An analysis of channel bank erosion and development of a catchment sediment budget model

Submitted by Victoria Jennifer Julie Janes to the University of Exeter as a thesis for the degree of Doctor of Philosophy in Geography, December 2013

I certify that all material in this thesis which is not my own work has been identified and that no material has been previously submitted and approved for the award of a degree by this or any other University.

Abstract

Increased sediment loads within river catchments have well-documented detrimental effects on water quality and catchment management plans are required to address reduction and mitigation of these problems. In order to do this it is essential that tools are available that deliver reliable sediment generation data at appropriate temporal and spatial scales. Currently, most sediment generation models do not include bank erosion individually as a sediment source. Therefore, to enable improved accuracy in predictions of future sediment pressures under environmental change, explicit modelling of the rates of sediment production by the bank erosion is required to provide a more complete representation of the catchment sediment budget.

In this study, an existing prototype national bank erosion index has been refined. Using Geographical Information Systems (GIS) digitised overlays, channel migration rates were calculated for several UK catchments. Relationships between the rate of channel bank erosion and factors controlling the rates of channel migration were investigated, including channel sinuosity, slope, upstream catchment area, and restriction of migration due to valley width. Significant correlations between bank erosion and sinuosity, upstream area and channel confinement were observed. The non-linear influence of channel planform geometry (curvature and sinuosity) on migration rates was further investigated using an existing meander migration model. A new bank erosion model was developed to incorporate the influence of both channel confinement and sinuosity. As the model incorporates the key physical controls on bank erosion, hence it is expected that it will have wide applicability in catchment- to national-scale bank erosion assessment.

A computationally efficient catchment routing model was developed. Data output from a newly developed catchment overland sediment and runoff estimation model (ADAS APT) was used as input to the routing model. The newly developed bank erosion model and an existing floodplain sedimentation model were incorporated within the routing methodology to provide a catchment sediment budget model. The model was applied to the Exe catchment, Devon, UK and validated against observational data. Model estimations of annual

sediment generation through bank erosion, sediment deposition on floodplains, and sediment load at the catchment outlet were within the range of observed values. The catchment sediment budget model developed in this thesis provides a more comprehensive representation of catchment sediment processes than existing alternative methodologies.

Acknowledgements

Firstly, I would like thank my supervisors Prof Andrew Nicholas, Prof Tim Quine and Prof Adrian Collins for their support, guidance and encouragement throughout the course of this project. I greatly appreciate all your help, without which this would not have been possible.

Thanks also to Dr Diane Fraser, for much help and guidance with the use of ArcGIS , various programming and IT issues.

To all my wonderful friends in the blue room, thank you for all your support. Be it in the form of cake, gossip, hot-chocolate (with cream, marshmallows and a flake) or a jogging partner, it was all greatly appreciated!

To my parents, I promise I'm done being a student now. Thank you for your support over the many years.

Finally to Richard, who is only just beginning his PhD journey. Thank you so much for your never-ending support and faith in me.

Contents

List of figures

List of tables

1.Introduction Chapter

The overall aim of this project is to develop a new model to estimate catchment sediment budgets within the UK. There are several existing models of overland sediment generation available: USLE (Wischmeier and Smith, 1962), SedNet (Prosser *et al*, 2001a), INCA-Sed (Jarritt and Lawrence, 2007), WEPP (Laflen *et al*, 1991), PSYCHIC (Davison *et al*, 2008) etc. PSYCHIC (**P**hosphorus and **S**ediment **Y**ield **CH**aracterisation **I**n **C**atchments) was developed by ADAS UK Ltd. and is used to estimate overland sediment production and transport to river channels at a catchment scale. PSYCHIC is currently being further developed within ADAS to create the APT model (ADAS Pollutant Transport model). This project aims to develop a model that can be coupled to the APT model to provide a catchment sediment budget model.

At present PSYCHIC does not contain any representation of sediment generation within river channels. ADAS have developed a national bank erosion index to estimate the volume of sediment generated as a result of bank erosion that reaches the catchment outlet. However, few existing sediment generation models currently predict the total volume of sediment entering the channel from bank erosion processes. Channel migration and associated bank erosion is a source of sediment within river catchments and as noted in several previous studies (Bull, 1997; Walling *et al*, 2005 etc.) may form a significant contribution to the total sediment budget within individual catchments. This thesis aims to develop a model to predict the volume of sediment produced by bank erosion processes that can then be coupled with other models, such as PSYCHIC/APT.

PSHYCIC/APT does not currently include a channel routing component. A computationally efficient routing model will be developed to enable the coupling of the overland sediment and water generation and delivery to the channel network (as estimated by PSYCHIC/APT) and a channel bank erosion model. Additional significant catchment sediment processes such as floodplain sedimentation will be incorporated within the model to achieve a comprehensive representation of the catchment sediment budget.

The sediment budget model that will be developed in this thesis can be coupled with existing overland sediment generation models. The aim is to improve the accuracy of sediment generation and load estimation, and

ultimately provide a more comprehensive representation of the catchment sediment budget. This information will better inform policy development and effective implementation of mitigation strategies.

In this chapter, a literature review will outline overland sediment generation processes, existing sediment generation models, and factors known to influence bank erosion. Additionally, the importance of sediments within the river system and the significance of bank erosion as a sediment source will be highlighted.

1.1.Literature review - Sediment generation

1.1.1. Processes of overland sediment generation

Surface processes within the river basin that act as sediment sources include wash/interrill processes (such as rainsplash erosion and soil wash) and rill and gully processes. Sediment models used to quantify these processes differ in terms of complexity, the processes that they include, and the input data required. As indicated by Merritt *et al*, (2003), the most appropriate model depends on the intended use of the model and the processes considered.

The rate of overland sediment generation within river catchments is highly variable both spatially and temporally. This is due to the numerous factors influencing rates of sediment generation processes. An understanding of sediment generation and transport processes within catchments is necessary to enable development and application of representative modelling methodologies. This section will discuss several processes of overland sediment generation, and factors influencing the rates of these processes.

1.1.1.1. Rainsplash erosion

Rainsplash erosion detaches sediment through the impact of raindrops falling on the soil surface. At height raindrops possess gravitational potential energy that is converted to kinetic energy as they fall. Kinetic energy is proportional to the mass and impact velocity of the raindrops and determines their erosivity. This is transferred to the soil surface and converted to a consolidating force (compacting the soil and forming a 'splash crater') and a disruptive force (dispersing the water). Less than 0.3% of the kinetic energy of the raindrop is used in transport of sediment particles (Knighton, 1998). The detachability of the soil by rainsplash impact depends upon the soil erodibility, which is a function of texture, cover, aggregate stability, and organic matter content.

The presence of vegetation results in a change in the erosive power of raindrops by altering the drop-size distribution. This induces effects that can both hinder and increase the rate of soil detachment. Vegetation causes some

drops to aggregate and increase in size. Larger drops lose proportionally less kinetic energy to air resistance than smaller drops and therefore have a larger kinetic energy for the same volume of water. Riezebos and Epema (1985) noted that raindrops with a prolate shape produce a soil detachment rate that is 2 to 3 times higher than that of raindrops with an oblate shape. Under vegetation fall heights of drops are reduced and more drops will have a prolate shape at impact, accounting for relatively intense splash erosion under vegetation. However, a low vegetation cover decreases the kinetic energy of the rain by up to 90% by protecting the underlying soil surface (Gregory, 1987). Additionally the presence of a litter layer provides a final barrier before the soil surface, reducing the kinetic energy acting on the soil surface decreasing erosion by up to 93.5%.

The slope gradient is a key factor controlling the transport of detached sediment particles as illustrated by Torri and Poesen (1992) as it acts through the addition of a gravity component to the drop detaching force. As slope gradient increases more sediment is moved downslope up to a maximum slope angle of ~18° (Morgan, 2005).

Morgan (2001) revised a previous soil-prediction model (Morgan-Morgan-Finney model) to estimate values of rainfall energy. The effective rainfall (ER) is split into direct throughfall (DT) and that which is intercepted and termed leaf drainage (LD):

$$LD = ER \times CC$$

$$DT = ER - LD$$

where CC is percentage canopy cover. The kinetic energy of the rainfall is then calculated as a function of rainfall intensity (I) using the relationship:

$$KE(DT) = DT(11.9 + 8.7\ Log\ I)$$

$$KE(LD) = (15.8 \times PH^{0.5}) - 5.87$$

$$KE = KE(DT) + KE(LD)$$

where PH is plant height. However alternative relationships have been observed between the kinetic energy of rainfall and rainfall intensity as shown in Table 1.1.

Table 1.1:Relationships between kinetic energy (KE, Jm^{-2} mm^{-1}) and rainfall intensity (*I*, mm/h)

Equation	Study
$KE=11.87+8.73\log_{10}I$	Wischmeier and Smith (1978)
$KE=9.81+11.25\log I$	Zanchi and Torri (1980) - Central Italy, in Morgan (2001)
$KE=8.95+8.44\log I$	Brandt (1989), in Morgan *et al*, (1998) used in EUROSEM
$KE=35.9(1-0.56e^{-0.034I})$	Coutinho and Tomas (1995) - Portugal, in Morgan (2001)
$KE=28.3[1-0.52\exp(-0.042I)]$	Van Dijk (2002), in Fornis *et al*, (2005)
$KE=11.93+7.82\log I$	Fornis *et al*, (2005) - Philippines
$KE=11.41+3.64\log_e I$	Brodie and Rosewell (2007) - Australia

EUROSEM (Morgan *et al*, 1998) estimates soil detachment by raindrop impact using the following equation:

$$DR = \frac{k}{\rho_s} KE e^{-zh}$$

where k is an index of the detachability of the soil (obtained experimentally), ρ_s is the particle density, KE is the total kinetic energy of the net rainfall at the ground surface, z an exponent depending upon the soil texture and h the mean depth of the surface water layer. However in this model the influence of a sloping surface on soil particle detachment is neglected. As noted in the previous section the presence of a slope has a significant effect on the rate of sediment movement by rainsplash erosion.

The formation of a surface seal is known as consolidation and occurs when finer particles are washed into the pores of the soil surface to form an

semi-impermeable layer up to 10 mm thick. The kinetic energy of rainfall breaks down aggregates within the soil, causing smaller soil units or individual particles to cover and fill pores of the soil below. This layer decreases infiltration capacity and hence increases surface runoff. The infiltration capacity can be reduced by up to 50% in one storm event (Knighton, 1998). Hoogmoed and Stroosnijder (1984) observed that a thin crust on the surface to be at least 10 times less permeable than the directly underlying soil. Most seals form almost completely within the first 5-10 minutes of rainfall when loose particles are available, however this varies with soil and rainfall characteristics (Bryan, 2000).

Crusting of the soil surface may occur when the soil surface hardens as it dries out after a rainfall event. This acts in a similar way to the surface seal. The probability of crust formation decreases as clay and organic matter content within the material increase as these provide greater strength to the soil. Loams and sandy loams are most vulnerable to crust formation.

Rainsplash erosion is most effective when combined with surface runoff as this allows rapid transport of detached sediment particles downslope and prevention of the formation of a surface crust. Additionally the presence of surface water causes an increase in splash erosion due to the turbulence caused by the impacting raindrops. Beuselinck *et al*, (2002) observed a significant increase in sediment delivery ratio (SDR) of surface flow in the presence of raindrop impact and that this effect is more pronounced on higher surface slopes. However as discharge increases the effect on SDR reduced as sediment export becomes more efficient. This increase was attributed to the Hairsine-Rose theory of rainfall re-detachment whereby previously deposited sediment particles are lifted into the water layer as a result of raindrop impact and rapidly acquire the velocity of horizontal flow. Fox and Byran (1999) highlighted the significance of the presence of a surface water layer for rainsplash erosion; they found splash erosion without a surface water layer never accounted for more than 20% of total interrill erosion, rain-impacted flow erosion (rainsplash erosion with a surface water layer) accounted for more than 80% of total erosion.

Kinnell (2005) identified that soil detachment by the action of raindrop impact and overland flow (either individually or acting in combination) can be divided into four separate sub-processes;

1. Raindrop detachment with transport by raindrop splash – a transport-limited process requiring the presence of a slope for net downslope movement of sediment.
2. Raindrop detachment with transport by raindrop-induced flow transport – raindrops penetrate overland flow to lift detached material into the flow and allow movement of sediment downstream, also transport-limited.
3. Raindrop detachment with transport by flow – raindrops not involved in the transport process but allow particles to be detached which would not have been by flow.
4. Flow detachment with transport by flow – when stream power enables sediment detachment and transport. Rill erosion occurs where this process is present.

The Hjulström curve (Figure 1.1) shows the water velocity required to transport, erode, or deposit sediment particles of different size diameter. From this it can be seen that less energy is required to keep sediment of a particular particle size in transport that to detach. Where the velocity of runoff flow (and hence shear stress acting on the sediment) is too low to detach particles, rainsplash erosion results in a greater force and soil detachment and runoff velocity is great enough to keep these particles in transport.

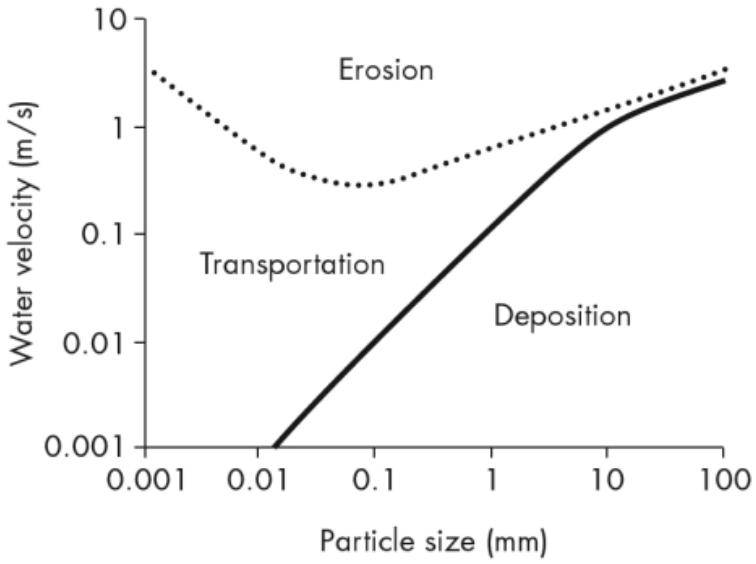

Figure 1.1: The Hjulström curve indicating the relationship between flow velocity and erosion, transport and deposition characteristics for different sized particles. Taken from Davie (2008).

1.1.1.2.Erosion by surface flow

Erosion by surface flow can occur through cavitation of solid rock, and removal of both unconsolidated non-cohesive sediments and cohesive sediments. To entrain sediment the forces moving the particle must be greater than those attempting to hold it in place. The presence of a surface water layer allows the rapid removal of sediment detached from the surface. Surface water may develop in two ways; the first is known as infiltration-excess overland flow and is known as Hortonian flow. This flow occurs when the infiltration capacity of the underlying soil has been exceeded due to the intensity of the rainfall and occurs at flow rates of 30-500 mh^{-1} (Knighton, 1998). The second form of surface runoff is known as saturated overland flow and occurs when the soil is completely saturated. This process, also known as the Hewlett hypothesis is therefore related to the antecedent moisture conditions present in the soil rather than the infiltration capacity and occurs at flow rates of 0.3-100 mh^{-1} (Knighton, 1998).

1.1.1.2.1. Curve number approach

The curve number approach is an empirical runoff estimation method developed by the US Soil Conservation Service in 1972. Runoff is calculated using the following equation:

$$R_s = 0 \ \ where\ P \leq I_a$$

$$R_s = \frac{(P - I_a)^2}{(P - I_a + S)} \ \ where\ P > I_a$$

Where P is total precipitation, I_a is initial retention/abstraction volume, commonly taken as $0.2S$ (Bras 1990), and S is the potential maximum surface retention. The surface retention volume is given as:

$$S = \left(\frac{1000}{CN}\right) - 10$$

CN is a parameter known as the curve number and is dependent on soil type (or Hydrologic soil group, HSG), hydrological condition, land-use or cover type, and 5-day antecedent moisture conditions (AMC). The curve number can range from 0-100 and given for various soil types and conditions, with higher numbers reflecting increased runoff. The influence of the curve number on the predicted volume of runoff is shown in Figure 1.2.

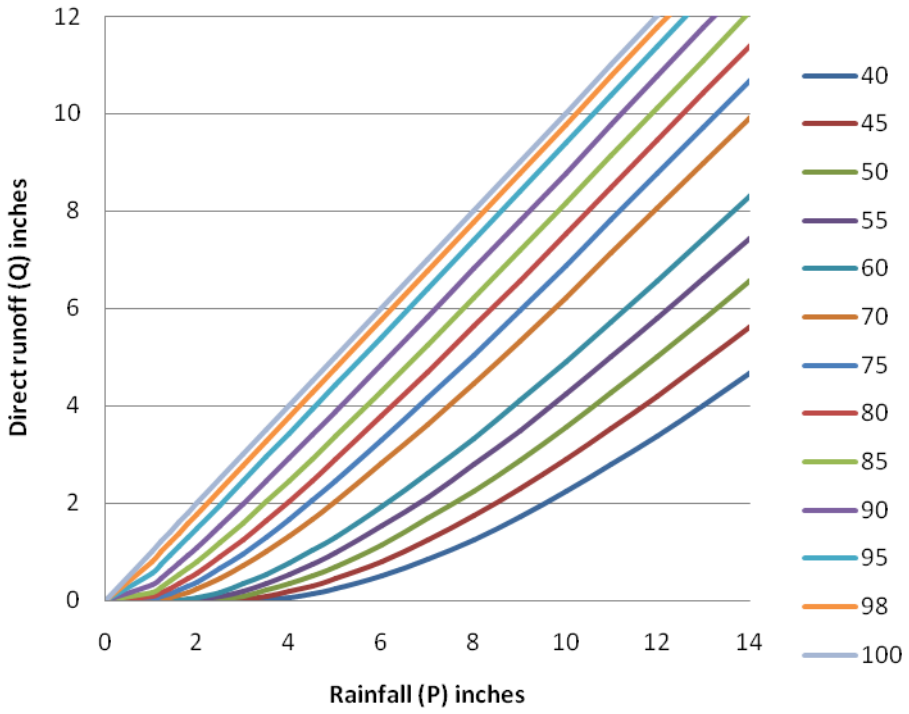

Figure 1.2: Solution of runoff equation, assuming *Ia*=0.2*S*.

Soils are classified into four HSGs depending on their infiltration rate (USDA, 1986):

- Low runoff potential - soils with high infiltration rates even if wet. High rates of water transmission (>0.3 in/hr). E.g.: Sand, loamy sand, or sandy loam.
- Moderate infiltration rates - moderately well to well-drained soils. Moderate rate of water transmission (0.15-0.3 in/hr). E.g.: Silt loam or loam.
- Slow infiltration rates - soils with a layer that impedes downward movement of water. Slow rate of water transmission (0.05-0.15 in/hr). E.g.: Sandy clay loam.
- High runoff potential - soils with slow infiltration rates, with high water table. Very slow rate of water transmission (0-0.05 in/hr). E.g.: Clay loam, silty clay loam, sandy clay, silty clay or clay.

The hydrological condition indicates the effects of cover type and treatment on infiltration and runoff, and is estimated from plant density. Good hydrologic condition indicates the soil has a low runoff potential for that specific

hydrologic soil group and cover type. Table 1.2 provides examples of curve numbers for a selection of agricultural soil-cover types. For each soil-cover type individual curve numbers are provided for different hydrologic conditions and each HSG.

Table 1.2: Runoff curve numbers for a selection of agricultural soil-cover complexes, (USDA 1986).

Land use cover	Treatment	Hydrologic condition	Soil group			
			A	B	C	D
Fallow	Bare soil		77	86	91	94
	Crop residue cover	Poor	76	85	90	93
		Good	74	83	88	90
Row crops	Straight row	Poor	72	81	88	91
		Good	67	78	85	89
	Contoured	Poor	70	79	84	88
		Good	65	75	82	86
	Straight row and contoured	Poor	70	80	87	90
		Good	64	75	82	85
Pasture, grassland, or range		Poor	68	79	86	89
		Fair	49	69	79	84
		Good	39	61	74	80
Meadow			30	58	71	78
Woods-grass combination		Poor	57	73	82	86
		Fair	43	65	76	82
		Good	32	58	72	79
Wood		Poor	45	66	77	83
		Fair	36	60	73	79
		Good	30	55	70	77

The AMC accounts for the variation in curve number between different storm events. The curve numbers displayed in tables (such as Table 1.2) are for average antecedent conditions, also known as AMC 2 and can be adjusted to account for a dry watershed not yet at wilting point (AMC 1, curve number is decreased) and a nearly saturated soil (AMC 3, curve number is increased) (Bras, 1990).

King *et al,* (1999) investigated the accuracy of the curve number method in Goodwin Creek, USA, and over an eight year period found the efficiency of the method to be 84% at a monthly timescale, and 43% for daily. Runoff was found to be consistently under estimated using this method. It was noted that

the CN method of runoff estimation is simple and robust, yet a major limitation is the inability of the method to account for rainfall intensity and duration.

Huang *et al*, (2007) conducted a similar study in the Loess Plateau, China, and in addition to calculating the CN using the standard method, they also calculated a measured value of CN using by collecting rainfall and runoff data, and calculating S using the equation:

$$S = 5\left[(P + 2Q) - \sqrt{Q(4Q + 5P)}\right]$$

Similarly to King *et al,* (1999) the study found that the standard method underestimated runoff depths in 85 out of 98 plot-runoff events. Additionally, no relationship was observed between the measured CN and the 5-day AMC, indicating the 5-day AMC was not a reasonable assumption for most storms in the study area. Therefore the inadequacy (and under estimation) of the AMC resulted in the underestimation of runoff.

Infiltration rate is therefore a major control on the generation of surface runoff. Water drains into the soil by gravity and capillary forces in voids between soil particles. In rainstorms these voids are filled so the capillary forces are reduced. The infiltration rate corresponds to the hydraulic conductivity of the soil, which varies between soil types (sandy soils have a high hydraulic conductivity and clay soils have low). Coarse-textured soils have greater infiltration rates than clay soils due to larger void spaces. Cracks and macropores within the material also greatly influence the transmission of water. Infiltration rate also has much spatial variability due to differing soil structures, compaction, initial moisture content and vegetation density. Additionally, saturated overland flow is important in the formation of rills, and areas of cultivated land with a perched water table (usually found in area where an impermeable layer prevents downward drainage of water from upper soil layers).

Erodibility of the soil depends largely on the soil texture, the amount of organic matter in the soil, and the soil profile (structure of the surface horizons and permeability). Sand silt and clay particles have different diameters (0.05-

2mm, 0.002-0.05mm, and <0.002mm respectively) and soil texture is determined by the percentage of these three components within the soil. Wischmeier and Mannering (1969) found soils with high silt, low clay and low organic matter content are more erodible. This is due to the lower permeability of these soils, and low resistance to particle detachment. Due to their high cohesion, clay-rich soils are less erodible as they resist detachment. Sandy soils are highly permeable and as a result runoff rates and erodibility of these soils are low.

Soils structure is the aggregation of soil particles. Developed soil structures contain cracks and large pores for storing water, thereby increasing infiltration and reducing runoff and erodibility. Aggregation also holds particles together which increases the soil resistance to raindrop impact. Decomposed organic matter (humus) binds mineral particles within the soil to form aggregates, enabling a developed structure to form within the soil. Therefore soils with higher soil organic matter content are less erodible.

As slope gradient increases soil detachment through surface runoff also increases. Fox and Bryan (1999) found that for a constant runoff rate soil loss increased approximately with the square root of slope gradient. They also noted that the influence of slope gradient was exerted through flow velocity as of all the hydraulic parameters soil loss was best correlated with flow velocity (R^2=0.80).

The rate of sediment detachment does not show a simple linear relationship with increased precipitation, as there are many other factors to consider, notably vegetation cover. The relationship between sediment yield and precipitation was investigated by Lanbein and Schumm (1958) who observed for the same value of effective precipitation (the amount of precipitation required to produce a known amount of runoff) annual sediment loads could vary tenfold due to different geologic and topographic factors. Additionally erosion was observed to reach a maximum with a mean annual precipitation of 300 mm and as precipitation increased further above this level the effect of increased vegetation cover providing protection to the underlying soil counteracted the erosive effect of increased rainfall causing soil loss to decrease with further increase of rainfall.

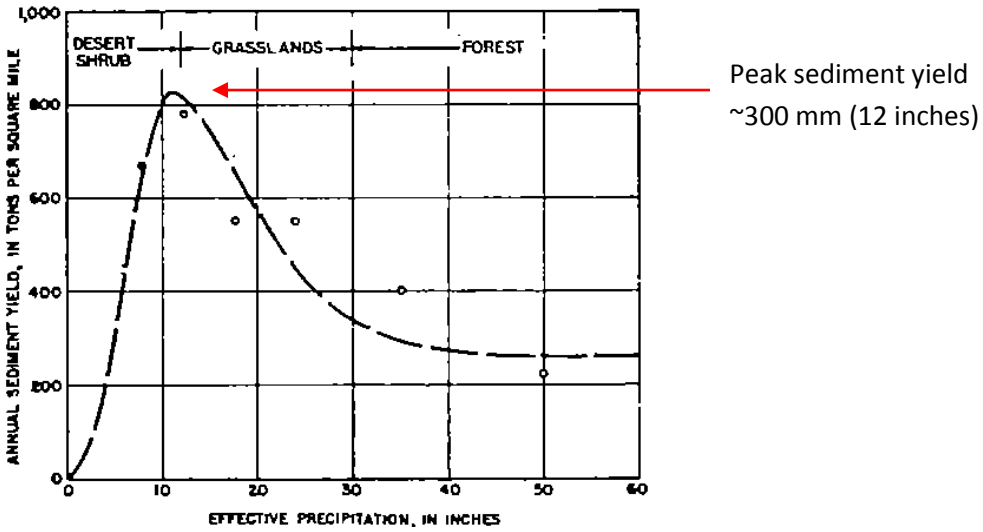

Figure 1.3: Climatic variation of yield of sediment, the Langbein-Schumm rule. Adapted from Langbein and Schumm (1958).

Sediment production rates may also vary seasonally due to the variation in the magnitude of events with changing seasons and also seasonal vegetation patterns. Wilson (1973) found that sediment yield was more a function of climate regime than of mean annual precipitation and high variability of seasonal rainfall produces maximum sediment yields. Seasonal patterns may produce wet and dry seasons with vegetation showing a similar pattern with peaks slightly lagging that of rainfall. This means the most vulnerable period is during the early wet season when rainfall is high and vegetation has not grown enough for sufficient protection. Monsoonal rainfall patterns and irregularity of rainfall fails to provide sufficient water for dense vegetation growth and high sediment yields can be expected (Douglas 1967). The influence of vegetation on soil erodibility was also highlighted in the section on rainsplash erosion (page 24) and Figure 1.3. The presence of vegetation protects the underlying soil thereby decreasing soil erodibility. Additionally, decaying plant matter increases the organic matter content within the soil, increasing resistance to soil detachment. Plant roots also have binding effect on the soil, increasing soil resistance and decreasing erodibility.

1.1.1.3. Rill processes

Small channels of more concentrated flow known as rills may develop within surface flow. Rills are surface microchannels 50-300 mm wide and up to 300 mm deep and are associated with infiltration-excess overland flow. Formation of rills occurs on slopes greater than 2-3° with probability of rill development increasing with increasing gradient due to increased overland flow and erosivity and decreased topsoil shear strength. Govers and Poesen (1988) noted that on slope gradients >30% more soil loss due to rill erosion is expected as rilling and channel sidewall processes become more active with increased slope gradient. Rill erosion may account for a significant proportion of the sediment removed from a hillslope, particularly on slopes with little vegetation cover where they can account for between 50 and 90% of total sediment removal (Knighton, 1998). The erosive potential of rills depends upon the spacing of the rills and the extent of the area with rill formation. Rills are discontinuous features and may be lost when the supply of sediment to the rill system is greater that the transporting capacity.

Rill initiation is dependent on both flow conditions and soil surface properties. The flow condition which can be indicated by the Froude number ($Fr = v/gR^{0.5}$ where v is the velocity of flow, g the acceleration due to gravity and R the hydraulic radius) has also been linked to rill formation; supercritical flows (Fr > 1) are associated with instability features which increase shear stress generating bed deformation and can trigger rill incision (Bryan, 2000). Additionally, Bryan and Rockwell (1998) observed the importance of hydraulic impedance (caused by the presence of a high water table) on moderate slopes (< 9°) for rill development. This effect is mainly due to a significant decrease in soil shear strength due to positive pore water pressures.

Rejman and Brodowski (2005) found rill erosion to contribute between 65 and 73% of total overland soil loss, and rates of rill erosion were ~5.9 kg m^{-3}. Studies in other areas have found similar values of contribution of rill erosion to total sediment loss; 58% (Kimaro *et al*, 2008). Additionally Rejman and Brodowski (2005) found the contribution of both rill and interrill erosion increased with slope length. Fox and Bryan (1999) observed a similar

relationship and noted that on longer slopes interrill runoff will attain a greater velocity thereby increasing interrill erosion rates.

Eventually rills may develop into larger more permanent features known as gullies. Gullies have steep sides and low width to depth ratios and generally only develop on slopes with a gradient of 12° or more. The generation of gullies is normally a result of increased surface runoff.

1.1.2. Sediment delivery ratio

Sediment delivery ratio is defined as the fraction of total erosion that is transported from a specific catchment within a particular time interval and can be conceptualised as:

$$SDR = Y/E$$

Where Y is annual average sediment yield per unit area and E is average annual erosion over that same area (Lu *et al*, 2004). Sediment delivery ratio (SDR) varies greatly both spatially and temporally due to its dependence on many factors including hydrology (rainfall, runoff, drainage pattern), topography, underlying lithology and also vegetation properties.

Walling (1983) observed the importance of antecedent soil moisture, season, and magnitude of annual precipitation on SDR. Additionally it was observed that as runoff is usually produced in only a small area of a river basin then the SDR will be related to the characteristics of this area as opposed to the whole watershed.

Lu *et al*, (2004) observed the influence of vegetation on SDR; the fraction of eroded sediment that reaches the channel is reduced by the presence of vegetation cover, and SDR remains constant for un-vegetated channels. Ebisemiju (1990) observed that ~88% of detached and entrained sediments were transported to the channel on bare slopes, whereas on fully vegetated slopes this figure decreased to 16%. On bare slopes runoff velocities will be greater and infiltration rates will be lower, therefore flow velocities and transport capacities will be higher.

The influence of basin size on SDR was investigated by Trimble (1977) who observed a SDR of 10% for basin size of 260 km^2 and SDR of 5% for a basin size of 1500 km^2. This relationship has been explained due to the decreasing slope and channel gradients associated with larger basins, and increased opportunities for sediment deposition or trapping on its course to the channel. However, Walling (1983) observed considerable variability of values of SDR between basins of a particular size, as shown in Figure 1.4.

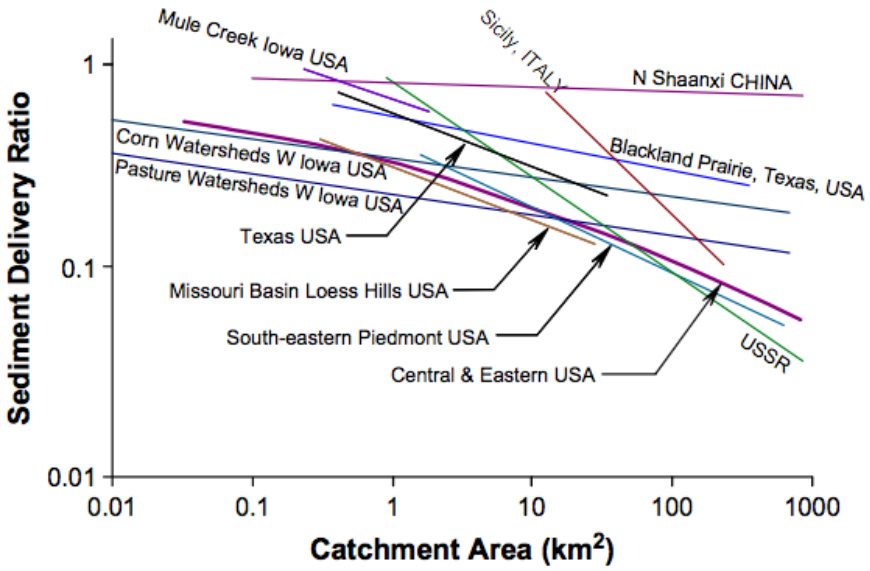

Figure 1.4: Relationships between sediment delivery ratio and catchment area observed in previous studies for various regions. Taken from Lu *et al*, (2006).

Many studies have also indicated the influence of season on SDR (Duijsings, 1987; Sarma 1986; Cabot *et al*, 2006; Wu *et al*, 2008). These studies observed that the relationship between SDR and season were an indirect effect of the rainfall patterns; higher suspended sediment was observed in seasons when rainfall was more intense, and is therefore more erosive and has a greater transport capacity. The transport capacity is the amount of sediment the water can carry and is determined by the flow velocity. In dry months there was a dominant sediment storage pattern.

SDR is a spatially lumped concept when in reality it is spatially distributed. Individual sediment sources have unique detachment, transport and

storage processes, local factors are influential on the volume of sediment that reaches the channel, and as noted previously runoff may only occur in a fraction of the basin rather than the whole. For this reason Ferro and Minacapilli (1995) used a spatially distributed approach to model SDR to account for sub-basin variability. Within each sub-basin section SDR is calculated as a function of travel time, unit length and slope characteristic of that particular section. Sub-basins were determined as areas of similar length and steepness.

Van Dijk and Kwaad (1998) created a delivery ratio method based on the probability of a land cell to generate surface runoff:

$$D_r = \alpha \left(\frac{H_c\sqrt{s}}{nl}\right)^{\beta} \qquad 0 \leq D_r \leq 1$$

where values of α and β were 9.53 and 0.79 respectively (Dickinson *et al*, 1986), H_c is a hydraulic coefficient indicating the probability of overland flow occurrence, s is the slope gradient , l is the length of the flow path between the cell and the channel, and n is Manning's roughness coefficient. The sediment delivered (SD) is calculated by multiplying the delivery ratio and the total soil loss of the cell (A):

$$SDR = D_r A$$

Sediment supplied to channel was calculated by accumulating SDR values from individual cells over the local drain direction map.

Lu *et al*, (2006) note importance of the factors influencing SDR that vary within a basin (such as topography, soil, hydrological variables and vegetation cover). In their study SDR over the Murray Darling basin was modelled using an adaptation of a model by Sivapalan *et al*, (2002) which was used to investigate catchment response to floods. The model consists of two independent components as shown in Figure 1.5. Soil erosion supplies the hillslope store with sediment (assumed at a constant rate) during an effective storm. The hillslope stores some of the sediment and delivers some to the channel network store. The SDR can then be calculated from the probability distribution of effective storm duration.

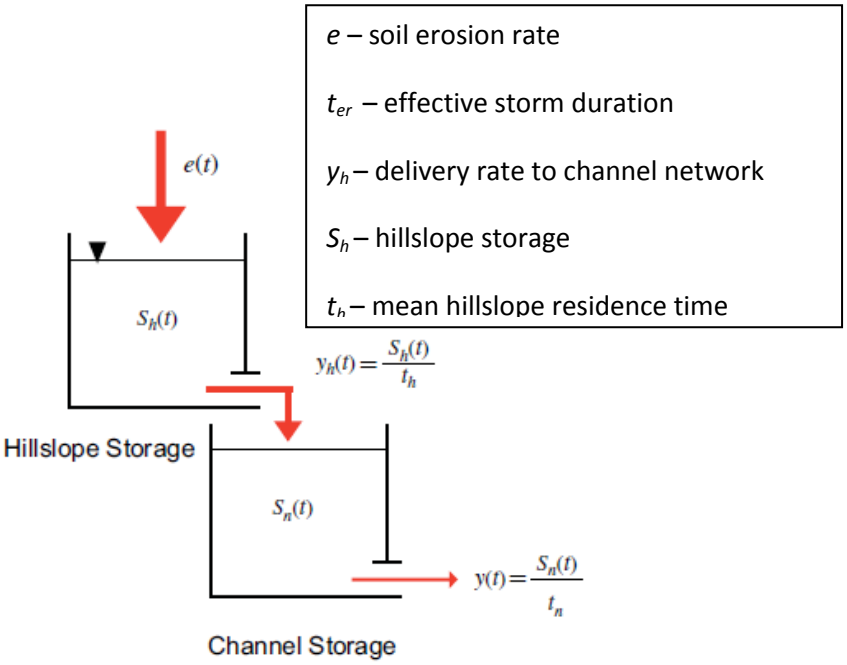

Figure 1.5: Diagram of a two storage lumped linear model of SDR at catchment scale. Adapted from Lu *et al*, (2006).

The sediment in the two stores is calculated by the following continuity equations:

$$\frac{dS_h(t)}{dt} = e(t) - y_h(t), \quad y_h(t) = S_h(t)/t_h$$

$$\frac{dS_n(t)}{dt} = y_h(t) - y(t), \quad y(t) = n(t)/t_n$$

where S_h is the sediment stored on a hillslope, S_n is the sediment stored in the channel network, y_h is the rate of delivery, and t_h and t_n are the mean hillslope and channel residence times respectively. The residence time of sediment is estimated as a function of particle size, accounting for the varying particle movements with water flow. The influence of land cover is accounted for as the basin is divided into smaller areas of similar land use, cover, and soil properties. GIS is used to estimate the mean hillslope travel time for water flow as a function of topographic features and soil properties. The travel time through each cell is estimated as the distance through the cell divided by the velocity of flow.

1.1.3.Overland sediment generation models

This section will outline some of the existing models used to represent overland sediment generation at catchment scale. These will include the Universal Soil-loss equation (USLE/RUSLE), WEPP (Water Erosion Prediction Project), SedNet (the SEDiment river NETwork model), INCA/INCA-Sed (Integrated Nitrogen Catchment model), CREAMS (Chemicals Runoff and Erosion from Agricultural Management Systems), SHETRAN (Système Hydrologique Européen TRANsport) and PSYCHIC (Phosphorus and Sediment Yield CHaracterisation In Catchments).

Sediment generation models can be defined as empirical or process-based. Empirical models are based on statistical relationships from previous research allowing a simple input-output relationship. The benefits of these models include the small amount of data required to run the model (in comparison to detailed process-based alternatives). The limitations of these models include that the empirical relationships used may be based on an un-representative dataset; a relationship between two variables in one area may not be the same as the relationship between the same variables in another. Process or physically based models involve solving physical equations to represent individual processes within the catchment. The benefits of these model types include minimal calibration as most parameters should be physically based and therefore have measurable values. The limitations of these models include the large amounts of data required for input, and also to validate the representation of processes within the models. Additionally these models are often computationally complex resulting in long simulation times.

The way in which spatial detail is represented within models can be defined as lumped or distributed. Lumped models treat modelled areas (for example sub-catchments) as single units, whereas distributed models involve separation of modelled areas into individual units. Distributed models permit representation of spatial variability.

The area the model is to be applied, availability of data (both spatial and temporal), and the requirements of the model output should be considered when selecting which model type should be used.

1.1.3.1. Universal Soil-Loss Equation

In response to the requirement to quantify soil loss in agricultural areas the Universal Soil-Loss Equation (USLE) was developed by Wischmeier and Smith in 1962 and reviewed in 1978. This empirical equation was based on experimental data collected within the USA and uses parameters that are universally acknowledged to influence erosion.

USLE was then revised by Renard *et al,* (1997) to produce the Revised Universal Soil-Loss Equation (RUSLE). RUSLE computes combined interill and rill erosion values and contains the same parameters as used in USLE but the equations used to calculate these parameters have been adapted.

Both USLE and RUSLE are based on the following equation:

$$E = R.K.LS.C.P$$

Where E is mean annual soil loss, R the rainfall-runoff erosivity factor, K the soil erodibility index, LS the topographic factor combining both slope length and gradient, C crop management factor and P conservation practice factor (Wischmeier and Smith, 1978 and Renard *et al*, 1997).

The rainfall-runoff erosivity factor (R) is the calculated from the sum of erosion index values from a normal year's rain. The erosion index is a measure of the erosive force of rain and calculated as the product of energy and maximum 30-minute intensity of each storm. Renard *et al*, (1997) note that data used to estimate R must include the effects of frequent moderately sized storms as well as occasional high magnitude events. In the development of erosion index their calculation was based on 22-year records so as to encapsulate cyclic variability in rainfall patterns, but recommend the use of longer records where possible. An equivalent R approach was developed for use in the farming areas in Pacific Northwest regions to reflect the combined effects of thawing soil and rain on snow and partly frozen soil (Renard and Ferreira, 1993).

The soil erodibility index (K) is defined as the mean annual soil loss per unit R for standard condition bare soil; recently tilled up and downslope with no conservation practice, and on a 5º slope of 22m length (Morgan, 2005). K

values are commonly estimated through use of a nomograph (see Figure 1.6), however this does not apply for some soil types.

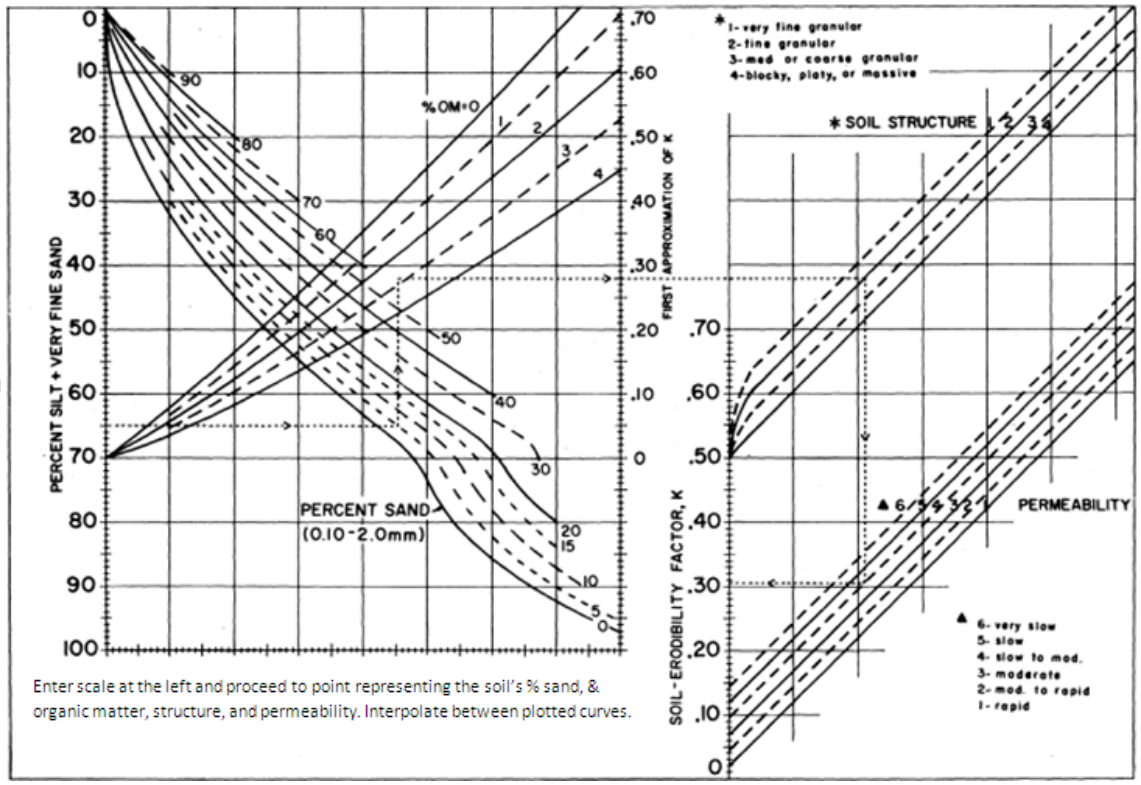

Figure 1.6: Soil-erodibility nomograph adapted from Wischmeier and Smith (1978).

RUSLE varies K seasonally, with variability highest in Spring due to soil 'fluffing' from freeze-thaw and when the soil is wet, and lowest in mid-autumn when soil is dry and compacted (Renard and Ferreira, 1993; McCool *et al*, 1995). Values of K range from ~0.013 – 0.059 SI units with high-sand and high-clay content soils having lower values than high-silt content soils (McCool *et al*, 1995). This is because clay soils are more resistant to detachment, sandy soils have coarse textures and therefore even though easily detached are not transported due to low runoff values, and soils with high silt contents are easily detached and tend to crust and produce high rates of runoff. K is also adjusted for rock within the soil profile to account for the effects on runoff due to the influence this has on soil permeability.

The topographic factor (LS) expresses soil loss under a given slope steepness and length to soil loss from standard condition (Morgan, 2005) and is calculated as:

$$LS = \left(\frac{x}{22.13}\right)^{n} (0.065 + 0.045s + 0.0065s^{2})$$

Where x is the slope length (m), n is varied according to steepness, and s is slope gradient. The reliability of RUSLE decreases with large slope lengths and therefore should not be used on slopes longer than 1000 ft (Institute of Water Research, 2002). RUSLE allows complex slopes to be represented by a series of segments allowing for a improved representation of the topographic effect compared with USLE.

The crop management factor (C) is a ratio of soil loss under a given crop to that from bare soil. This takes into account the annual variation in cover by dividing the year into different stages of crop growth: fallow, seed-bed (secondary tillage formation), establishment, development, maturity, and residue/stubble-harvest (Morgan, 2005). Values of C vary depending on crop type (see Table 1.3), yield, plant density, and nature of previous crop.

In RUSLE a sub-factor method is used to compute soil loss ratio and is given by the equation:

$$C = PLE, CC, SC, SR, SM$$

where PLE is prior land use, CC is the crop canopy, SC is surface/ground cover, and SR is surface roughness (Renard *et al*, 1997). Values of C range from near zero for well-protected soil to1.5 for finely tilled surface with a large volume of surface runoff and highly susceptible to erosion (McCool *et al*, 1995). PLE accounts for the residual effects of cropping, CC accounts for the influence of the canopy layer reducing the rainfall energy (similar to that illustrated in Table 1.3), surface cover reduces transport capacity of runoff as does surface roughness.

Table 1.3: C-factor values for use in USLE. Taken from Morgan (2005).

Table continued on next page.

Practice	Average annual C-factor
Bare soil	1.00
Forest or dense shrub, high mulch crops	0.00
Savanna or prairie grass in good condition	0.01
Overgrazed savanna or prairie grass	0.10
Maize, sorghum or millet: high productivity conventional tillage	0.20-0.55
Maize, sorghum or millet: high productivity conventional tillage	0.50-0.90
Maize, sorghum or millet: low productivity no or minimum tillage	0.02-0.10
Maize, sorghum or millet: high productivity chisel ploughing into residue	0.12-0.20
Maize, sorghum or millet: low productivity chisel ploughing into residue	0.30-0.45
Cotton	0.40-0.70
Meadow grass	0.01-0.025
Soya beans	0.20-0.50
Wheat	0.10-0.40
Rice	0.10-0.20
Groundnuts	0.30-0.80
Palm trees, coffee, cocoa with crop cover	0.10-0.30
Pineapple on contour: residue removed	0.10-0.30
Pineapple on contour: with surface residue	0.01
Potatoes: rows downslope	0.20-0.50
Potatoes: rows across-slope	0.10-0.40
Cowpeas	0.30-0.40
Strawberries: with weed cover	0.27
Pomegranate: with weed cover	0.08
Pomegranate: clean-weeded	0.56
Ethiopian tef	0.25
Sugar cane	0.13-0.40
Yams	0.40-0.50
Pigeon peas	0.60-0.70
Mungbean	0.04
Chilli	0.33

Practice	Average annual C-factor
Coffee: after first harvest	0.05
Plantains: after establishment	0.05-0.10
Papaya	0.21

The P factor represents the influence of any erosion-control in practice within the area. It is derived from the ratio of soil loss where practice is applied to soil loss where it is not. No soil erosion practice would yield a P value of zero, typical P values range from 0.01-0.9 (Morgan, 2005) and will vary according to slope steepness. P factor values are considered the least reliable of RUSLE due to their lack of experimental data reflecting the many possible scenarios (Renard and Ferreira, 1993; McCool *et al,* 1995).

Later developments of RUSLE have included a 2D-RUSLE using upstream contributing area instead of slope length to estimate LS. Desmet and Govers (1996) estimated using GIS using a formula based on slope length factor of grid cells, drainage area at the inlet of cell, slope length and aspect. This version accounts for the effects of flow convergence, and captures both rill and interill erosion.

1.1.3.2. WEPP

The Water Erosion Prediction Project (WEPP) was a research project initiated by the US Department of Agriculture in 1985 and is a process-based model developed to replace the factor based erosion prediction of USLE. Laflen *et al,* (1991) noted the wider applicability of process-based models to predict spatial and temporal variability compared to empirical models. WEPP predicts both soil erosion and deposition, and operates on a daily time step, and either a hillslope or watershed scale.

Weather and climate data are generated from a stochastic weather generator that provides mean daily precipitation, daily maximum and minimum

temperatures, mean daily solar radiation, and mean daily wind direction and speed. Infiltration is calculated using the Green-Ampt equation and runoff is calculated as the difference between rainfall and infiltration and is routed using kinematic wave equations. The model is therefore limited to areas which are dominated by Hortonian/rainfall excess overland flow (Flanagan *et al*, 2007). Winter processes (such as frost and thaw development in the soil), irrigation, water balance, plant growth, and residue decomposition are also represented in the model. Soil parameters included within the model are

- Random roughness – related to tillage
- Oriented roughness – height of ridges left by tillage
- Bulk density – total pore volume
- Wetting-front suction – related to infiltration
- Hydraulic conductivity – controls infiltration and runoff
- Interrill erodibility – measure of soil resistance to detachment by raindrop impact
- Rill erodibility – measure of the soil resistance to detachment by concentrated rill flow
- Critical shear stress – threshold parameter above which a rapid increase in soil detachment per unit increase in shear stress occurs.

Interrill detachment (D_i) is proportional to the product of effective rainfall intensity (I_e) and interrill runoff rate (σ_{ir}):

$$D_i = K_i I_e \sigma_{ir} SDR_{rr} F_n (R_s/W)$$

where $SDRrr$ is the sediment delivery ratio, F_n accounts for irrigation, R_s and W are the rill spacing and width, and k_i is a baseline interrill erodibility (Nearing *et al,* 1989). Rill detachment (D_c) is modelled as a function of the shear stress of the flow acting on the soil (τ_f), and resistance of the soil to detachment (τ_c):

$$D_c = K_r(\tau_f - \tau_c)$$

where K_r is the rill erodibility of the soil. Rill detachment does not occur when the shear stress of the flow is less than the critical shear stress of the soil, and deposition occurs if the sediment load is greater than the transport capacity.

The watershed model links the hillslope models to the channel network. Channel shape is assumed to be triangular and erosion of channel bed occurs when shear stress of the flow exceeds the critical shear stress of the bed and sediment load is less than the transport capacity.

Tiwari *et al,* (2000) evaluated the performance of WEPP with observational data at 20 locations and the R^2 value was 0.71 when using the average annual values of soil loss, indicating the model performed well. When the model performance was analysed for yearly soil loss values the R^2 was 0.40, due to the variability in annual observations. It was noted that similarly to other soil erosion models, WEPP overestimates soil loss for small values, and underestimates high values. The model sensitivity to erodibility parameters was also noted, and therefore further refinement in the calibration process for these parameters would significantly improve model performance.

Pieri *et al*, (2007) analysed the accuracy of WEPP using experimental plot data in the Centonara Watershed near Bologna, Italy for a period of 7 years. The results indicated WEPP accurately simulated the water balance for the plots yet tended to under-predict the sediment yield. The authors noted the importance of calibration of the model's erodibility parameters for the study site.

Singh *et al*, (2012) assessed the accuracy of WEPP in a watershed in eastern Himalaya and found the Nash-Sutcliffe simulation coefficients (a measure used to assess predictive accuracy of models, with values of 1 indicating perfect simulation) for model simulations of runoff and sediment yield during the validation period to be 0.87 and 0.90 respectively. Deviations of the simulated values from the measured were within ±20% and goodness-of-fit test statistics indicated the model simulated daily runoff and sediment yield with reasonably good accuracy. Sensitivity analysis revealed sediment yield outputs were most sensitive to rill erodibility parameter, and runoff outputs were most sensitive to the hydraulic conductivity parameter. Again, it was observed that the model slightly under-predicted both runoff and sediment yields.

Ascough *et al*, (1997) noted the watershed model neglected partial area response, headcutting, bank erosion, and perennial streams which limited the model accuracy. Merritt *et al*, (2003) noted the WEPP models limitations to include the large computational and data requirements which may limit its

applicability. The model includes a number of parameters that require calibration against observational data, which may not be available. Additionally, Merritt *et al*, (2003) noted that the rill-interrill concept of erosion may not be applicable to soils that have not been cultivated and do not have rill formations. For large catchments error accumulation may become an issue, as simulations are performed on individual hillslopes and then these are summed to the catchment scale. Whilst WEPP is a process-based model the number of parameters involved means the model contains empiricism. As noted by Singh *et al,* (2012) and Pieri (2007) the model is sensitive to certain parameters and it is important to carefully calibrate parameters to the site where the model will be used.

1.1.3.3. SedNet

SedNet (the Sediment River Network Model) was developed by the Australian National Land and Water Resources Audit (NLWRA) to predict mean annual transport and deposition of suspended and sediment load considering three sediment sources; sheetwash, gully erosion and streambank erosion. The river is split up into links representing the reach between two nodes. Sheetwash erosion is modelled using RUSLE and gully erosion is estimated from aerial photograph interpretation.

Within the SedNet model, suspended sediment is assumed to be supply limited and the only deposition represented was floodplain deposition calculated from the fraction of total discharge that flows overbank (Q_x-Q_{bx}/Q_x):

$$D_x = \frac{Q_x - Q_{bx}}{Q_x}(TIF_x)\left(1 - e^{-\left(\frac{vA_{fx}}{Q_x - Q_{bx}}\right)}\right)$$

Where TIF_x is total incoming sediment, v is settling velocity of suspended sediment, and A_{fx}floodplain area (Prosser *et al*, 2001a).

The bedload sediment transport is assumed to be transport limited within SedNet and therefore deposition of bedload materials occur when the loading of sediment is greater than the transport capacity (STC_x) which is calculated as:

$$STC_x = \frac{86{S_x}^{1.3} \sum {Q_x}^{1.4}}{\omega {w_x}^{0.4}}$$

where ω is the settling velocity of bedload sediment (Prosser *et al*, 2001a). Thus when the sediment yield from the link is less than or equal to the transport capacity no deposition occurs.

Bank erosion (BC_x) is assessed using a relationship between bankfull discharge ($Q_{1.58}$), the length of the link (L_x), bank height, and sediment bulk density which is set at a constant value for the whole catchment (Prosser *et al*, 2001a). The mean annual sediment supplied from bank erosion is calculated as:

$$BC_x = 18(Q_{1.58})^{0.6} L_x$$

In sections of the streams where vegetation has been cleared from stream banks the following equation is used:

$$BC_x = 18(1 - PR)(Q_{1.58})^{0.6} L_x$$

Where PR is the proportion of stream length with vegetation still in place (Prosser *et al*, 2001a).

Prosser *et al*, (2001b) note limitations of the SedNet model, including the hillslope sediment delivery ratio (HSDR). Not all the sediment that is eroded from hillslopes will reach the river channel (as illustrated in the Sediment delivery ratio section). The HSDR modulates the supply of sediment to rivers from overland erosion processes, increasing the HSDR increases the suspended sediment load per unit catchment area and Prosser *et al*, (2001b) used the value 0.05-0.1 in this particular study. Without a low HSDR, Prosser *et al*, (2001a) noted that the supply of sediment to streams is then dominated by hillslope eroded sediments. However, the ratio remains poorly defined by measurements within specific catchments making calibration of this parameter difficult.

SedNet has been applied at a catchment scale in several previous studies; Bartley *et al*, (2004) applied the model to the Bowen catchment, a sub-catchment to the Burdekin catchment in Queensland, Australia. The model was used to determine the main processes and areas within the catchment

contributing to sediment generation, and assess the impacts of management strategies. The model estimated an annual sediment delivery of ~1.3 million tonnes per year, and found hillslope erosion was the greatest contributor of sediment and nutrients (72%). It was again noted that an improved understanding of the spatial variability of the hillslope sediment delivery ratio within and between catchments would lead to greater accuracy in model outputs. Additionally, the lack of bank erosion data within the catchment meant the study was reliant only on model outputs.

Armour *et al*, (2009) used the model to calculate sediment, nitrogen and phosphorus loads in the Tully-Murray catchment in Australia, and evaluate land management strategies on pollutant loads. The modelled flows and annual average concentrations of sediment, N and P under current conditions were found to be very similar to observed values indicating the model provides a good representation of catchment processes.

1.1.3.4. INCA

The model INCA (Integrated Nitrogen Catchment Model) was first developed by Whitehead *et al*, (1998) and is a dynamic, semi-distributed model predicting daily and annual land use specific Nitrogen fluxes. INCA-P (Integrated Catchments model for Phosphorus) was then developed by Wade *et al*, (2002) producing the same output for Phosphorus. The INCA-P model requires input hydrological data (obtained from MORECS model, Hough *et al*, 1997), land management practices, and flow rates and concentration of P from sewage outlets. Firstly sub-catchment boundaries and the area of each land-use type are calculated in GIS. A land-phase hydrological model calculates the flow of effective rainfall through 3 pathways; soil water, groundwater, and direct runoff.

Jarritt and Lawrence (2007) produced a sediment delivery model (INCA-Sed) based on INCA to estimate in-stream suspended sediment concentrations. Three sources of in-stream sediment sources were considered within the model;

1) Delivery from adjacent sub-catchment slope by overland flow.

2) Entrainment of non-cohesive materials from the channel bed.
3) In-stream sources such as channel banks.

The land-phase model of the original INCA model was modified to account for the first of these sources: in the original INCA model direct runoff is generated when soil zone flow exceeds a user-defined threshold value, and therefore resembles saturation excess overland flow. INCA-Sed incorporates a representation of infiltration excess overland flow by modelling the contribution of rainfall excess to direct runoff as in areas of sparse vegetation cover the importance of this type of runoff was noted. Additionally, transport-limited and supply-limited constraints were included within the model to account for variations in sediment transfers within catchments.

Entrainment and deposition of multiple grain size classes are simulated within the model. Due to low settling velocities of fine sediments (such as silt and clay) these sediment fractions are deposited within the model during low flows, to levels below observed 'background' sediment concentrations. These sediment fractions were considered to be from in stream sources such as bank erosion and are represented within the model using the following equation:

$$m_{rel} = a_9 Q^{a_{10}}$$

where m_{rel} is the mass of sediment released (kg m^2 s^{-1}), Q is the reach discharge, and a_9 and a_{10} are calibration parameters. It was noted that these processes are not fully characterised within the model, and consequently only the broadest seasonal trends in sediment concentrations are reproduced by the model.

Rankinen *et al,* (2010) applied the model to four study catchments in Finland and found the model was able to reproduce the magnitude of sediment load derived from different land use classes, however the timing of sediment peaks was not captured by the model. This was attributed to the lack of temporal variability of erosion and delivery parameters within the model.

1.1.3.5. CREAMS

The Chemicals, Runoff, and Erosion from Agricultural Management Systems model (CREAMS) was developed in 1980 to evaluate the effects of agricultural practices on pollutants in surface runoff and soil water. The model applies to small watersheds and assumes uniformity of soil, topography, land use, and rainfall within the watershed. A process-based approach is used to estimate soil loss and the model operates on a daily time-step (between storm events) and contains representation of overland flow, channel flow, and impoundment.

Runoff within CREAMS is estimated using the curve number procedure (as described previously) that was modified to include a depth-weighted retention parameter, to represent variation in soil moisture storage with soil depth. There are seven computational soil layers within the model, which are defined based on effective rooting depth within the soil (Knisel and Williams, 1995). The model represents interrill erosion by raindrop impact, and rill erosion by overland flow. In addition to sediment detachment, sediment deposition (Dp) is also estimated as a function of the transport capacity (Tc):

$$Dp = 0.5Vf(Tc - G)$$

where Vf is the fall velocity of the particle class, G is the sediment load, 0.5 is a factor that accounts for the tendency of raindrop impact to keep sediment suspended in flow (Lane *et al*,1992). Transport capacity is calculated using the equation by Yalin (1963). The model also accounts for snowmelt, simulation of frozen soil (decreasing storage), soil evaporation, plant evaporation, evapotransporation and soil water depletion by evapotranspitation, and irrigation.

Within the channel element of the model sediment is routed using the same method and lateral inflow from overland flow is included. Discharge within the channel is assumed to vary directly with upstream drainage area, velocity of flow is estimated using Manning's equation, and detachment by flow is computed as a function of excess shear stress and a soil erodibility parameter. Channels are assumed to have a rectangular form and channel bed erosion is

calculated as a function of shear stress and mass density of soil. Channel widening is calculated as a function of shear stress and soil density.

1.1.3.6. SHETRAN

SHETRAN (Système Hydrologique Européen TRANsport) developed at the University of Newcastle is a 3D semi-distributed physically-based model of hydrology and sediment generation and transport within river catchments. River basins are represented as columns of grid cells (from 1 km^2 grid resolution). The channel network is represented as a series of channel links between grid cells. As the model is physically-based several parameter values can be measured, however parameters are estimated from point-measurements and values may vary at a finer spatial resolution than the model represents (i.e. sub-grid scale). SHETRAN requires detailed input data including weather station data, DEMs (Digital Elevation Maps), geology and land use maps, vegetation cover, cross-sectional channel survey data, and sediment particle size data meaning creating a preliminary data set for a new basin takes at least a few weeks (Ewen *et al*, 2000).

The three main components of the model are water flow, sediment transport, and solute/contaminants transport. It is assumed flow is not influenced by sediment transport, and sediment transport is not influenced by contaminants. Hydrological processes represented in SHETRAN include interception of rainfall, evaporation and transpiration, infiltration, ground-water seepage discharge, surface runoff, aquifer storage, and abstraction. Flow is calculated using 2D diffusion approximation of the Saint-Venant equations.

Sediment processes represented within SHETRAN include erosion by raindrop and leaf drip impact, deposition and storage of sediment (based on transporting capacity of overland flow), overbank transport, and channel bank erosion. The bank erosion component within SHETRAN is based on the exceedance of critical shear stress at channel banks:

$$E_b = k_b \left(\frac{\tau_b}{\tau_{bc}} - 1 \right) \quad if\ \tau_b > \tau_{bc}$$

Shear stress (τ_b) acting on channel banks is calculated as:

$$\tau_b = K\tau$$

where K is a proportionality constant calculated as:

$$K = a_4 + b_4 \frac{B}{H}$$

The constants a_4 and b_4 are estimated from the channel width to depth ratio, and range between 0.05-0.75 and 0.0-0.41 respectively (Lukey *et al*, 1995). Critical shear stress is calculated either using the Shield's equation or using an equation to account for the silt-clay content of the channel bank. The volume of sediment eroded is proportional to an empirical parameter, bank material erodibility coefficient (k_b). The bank erosion component does not account channel form/sinuosity or vegetation characteristics.

1.1.3.7. PSYCHIC

The model PSYCHIC (**PH**oshorus and **S**ediment **Y**ield **CH**aracterisation **I**n **C**atchments) is a processes-based model of phosphorus (P) and suspended sediment (SS) mobilisation and its subsequent transport and delivery to river channels. Developed by Davison *et al*, (2008) the model operates at catchment scale by estimating the risk of P originating within each individual spatial unit reaching the river channel. The input data required for the model is outlined in Table 1.4.

The model structure is outlined in Figure 1.7. Sources of soil P include manure and fertiliser applications and livestock excreta. Mobilisation of P is driven by kinetic energy of raindrops and surface runoff over land enables transport of mobilised P. Within PSYCHIC these processes are modelled using a mean climate drainage model (MCDM) as outlined by Anthony (2003), and the Morgan-Morgan-Finney model (Morgan, 2001) as outlined in the previous section.

Mobilised sediment is delivered to the channel by rapid overland flow or slower sub-surface lateral flow depending on the connectivity of the landscape, estimated through the surface connectivity, which is calculated from the drainage density and distance to the river from each grid square.

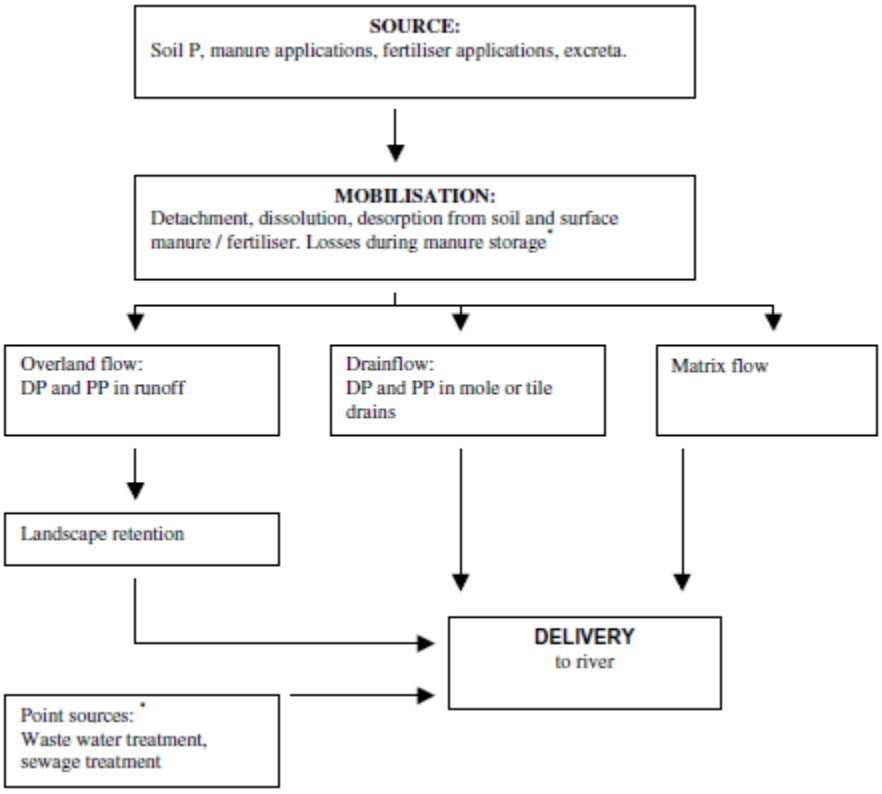

Figure 1.7: Modelling framework of PSYCHIC - conceptual diagram of mobilisation and delivery of agricultural P sources. Taken from Davison *et al*, (2008).

Strömqvist *et al*, (2008) reviewed the predictive capabilities of the PSYCHIC model for the Hampshire Avon and Herefordshire Wye. They noted the model's constraints for computing short-term events due to the use of climate data as an input (see Table 1.4), and that the model performance improved when predicting longer-term data. Additionally it was indicated that the model uncertainty would increase with decreasing catchment size as the parameterisations of mobilisation and delivery have been developed from localised empirical studies. Most importantly Strömqvist *et al*, (2008) commented on the lack of representation of processes such as channel bank erosion and indicated how inclusion of this sediment source would significantly improve the model.

Table 1.4: Principal input data used in PSYCHIC at catchment scale. Adapted from Davison *et al*, (2008).

Data input used in PSYCHIC	Dataset
Area of major crops, livestock numbers and type	MAGPIE Database (Defra) and CEH Land Cover imagery
P applications; manure and excretal returns (monthly)	Manure management database (Defra)
Dominant soil series per 1km^2	NATMAP2 (NSRI)
Soil series characteristics	SOILSERIES (NSRI)
Monthly climate data	
Index of proximity to surface water	
Mean slope per 1 km^2	
Number of people per 1km^2	

Collins *et al*, (2009) developed the PSYCHIC model to allow agricultural sediment source projections for 2015. PSYCHIC was used to estimate sediment delivery to rivers, and sediment delivery from channel banks was estimated using a national index calculated from river flow regime, critical shear stress, and hence the percentage of the year in which critical shear stress is exceeded. Bank shear stress is calculated according to the equation developed Guo and Julien (2005):

$$\frac{\tau}{\rho g s h} = \frac{b}{2h}\left[1 - \frac{4}{\pi} tan^{-4} \exp\left(\frac{-\pi h}{b}\right) - \frac{\pi h}{4b} \exp\left(\frac{-h}{b}\right)\right]$$

where b and h are channel width (m) and flow depth (m) respectively and calculated as:

$$b = 4.33.Q^{0.5}$$

$$h = \frac{Q}{b.v}$$

where Q is the bankfull flow (m^{3}s^{-1}) and v is flow velocity (m s^{-1}) calculated as:

$$v = 10^{-0.583} \bar{Q}^{0.283} \left(\frac{Q}{\bar{Q}}\right)^{0.495}$$

where $\bar{Q}$ is the long-term mean flow.

The critical shear stress is calculated using the equation developed by Julian and Torres (2006):

$$\tau_c = 0.1 + 0.1779.SC^2 - 2.34 \times 10^{-5}.SC^3$$

where SC is the total silt-clay content. The percentage of the year in which shear stress exceeds critical shear stress (D) can then be calculated for a river channel. The catchment area averaged bank erosion rate (B, kg ha^{-1}) was then calculated as:

$$B = 0.0225\left(\frac{D.L.H}{A}\right)^{1.58}$$

where is the river channel length (km), H is the bank full channel depth (m) and A is the area of the catchment.

Collins *et al*, (2009) noted that this method had a general tendency for over-prediction, which was attributed to the absence of longer-term floodplain sediment retention. Limitations of this approach include that percentage exceedance of critical shear stress and total silt-clay content are the factors included in bank erosion estimates. Other factors including vegetation cover and change in discharge are not considered. Additionally it assumed that the system is in equilibrium, which may not be true for some situations.

Currently PSYCHIC is being re-developed within ADAS and will be replaced by a new model known as the APT model (**A**DAS **P**hosphorus **T**ransport). Similarly to PSYCHIC the model will output both water and sediment delivery to the channels. Overland flow will be estimated using the curve number approach.

1.1.4.The importance of sediment within river systems

Increased sediment loads within river catchments have well-documented detrimental effects on river systems (Bilotta and Brazier 2008; Edwards and

Withers, 1998; Heathwaite and Johnes, 1996; Owens *et al*, 2005; Wood and Armitage, 1997). Physical effects of increased sediment loads include increased turbidity within the water column, causing a reduction in the depth of the photic zone. Increased sedimentation rates within channels cause a shift in channel morphology and habitat dynamics. Sediments are also a key vector for the transport of nutrients, trace and heavy metals, and a range of additional harmful substances that greatly influence the chemical composition of the water (FAO, 1996; USGS, 2007). Table 1.5 indicates potential contaminants that may enter river systems with sediment. Chemical changes to water caused by sediment-associated pollutants raise issues within the river ecosystem (e.g. eutrophication, toxicity to aquatic habitats), and the potential for human consumption of water due to increased levels of toxins and pathogens. Biological and ecological effects of increased sediment include impacting and altering sensitive habitats and subsequent reduction in biodiversity (e.g. decreased salmon spawning gravel as observed by Theurer *et al*, 1998 and Soulsby *et al*, 2001), reduced primary and secondary productivity due to reduced depth in the photic zone, and associated pollutant issues. The delivery of sediment and associated nutrients and contaminants to rivers therefore has important implications for river ecosystem health and the supply of potable water.

Table 1.5: Examples of sediment associated contaminants and their sources. Taken from Taylor and Owens (2008).

Material	Sources
Sediment (organic and inorganic)	Erosion from rural, agricultural and forested land, channel banks, urban road dust and construction, STW solids, atmospheric deposition, inputs from tidal areas and coastal zone (during flood and ebb tidal cycle)
Metals and metalloids (Ag, Cd, Cu, Co, Cr, Hg, Ni, Pb, Sb, Sn, Zn, As)	Geology, mining, industry, acid rock drainage, sewage treatment, urban runoff
Nutrients (P, N)	Agricultural and urban runoff, wastewater and sewage treatment
Organic compounds (pesticides, herbicides, hydrocarbons, PCBs, PAHs, dioxins)	Agriculture, industry, sewage, landfill, urban runoff, combustion
Xenobiotica and antibiotics	Sewage treatment works, industry, agriculture
Radionuclides (^{137}Cs, ^{129}I, ^{239}Pu, ^{230}Th, ^{99}Tc)	Nuclear power industry, military, geology, agriculture (secondary source)

The EU Water Framework Directive (WFD) states that all rivers in the UK should achieve 'good' status by 2015. This includes both chemical and ecological status and involves a regulation of sediment levels due to the detrimental effects of sediment on river ecosystems. Currently over 70% of rivers, lakes, estuaries, coastal waters, and groundwater in England and Wales fail to meet the 2015 targets, (Environment Agency, 2012). Reasons for failure include alien species pressures, diffuse, point and combined source pollution, physical alternation, and water abstraction. In response to the WFD, River Basin Management Plans have been developed which seek to tackle issues associated with diffuse pollution, including sediment. Additionally the England Catchment Sensitive Farming Delivery Initiative (ECSFDI) aims to reduce diffuse water pollution from agriculture. In order to inform the revisions to policy-driven management plans and advice programmes, modelling is required to predict expected sediment pressures under future climate, land use and catchment management scenarios. Therefore, to enable improved accuracy in predictions of future sediment pressures under environmental change, greater accuracy of modelling rates of sediment generation is required.

This section has outlined the environmental effects of changes to the sediment load within rivers, highlighting the importance of management strategies. Catchment modelling of sediment processes enables both further understanding of sediment movement within river systems, and also provides a means to assess the effectiveness of potential mitigation strategies. The catchment models that have been discussed in this section include only a simplistic representation of bank erosion, or exclude this process as a sediment source. The following section will discuss the factors influencing rates of channel bank erosion, and an provide an indication of the significance of this process to catchment sediment budgets.

1.1.5. Factors influencing bank erosion

Numerous factors have been noted to influence the rate of channel migration and bank erosion related to bank stability, channel geometry, discharge and flow regime of the channel, catchment characteristics, vegetation, channel lithology and geology, and climatic conditions. The influence of several of these factors will be discussed below. Due to the complex relationship between bank erosion and controlling factors, bank erosion rates have been observed to be highly variable both between and within individual river catchments (Bull, 1997; Couper *et al*, 2002; Hooke, 1980; Hooke, 2008; Lawler *et al*, 1999; Leys and Werritty, 1999;).

1.1.5.1. Controls of bank stability

Channel bank collapses through mass movement processes are a significant sediment source within fluvial systems. Mass movement occurs when the shear strength of a slope (the frictional resistance within the material to resist failure) is overcome by the shear stress (forces acting to deform a slope, mainly gravity acting upon the weight of the slope). The forces acting on a slope are illustrated in Figure 1.8.

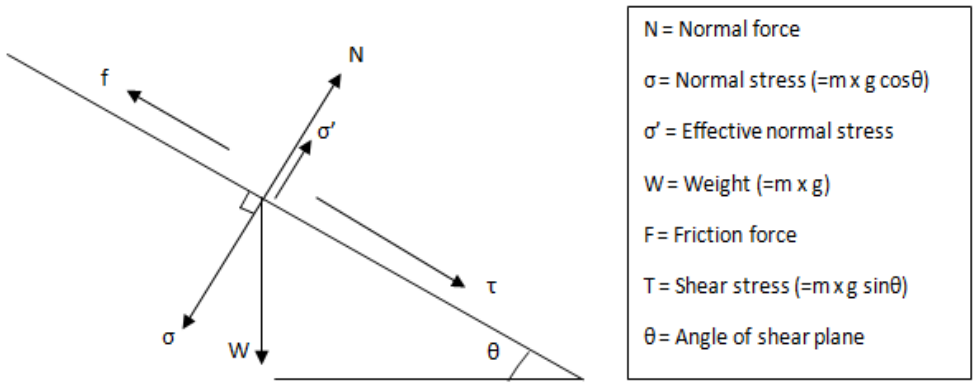

Figure 1.8: Forces acting on a slope.

Due to the mechanical forces acting on a channel banks, it follows that an increase in bank height increases the weight of the channel bank and hence the shear stress acting upon it, thereby increasing the likelihood of bank failure. Several studies have noted the influence of channel bank size on the rate of bank erosion (Michelli and Kirchner, 2002; Walling, 2005; Walling et al, 2006). Walling (2005) noted that channel erosion would be expected to be more significant in larger catchments with well-developed channel banks. Channel bank height ratio (defined as the bank height divided by the bankfull depth at the foot of the bank) can be used to assess the probability of bank erosion; as shown in Figure 1.9, as bank height ratio increases about 1.0 the probability of bank erosion increases (EPA, 2013).

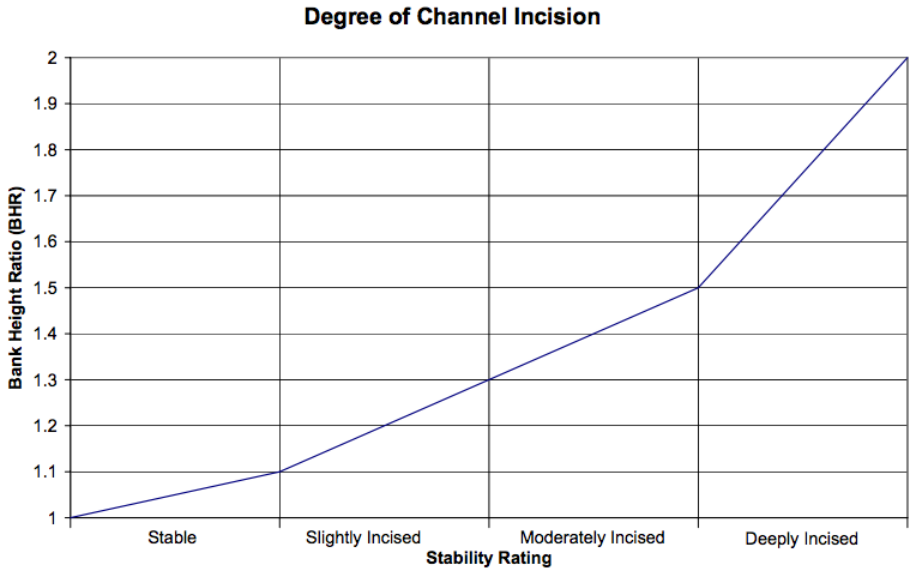

Figure 1.9: Relation between bank height ratio and channel bank erosion risk. EPA (2013).

The normal stress is only exerted at points of contact within the slope and not within voids. Below the water table water fills voids within the slope resulting in a pressure greater than atmospheric creating a buoyancy effect on the overlying material. This buoyancy opposes the normal stress (σ). Therefore effective normal stress (σ') can be calculated as:

$$\sigma' = \sigma - u_w$$

where u_w is pore-water pressure.

Cohesion (c) is the inherent strength within a slope due to the chemical bonding, adhesion and electromagnetic and electrostatic forces. The contribution of cohesion to the shear strength of a slope is shown in Figure 1.10. Cohesive forces are largely derived from cementing materials binding the aggregate together. These forces are not controlled by compressive forces but by chemical bonds between the particles that may result in cohesive strengths of several $kN^{-1}m^{-2}$ (Selby, 1982). Capillary cohesion occurs when water films form around particles within slope material due to a negative pore water pressure.

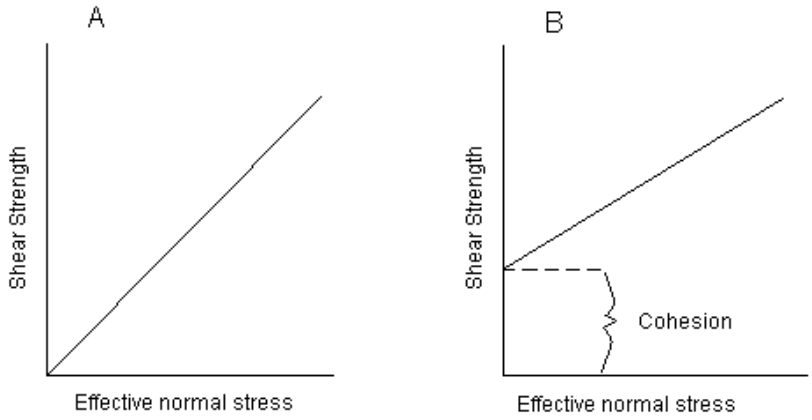

Figure 1.10: Relationship between shear strength and effective normal strength for two types of slope materials; A has a frictional component only related to effective normal strength, B has a initial strength from cohesion which is irrespective of effective normal stress. Adapted from Summerfield (1991).

Hooke (1980) found the percentage silt-clay content of the bank material was the dominant factor controlling width averaged bank retreat rates, explaining 46% of the variation in mean rates. Couper (2003) observed that banks with high silt-clay content are more susceptible to subaerial (overland based) processes, which in turn will influence the spatial variability of bank erosion rates. Additionally it was noted that different processes act on the upper

and lower parts of the bank ('vertical zoning') and that higher silt-clay content in the lower part of the bank increases resistance to hydraulic processes.

Julian and Torres (2006) combined results from previous studies with their own to illustrate the importance of different independent flow variables on erosion rates of channel banks with varying specific silt-clay content (see Figure 1.11). Additionally, it was noted that bank erosion rates increased exponentially as the critical shear stress measured at the bank decreased (R^2=0.98, p=0.012).

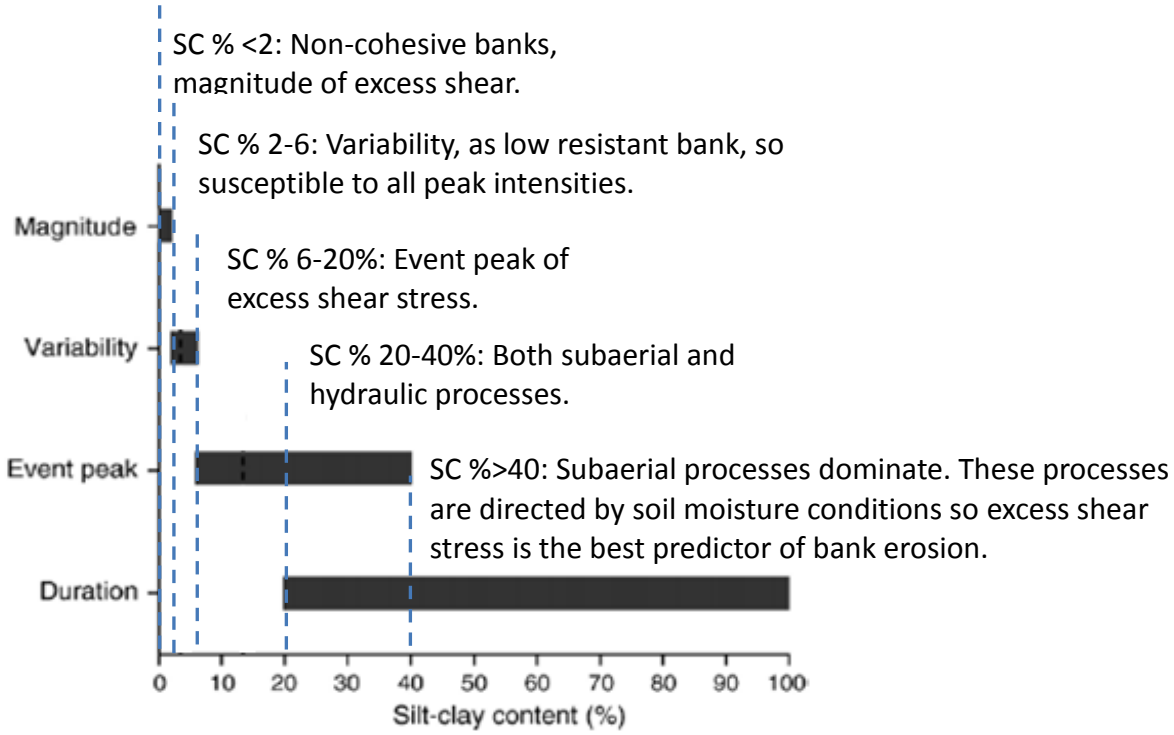

Figure 1.11: Conceptual model of best independent flow variable as predictors of erosion rates of cohesive river banks. Adapted from Julian and Torres (2006).

Soil aggregation is particularly important when considering a non-coherent soil's susceptibility to erosion. Aggregation involves physical stresses that can force particles together or apart, such as frost and root action, compression and shrinkage. Aggregation also involves binding agents that

cement particles with varying strength; these include mineral deposits and various electrostatic bonds.

The shear strength of a slope can be estimated from the Coulomb-Terzaghi shear strength equation:

$$s = c + \sigma' . tan\emptyset$$

where $tan\emptyset$ is the slope angle. Increased soil moisture content decreases the internal friction within the soil layer, reducing the shear strength of the channel bank and promoting bank failure. Therefore, some of the variability in observed bank erosion rates may be explained by variation in the volume of precipitation. The presence of water will therefore increase the probability of a mass movement occurring and also influence both speed and form of the mass movement process. Atterberg limits are used to distinguish between four physical states (solid, semi-soild, plastic and liquid) the boundaries of which differ depending in the composition of the material. Materials mainly composed of silt generally have lower Atterberg limits and strength than those composed mainly of clay and therefore with identical moisture contents silt materials generally fail before clay. When materials are saturated so that point-to-point contact does not occur any inter-particle friction within the material is lost. This is known as Liquefaction and causes a reduction in shear strength to negligible values.

Corrasive action (or abrasion, abrasive action of materials transported within the water acting to erode the surface) allows undercutting of channel bank slopes that leads to instability of the slope material. Corrosion of bank material (removal of soluble materials) may contribute to a reduction of bank strength. These processes can eventually lead to bank collapse, which occurs when the shear strength of the slope is reduced below a threshold value (the critical shear stress). Ashbridge (1995) noted bank retreat occurred through a cycle, whereby channel banks are weakened by corrasion and corrosion, allowing bank collapse to occur, and collapsed material to be removed by corrasion.

Weathering of bank material above the water level will lead to weakening of channel banks. The rate of weathering processes is largely dependent on the

lithological and structural properties of the parent material as this determines the susceptibility to certain processes particularly chemical processes; the presence of faults, joints, and fractures within the rock allow water to reach a larger surface area of the rock leaving it vulnerable to chemical weathering processes and allowing weathered material to be transported away. Mineral stability has been observed to be inversely proportional to the temperature at which it was formed (Smithson *et al*, 2008). Additionally as indicated by Goldich's weathering sequence (1938) the mineral composition of the parent material will determine how resistant it is to weathering processes (see Figure 1.12). Initial breakdown of material by mechanical processes increases the surface area of the material leaving it more susceptible to chemical processes.

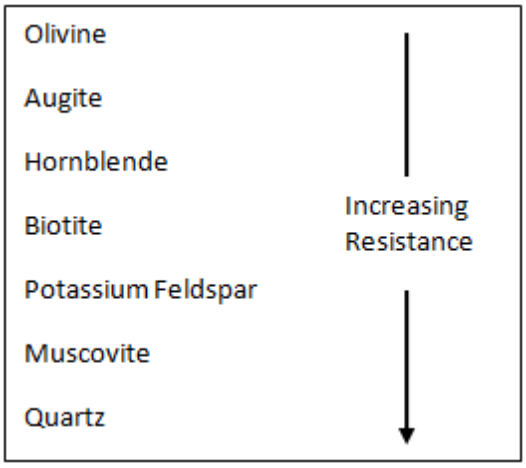

Figure 1.12: Goldich's (1938) weathering series for silicate minerals.

It has long been understood that climate also has a significant role determining the rates of weathering processes as demonstrated by Peltier (1950). Firstly the presence of water allows certain processes (namely chemical) to occur whilst transporting weathered material away. Secondly as illustrated by the Ahrenius equation temperature increases the rate at which chemical reactions may occur; with every 10°C increase in temperature the rate of chemical reactions may double. Additionally large diurnal variations in temperature allow processes such as insolation to become more significant.

The presence of vegetation may increase the rate of weathering processes. The presence of roots may increase the rate of physical rock break-up, thereby increasing rock surface area allowing the rate of any chemical processes present to increase. Furthermore the presence of a developed root system will allow a supply of water to reach the parent material, increasing the rate of weathering processes. Organic acids produced by bacteria that break down plant material will result in weathering by chelation.

Bank erosion rates also show seasonal variation; Gardiner (1981) observed over 90% of total bank erosion recorded over 1 year occurred during winter months, due to wetting of channel banks resulting in decreased shear strength. Ashbridge (1995) also observed an increase in erosional activity during winter months and attributed this to a maximum in the frequency and magnitude of storm events from October to March. Additionally, the importance of freeze-thaw during winter months in 'preparing' channel banks for erosion has been noted by several authors: (Gardiner, 1981; Lawler, 1986; Lawler, 1993). Vegetation die-back during the winter months may also lead to a decrease in bank stability and hence an increase in erosion (Thorne, 1990).

1.1.5.2. Channel planform

Channel sinuosity induces changes to flow patterns within the river channel. Bends within the channel induce helical flow of water within the channel, which then focuses river energy on the outside of the river bend (see Figure 1.13).

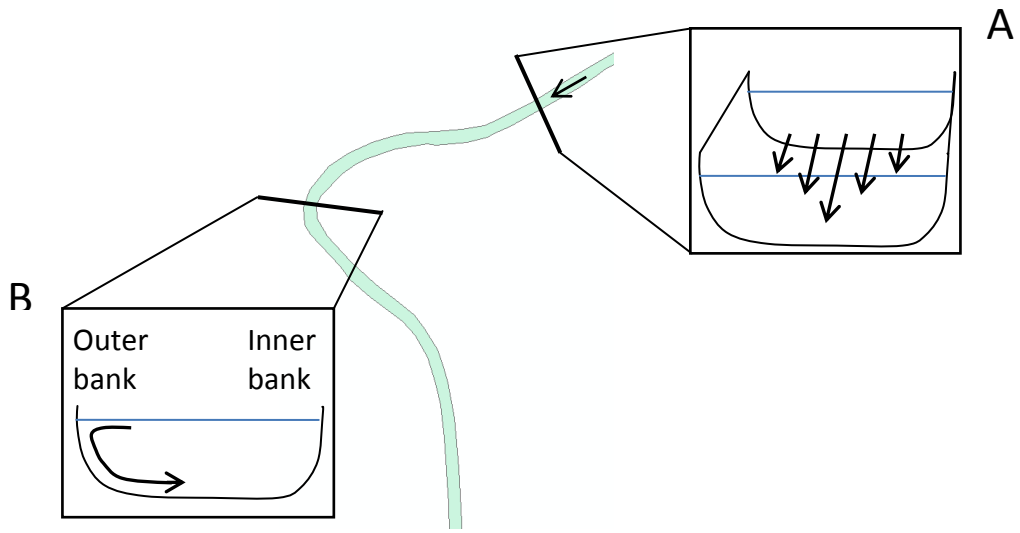

Figure 1.13: Meandering river channel, arrows indicate flow direction. A: Cross-section at a straight section of the channel, the flow is straight within the channel, with the high velocity flow in the centre of the channel. B: Cross-section at a point of high channel curvature, here secondary flow cells develop and high velocity flow is directed towards the outer bank, resulting in bank erosion.

The influence of channel curvature on migration rates is well accepted. A non-linear relationship exists between channel curvature per channel width, or channel curvature ratio (rc/w), and the rate of channel migration. This relationship was first noted by Hickin and Nanson (1975) on the Beatton river in Canada, whereby migration rate increased with rc/w up to a value of 3.0, and with further increase of rc/w above this value migration rates decreased. This relationship was then tested on a further 18 reaches of river in Canada and a similar relationship was found; width averaged migration rates were found to rapidly increase with channel curvature ratio up to 2.0-3.0, and decrease with values >3.0 (Nanson and Hickin, 1986). In a study of a reach of the Red River, USA, Thorne (1991) also observed a peak in bankline migration in bends with rc/w between 2 and 3. A Similar pattern was also observed by Hooke (1997) and others (see Figure 1.14).

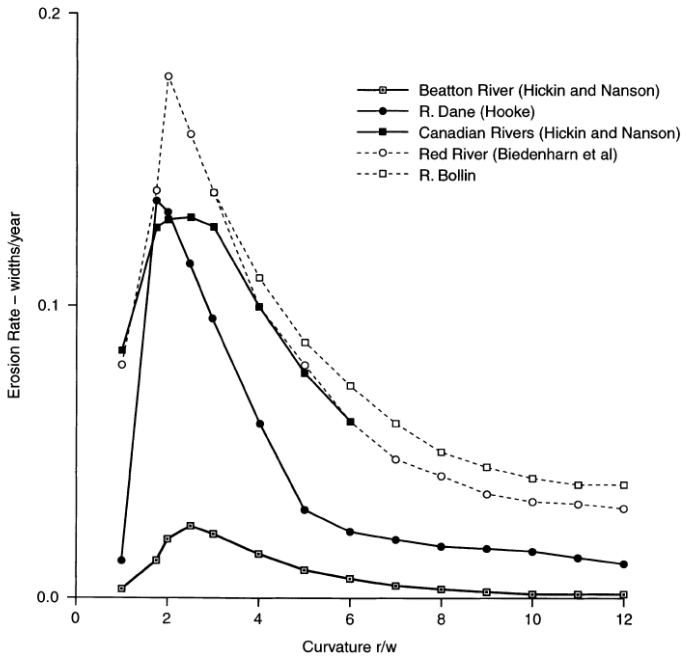

Figure 1.14: Compilation of plots of migration rates against channel curvature ratio. Taken from Hooke (2003).

Contrary to these findings, in a study of the Mississippi river Hudson and Kesel (2000) found a peak in migration rate to occur at channel curvature values of ~1.0. It is thought this is due to the complexity of floodplain sediments in the lower Mississippi valley, which influence channel migration; bands of resistant material prevent the channel from migrating freely. A similar effect of channel confinement was observed by Hooke (1987). Additionally, Beeson and Doyle (1995) investigated bank erosion of 748 bends in 4 streams as a result of the 1990 floods in southern British Columbia, Canada and found no clear relationship between bank erosion and channel curvature. However, the influence of channel bank vegetation was noted and attributed for the lack of relationship observed between channel curvature and bank erosion in this location.

Hickin (1978) examined the flow patterns within meander bends that result in the observed relationship between channel curvature ratio and migration rate. It was found that the strength of secondary flow, and hence energy expenditure, increased rapidly as rc/w decreased from 4.0 to the data minimum of 1.41. As rc/w decreased from 3.0, the maximum velocity filament shifted from the outer to the inner bank (concave to convex) resulting in channel

migration slowing to negligible amounts. This pattern is illustrated in Figure 1.15. From this, Hickin (1978) described a model of 3 stages of development and migration in channel bends according to flow channel geometry and resulting flow structure:

- Initiation (rc/w >4.0): only a slight asymmetry in channel cross-section, velocity distributed to outer bank, secondary circulation weak, migration rates low. Straight channel.
- Growth (rc/w=3.0-4.0): increased asymmetry in channel cross-section, velocity distributed to outer bank secondary circulation increases intensifying helical flow, migration rates high. Active meander.
- Termination (rc/w<3.0): further increased asymmetry in channel cross-section through deepening at the outer bank, secondary circulation moves towards the inner bank to a more central position in the channel, channel migration ceases. Stable meander.

These 3 stages of channel development in relation to the curve identified from the relationship between rc/w and migration rates is illustrated in Figure 1.16. A pattern of channel development resembling this model was observed on the Hanjiang river, China, by Jiongxin (1996).

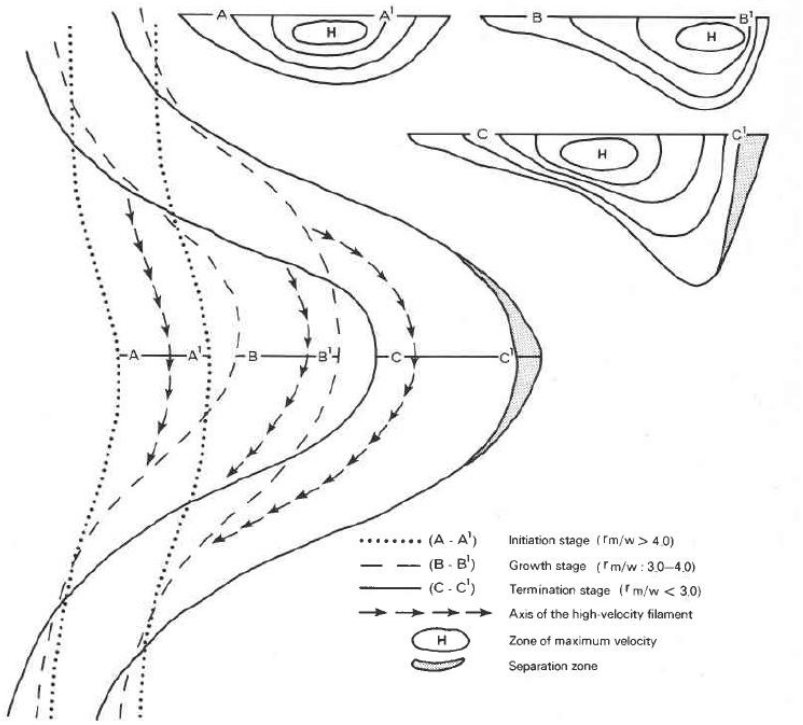

Figure 1.15: Model of changing flow structure in a channel bend according to rc/w. Taken from Hickin (1978).

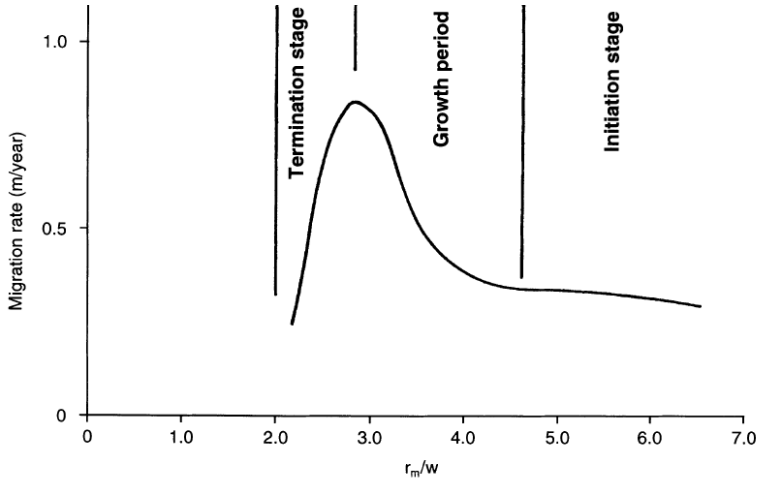

Figure 1.16: Model of non-linear relationship between rc/w and channel migration and stages of development as proposed by Hickin (1978). Taken from Hooke (2003).

The influence of up-stream channel geometry has also been noted in several studies (Carson and Lapoint, 1983; Davies and Tinker, 1984; Furbish,

1991; Seminara *et al*, 2001; Zolezzi and Seminara 2001). This is due to the presence of helical secondary flow circulation within the channel, which results in the point of maximum near bank flow velocity being located downstream of the point of maximum channel curvature. Consequently, channel meanders migrate downstream, as observed by Hooke and Yorke, (2010). Secondary flow circulation will be discussed in detail in chapter two.

Channel sinuosity is inversely related to radius of curvature. Therefore a relationship between channel sinuosity and bank erosion would be expected to exist, and has been observed in previous studies (Abam, 1993; Schilling and Wolter, 1999). This will be discussed in detail in chapter two. Additionally, several authors have noted the relationship between channel sinuosity and the occurrence chute cut-off; Stølum (1996) noted meanders migrated freely until reaching a critical value of sinuosity (3.14±0.34) at which point cut-offs occur and the sinuosity oscillates in accordance with cut-off occurrence. Schumm (1994) noted a maximum sinuosity of just over 3 in 24 reaches of the Mississippi. Micheli and Larsen (2011) noted cut-offs to occur at an average sinuosity of 1.97±0.1 and at rc/w values of 2.1±0.2. On the river Dane, UK, Hooke and Yorke (2010) observed a maximum sinuosity of 2.66 in 1984, after which a cut-off occurred, and a maximum of 2.93 in 2007.

Chute cut-offs have also been used to provide a basis for the theory that channel meandering is an autogenic process; Gautier et al, (2007) noted that cut-offs do not coincide with periods of peak flow and concluded that instead they indicated the self-regulating behaviour of river channels. Additionally, Stølum (1996, 1998) believed cut-offs occurred to allow self-organisation of the channel by restricting sinuosity. On the river Bollin in Cheshire, UK, Hooke (2003) noted sinuosity increased over time from 1.52 to a maximum of 2.92 over 139 years, at which point cut-offs occurred to reduced the channel sinuosity. This fits with Hooke's (2007a) definition of self-organised critically theory of channel meanders as '*when a state is reached in the system in which sudden readjustment occurs to regain order and reorganisation*' (Hooke, 2007a). The evolution of channel sinuosity under the theory of self-organised critically is that as a channel develops channel sinuosity increases over time until the supercritical sinuosity is reached, at which point cut-offs occur causing sinuosity to decrease from the supercritical value. Channel sinuosity then

oscillates around a more stable value (Hooke 2003). Hooke (2007b) noted that active channel bends showed a sequence of evolution, and that channel curvature ratio alone does not adequately describe the characteristics of bend evolution. On a study of the river Dane, UK, Hooke and Yorke (2010) noted that the development of a channel from a low sinuosity curve through to cut-off took 80-150 years, and the development of compound bend took between 50 and 100 years.

The occurrence of chute cut-offs may also influence the rate of bank erosion; Brice (1973) noted a cut-off may result the rapid growth of adjoining meanders. However, this effect was not observed far downstream from the cut-off. Contrary to this, Hooke (2007a) did not notice any increase in bank erosion up or downstream of a cut-off or development of new bends within these regions.

1.1.5.3. Discharge - magnitude vs. frequency

As discharge increases, the applied shear stress by the channel flow on bank material also increases. Hooke (2008) observed higher discharge years resulted in greater bank erosion. Several studies have investigated the influence of peak flow on bank erosion rates. Hooke (1979) found that event peak flow had the strongest correlation with bank erosion at a site on the Exe (R^2=0.4635). Peak discharge was also noted to be the most significant variable at a site on the Creedy. Julian and Torres (2006) also noted the importance of event peak discharge on bank erosion at scales of 150m, 240m, and 425m (R^2=0.996, 0.848 and 0.933 respectively). In addition to event peak, variability of event peak was identified as an explanatory variable of bank erosion and was identified to be more significant than event peak where critical shear stress of the slope was low. In a study on the Rio Beni, Bolivia, Gautier *et al*, (2007) noted that flood intensity was the main factor controlling bank erosion. Using compound specific stable isotope sediment tracing, Blake *et al*, (2012) estimated a single storm event in March 2008 resulted in generation of 1.3t (±0.8) of sediment from bank erosion on the Furze Brook catchment (UK).

The relative importance of high magnitude events of low frequency versus low magnitude events of high frequency is a long running debate throughout Geomorphological science. Wolman and Miller (1960) found events which occured more than once per year account for 78-95% of total suspended load and event with a recurrence interval of less than 10 years account for 98-99% of total sediment load. Since this paper many other studies have highlighted the importance of events of moderate frequency and magnitude in transporting sediments and transforming the landscape (Dury, 1973; Webb and Walling, 1982; Biedenharn and Thorne, 1994; Nash, 1994; Torizzo and Pitlick, 2004; Gomez *et al*, 2007). Thornes (2003) states that '*it is the product of magnitude and frequency that results in the most important events, being those of intermediate size and frequency*.'

Contrary to Wolman and Miller's theory, Baker (1977) observed that rare floods of high magnitude do have significant impacts on semi-arid areas (central Texas) due to a feedback mechanism which enhances response to rainfall in areas of intense but infrequent events. Several others studies have observed the importance of catastrophic events in arid/semi-arid areas (Kemp, 2004; Nash, 2001; Pickup, 1991; Tooth, 2000) and have attributed this to the reduced vegetation cover leaving them more vulnerable to the effects of high magnitude events.

Schumm (1972) indicated the importance of geomorphic thresholds, both extrinsic (e.g. climate) and intrinsic (e.g. lithology) and how events of high magnitude will become increasingly influential when systems are close to thresholds.

Wolman and Miller hypothesised that with increasing variability of runoff and decreasing drainage basin area the importance of high magnitude events would increase. However, Nash (1994) observed no correlation between these two variables and effective discharge. Several studies have observed the range of effects a flood of a particular magnitude can have between different locations (Miller, 1990; Magilligan, 1992; Fuller, 2008). These variations are due to local variations of variables such as channel morphologies (influencing stream power), lithologies, vegetation type and cover etc.

The importance of events of a particular magnitude is dependent on the time scale at which the system is observed. As indicated by Couper and Maddock (2001) over short time-periods, the concept of process dominance has a temporal aspect in addition to spatial. They noted that over time periods of several years or more, mass failure and fluvial erosion through high magnitude events can be expected to account for a larger proportion of bank erosion, whilst over shorter time periods more frequent and lower magnitude events and processes would dominate. Whilst events of higher magnitude may result in increased rates of bank erosion for very short time periods, Hooke (1980) noted that most erosion occurs during, or in association with events that occur several times a year. In relation to channel migration, the influence of the range of flow between mean annual discharge and mean discharge during the month of highest flow has long been noted (Carlston, 1965). Phillips (2002) and Surian *et al,* (2009) noted a bimodal distribution of the dominant discharge; frequent flows of moderate magnitude maintain the general channel morphology whilst higher magnitude floods with longer recurrence intervals are required for transport of coarse bed materials and channel bank erosion.

Other factors influencing bank erosion can act to form high/low thresholds thereby increasing/decreasing the importance of high magnitude events respectively. For example, where bank material is weak, stream power and event magnitude does not need to be large to cause bank erosion and hence the importance of high magnitude events is not great.

1.1.5.4. Catchment characteristics

Several studies have also noted an increase in bank erosion rate corresponding to an increase in drainage basin area (Hooke, 1980; Birkinshaw and Bathurst, 2006). This was attributed to drainage basin area represents a surrogate of discharge and as noted above, this represents the relationship between forces acting on the bank. The influence of drainage basin area will be discussed in more detail in chapter two.

Channel migration may be restricted by valley walls (Lewin and Brindle, 1977; Milne, 1983; Rapp and Abbe, 2003). Lateral confinement of channel

migration and the influence on bank erosion will be discussed in more detail in chapter two.

As velocity of channel flow increases the force acting on channel banks and hence the potential for channel bank erosion increases. As channel bed slope increases the velocity of flow also increases. Therefore it can be expected that bank erosion rate may increase with an increase in channel bed slope. Several studies have noted differing channel forms corresponding to different values of channel slope (Schumm and Khan, 1972; Montgomery and Buffington, 1997). The influence of channel slope will be discussed in more detail in chapter two.

1.1.5.5. Vegetation

The presence of vegetation on slopes has both mechanical and hydrological effects that may act to either increase or decrease slope, or bank stability. Micheli and Kirchner (2002) noted that the presence of vegetation decreased the rate of bank erosion; channel banks without wet meadow vegetation eroded at a rate 10 times that of channel banks with wet meadow vegetation. Beeson and Doyle (1995) noted bank erosion was 30 times more prevalent on non-vegetated bends than on vegetated bends after a flood event.

The mechanical influence of vegetation is due to the tensile strength of roots that act to reinforce the soils stability. Soil stabilisation may also occur through anchorage of superficial layers to deeper stable layers, or bedrock, (Mattia *et al*, 2005). The binding of soil particles by roots also increases shear strength and reduces erosion rates. The adverse mechanical effects on stability include the increased weight on the slope from the vegetation which increases the downhill force, and shear stress. Also, the presence of vegetation increases wind exposure and allows the dynamic force to be transmitted to the soil. The magnitude of these effects varies greatly between species type and environmental conditions and it is considered that the overall influence of mechanical effects of vegetation promote slope stability (Simon and Collinson, 2002).

The hydrological effects of vegetation on bank stability include the interception of rainfall at the soil surface thereby reducing the magnitude of surface erosion. Additionally plant roots absorb water which is then released through evapotranspiration to decrease the water content of soil. This increases the internal friction within the soil layer, hence promoting slope stability.

Simon and Collison (2002) investigated both the mechanical and hydrologic effects of vegetation on streambank stability by calculating the factor of safety of the channel banks throughout the year. The factor of safety of a slope (or bank) is calculated as by dividing the forces resisting movement (slope strength) by forces driving movement (shear stress acting on slope). An decrease in values indicates a decrease in slope stability, with values <1.0 indicates unstable slopes. As can be seen from Figure 1.17, throughout the vast majority of the year the presence of vegetation vastly increased the factor of safety of the streambank. Tree roots increased soil strength by 2-8kPa and grass roots contributed 6-18kPa, with the mechanical and hydrologic effects tree cover increasing the factor of safety by 32% and 71% respectively, and grasses 70% and -15%. Abernethy and Rutherford (1998) noted spatial zoning in the dominance of each process group; where direct fluvial entrainment is responsible for bank erosion the vegetation acts to reduce flow velocities and hence bank erosion, whereas in areas where bank slumping/collapse is dominant the mechanical influence of vegetation (through root reinforcement) reduces bank erosion. Therefore the magnitude of the influence of vegetation on bank erosion rates, and also the process by which vegetation influences bank erosion rates will vary both spatially and temporally.

Seasonal variation of vegetation cover will also influence bank stability (as indicated in Figure 1.17) and hence bank erosion rates. Additionally, changes in channel discharge (which may be linked to seasonal influence) may affect vegetation cover, which in turn will affect bank erosion rates. As hypothesised by Hooke (2008), low flow years could allow increased vegetation establishment on channel banks, resulting in a decline of bank activity. Additionally it was noted how warmer winters could restrict vegetation die-back, resulting in the same effect.

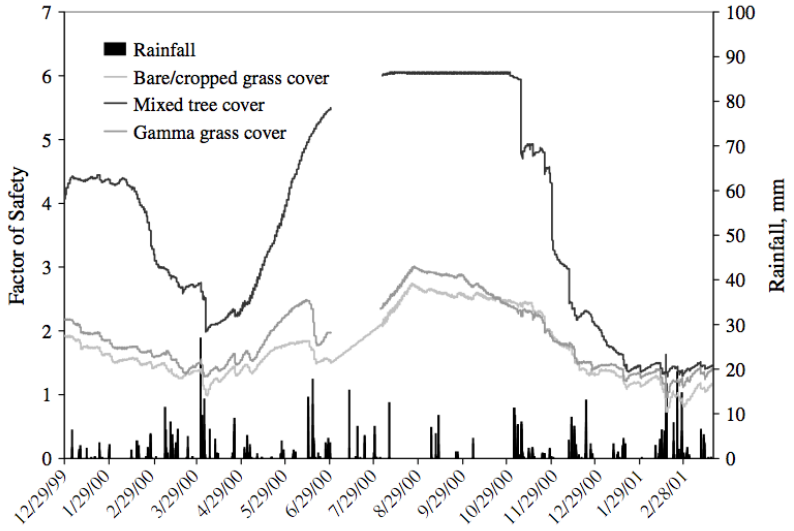

Figure 1.17: Variation of rainfall and factor of safety values over time for three streambank vegetation covers, taken from Simon and Collison (2002).

1.1.5.6. Anthropogenic influences

Land use change may alter the infiltration capacity of the soil, causing an increase in surface runoff production. Compaction by trampling/machinery decreases pore spaces within the soil, reducing the capacity of water that may be stored within the soil. Kosmas *et al*, (1997) observed this effect on land used for vine production in the Mediterranean region; the aggregate stability and organic matter content of the soils decreased through heavy machinery use and clearance of additional vegetation. As a result, runoff volumes of up to 32% of the annual precipitation were observed, compared to 0-2.6% in 'semi-natural' areas used for olive production.

Clearance of natural vegetation within an area greatly reduces the protection of the soil surface to the erosive energy of rainfall. Gregory (1987) noted vegetation cover decreases the kinetic energy of the rain by up to 90% by protecting the underlying soil surface. Without the protective layer the soil surface is exposed to the full force of rainfall allowing a greater volume of sediment to be dislodged through raindrop impact. Furthermore, the removal of a litter layer on the ground surface also increases the vulnerability of the soil surface to erosion.

Land use changes that result in changes to the volume of runoff generation throughout catchments will also result changes to the response time and magnitude of peak discharge in response to rainfall events. Costa *et al*, (2003) compared 2 twenty-year periods in the Tocantins catchment, Australia, and observed an increase in rainy season discharge of 28%, and an increase in annual mean discharge of 24% between the two periods. These changes were attributed to the 19% increase in agricultural land use between these two periods, causing in a decrease in both evapotranspiration rates, and the infiltration capacity of the land, resulting in increased runoff generation. Soil conservation strategies have also been shown to result in a decrease of peak flow magnitude; Potter (1991) anlaysed flood peaks in the Pecatonica river, Wisconsin, USA from 1940-1984 and observed a decrease in flood peaks and an increase in the rising time of flows in response to rainfall events. These changes could not be attributed to climatic or construction within the catchment, but were believed to be the result of soil conservation practices, including the filling of gullies (formed through soil erosion) within the catchment, and conservation tillage practices. Conservation tillage involves leaving crop residues on the soil to enhance soil roughness and increase soil moisture content (thereby decreasing runoff volumes and velocities).

Anthropogenic influence may also affect rates of channel migration and bank erosion, and construction and catchment management may act to prevent rates of bank erosion. For example, Michalkova *et al*, (2011) noted the influence of flood control structures within the Sacramento river; the construction of weirs within the river reduced bank erosion rates by reducing downstream peak flows. Additionally it was noted that after the construction of the Shasta Dam the channel width and peak flows reduced, as did bank erosion rates. Winterbottom (2000) also noted a 34% reduction in mean channel width, and a decrease in channel braiding on the rivers Tay and Tummel, Scotland between 1971 and 1994 and attributed these changes to flood embankment construction. Similar observations have been made in several other locations; Piave River, Italy (Surian, 1999); Brenta River, Italy (Surian and Cisotto, 2007); Arno River, Italy (Rinaldi, 2003); Dunajec River, Poland (Zawiejska and Wyzga, 2010); Somesu Mic River, Romania (Persoiu and Radoane, 2011).

Land-use may affect bank erosion rates through increasing rates of bank erosion through trampling or overgrazing by livestock (Kondolf *et al*, 2002; Lyons *et al*, 2000; Zaimes *et al*, 2006). Myers and Swanson (1992) noted the magnitude of the influence of livestock grazing depended on the stream type, and some streams were more sensitive than others. Neller (1988) observed bank erosion in an urban area to be 3.6 times higher than in a nearby rural section of the catchment. This was attributed to a change in runoff conditions associated with the urban development.

The removal of vegetation decreases the shear strength of the soil through lack of root binding leaving the area more prone to mass movement processes. Roberts and Church (1986) increased bank erosion rates and sediment supply to rivers in response to increased logging within British Columbia. As roots remove moisture from the soil additional soil moisture content results in reduced cohesion of the soil thereby enhancing the susceptibility to mass movement. Increased bank erosion rates in response to the removal of bank stabilising vegetation for agriculture have been observed in previous studies (Allan *et al*, 1997; Kondolf *et al*, 2002). Michalkova *et al*, (2011) noted a significant difference between mean annual bank erosion rates between riparian and agricultural areas, however they noted that land use change did not influence the frequency of bank erosion as this was controlled by the hydrological pattern and channel geometry.

1.1.6.The contribution of bank eroded sediment to the sediment budget

The previous section highlighted the distinct variation of bank erosion rates within and between catchments observed in previous studies. Evidently the rate of channel migration and bank erosion is controlled by complex inter-relation of numerous variables, resulting in the high spatial and temporal variability of observed rates.

Several studies have noted the significance of bank erosion as a sediment source of varying magnitude within UK catchments (Table 1.6) and worldwide (Figure 1.18) the reasons for which will be discussed in further detail in a later section. From a compilation of previous studies Walling (2005)

observed that channel erosion generally accounts for 4-40% of suspended sediment load within UK catchments. Additionally the increased significance of bank erosion within upland catchments was noted. This corresponds with observations by Carter *et al*, (2003) who found bank erosion forms a greater percentage of the suspended sediment load within upper reaches of catchments (43-80%) than in lower reaches (18-33%). The difference in magnitude of the contribution of bank erosion to the sediment budget in upper and lower reaches of the catchment may be due for a number of reasons including dilution from other sources. Upper catchments may have smaller areas of cultivated land due to steeper slopes. Cultivated land is more susceptible to soil erosion (as will be discussed in a later section) and therefore more sediment is delivered to the channel in lower reaches.

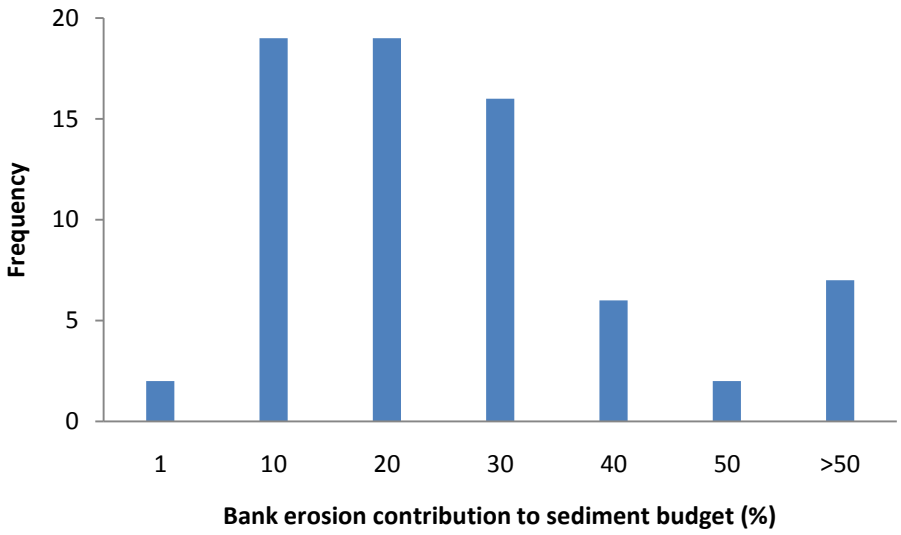

Figure 1.18: Contribution of bank erosion to the sediment budget within several catchments in the UK, and worldwide as observed from previous studies.

Table 1.6: Percentage contribution of bank erosion to the sediment budget at several locations within the UK as found in previous studies. Table continues on next page.

Reference	Catchment	Percentage of budget
Ashbridge (1995)	Culm	19.0
Bull (1997)	Severn	17.0
Carter *et al,* (2003)	Aire	43-84
Collins (2007)	Exe	5.3
	Severn	7.5
	Plynlimon	12.0
Collins *et al,* (1997a)	Hore	25.5
	Higher Chapeltown	2.5-30
	Cruwys Morchard	2.6-4
	Bickleigh	3.5-21.5
	Little Silver	3.7
Collins *et al,* (1997b)	Upper Hore	25.5
	Abermule	22
	Hafren	4.3
	Dart	5
Gardiner (1981)	Lagan	4
Gruszowski *et al,* (2003)	Leadon	8
He and Owens (1995)	Culm	12
Heywood (2003)	Nadder	14
	Upper Avon	8
	Wylye	11
	Lower Avon	19
Nicholls (2001)	Torridge	23
	Waldon	21
	Upper Torridge	21
Owens *et al,* (2000)	Tweed	39
	Teviot	39
	Ettrick Water	48
Russell *et al,* (2001)	New Cliftonthorpe	6
	Lower Smisby	6.2

Reference	Catchment	Percentage of budget
	Jubilee	12
	Belmont	11
Walling *et al,* (1999)	Swale	28.2
	Ure	37.2
	Nidd	15.1
	Ouse	37.3
	Warfe	22.5
Walling *et al,* (2006)	Pang	1
	Langbourn	1
Walling *et al,* (2008)	Upavon East	22
	Upavon West	22
	Chitterne Brook	9
	Till	15
	Sem	12
	Nadder	24
	Ebble	15
	Frome	25
	Stretford Brook	20
	Dore	15
	Worm Brook	20
	Garren Brook	25
Walling and Woodward (1995)	Culm	10

The magnitude of bank erosion as proportion of the sediment budget varies with timescale over which it is observed. For example, Gruszowki *et al*, (2003) found channel banks to supply an average of 8% of the total sediment budget. However, during one of the sampling periods bank sediment accounted for 62.9%, possibly due to a major bank collapse event. Additionally, Bull (1997) noted that bank-derived sediment accounted for an average of 17% of suspended sediment load on an annual timescale, 38% average at monthly timescale, and an average of 64% at event timescale.

As noted by Walling and Collins (2008), it is important that management strategies that seek to control sediment levels are based on a holistic understanding of sediment dynamics within individual catchments. Policy developers should consider the sediment budget as a whole before implementing management strategies. To do this all sediment sources to the catchment should be considered, hence the requirement to quantify bank eroded sediment generation within sediment budget estimations.

1.1.7.Synthesis of literature and gaps in current knowledge

The literature presented within this section has reviewed several factors influencing the rate of overland sediment generation processes. Additionally, several catchment scale models exist that include physical representation of these processes, a selection of which have been detailed in this chapter. The environmental importance of sediment within river catchments, including ecological and chemical, has also been indicated and therefore the requirement to understand and predict sediment generation within catchment systems.

This section also highlighted the significance of bank erosion as a source of sediment generation within catchments and the numerous factors influencing rates of bank erosion as identified in the literature. Several of the existing catchment models presented here do not include bank erosion as a sediment source, and others include only a simplistic representation of this process.

1.2.Objective of thesis

As indicated previously, the overall aim of this thesis is to develop a catchment sediment budget model. The model should include factors such as bank erosion and floodplain sedimentation, thereby providing a comprehensive representation of catchment sediment processes. Figure 1.19 illustrates the format of this thesis, and how the following chapters will contribute to the catchment sediment budget model that will be developed within the final chapter of this thesis.

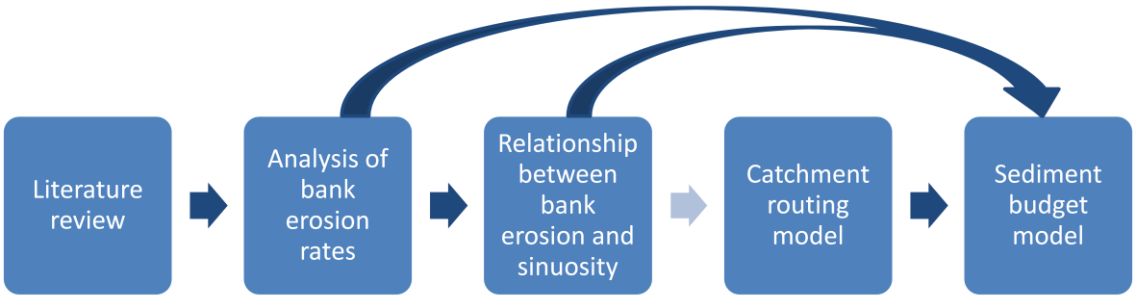

Figure 1.19: Schematic diagram illustrating the structure of this thesis.

Firstly, this thesis will analyse the influence of several of the physical characteristics on bank erosion rates within UK catchments (chapters two and three). These factors will then be incorporated within a new bank erosion model that will be developed in chapter five. The new model will be a development on existing methods due to the improved representation of spatial variation of bank erosion rates. This will be achieved by inclusion of additional factors that have been observed to influence bank erosion rates within the model.

A catchment scale routing model will be developed within chapter four. In chapter five the bank erosion model and a representation of floodplain sedimentation will be incorporated within this routing model to provide a

sediment budget model. Data from an existing overland sediment generation model will be used as input data to the budget model. The model will be applied at a catchment scale, and should be suitable for application nation-wide. To allow coupling to existing overland sediment generation models the model should be computationally efficient and not rely on large input datasets. The model will then be used to assess the impacts of climate change scenarios. The sediment budget model will provide a more comprehensive representation of catchment sediment processes than previous models.

The objectives of each of the chapters of this thesis are:

- Chapter two - analyse the influence of physical factors on bank erosion rates within UK catchments.
- Chapter three - using model outputs analyse the relationship between sinuosity and bank erosion over longer time scales.
- Chapter four - develop a computationally efficient catchment routing model.
- Chapter five - develop a bank erosion model incorporating the findings from chapters two and three, and include this and a floodplain sedimentation model within a catchment sediment routing model.

2.Analysis of bank erosion rates from UK catchments

2.1. Introduction

The rate of channel bank erosion varies greatly between and within individual river catchments. Several factors have been correlated to rates of river bank erosion include meteorological factors (Ashbridge, 1995;), river discharge (Julian and Torres, 2006), composition of bank material (Hooke, 1980), channel planform (Hooke and Yorke, 2010; Howard and Hemberger, 1991), restriction of channel migration within valley walls (Tooth *et al*, 2002), and influences due to vegetation (Simon and Collison, 2002). Additionally, anthropogenic influences; including land use change, construction, and river management strategies have been observed to accelerate/decelerate bank erosion processes (Kondolf *et al*, 2002; Myers and Swanson, 1996; Roberts and Church, 1986). Existing bank erosion models neglect the influence of several of factors known to influence channel bank erosion rates (Darby and Thorne, 1996; Langendoen *et al*, 2010; Luppi et al, 2008; Mosselman, 1998).

In order to improve upon existing models, more of the physical controls of bank erosion which have been identified in the literature should be included in model calculations. The objectives of this study include development of a widely applicable bank erosion model which offers improvements over existing models in 1) physical representation, and 2) quality of predictions. Therefore, the first stage of this study aims to investigate relationships between physical controls of bank erosion such as sinuosity, channel confinement within a valley, channel slope, and upstream catchment area.

As the model developed would be required to be applied nationally, at a catchment scale, relationships developed from the study should be based from observations from several catchments. Therefore, rates of bank erosion and volume of eroded sediment are estimated for several individual river sub-catchments within the UK. Factors known to influence bank erosion such as channel sinuosity, upstream catchment area, channel slope, and channel confinement by valley walls were also calculated for each of these sub-catchments. Relationships between rates of bank erosion and these

independent variables were then explored using statistical techniques such as correlation and multiple linear regression. Using variables shown to have a statistically significant influence, a regression model was developed to predict bank erosion. Sub-catchments observed not to fit the regression model well were then analysed in further detail to examine if factors not accounted for within the regression model could explain differences between predicted values and GIS estimated rates.

2.1.1. Objectives and Justification

The objectives of this chapter include;

- Calculate bank erosion rates for several UK river catchments over a time period exceeding 100 years
    - Identify the magnitude of bank erosion as a sediment source
    - Identify the spatial variation of bank erosion rates
- For the same catchments calculate values of factors known to influence bank erosion including
    - Upstream catchment area
    - Channel slope
    - Sinuosity
    - Channel confinement
- Analyse the statistical significance of these factors and their contribution to bank erosion rates
- Use regression analyses to evaluate the predictive capabilities of these factors for estimating bank erosion rates.

As noted in the previous chapter, several studies have observed the significance of river bank erosion as a sediment source of varying magnitude within UK catchments (Bull, 1997; Carter *et al*, 2003; Walling, 2005 etc.). From studies reviewed in chapter one, the contribution of bank erosion to the sediment budget within UK catchments has been observed to be within the range of 10-40%. This chapter will establish bank erosion rates for several catchments within the UK, identify the importance of bank erosion as a

sediment source within these catchments, and note the variation of bank erosion rates both within and between catchments.

The relationships between bank erosion and factors not currently included within existing bank erosion models will be analysed. Using multiple regression a predictive equation of bank erosion can be developed from these independent factors.

Existing sediment generation models do not explicitly include bank erosion as a sediment source. As noted by Walling and Collins (2008), it is important that management strategies that seek to control sediment levels are based on a holistic understanding of sediment dynamics within individual catchments. Policy developers should consider the sediment budget as a whole before implementing management strategies. To do this all sediment sources to the catchment should be considered, hence the requirement to quantify bank eroded sediment generation. The findings from this chapter will then be incorporated into a new/existing bank erosion model (later in this thesis), with the aim of improving the accuracy of bank erosion predictions within UK catchments. This can then be coupled to existing sediment generation models to improve the accuracy of sediment generation predictions.

2.1.1. Background

Several factors are known to influence the rate of channel bank erosion (see Figure 2.1). These include factors relating to channel planform and geometry (Hooke and Yorke, 2010), discharge and flow regime of the channel (Julian and Torres, 2006), vegetation (Simon and Collison, 2002), lithology and geology (Tooth *et al*, 2002), seasonality (Ashbridge, 1995) etc. Several of these factors have been discussed in detail in the previous chapter. Due to the complex nature of the relationship between bank erosion and the numerous controlling factors, bank erosion rates have been noted as highly variable both within (Ashbridge, 1995; Bull, 1997; Couper and Maddock, 2001; Lawler *et al*, 1999) and between catchments (Walling *et al* , 2002; Walling, 2005).

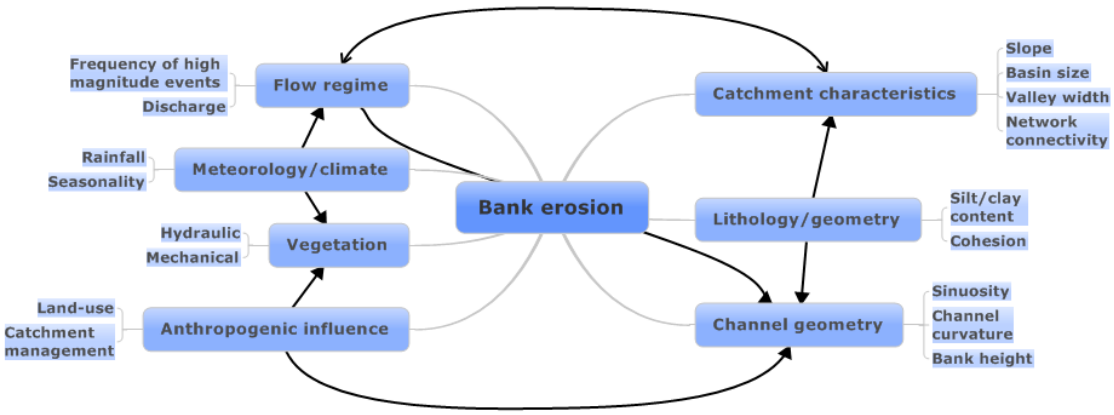

Figure 2.1: Diagram indicating several of the factors which influence bank erosion rates, and how they are interlinked.

In the previous chapter it was demonstrated that physical channel characteristics influence bank erosion rates, therefore, this chapter aims to investigate and analyse the relationship between bank erosion and some variables not currently included within existing bank erosion models; channel slope (profile), sinuosity (channel planform), upstream catchment area, and channel confinement.

2.1.1.1. Channel profile control

Empirical studies have provided evidence of the influence of slope on channel planform. For example, Schumm and Khan (1972) noted that at very low values of slope channels remain relatively straight, with slopes greater than 0.002 a meandering thalweg begins to develop and that meandering increases with increasing slope up to a slope value of 0.016 at which point braided channels develop. Montgomery and Buffington (1997) also indicate how slope and drainage area influence the form of channel; bedrock reaches have the greatest channel bed slopes, slopes >0.065% are likely to have a cascade morphology, 0.03-0.065% step-pool morphology, 0.015-0.03% plane-bed morphology, and slopes of <0.015% pool-riffle morphology. As bank erosion rates vary with channel planform (as discussed in the previous chapter),

channel slope may indirectly influence bank erosion rates through controlling the channel planform.

These empirical findings are broadly consistent with theoretical relationships between slope and energy. According to Manning's equation, the mean velocity of river flow ($\bar{v}$) increases with channel slope:

$$\bar{v} = \frac{R^{2/3} s^{1/2}}{n}$$

where R is the hydraulic radius, s is the channel slope, and n the Manning's roughness coefficient. An increase in velocity of channel flow increases the force acting on channel banks and hence the potential for channel bank erosion increases. As slope increases stream power (Ω) also increases:

$$\Omega = \rho_w g Q s$$

where ρ_w is the water density, g the acceleration due to gravity, and Q the discharge. Stream power is the rate of energy supply in the channel for transporting and eroding sediment, therefore it can be expected that bank erosion rates may increase with an increase in channel bed slope.

2.1.1.2. Channel planform controls

Channel curvature induces changes to flow patterns within the river channel. The centrifugal force acting on the primary (downstream) flow within the channel results in water flow being forced towards the outer channel bank. The influence of channel bed friction results in lower flow velocities with decreasing depth within the water column. The magnitude of centrifugal force increases as the velocity of the flow increases, meaning the force acting on the upper part of the water column is greater than that acting further down. As the water is moved towards the outer bend a water surface slope forms, generating a pressure gradient force acting towards the inner bank. The combination of the centrifugal, pressure gradient, and frictional forces within the channel result in the formation of secondary circulation cells (see Figure 2.2 A and B). The influence of the primary, downstream velocity on the secondary circulation cell causes the cell to become helical (see Figure 2.2 C).

The secondary circulation results in high velocity flow and hence increased shear stress acting on the outer channel bank, which increases bank erosion rates at the outer bank. Due to the helical nature of the cell, the point where the high velocity flow (and hence maximum bank shear stress) reaches the channel bank is located downstream of the point of maximum bend curvature (bend apex). This results in the downstream migration of meander bends, as has been observed in several studies (Carson and Lapointe, 1983; Hooke and Yorke, 2010; Nicoll and Hickin, 2010;).

A

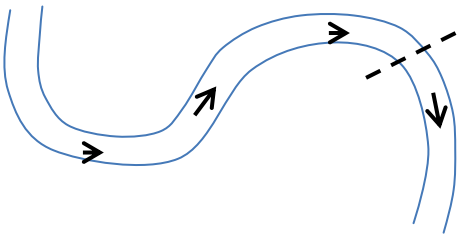

B

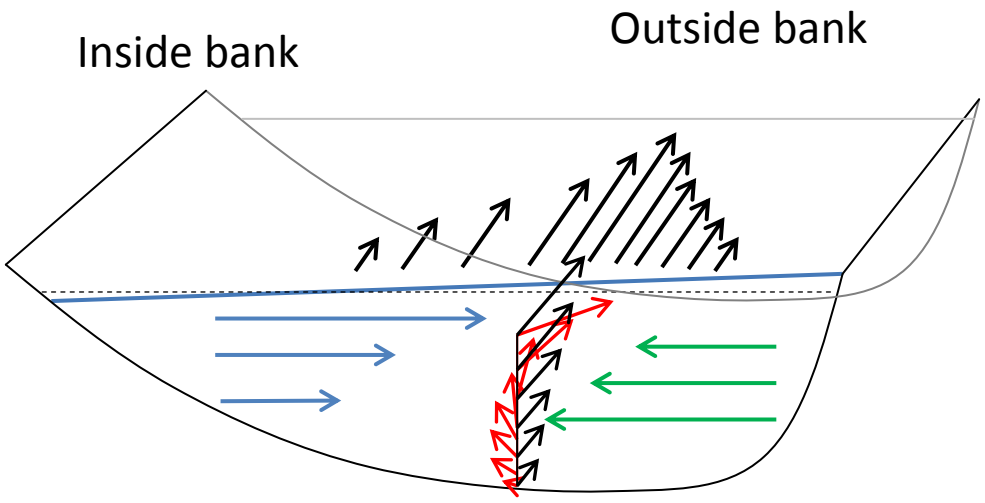

C

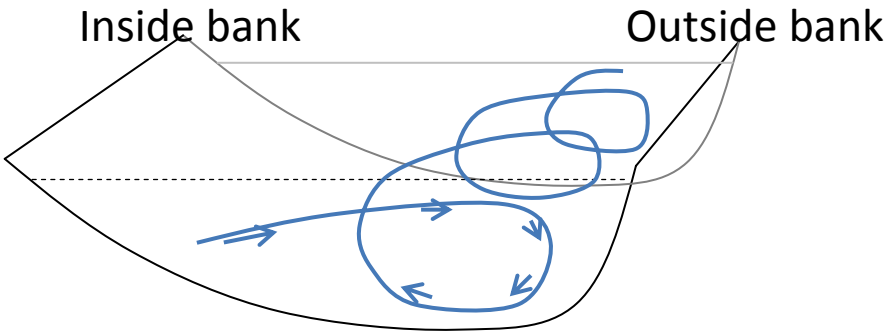

Figure 2.2: A) Hypothetical meandering channel, illustrating cross-section depicted in B and C. B) Black arrows indicate primary flow direction and magnitude (flow velocity is lower towards channel sides and lower in the water column due to friction of the channel). Blue arrows show the direction and magnitude of centrifugal force (magnitude of the force decreases with increased depth in the water column due to the decreased velocity). The blue line represents the water surface slope as a result of water movement by the centrifugal force, and results in a pressure gradient (green arrows). The red arrows represent the resulting direction of secondary flow. C) Helical cell formation of secondary flow.

The secondary flow generated in curved channels as described above results in the observed relationship between channel curvature ratio (the radius of curvature of the channel divided by the channel width) and channel migration rate (as detailed in the previous chapter, section 1.2.4.2). Channel curvature is linearly related to channel sinuosity; as channel curvature decreases, sinuosity increases. It follows that a relationship between channel sinuosity and migration rate should exist. This has been observed in Walnut Creek, Iowa by Schilling and Wolter (1999), who noted that sinuosity varied from 1-2.3, with channelized areas having an average bank retreat rate of <0.05ft/yr and meandering reaches showing active channel erosion and retreat rates >0.2ft/yr (see Figure 2.3). Abam (1993) also noted that increased sinuosity resulted in bank failure at the concave bank due to scour and toe erosion. In a study with data from 450 rivers in Canada, the USA and New Zealand Rosgen (1994) found as slope decreased, sinuosity increased causing an increase in channel migration and bank erosion.

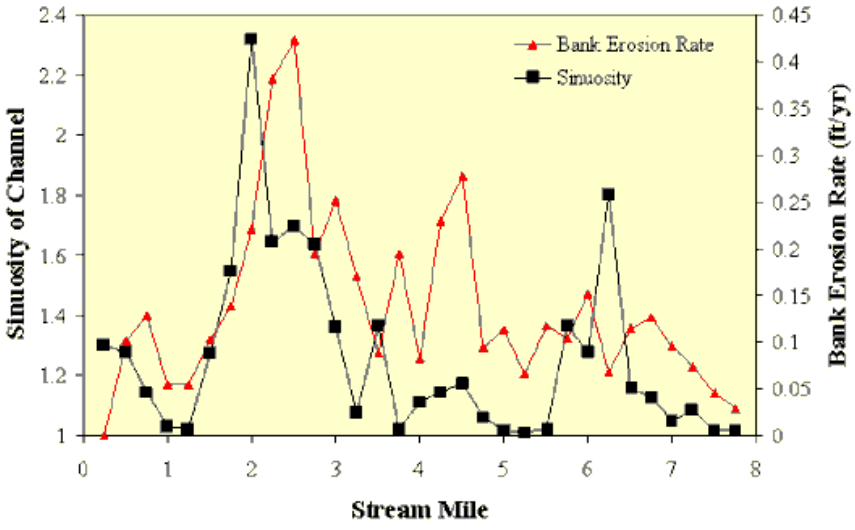

Figure 2.3: Channel sinuosity and average bank erosion rates observed in Walnut Creek, Iowa. Schilling and Wolter (1999).

2.1.1.3. Catchment area control

Hooke (1980) noted that bank erosion rate was related to catchment area, and this explained 53% and 39% of variation in mean and maximum erosion rates respectively. It is suggested that this is because catchment area represents a surrogate of discharge and hence indicates the positive relationship between bank erosion rate and discharge; as discharge increases the shear stress acting on the channel banks increases, causing increased bank erosion. Birkinshaw and Bathurst (2006) also noted that as basin area increases, the volume of sediment derived from bank erosion also increases. Bull (1997) observed that downstream sites had significantly larger rates of erosion than upstream locations, due to an increase in bank failure events.

2.1.1.4. Valley confinement control

Channel migration may be restricted by valley walls. Lewin and Brindle (1977) first identified channel confinement and described 3 degrees of confinement based on decreasing relative valley width:

1) Occurs within wide-floored valleys so contact with valley walls is infrequent.
2) When floodplain is narrower than the amplitude of the meandering channel, so that boxed, sinusoidal pattern is present with contacts with the valley wall at each wavelength of the channel.
3) When meander geometry appropriate to channel discharge in a free meander medium is prevented from developing due to valley wall restriction.

Rapp and Abbe (2003) define confined channels as those with a valley width of less than 2 channel widths, moderately confined channels with a valley width of between 2 and 4 channel widths, and unconfined channels with a valley width greater than 4 channel widths. Alternatively, a confinement ratio for channels can be calculated from the width of the valley floor or floodplain divided by the width of the bankfull channel. Hall *et al*, (2007) define confined

channels as having a confinement ratio of less than or equal to 3.8, and unconfined channels with a ratio of greater than 3.8.

Milne (1983) found low sinuosity in channels was partly due to lateral confinement of the channel by valley walls which prevents free meander development. Tooth *et al*, (2002) noted where valley width was confined due to bedrock geology sinuosity values were ~1.10-1.34 and where valley width did not restrict sinuosity of meander migration sinuosity values were ~1.75. Nicoll and Hicken (2010) observed confined channels had a higher wavelength and curvature than unconfined rivers. Un-confined channels within their study region showed a pattern of downstream translation, with few channel cutoffs occurring, causing bend over-tightening and a decrease in channel curvature. Additionally, un-confined freely meandering rivers can migrate outwards which reduces channel-bend radius. As it is not possible for these mechanisms to operate in confined channels, channel curvature and wavelength remain higher than un-confined developing channels.

Fotherby (2009) also noted the influence of valley confinement as a factor determining the river pattern in the Platte River, USA; areas of the channel which were confined by the river valley were noted to be less braided. This was attributed to confinement restricting the tendency of flow to divide into multiple channels.

2.2.Methodology

Field observational data of bank erosion rates using techniques such as erosion pin methodologies are time consuming and therefore only cover a small spatial area. Additionally, data sets using this methodology do not cover a sufficiently long time period. Therefore, in this chapter a methodology using GIS is illustrated, similar to simple polygon overlay as used in previous studies (Hooke and Kain, 1982; Gurnell et al, 1994). This involves digitising channel positioning from historical Ordnance Survey maps, thereby allowing observation of channel migration over a period of approximately 150 years (depending on the catchment).

The chapter also aims to investigate importance of several physical controlling factors on the rate of bank erosion. These include; channel slope, sinuosity, channel confinement, and upstream catchment area. The statistical significance of the relationship between bank erosion rate and these factors will then be analysed, and their predictive capabilities assessed using regression techniques.

Bank erosion rates will be calculated for individual Water Framework Directive (WFD) sub-catchments. Catchments chosen were selected to represent the range of rainfall patterns across England and Wales. The catchments chosen cover a range of catchment types (i.e. different underlying geologies and channel characteristics etc.). Due to the large spatial coverage of bank erosion data obtained from several catchments using the GIS methodology, this will allow development of empirical relationships between bank erosion rates and several physical controlling factors that will be representative for the UK. In later chapters, an existing bank erosion index will be modified to incorporate physical factors observed to be significant to bank erosion rates within this chapter. The model will be required to be applied nationally, at a catchment scale. Therefore this indicates the requirement to obtain data covering a large area, so that relationships are representative of catchments within the UK.

As noted in the literature review section, several factors influence rates of bank erosion, some of which will not be included in the regression model. Therefore, in sub-catchments where the model does not perform well (i.e. data points with large residual values) factors known to influence bank erosion that

are not included in the model will be investigated. Land cover and geology of sub-catchments will be noted to investigate if these variables could account for observed differences between GIS bank erosion estimates, and the predicted values from the regression model.

2.2.1. Digitising channels in GIS

Historical ordnance survey maps were downloaded in digital form from the EDINA Digimap website. Ordnance survey maps were originally produced in 1840 and have involved different mapping series, each with revisions, up to present day. The dating and coverage of the maps varies between each mapping series.

County Series maps created between 1846 and 1969 are available in a first edition and 3 revisions. In 1880 the first national survey of maps was commissioned. Each county was surveyed individually (hence the name of the series), meaning surveying of neighbouring counties occurred at different dates. These are also available to download in national grid format, equivalent to contemporary national grid tiles. From 1944 onwards the mapping process was transferred to a national grid format. First edition and up to 4 revisions are available up to 1990s. The dates and coverage of each mapping series is indicated in Table 2.1.

Table 2.1: Historical Ordnance Survey map series, publishing dates, and coverage.

Series Name	Published	Coverage
First County series survey	1846-1901	Poor in NE England
County series 1st revision	1888-1915	Poor for N Yorkshire and parts of SW England
County series 2nd revision	1903-1949	Poor for Cornwall, Wales, Lincolnshire and Scottish/English border
County series 3rd revision	1922-1969	Concentrated in urban areas
National Grid 1	1943-1993	High
National Grid 1st revision	1944 onwards	Concentrated in urban areas
National Grid 2nd revision	1946 onwards	Revisions only
National Grid 3rd revision	1951 onwards	Revisions only
National Grid 4th revision	1953 onwards	Revisions only

The dates of the map created within one mapping series may vary as these maps are made up of separate historic maps which have been joined together. Neighbouring maps within the same map edition have often been surveyed and revised at different dates. An estimate of the age of one map layer was taken from the range of years of map creation given (often up to 15 years). The difference in the years of map creation means that the catchments chosen for digitising do not all have data from the same time periods as each other (i.e. different years are represented in different catchments).

Maps produced before World War 2 County Series were produced from separate county surveys and consequently the map data may overlay at county boundaries. This may also account for the variation in year of map creation within some layers. Additionally, maps taken from the edge of a county map will contain white space with neighbouring counties left blank leaving gaps in the data. This problem was noted when downloading data for the river Wye as sections of this river lie on the boundary between Gloucestershire and Monmouthshire. Between maps the weight of lines and notation can be seen to vary slightly, although this was not a major problem when observing channel positioning. However, it was noted in some older maps (particularly 1890s)

upper sections of rivers were poorly represented with often only a single line representing the channel. This will introduce errors as it is impossible to accurately digitise both channel banks.

Catchment areas were downloaded in groups of national grid tiles and imported into GIS using ArcInfo as .tif files, with British national grid co-ordinates projected as the data frame. The channels were then digitised from the historic data to produce polygon shapefiles of the channel.

Satellite images provided too poor resolution to enable channel bank digitisation. Additionally, in rural sections when zoomed in sufficiently to see the channel it was difficult to identify features to geo-reference these images to maps. Therefore these were not used in the digitising process. Data from Mastermap (also accessed through EDINA Digimap) was downloaded in sections over the catchment areas. Water themes were selected for download (from the topography layer) and then using InterpOSe dotted eyes application the relevant data layers were extracted to input into GIS as shapefiles. The mastermap topography layer is updated bi-annually and the date of the map creation used for this analysis was June 2010.

The mastermap shapefiles were joined to form shapefiles for individual rivers using the union tool. The mastermap data includes all features that contain, delimit or relate to real-world objects containing water. Therefore many features such as drainage systems, ponds, lakes etc were shown within the layer. The layers were then clipped using a shapefile of the most recent digitised period with a buffer of 20m to ensure the channel was incorporated within the clipped image but allowed unwanted water features to be eliminated. However, there are some errors associated with this method as some sections of the mastermap features not included in the main channel may still be present within the 20m buffer of the previous time period. Each channel shapefile contained many individual polygons due to the nature of the mastermap data. Each channel was converted to one polygon to allow analysis using the merge tool.

Rather than rasterising the polygons to calculate areas of channel erosion and deposition this was done by direct comparison of polygons. This meant the resolution was determined by the digitisation of the mapped river,

and the original mapping as opposed to the resolution dictated by the cell size of the raster image. Each year's polygon was given an additional field according to the year it represented (e.g. Y_1890, Y_1940 etc.). This field was then given a value, with each time period given an increasing number on a binary scale. The polygons were then overlaid using the union tool and a new field (Y_flag) created which calculated the sum of the two year input fields. For example Y_1890 = 1 and Y_1940 = 2, on the union polygon where both channels were present Y_flag =3, where there was only the channel in 1890 Y_flag=1 and where the channel was only present in 1040 Y_flag=2. These numbers could then be interpreted as 1=deposition, 2=erosion and 3=no change (as illustrated in the Table 2.2). This methodology is similar to '*Simple polygon overlay analysis*' as described by Gurnell *et al* (1994). This process was conducted for 2 consecutive map dates at a time i.e. 1890-1940, 1940-1970, 1970-2010. The corresponding areas of erosion and deposition were then calculated in m^2 using the 'Calculate Geometry' tool within GIS.

Table 2.2: Simple polygon overlay analysis method used to estimate bank erosion.

		Year 1	
		Channel	**No Channel**
Year 2	**Channel**	No change	Erosion
	No Channel	Deposition	No Change

It was noted that this method of calculation of bank erosion rates was inaccurate for any areas where the channel had migrated to a degree that the channel two polygons from the time periods represented did not overlap (as illustrated in Figure 2.4). This resulted in an underestimation of bank erosion as an area, or 'island' of bank erosion was omitted from the estimation. Therefore, each time overlay for each WFD sub-catchment was examined individually and any 'erosion islands' were digitised and their area added to the erosion area calculated for the corresponding sub-catchment from the overlay process. However, it was also noted that this methodology will overestimate bank erosion where erosion has occurred by avulsion rather than migration.

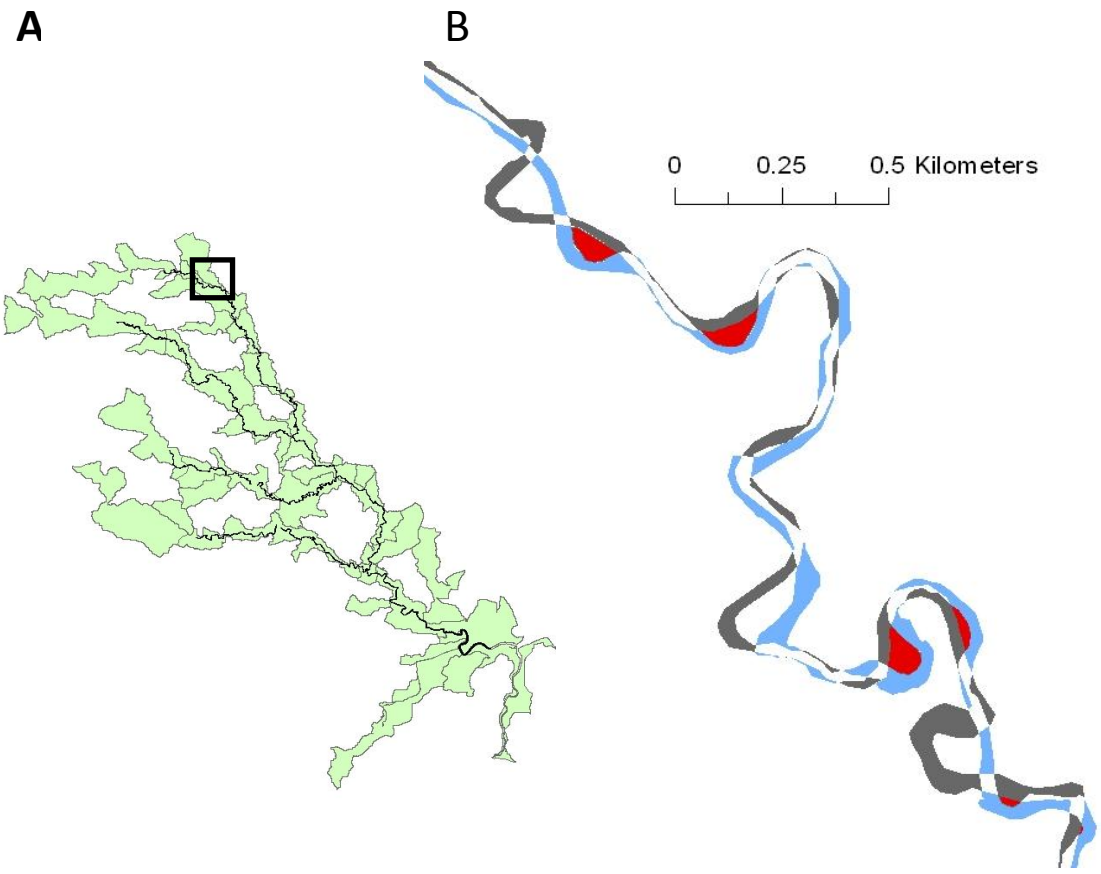

Figure 2.4: A) Ouse catchment and digitised channels. Square shows the location of B. B) Example of island inclusion methodology, example taken from a section of the Swale 1940-1975 time period. Blue channel: 1975, Grey channel: 1940, White channel: Both time periods, no channel change. The five red sections indicate areas which the channel has eroded through during the time period. The area of these red polygons was added to the total erosion for this sub-catchment. The meander loop at the top left of the image indicates a chute cut-off and therefore the area between the two channel overlays has not been eroded and so is not added to the total erosion area. Flow is from top to bottom of image.

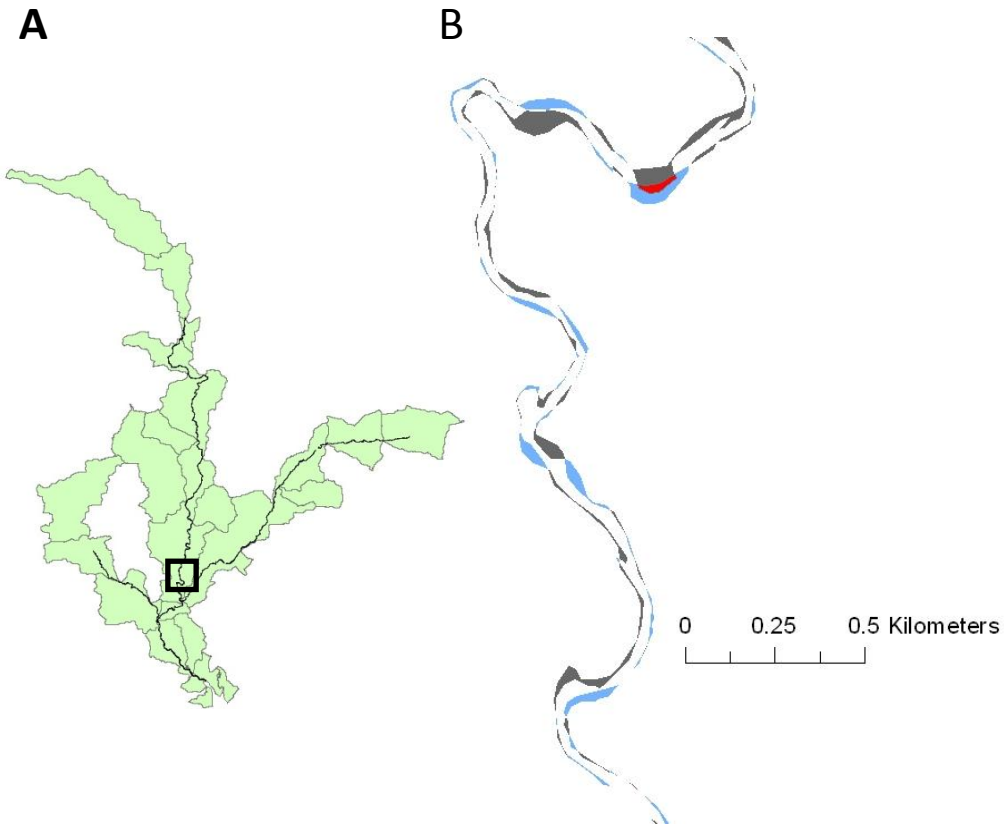

Figure 2.5: A) Exe catchment and digitised. Square shows location of B. B) Example taken from a section of the Exe 1962 (grey channel) -1970 (blue channel). Flow is from top to bottom of image.

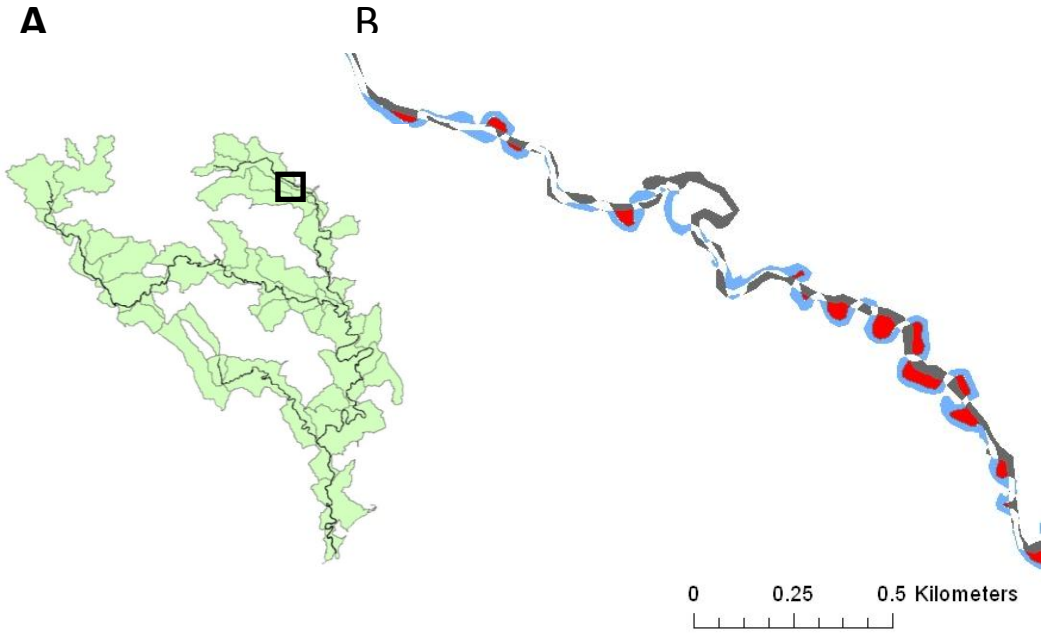

Figure 2.6: A) Wye catchment and digitised channels. Square shows location of B. B) Example taken from a section of the Lugg 1890 (grey channel) -1975 (blue channel).

The catchments included for digitising and analysis were chosen from listed priority catchments of the England Catchment Sensitive Farming initiative (CSF). Catchments were selected to enable representation of the variety of rainfall patterns and geologies (hence catchment types) across England and Wales. Chosen catchments are shown in Figure 2.7 and time periods represented are as follows:

- River Exe, Devon (Exe, Culm and Creedy) - 1890, 1962, 1970, 2010.
- River Avon, Hampshire (Avon, Bourne, Ebble, Wylye, Nadder) - 1890, 1926, 1985, 2010.
- River Ouse, Yorkshire (Ouse, Swale, Ure, Nidd, Wharf) – 1860, 1940, 1975, 2010.
- Rivers Test and Itchen, Hampshire – 1875, 1940, 1985, 2010.
- River Wye, Herefordshire (Wye, Monnow, Lugg) – 1890, 1975, 2010.
- River Stour, Kent (Stour, East Stour, Little Stour, Sarre Penn) – 1875, 1940, 1985, 2010.
- River Eye, Leicestershire – 1890, 1950, 1983, 2010.

Sources of error within the GIS methodology include geo-referencing errors. Whilst the historical maps have been digitised prior to download some geo-referencing errors may still be present. Other sources of uncertainty include channel bank-line positioning, and errors from the mapping process.

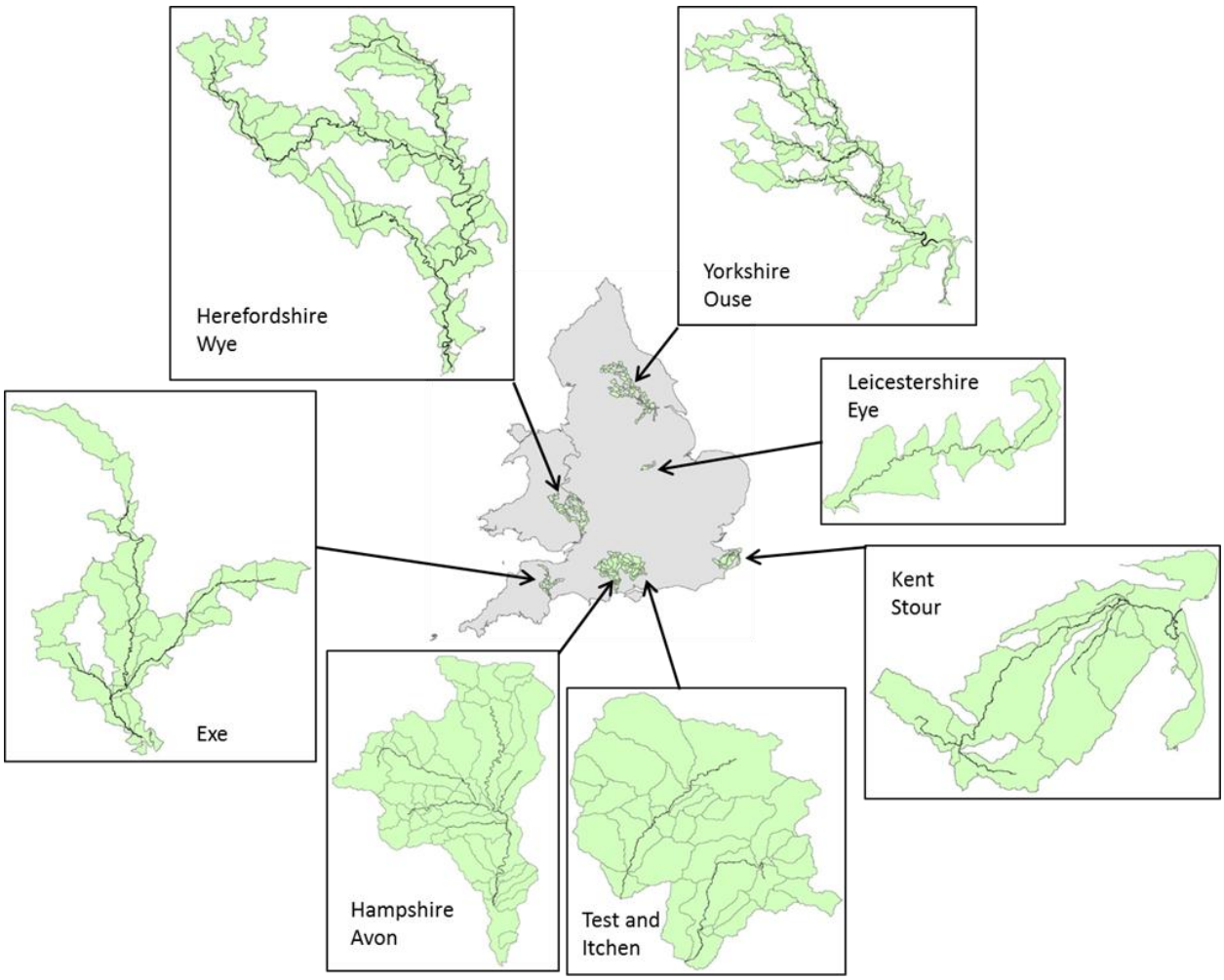

Figure 2.7: Location of the catchments chosen for digitising. The channels digitised within the catchments (and sub-catchments) are also shown.

2.2.2. Eroded sediment estimation

Channel erosion derived from GIS was estimated as an area (m^2). However, for comparison with sediment yield data it is necessary to convert these data to volume and mass. This requires use of bank height and sediment bulk density data. Channel bank heights were estimated from River Habitat Survey (RHS) data from the Environment Agency (Environment Agency, 2008). As survey points were randomly placed within catchments all RHS points within individual WFD sub-catchments, the values of bank height within an individual sub-catchment were averaged to produce an individual value of bank height for each sub-catchment. Where no RHS data points were present within a sub-catchment, the bank height of the nearest data point was used. There will be

errors associated with this method of bank height estimation as bank heights may vary considerably within individual sub-catchments. Whilst bank height may influence migration rates, bank height was not used as an independent variable due to the limitations associated with estimating bank height values.

Sediment volume was then converted to dry mass (kg) by multiplying by an assumed density of 1400kg m^3. This value was chosen as average floodplain sediment density observed in previous studies (see Table 2.3). The existing ADAS bank erosion index estimates bank eroded sediment reaching the catchment outlet as a mass of sediment (kg $ha^{-1}yr^{-1}$). After considering the proportion of bank eroded sediment that is deposited (i.e. through floodplain sedimentation) and does not reach the catchment outlet, calculation of bank erosion rates as a mass of sediment allow comparison of GIS derived bank erosion rates and estimates from the existing bank erosion index. The mass of sediment was then divided by the area of the sub-catchment to give a value of kg ha^{-1}, which was then divided by the number of years the overlay period covered to give a value in kg ha^{-1} yr^{-1}.

Retreat rates of the channel were estimated using the erosion area polygon of each sub-catchment divided by polygon length of the channel polygon, (giving a retreat rate for the whole time period in m). This was then converted into an annual retreat rate estimate (m yr^{-1}) by dividing by the number of years the time period covered, and a width averaged retreat rate (m m^{-1} yr^{-1}) by dividing by the average channel width

2.2.3. Estimation of Sinuosity

Channel sinuosity for each sub-catchment was calculated from the channel length divided by the straight line distance of the channel. Channel length was estimated from channel polygon values of channel area and perimeter. Straight line distance (from headwaters to outlet) was calculated by direct measurement in GIS. The sinuosity for each sub-catchment was calculated for each time period digitised. The values of sinuosity used in regression analysis were taken as an average of the sinuosity over all time period representations.

Table 2.3: Bulk density of floodplain sediment from previous studies. The average of these was used as a constant to convert volume of bank eroded sediment to mass of eroded sediment.

Bulk density kg m^3	Location	Reference
1600	Rivers in SE Australia	Erskine and Saynor (1996)
1455	Detroit River, USA	Jespen *et al*, (1997)
1305	"	"
1785	"	"
1230	Los Alamos, USA	Reneau *et al*, (1998) in Malmon *et al*, (2005)
1002	Georgia, USA	Craft and Casey (2000)
1500	Australian rivers	Prosser (2001b)
1300	Neman, Lithuania	Vaikasas and Rimkus (2003)
1050	Neckar, Germany	Gerbersdorf *et al*, (2007)
1360	New Zealand	Environment Waikato (2007)
1800	Australian rivers	Hazelton and Murphy (2007)
1700	"	"
1600	"	"
1400	"	"
1800	USA rivers	Lauer and Parker (2008)
1150	Cumberland, Canada	Van Asselen *et al*, (2010)
1220	"	"
1320	"	"
1260	"	"
1400	"	"
1300	"	"
1350	"	"
1470	"	"
1420	"	"
1550	"	"
1650	"	"
1700	"	"
1000	Culm, Dvon	Walling and Bradley (1989)
1417		Average

2.2.4.Estimation of Slope

Ordnance Survey contours from land-form profile data were downloaded from Digimap. This data was then converted using the productivity suite from ESRI, and then loaded in GIS. This data has an accuracy of ±2.5m for 5m intervals. The height at the headwater and outlet of each channel within each sub-catchment was taken from the contour data and the slope calculated (height at top of catchment minus height at bottom, divided by straight line distance).

2.2.5. Estimation of Channel Confinement

The degree of channel confinement within a valley can be expressed in several different ways. In this analysis 4 different methods of estimating channel confinement were calculated and their relationship with erosion rates was investigated. These methods are outlined below:

1) **Confinement ratio using channel width** – This was calculated as the floodplain width divided by the bankfull channel width, as used in previous studies (Hall *et al*, 2007; Rapp and Abbe, 2003). Hall *et al*, (2007) stated that confined channels had a ratio of ≤3.8 and unconfined channels >3.8.
2) **Confinement ratio using meander belt width version A** – Meander belt width was calculated as channel width multiplied by sinuosity for each WFD. The confinement ratio was then calculated as floodplain width divided by belt width.
3) **Confinement ratio using meander belt width version B** – Mackey and Bridge (1992) found the following relationship between belt width (B) and channel width (w):

$$B = 6.89w^{0.99}$$

The data used to form this relationship was taken from 98 field observations and produced a correlation coefficient R=0.94. The confinement ratio was then calculated as floodplain width divided by belt width, as calculated from this relationship.

4) **Confinement ratio using meander belt width version C**– Williams (1986) found the following relationship between belt width (B) and channel width (w):

$$B = 4.3w^{1.12}$$

The data used to form this relationship was taken from 153 sites in various countries and produced a correlation coefficient R=0.96. The confinement ratio was then calculated as floodplain width divided by belt width, as calculated from this relationship.

The floodplain data used to calculate channel confinement was provided by ADAS, and covers the Environment Agency flood zone 3. Flood zone 3 as defined by the EA represents the area which has a 1 in 100 or greater probability (>1%) of annual flooding (100 year return period). The width of the floodplain for each sub-catchment was estimated from the floodplain polygon area and perimeter (using the same method as channel width).

2.2.6. Correlation and regression analysis

The relationships between bank erosion rate (in both kg ha^{-1} yr^{-1} and m m^{-1} yr^{-1}) and the independent variables (sinuosity, slope, channel confinement, and upstream catchment area) were analysed using statistical techniques. Both Pearson's correlation and regression are forms of parametric statistical tests meaning all input variables must be normally distributed. Therefore, initially the distribution of all input variables was assessed by calculating descriptive statistics for all variables. For normally distributed data the mean median mode should be a similar value, the skewness statistic should be between +1 and -1, and the value of kurtosis should be between +3 and -3 (Norušis, 2005). Any data that is not normally distributed may be transformed using the $\log_{10}$ transformation to achieve normality (see Figure 2.8). Pearson's correlation was then used on data to assess the strength of relationships between each of the independent variables individually and bank erosion rate. Additionally, scatterplots were used to assess relationships between variables are linear.

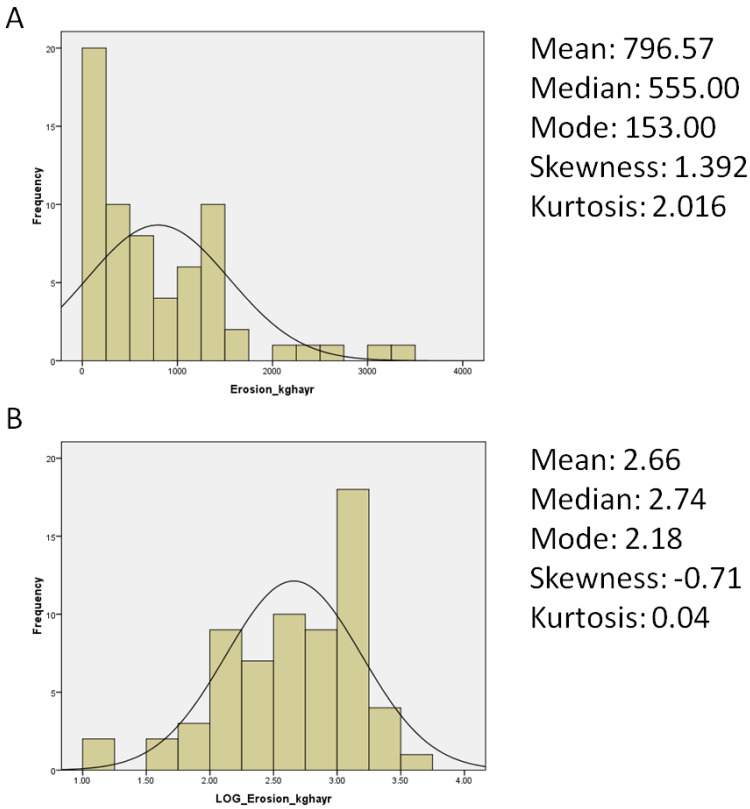

Figure 2.8: Output from normality test for A - Erosion (kg ha yr) and B - after log transformation.

A multiple regression analysis was then used to assess to what extent the variance of bank erosion can be explained by the combination of the independent variables. Before regression analysis the independent variables were checked to ensure they were independent from each other (no significant correlations between pairs of independent variables). This ensures no independent variables are duplicates, thereby avoiding statistical redundancy and ensures the assumption of no multicollinearity is true.

2.2.7. Analysis of residual values

From each of the regression analyses, standardised residual values were noted. These values represent the difference between the observed (GIS estimated value) and predicted (from the regression equation) values. Residual values for each regression were analysed individually. Within these sub-catchments, land cover and geology were investigated to see if these variables

could account for the observed differences between the estimates from GIS and the model predicted values. Land cover and geology data were obtained from the Centre for Ecology and Hydrology (CEH) and the Digimap website, the details of the data are outlined below.

Land Cover Map (LCM) 2007 data with 1km^2 resolution was downloaded from the CEH. This data was then used in GIS to establish the dominant land cover classification (as defined by CEH documentation, see Appendix A Figure 119) both next to the channel and within the basin of these sub-catchments. Geology data was downloaded from the Digimap website, which provided bedrock classification within individual sub-catchments and corresponding British Geological Survey definitions for each classification.

The predominant land-cover and geology type in each of the sub-catchments was noted and then compared with residual values. An average residual value for each land-cover and geology type was noted to establish if any classification was predominant in areas where the models over/under predicts bank erosion values. Un-standardised residual values were also correlated against dependent variables used in the regression models to investigate if any of the dependent variables individually contributed to the error in regression model prediction.

2.3.Results and Analysis

Figure 2.9 and Appendix A Table 77 show the erosion estimates from the GIS overlay data.

Table 2.5 indicates the mean rates of bank erosion calculated for each of the 7 catchments for which data was collected in this study, and indicates the largest erosion rate as calculated as a mass of sediment (kg ha^{-1} yr^{-1}) was observed in the Eye catchment, and the lowest was observed in the Test and Itchen. Table 2.5 also indicates the catchments with the largest annual retreat rates were the Avon and Exe, the largest width averaged retreat rate observed was in Stour, and the smallest retreat rates were observed within the Wye. The data presented here are the average values of all time period overlays for each sub-catchment. The minimum, maximum, and average values of bank erosion as calculated using each unit of measurement are shown in Table 2.4. The values of retreat rate obtained from this are of similar magnitudes to rates calculated from previous studies for the same catchments Table 2.6.

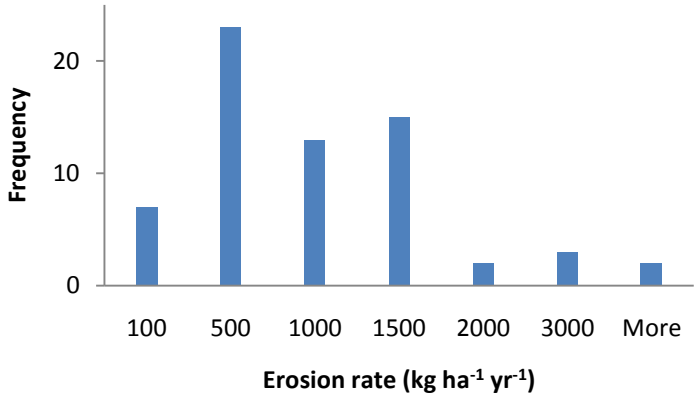

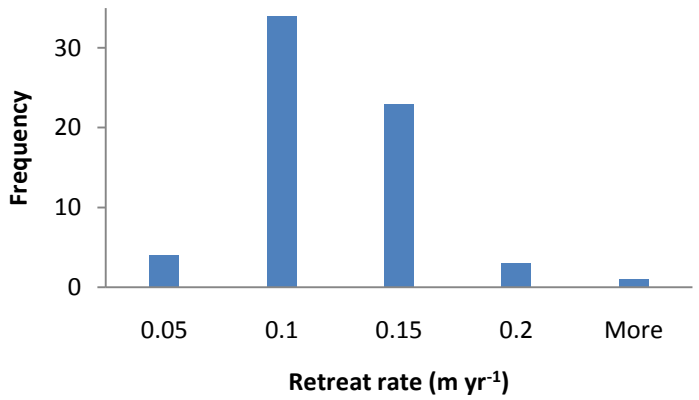

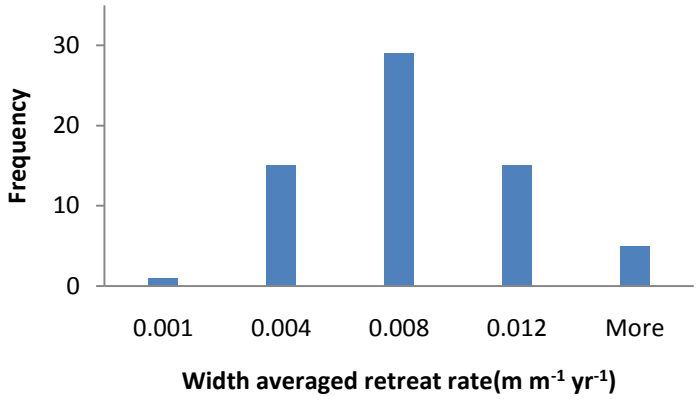

Figure 2.9: Histograms showing bank erosion as Erosion rate (kg ha^{-1} yr^{-1}), retreat rate (m yr^{-1}), and width averaged retreat rate (m m^{-1} yr^{-1}) calculated for all 65 sub-catchments from GIS.

Table 2.4: Rates of bank erosion calculated from the 65 sub-catchments.

	Erosion (kg ha^{-1} yr^{-1})	Retreat rate (m yr^{-1})	Width averaged retreat rate (m m^{-1} yr^{-1})
Min	9	0.0279	0.0008
Max	3321	0.2291	0.0138
Ave	786	0.0976	0.0063

Table 2.5: Mean rates of bank erosion for each catchment.

Catchment	Mean Erosion (kg ha^{-1} yr^{-1})	Mean Retreat rate (m yr^{-1})	Mean Width averaged retreat rate (m m^{-1} yr^{-1})
Avon	412	0.1166	0.0082
Exe	1185	0.1141	0.0078
Eye	1389	0.0863	0.0072
Ouse	1051	0.1046	0.0049
Stour	172	0.0746	0.0091
Test and Itchen	118	0.0897	0.0059
Wye	1095	0.0744	0.0039

Table 2.6: Rates of bank erosion from Ouse and Exe catchments observed from previous studies.

Bank erosion rate	Unit	Location	Time period	Reference	m yr^{-1}
0.63	m/yr	Exe	1974-1976	Hooke (1980)	0.630
0.62					0.620
1.18					1.180
1.03					1.030
0.24		Culm (upper)			0.240
0.18		Culm (lower)			0.180
0.26		Creedy			0.260
82.7	mm	Swale	Mar' 1996-May 1997	Lawler et al (1999)	0.071
239.7					0.205
337.6					0.289
116.8					0.100
440.1					0.377
424.9					0.364
320					0.274
93					0.080
166.3		Ure			0.143
77.7		Ouse			0.067

Table 2.7 shows the minimum, maximum, and average values of each of the independent variables for the 65 sub-catchments. Appendix A Tables 78 and 79 in the appendix show the values estimated for each sub-catchment.

Table 2.7: Range of values of independent variables calculated for the 65 sub-catchments.

	Upstream Catchment area (km^2)	Average Sinuosity	Slope	CC1	CC2	CC3	CC4
Min	24	1.1118	0.0000	1.8	1.0	0.3	0.3
Max	4605	2.5434	0.0640	98.1	74.0	14.5	18.3
Ave	840	1.5662	0.0037	12.2	8.0	1.8	2.1

2.3.1. Prior to multiple regression analysis

Relationships between erosion rate (kg ha^{-1} yr^{-1}) and independent variables (total upstream area, sinuosity, slope and channel confinement), and also between width averaged retreat rate (m m^{-1} yr^{-1}) and the independent variables were analysed. The analysis of these relationships is outlined below.

On inspection of the digitised channels in ArcGIS there was a clear geo-referencing error in the 1926 map layer for the river Wylye (Avon catchment); for this time period the channel was shifted to the right of the other 3 time periods represented. Therefore erosion estimates were re-calculated, removing the 1926 layer from analysis. The re-calculated erosion values are shown in Table 2.8. The regression analysis was the performed using this data for the river Wylye.

Table 2.8: Results after 1926 Wylye layer removed.

Number	Channel	Total kg/ha/yr	Retreat rate/yr	Width averaged retreat rate
10	Wylye	686	0.114199	0.008203
11	Wylye	9	0.080513	0.008029
12	Wylye	153	0.070860	0.006122

2.3.1.1. Distribution of variables

As indicated in Appendix A Table 80, all variables considered for this analysis except retreat rate and width averaged retreat rate are not normally distributed. Therefore, the values of non-normally distributed variables were transformed by taking the logarithm to the base 10 to achieve normal distribution. Values of variable slope are very low (0-0.064) and therefore a logarithmic transformation was unsuitable. Slope was transformed by adding a constant of 0.0001 to all values and then taking the logarithm to the base 10. The distribution of the transformed variables was then assessed in the same way, which indicated the transformation had resulted in normal distribution.

2.3.1.2. Correlation of variables

Table 2.9 shows the correlation matrix for the transformed variables. The dependent variables are erosion (kg $ha^{-1}yr^{-1}$) and width averaged retreat rate (m yr^{-1}). Before regression analysis the independent variables must be checked to ensure they are independent from each other (no significant correlations between pairs of independent variables). This ensures no independent variables are duplicates, thereby avoiding statistical redundancy and ensures the assumption of no multicollinearity is true. Variables were assumed independent where the statistical significance of the relationship is less than the 99% level. Additionally, the tolerance statistic (output from the regression model) should be >0.1, indicating multicollinearity is not an issue within the model. It is clear from Table 2.9 that the variables CC1, CC2, CC3 and CC4 are significantly correlated (at the 99% level) and therefore should not all be put into the regression analysis. This is to be expected as all these variables represent channel confinement, so are showing the same thing. Therefore only one of the channel confinement variables was selected for each regression analysis.

Table 2.9: Correlation matrix for independent variables. * indicates a significant relationship at the 95% level, and ** at the 99% level.

	Log Sinuosity	Log Slope	Log Upstream area	Log CC1	Log CC2	Log CC3	Log CC4
Log Sinuosity		-0.155	0.287*	-0.054	-0.257*	-0.052	-0.076
Log Slope	-0.155		-0.178	-0.101	-0.002	-0.103	-0.083
Log Upstream area	0.287*	-0.178		0.062	0.021	0.067	0.015
Log CC1	-0.054	-0.101	0.062		0.956**	1.000**	0.998**
Log CC2	-0.257*	-0.002	0.021	0.956**		0.956**	0.960**
Log CC3	-0.052	-0.103	0.067	1.000**	0.956**		0.997**
Log CC4	-0.076	-0.083	0.015	0.998**	0.960**	0.997**	

Table 2.10: Correlation of independent and dependent variables. * indicates a significant relationship at the 95% level, and ** at the 99% level.

	Log Erosion (kg ha^{-1} yr^{-1})	Retreat rate (m yr^{-1})	Width averaged retreat (mm^{-1} yr^{-1})
Log Sinuosity	0.395**	0.052	-0.219
Log Slope	-0.047	0.043	0.196
Log Upstream area	0.314*	-0.052	-0.482**
Log CC1	0.097	-0.006	0.493**
Log CC2	0.054	-0.036	0.520**
Log CC3	0.101	-0.004	0.489**
Log CC4	0.058	-0.017	0.533**

2.3.2.Regression of Erosion rate (kg $ha^{-1}yr^{-1}$)

All independent variables were correlated with the dependent variables to establish which independent variables should be input into the model (see Table 2.10).The variable sinuosity has a significant relationship with upstream area and channel confinement version 2 (R=0.287 and R=-0.257 respectively). However the strength of these relationships is weak and some level of collinearity is unavoidable as noted by Field (2005), therefore it is not necessary to remove this variable from the multiple regression analysis. Furthermore, the tolerance statistic from regression analysis can be used to check that multicollinearity is not a problem when these variables are used together. This statistic expresses the proportion of variability of each independent variable that is not explained by its linear relationships with other independent variables and should be >0.1 (Norušis, 2005).

Upstream area and sinuosity both show a statistically significant relationship with erosion rate (at the 99 and 95% levels respectively) and therefore were both included within the regression model. The variable slope was not included within this regression model as this showed a very weak relationship with erosion rate (-0.047). None of the channel confinement variables showed a statistically significant relationship with erosion rate (kg ha^{-1} yr^{-1}). However variables with an R value >0.100 or <-0.100 were included within initial regression models, as whilst individual variables may not be statistically significant, when combined with other variables they may show a significant relationship and enhance the R and R^2 values produced by the model. The version of channel confinement to be used will be version 3 (Mackay and Bridge, 1992) as this has the largest correlation with erosion rate out of the 4 channel confinement variables (1: R=0.097; 2: R=0.054; 3: R=0.101; 4: R=0.058). The three independent variables that will be entered into the regression model for dependent variable erosion kg ha^{-1} yr^{-1} will therefore be upstream area, sinuosity and channel confinement version 3.

Figure 2.10 shows scatterplots of each of log values of erosion rate and each of the independent variables to be entered into the model. It can be seen that as upstream area, sinuosity and valley confinement version 3 increase the erosion rate also increases. Although when considered individually none of the

independent variables show a high correlation with the dependent variable, it is possible that a combination of the independent variables may explain more of the variance in the dependent variable. (Norušis, 2005).

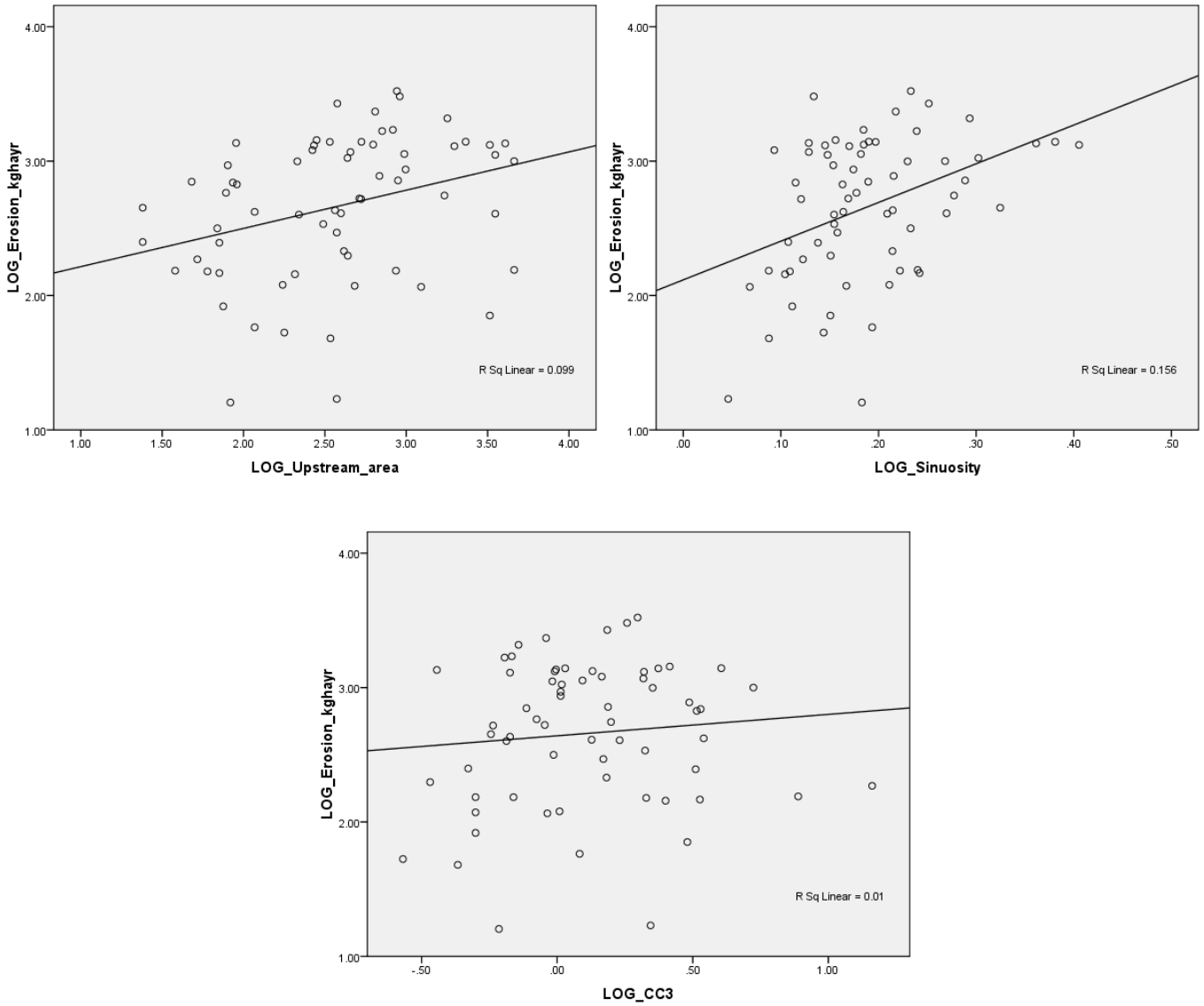

Figure 2.10: Scatter plots of the dependent variable (Erosion kg ha^{-1} yr^{-1}) against each independent variable entered into the regression model.

A regression analysis was performed on the data before removing values for the Wylye sub-catchment (geo-referencing errors) and produced R=0.459 and R^2=0.211. Whilst the values for the Wylye sub-catchment did not all produce large residuals for this initial regression analysis or erosion rate m yr^{-1}, due to the observed error in the data set this regression analysis was run with the 1926 Wylye data removed.

The regression output is shown in Table 2.11. From this it can be seen the absolute correlation between the three independent variables and erosion rate (R value) is 0.460. The regression model explains 21.1% of the variance. The adjusted R squared value indicates how well the model generalises and how well the regression equation would perform on another sample. As the R^2 and adjusted R^2 values are similar (0.211 and 0.172 respectively) this indicates the model generalises well. Figure 2.11 shows the observed and predicted values, regression line, and 95% confidence and prediction intervals. The 95% confidence intervals are calculated using the standard error of the predicted mean value, hence the confidence interval is narrowest for values close to 2.66 (the sample mean). Several of the data points do not fall within these lines as the interval predicts for mean values, not individual cases (Norušis, 2005). The wider dashed lines indicate the 95% prediction intervals for individual cases; these are calculated using the standard error of individual prediction. As the standard error of the individual prediction is always larger than the standard error of the mean prediction the prediction intervals are always larger than the confidence intervals (Norušis, 2005).

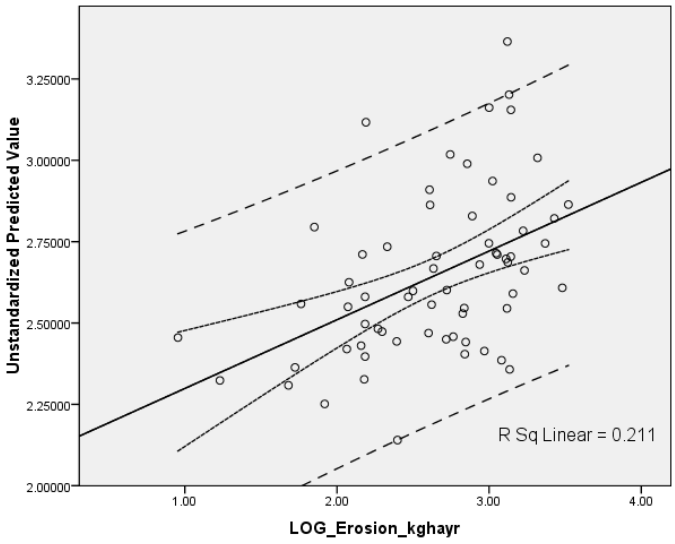

Figure 2.11: Scatterplot of observed vs. predicted values of width averaged retreat rate (m m^{-1} yr^{-1}) and the regression line after geo-referencing errors removed. The fine dashed lines indicate the 95% confidence intervals, and the wider dashed lines in

The regression model produces a predictive equation as shown below:

$$Log_{10}Erosion\ rate = 1.650 + (0.195 \times Log_{10}Upstream\ area) + (2.545 \times Log10Sinuosity + (0.160Log10Channel\ confinement\ v3)$$

Table 2.11: Regression output for dependent variable erosion kg^{-1} ha^{-1} yr^{-1}.

R	R Square	Adjusted R Square	Durbin-Watson	ANOVA F	Sig.
0.460	0.211	0.172	1.509	5.443	0.002

Variable	Unstandardized coefficients		Beta	t	Sig.	Tolerance
	B	Std. Error				
(Constant)	1.650	0.290		5.694	0.000	
Log Sinuosity	2.545	0.888	0.341	2.867	0.006	0.912
Log Upstream area	0.195	0.110	0.211	1.768	0.082	0.911
Log CC3	0.160	0.185	0.099	0.865	0.391	0.990

The t statistic of the regression model indicates the significance of the contribution of an independent variable to the model. From Table 2.11, we can reject the null hypothesis (that the independent variables do not contribute significantly to the regression model) for the variable sinuosity at the 99% level (as p=0.006). However the t statistic indicates the variables upstream area and channel confinement do not contribute significantly to the model (p=0.082 and 0.391 respectively). The model was re-run with these variables removed and the model's R and R^2 values significantly decreased (R=0.397 and R^2=0.157). Therefore these variables were left within the model.

2.3.2.1. Residuals

By examination of the residuals and their relationships to other variables entered into the regression model it is possible to detect any violation of assumptions required for multiple regression analysis. Residuals are the prediction errors of the regression model and can be used to identify observations that deviate sharply from the predictions (Allison, 1999). The residuals of the regression are shown in Appendix A Table 81. 99% of the

standardized residuals should be between -2.58 and +2.58 (Norušis, 2005). According to this there is only one observation value which the model does not predict well; Wylye no.11, WFD 33 (-3.12). This sub-catchment has the lowest value of erosion rate (9kg/ha.yr). Regression models often have less accuracy when predicting high and low values which explains the occurrence of these residuals. However, this case does not have a significant influence on the regression coefficients on the model as it does not have a significant leverage value (see Figure 2.15) and therefore removing this would not significantly alter the regression coefficients (see Figure 2.16).

Figure 2.12 indicates the spread of the residuals does not change over the range of the independent variable; the assumption of constant variances is not violated. Figure 2.13 indicates the linearity assumption is not violated as the relationship between the residuals and the independent variables shows a strong linear relationship.

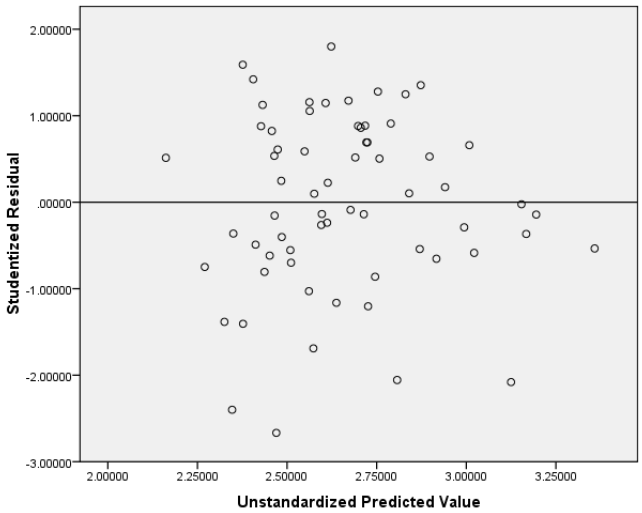

Figure 2.12: Scatterplot of residuals against predicted values of dependent variable to check the assumption of constant variance.

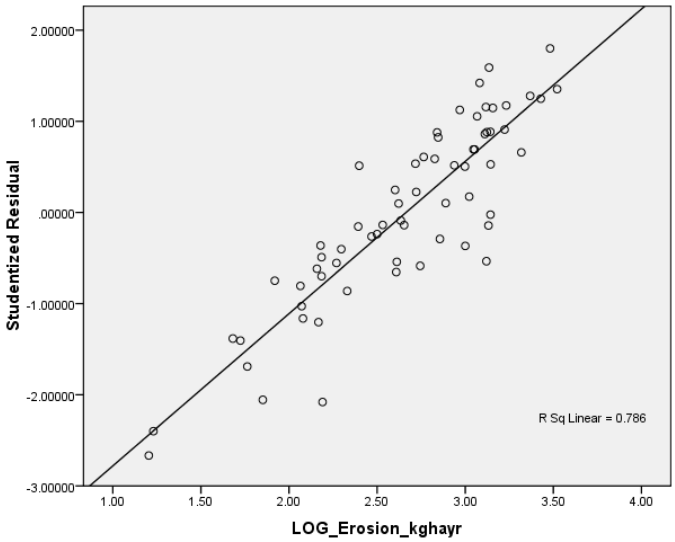

Figure 2.13: Scatterplot of residuals against the independent variable to check the linearity assumption. The linear relationship between the dependent variable and residuals indicates this assumption of regression is not violated.

The ANOVA F statistic = 5.443, p =0.02 indicates that there is a linear relationship between erosion rate and the independent variables. The Durbin-Watson statistic ranges from 0 to 4 and a value of ~2 indicates there is no correlation between successive residuals. Norušis, 2005 indicate this value should be between 1.5 and 2.5. The value of the Durbin-Watson statistic is 1.509 indicates the assumption of independence is not violated. As shown in the model output (Table 2.11) the tolerance statistics are all above 0.1 (0.912, 0.911, 0.990) and therefore multicollinearity is not an issue within the model.

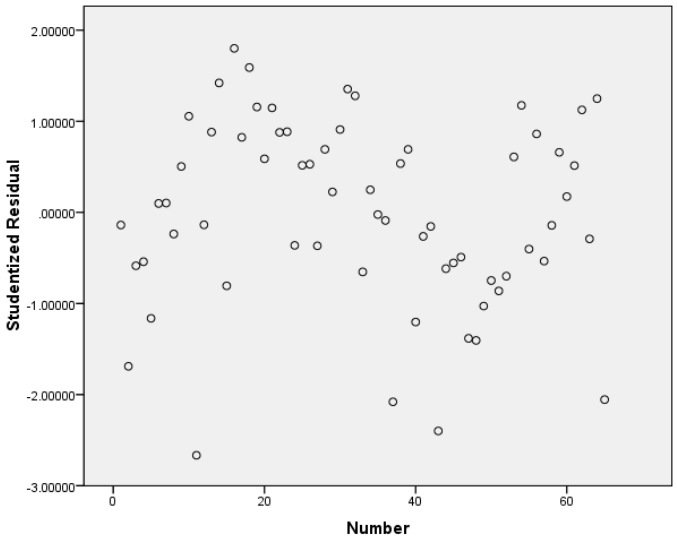

Figure 2.14: Scatterplot of residuals against case number to check the assumption of independence.

Centred leverage values should be plotted to see if unusual values are having a large influence on regression coefficients. Leverage is the distance between the values of independent variables for a case and the average for all cases, and high leverage values are calculated as >2p/N (where p is the number of independent variables, and N is the number of cases (Norušis, 2005). From Figure 2.15 two leverage points may be identified as points 45 and 1 (Sarre Penn 5 and Avon 5 respectively). Number 45 had the largest value of channel confinement ratio; 14.5, the second largest being just 7.74. Case 1 had the joint lowest upstream catchment area (24 km^2). Neither case number 1 or 45 produces a high residual (-0.12 and -0.49). Additionally, the Cook's value (see Figure 2.16) for these two cases are low; Cook's leverage value indicates the magnitude of the change in the regression coefficient if a case is removed, therefore the regression coefficients would not change significantly if these two cases were removed.

The high residual value (case 11, Wylye) is classified as a high leverage value. However, the Cook's value is low which explains why when removing this case the regression coefficient does not change much (R= 0.464 R^2= 0.215).

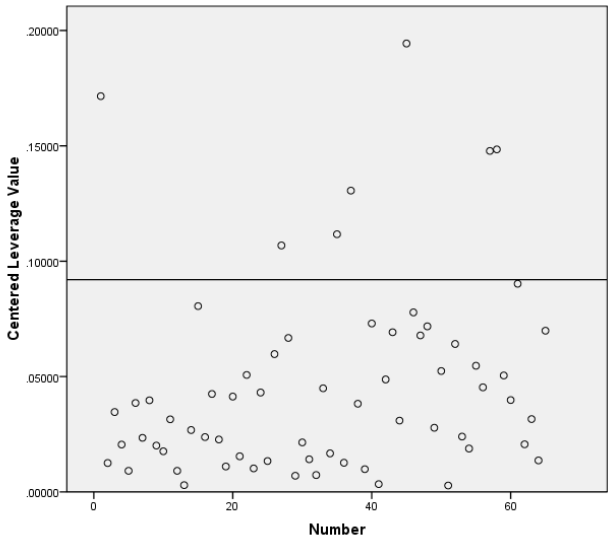

Figure 2.15: Centred Leverage average values for each case.

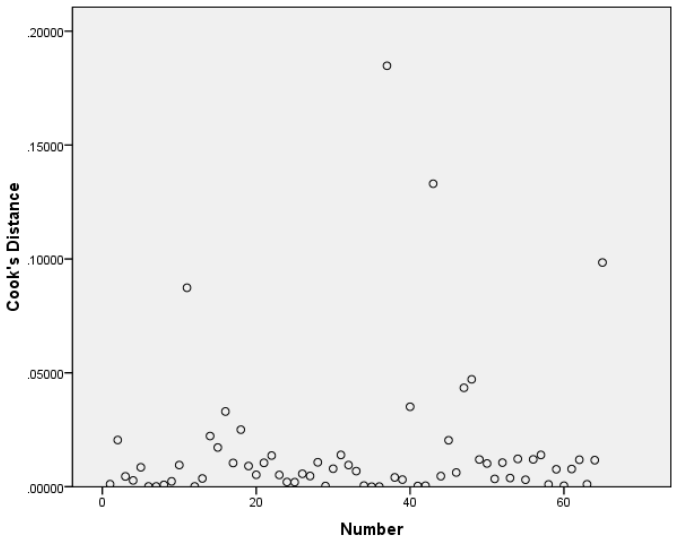

Figure 2.16: Cook's leverage value for each case.

2.3.3. Regression of Width averaged retreat rate m m^{-1} yr^{-1}

The variables upstream area and channel confinement both show a statistically significant relationship with width averaged retreat rate at the 99% level and will therefore be included within this regression model. For the regression analysis of width average retreat rate, the version of channel confinement to be used will be version 4 (Williams, 1986) as this has the largest correlation with erosion rate out of the 4 channel confinement variables (1:

R=0.493; 2: R=0.520; 3: R=0.489; 4: R=0.533). As before, variables with a correlation >0.100 or <-0.100 will also be included within initial regression models. Therefore both slope and sinuosity were also included within the regression model (R=0.196 and R=-0.219 respectively). The four independent variables that will be entered into the regression model for dependent variable erosion width averaged retreat rate m m^{-1} yr^{-1} will therefore be upstream area, sinuosity, slope and channel confinement version 4.

Figure 2.17 shows scatterplots of each of log values of width average retreat rate and each of the independent variables to be entered into the model. It can be seen that as upstream area and sinuosity increase the width average retreat rate also decreases, whilst as slope and channel confinement increase width average retreat rate also increases.

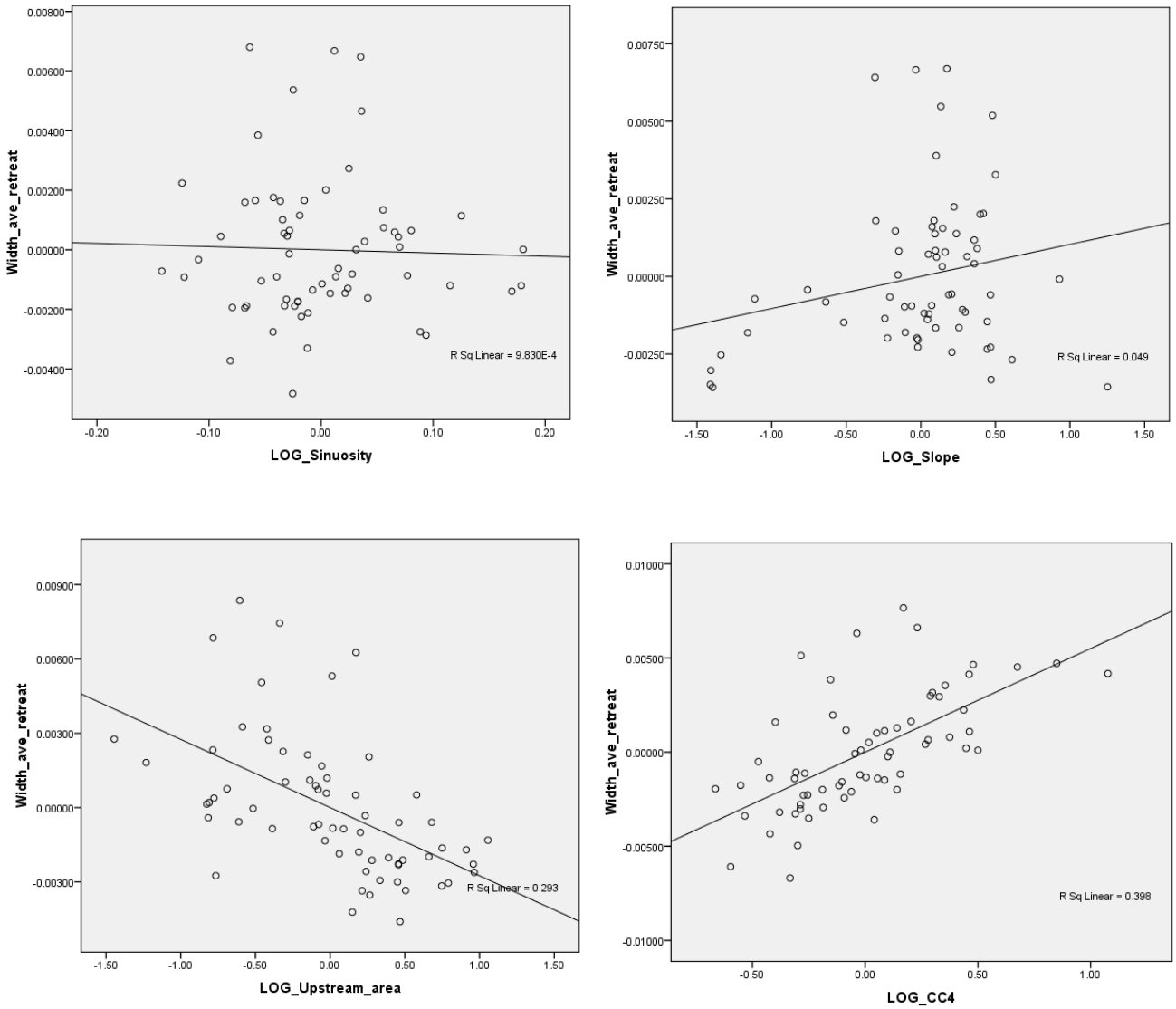

Figure 2.17: Scatterplots of dependent variable (width averaged retreat rate) against independent variables input into the regression model (sinuosity, slope, upstream area, channel confinement version 4).

The regression output is shown in Table 2.12. From this it can be seen the absolute correlation between the three independent variables and erosion rate is 0.790. The regression model explains 62.4% of the variance. As the R^2 and adjusted R^2 values are similar (0.624 and 0.599 respectively) indicating the model generalises well. Figure 2.18 shows the observed and predicted values and the fit of the regression line.

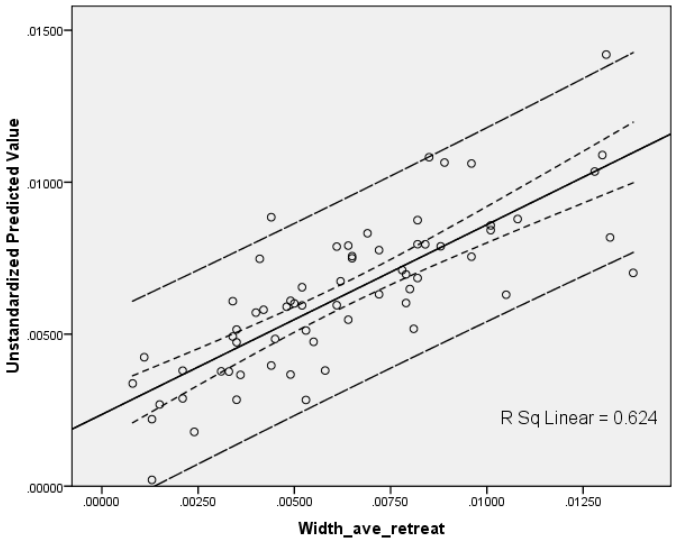

Figure 2.18: Scatterplot of observed vs. predicted values of width averaged retreat rate (m m-1 yr-1) and the regression line after geo-referencing errors removed. The fine dashed lines indicate the 95% confidence intervals, and the wider dashed lines indicate the 95% prediction intervals.

The regression model produces a predictive equation as shown below:

$$Width\ averaged\ retreat\ rate = 0.015 - (0.003 \times Log_{10} Upstream\ area) + (0.001 \times Log_{10} Sinuosity) + \left(0.001 \times Log_{10}(Slope + 0.0001)\right) + (0.005 \times Log_{10} Channel\ confinement\ v4)$$

Table 2.12: Regression output for dependent variable width averaged retreat rate.

R	R Square	Adjusted R Square	Durbin-Watson	ANOVA F	Sig.
0.790	0.624	0.599	1.707	24.932	0.000

Variable	Unstandardized coefficients		Beta	t	Sig.	Tolerance
	B	Std. Error				
(Constant)	0.015	0.002		9.458	0.000	
Log Sinuosity	0.001	0.004	0.012	0.138	0.890	0.899
Log Slope	0.001	0.000	0.183	2.258	0.028	0.949
Log Upstream area	0.003	0.000	-0.486	-5.820	0.000	0.899
Log CC4	0.005	0.001	0.595	7.463	0.000	0.985

From Table 2.12, we can reject the null hyposthesis (that the independent variables do not contribute significantly to the regression model) for the variables upstream area and channel confinement at the 99% level, and slope at the 95% level. However, the t statistic is not significant for the variable sinuosity, indicating this does not contribute significantly to the model (t=0.138, p=0.890). Therefore the model was re-run with this independent variable removed from the model (see section 2.3.4. p131).

2.3.3.1. Residuals

The residual values (see Appendix A Table 82) indicate there is only one observation value which the model does not predict well; Bourne no.5, WFD 23. This sub-catchment has one of the highest width-averaged retreat rate for the whole dataset. As noted previously, regression models often have less accuracy when predicting high and low values which may partly explain the occurrence of this residual. Appendix A Figure 122 shows a histogram and a P-P plot indicating that the standardized residuals are normally distributed.

Figure 2.19 indicates the spread of the residuals does not change over the range of the independent variable; the assumption of constant variances is not violated. Figure 2.20 indicates the linearity assumption is not violated as the relationship between the residuals and the independent variables shows a

strong linear relationship. Additionally, the ANOVA F statistic = 5.434, p =0.002 meaning we can reject the null hypothesis that there is no linear relationship between erosion rate and the independent variables. Figure 2.21 indicates the independence assumption is not violated as there is no relationship between each residual. Additionally, the value of the Durbin-Watson statistic is 1.707 which indicates the assumption of independence is not violated. As shown in the model output (Table 2.12) the tolerance statistics are all above 0.1 (0.899, 0.945, 0.899, 0.985) and therefore multicollinearity is not an issue within the model.

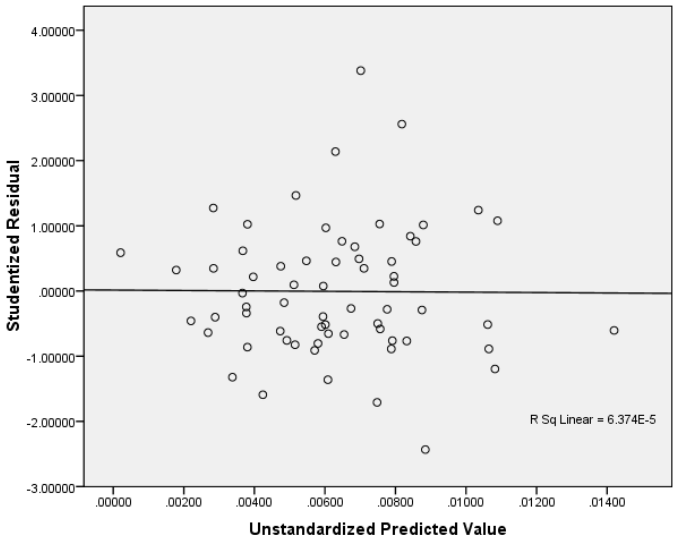

Figure 2.19: Scatterplot of residuals against predicted values of dependent variable to check the assumption of constant variance.

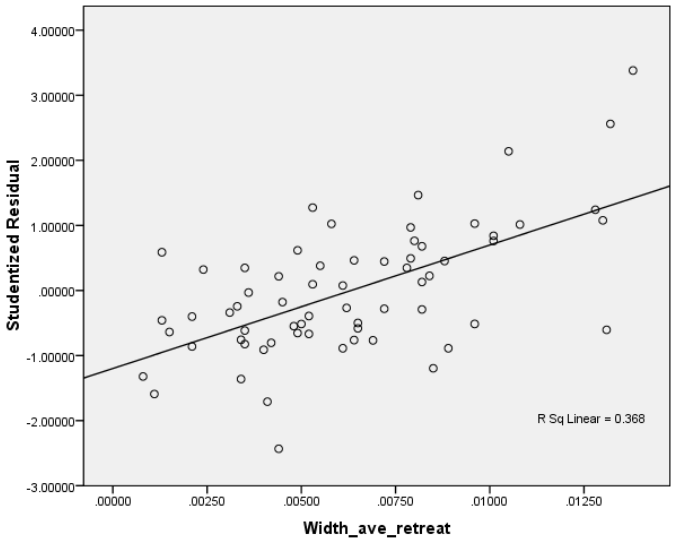

Figure 2.20: Scatterplot of residuals against the independent variable to check the linearity assumption.

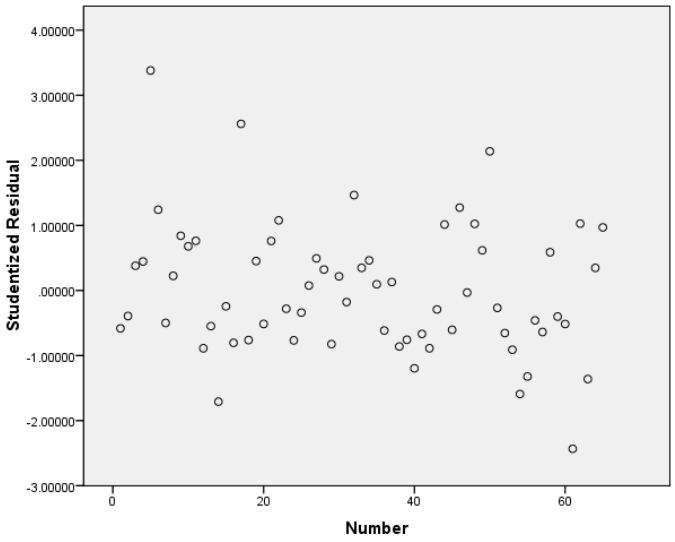

Figure 2.21: Scatterplot of residuals against case number to check the assumption of independence.

From Figure 2.22 four leverage points may be identified as points 45, 61, 52 and 1 (Sarre Penn 5, Munnow 1, Itchen 30 and Avon 5). Case 45 had the largest value of channel confinement ratio; 14.5, the second largest being just 7.74. Case 61 has the steepest slope gradient; 0.064, and the second steepest is just 0.019. Case 52 has the second smallest upstream area (38 km^2). Case 1 had the joint lowest upstream catchment area (24 km^2). Cook's leverage value indicates the magnitude of the change in the regression coefficient if a case is removed. Neither cases 45,52 or 1 has high residuals (-0.54, -0.59, and -0.52 respectively) and the cook's value (see Figure 2.23) indicates the regression coefficients would not change significantly if they were to be removed and the model re-run.

Case 61, Munnow is not classified as a high residual as it is not >2.5 or <-2.5. However, this case does produce the lowest residual from the dataset (-2.19) meaning the model over predicts the width averaged retreat rate for this variable. From Figure 2.23 it can be seen that removing this variable will have the most significant impact on the regression coefficients. Therefore, this case was removed from the data set and the regression analysis was re-run.

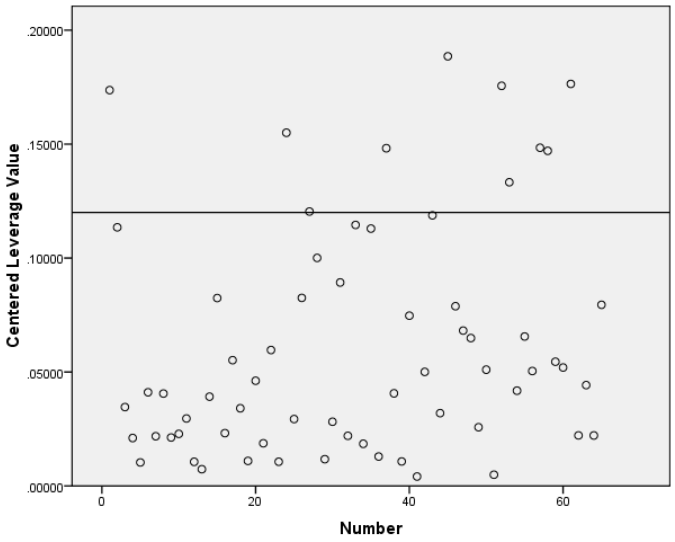

Figure 2.22: Centred leverage values for each case, (width averaged retreat after removing geo-referencing errors).

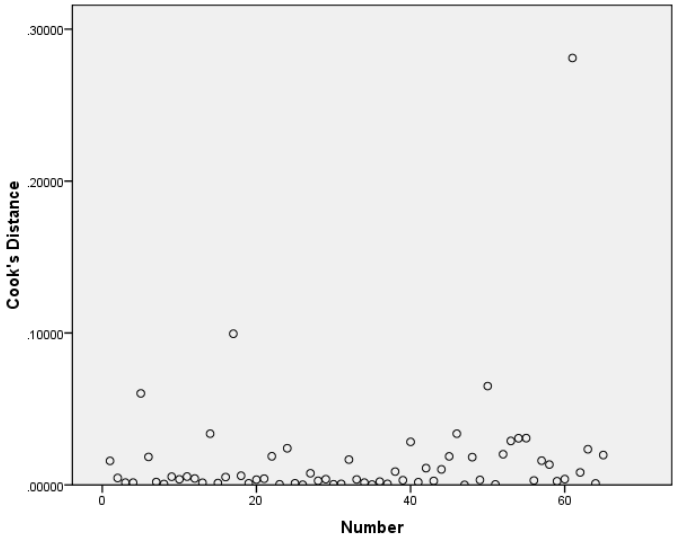

Figure 2.23: Cook's leverage values for each case, (width averaged retreat after removing geo-referencing errors).

2.3.4. Regression of Width averaged retreat rate m m^{-1} yr^{-1} removing case 61 and sinuosity variable

The regression model to estimate erosion as a width averaged retreat rate was re-run removing case 61 and the variable of sinuosity, and the results of the updated model are shown in Table 2.13. The absolute correlation between the three independent variables and erosion rate is 0.812 (compared

to 0.790 from the previous model). The regression model explains 66.0% of the variance. The R^2 and adjusted R^2 values are 0.660 and 0.643 respectively, which is an improvement upon the previous model (0.624 and 0.599 respectively). These results indicate the revised regression model (removal of case 61 and independent variable sinuosity) has greater accuracy when reproducing the observed values of bank erosion from the dataset. Figure 2.24 shows the observed and predicted values, regression line, and 95% confidence and prediction intervals.

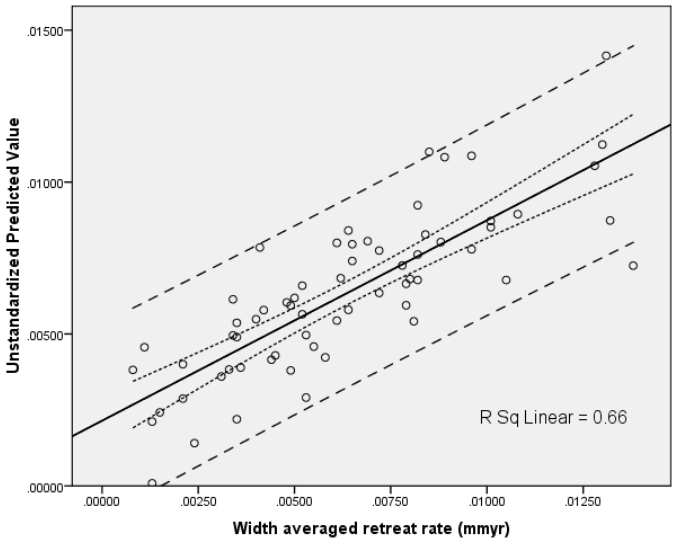

Figure 2.24: Scatterplot of observed vs. predicted values of width averaged retreat rate (m m^{-1} yr^{-1}) and the regression line after geo-referencing errors and case 61 removed. The fine dashed lines indicate the 95% confidence intervals, and the wider dashed lines indicate the 95% prediction intervals.

The regression model produces a predictive equation as shown below:

$$Width\ averaged\ retreat\ rate = 0.017 - (0.003 \times Log_{10} Upstream\ area) + \left(0.001 \times Log_{10}(Slope + 0.0001)\right) + (0.005 \times Log_{10} Channel\ confinement\ v4)$$

Table 2.13: Regression output for dependent variable width averaged retreat rate after case 61 removed, and sinuosity not input as a variable into the model.

R	R Square	Adjusted R Square	Durbin-Watson	ANOVA F	Sig.
0.812	0.660	0.643	1.628	38.749	0.000

Variable	Unstandardized coefficients		Beta	t	Sig.	Tolerance
	B	Std. Error				
(Constant)	0.017	0.002		10.242	0.000	
Log Slope	0.001	0.000	0.233	3.074	0.003	0.989
Log Upstream area	0.003	0.000	-0.509	-6.717	0.000	0.990
Log CC4	0.005	0.001	0.565	7.497	0.000	0.998

2.3.4.1. Residuals

Residuals of the regression are shown in Appendix A Table 83. According to this there is only one observation value which the model does not predict well; Bourne no.5, WFD 23. As noted previously this sub-catchment has a high width averaged retreat rate. Appendix A Figure 123. shows a histogram and a P-P plot indicating that the standardized residuals are normally distributed.

The ANOVA F statistic = 38.749, p =0.000 indicates that there is a linear relationship between erosion rate and the independent variables. The value of the Durbin-Watson statistic is 1.628 indicates the assumption of independence is not violated. As shown in the model output (Table 2.13) the tolerance statistics are all above 0.1 (0.989, 0.990, 0.998) and therefore multicollinearity is not an issue within the model.

2.3.5. Final correlations

The final correlations between bank erosion rate and the independent variables are shown in Table 2.14. The regression coefficients are also shown. The regression coefficients and, correlation coefficients when bank erosion rate

is calculated as width averaged retreat rate are higher than when calculated as a sediment volume. This is likely to be due to the error introduced to the bank erosion calculation when calculating a volume of sediment through bank height and sediment density estimation.

Table 2.14: Final correlations between dependent and independent variables. Yellow indicates a significant relationship at the 95% level, and red at the 99% level. Asterix indicate variables included into the regression equations, the coefficients for which are shown at the bottom of the table.

	Log Erosion (kg ha^{-1} yr^{-1})	**Width averaged retreat (m m^{-1}yr^{-1})**
Log Sinuosity	0.397*	-0.214
Log Slope	-0.046	0.263*
Log Upstream area	0.315*	-0.544*
Log CC1	0.091	0.529
Log CC2	0.047	0.549
Log CC3	0.095*	0.525
Log CC4	0.052	0.569*
R	0.460	0.812
R^2	0.211	0.660

2.3.6. Analysis of residuals

In this section, individual data points from the regression analysis with high residual values will be analysed in further detail. As noted previously, high residuals are classified as those with a value of >2.5 or <-2.5. Using this classification, each of the regression analyses only produced one high residual, indicating the models accurately represent the dataset.

As noted in the methodology, Land Cover Map 2007 data was obtained through CEH (Centre of Ecology and Hydrology). This was used to obtain land-use classifications for sub-catchments. Individual classifications used and their

descriptions can be found in Appendix A Figures 119 and 120. Geology data for sub-catchments was also obtained from Digimap. Vegetation and geology characteristics were analysed within sub-catchments too deduce if these factors could account for differences between GIS estimates and regression predicted values of bank erosion.

2.3.6.1. Residuals from Erosion kg ha^{-1} yr^{-1} regression: Number 11 Wylye Residual value -3.12 (Model over predicts)

As noted previously, this sub-catchment has the lowest value of erosion rate (11kg ha^{-1} yr^{-1}). Regression models often have less accuracy when predicting high and low values which may partly explain the occurrence of this residual. Due to the significance of upstream catchment area within the regression model, this could partly explain the error in prediction of this data point.

The geology type observed in the sub-catchment is a combination of sandstones, mudstones, and chalk. Catchments of different geologies show variations in the relationship between discharge and catchment area (Chaplin, 2005). Sandstones and chalk geologies have high rates of permeability (up to 20 and 5 m day^{-1} respectively). This means infiltration rates where these geologies are present will be high, resulting in low rates of surface runoff and lower discharge within channels. Consequently, bank erosion rates in these areas may be lower than predicted by the model, as geology is not accounted for within the model. However, as noted in Table 2.17, chalk and sandstone have a low value of strength compared to lithologies observed in other sub-catchments. This should result in increased bank erosion rates.

2.3.6.2. Comparison of residuals (Erosion kg ha^{-1} yr^{-1} regression) and land-use and geology

Land-cover classifications in the area according to the Land Map 2007 data included arable and horticulture, grassland, woodland, heather, and urban. The majority of the catchments were arable and horticulture and grassland. The average residual value for each classification is shown in Table 2.15. Urban may areas appear to be associated with negative residuals, which could be due

to associated construction and bank protection in these areas resulting in a decrease in bank erosion. However it should be noted that this land classification was only observed in 3 sub-catchments, therefore this would require further analysis to draw significant conclusions. Clay catchments appear to be related to areas of positive residuals, which could be a result of lower rates of permeability causing increased runoff and discharge peaks, resulting in increased bank erosion. However there were only 4 sub-catchments observed with this geology type and further analysis would be required to draw significant conclusions from this.

Table 2.15: Average residual value for each land cover and geology classification for regression of erosion rate (kg ha^{-1} yr^{-1}).

Classification	Residual
Arable and horticulture	0.01
Grassland	-0.17
Woodland	-0.21
Heather	0.60
Urban	-1.19
Mudstone	-0.02
Sandstone	-0.12
Clay	1.08
Chalk	-0.04

2.3.6.3. Correlation of residuals with dependent variables

Un-standardised residuals were correlated with dependent variables used in the regression model (sinuosity, upstream catchment area and channel confinement v3). The results of the correlation are shown in Table 2.16. This indicates none of the dependent variables individually contribute significantly to the error in the regression model.

Table 2.16: Correlation of un-standardised residuals with dependent variables for regression of erosion rate (kg ha^{-1} yr^{-1}).

	Correlation	Significance
Log_Sinuosity	0.000	1.000
Log_Upstream area	0.000	1.000
Log_CC3	0.109	0.385

2.3.6.4. Residuals from Width average retreat m m^{-1} yr^{-1} regression: Number 5 Bourne - Residual value 3.39 (Model under predicts)

As noted previously, this sub-catchment has the highest width averaged retreat rate for the whole data set (0.0138m m^{-1} yr^{-1}). Regression models often have less accuracy when predicting high and low values which may partly explain the occurrence of this residuals.

The geology type in this catchment is chalk (Newhaven and Seaford formations). As noted in Table 2.17, chalk has a low value of strength compared to lithologies observed in other sub-catchments. This may result in an increase in bank erosion rates. As geology is not accounted for by the regression model, this may partly explain the difference between bank erosion rates estimated from GIS and those predicted using the regression model. However as noted previously (section 2.3.6.1), chalk is a permeable lithology, which may result in a decrease in bank erosion (due to decreased runoff and discharge). The difference between the influence of geology between these two residuals could be due to the combination of lithologies observed in the previous example (Wylye - Sandstone, mudstone and chalk) compared to this example (Bourne - chalk only). In the previous example the variation of lithologies may result in a higher shear strength of bank material, thereby the resulting effect is the increased permeability of the lithology (resulting in decreased bank erosion, and the model over predicts). In this example, as only chalk is present the resulting effect is the low shear strength of channel banks (resulting in an increase of bank erosion, and the model under predicts).

Table 2.17: Relative rock strength. Taken from Look (2007).

Uniaxial compressive strength (MPa)	*Strength*	*Rock classification*		
		Sedimentary	*Metamorphic*	*Igneous*
10	Lowest	Salt, Chalk		Welded tuff
20	↑	Shale, Coal, Gypsum, (2) Triassic sandstone, Jurassic limestone		Porphyry, Granadiorite
40	↕	Mudstone, Sandstone, Clay – Shale	Phyllites	
60	↕	Carboniferous sandstone, Limestone, (2) Dolomite, Siltstones	(2) Schist, Micaschists	Granadiorite
80	↕		Slate, Quartzite	Granite, Rhyolite Serpentinite
100	↕	(2) Carboniferous limestone, Dolomite, Siltstone, (2) Sandstone	(2) Marble, Schist Quartzites	Granite, Pegmatites
150	↕	Greywackes	Gneiss	(2) Granite, Granadiorite, Rhyolite
200	↕		Quartzite	Granite, Diorite
250	Highest		Hornfels	Basalt

2.3.6.5. Comparison of residuals (Width average retreat m m^{-1} yr^{-1}) regression with land-use and geology

The average residual value for each land-cover and geology classification is shown in Table 2.18. Heather may be related to areas of negative residual, which could be due to the presence of Heather on acidic soils such as heathlands and moorlands, which are relatively infertile with low-growing vegetation. As noted in the literature review (section 1.1.5.5) reduced vegetation cover may increase bank erosion rates, and therefore areas with Heather as the dominant land classification may show increased rates of bank erosion. It should be noted that this land classification was only observed in 2 sub-catchments and therefore further analysis would be required to draw significant conclusions from this. Chalk catchments may be related to areas with high positive residual values, and clay catchments may be related to areas of negative residuals. However there were only 4 sub-catchments observed with these geology types and therefore further analysis is required to draw significant conclusions from this.

Table 2.18: Average residual value for each land cover and geology classification from regression of width average retreat rate.

Classification	Residual
Arable and horticulture	0.13
Grassland	-0.19
Woodland	0.20
Heather	-0.58
Urban	0.28
Mudstone	-0.28
Sandstone	0.07
Clay	-0.66
Chalk	0.46

2.3.6.6. Correlation of residuals with dependent variables

Un-standardised residuals were correlated with dependent variables used in the regression model (slope, upstream catchment area and channel confinement v4). All correlations were 0. This indicates none of the dependent variables individually contribute significantly to the error in the regression model.

In addition to factors analysed here (vegetation/land-use and geology) other factors not accounted for by the model may result in differences between the estimated GIS bank erosion rates and the regression model predicted values. These include channel bank soil properties, over-grazing of cattle, channel flow regime, and channel geometry. Therefore, in the following chapter the influence of channel geometry on migration rates will be analysed in further detail using channel migration models.

2.4.Conclusions

The bank erosion rates observed within this study from GIS data indicate that in several catchments within England and Wales bank erosion generates a significant volume of sediment. Additionally, the variability of bank erosion rates both within and between catchments was noted. Bank erosion rates vary both spatially and temporally due to the numerous factors which influence bank erosion, and their complex inter-relation.

The statistical analysis has shown that sinuosity and upstream area significantly influence bank erosion rates (when calculated as a volume in kg ha^{-1} yr^{-1}), and upstream area, slope, and channel confinement significantly influence bank erosion rates when calculated as a width averaged retreat rate (m m^{-1} yr^{-1}). The regression analysis indicates that the variables sinuosity, upstream area and channel confinement have a correlation coefficient of 0.460, and explain 21% of the variance of bank erosion rates calculated as a volume in kg ha^{-1} yr^{-1}. The variables upstream area, slope, and channel confinement have a correlation coefficient of 0.812, and explain 66% of the variance of bank erosion rates calculated as a width averaged retreat rate in m m^{-1} yr^{-1}. The difference in the strength of the correlation and regression coefficients between the two forms of dependent variable is due to the error induced when calculating erosion rates as a volume (kg ha^{-1} yr^{-1}), as this requires an estimation of channel bank height and floodplain sediment density. Calculation of bank erosion rates as a width averaged retreat rate (m m^{-1} yr^{-1}) does not require estimation of these variables, and therefore the error in calculation of bank erosion rate is smaller.

Both regression analyses produced only one high residual each, indicating the adequacy of the regression equation to represent the data. These residuals are likely to be the result of factors not included within the regression model (such as geology, lithology, land-use etc.).

Several assumptions are involved with regression analysis;

- All observations are independent
- A linear relationship exists between the dependent and the independent variables

- For each value of the independent variable there is a normal distribution of values of the dependent variable
- The distributions have the same variance.

Analysis of each regression model output was conducted to check none of the assumptions of regression were violated. Durbin-Watson and collinearity statistics were used to ensure the assumption of independent observations was met. Scatter plots of all independent variables against the dependent variables were used to check relationships were linear. It was noted that the relationship between sinuosity and bank erosion was not completely linear when measuring erosion as a width averaged retreat rate (m m^{-1} yr^{-1}); this was therefore not included in this regression model. Additionally scatterplots of residual values were used to confirm a linear model was suitable for the data. To ensure the assumption of equal variance is met the distribution of residual values from the regression models was analysed; residual values should be normally distributed if variance assumption is true. Model outputs were also checked for the existence of influential points by analysing Centred Leverage Values and Cook's distance. These tests ensured all data points should contribute approximately equally to the model, any data points which significantly altered model coefficients were removed. From this analysis it was clear that the assumptions required for regression analysis were true and therefore a linear regression analysis was a suitable method of analysis for this data set.

The limitations of the regression modelling approach primarily include the omission of additional dependent variables which influence bank erosion as indicated in Figure 2.1, such as land-use, geology, climate etc. The influence of land cover type and geology was considered when analysing residuals from the regression models, and the possible influence of chalk catchments resulting in the model under estimating bank erosion rates (producing positive residual values) was noted. Additionally the regression approach used in this study does not give any provide a means of assessing the variability of bank erosion and/or relationships between bank erosion and controlling factors across England and Wales. Further analysis could include an assessment of the spatial variability of these factors.

Only one set of coefficients was used in each of the regression equations produced in this chapter. Further analysis of the relationships could be performed using methods such as monte-carlo analysis; varying the values and combinations of coefficients within the model equations to produce multiple sets of equations. This would enable quantification of uncertainty within the estimation of coefficient values, and also further analysis of the sensitivity of the equations to these parameters.

Before regression analysis was performed the independent variables were correlated to check for collinearity and interaction between independent variables. Additionally, the tolerance statistics from model outputs were checked to ensure multicollinearity was not an issue within the models. Further analysis to investigate interaction between variables, (and a measure of the accuracy of the model vs. the number of parameters) could be conducted by means of the Akaike information criterion (AIC).

Whilst the regression model is based on data taken from several catchments from within England and Wales, inclusion of additional catchments within the data analysis process would result in greater confidence in correlations and regression models produced. Due to time constraints of the study it was not possible to increase the spatial coverage of the data. The spatial coverage of the data is still considerable in comparison to similar previous studies and therefore the findings from this study build upon existing literature.

The methodology used within this chapter has enabled identification of factors influencing bank erosion and their relative significance. The bank erosion model to be developed using this information will provide an annual estimate of bank eroded sediment. Therefore, any errors and limitations within the methodology used within this chapter should not have a significant effect on the accuracy of this bank erosion model.

In the following chapters, the relationship between bank erosion rate and channel sinuosity will be analysed over longer time scales using channel migration models. Additionally, the influence of upstream area, sinuosity, and channel confinement, will be incorporated within an existing bank erosion model, with the aim of improving the predictive capabilities of the model by

inclusion of additional physical factors which have been shown in this chapter to influence bank erosion rates.

3.Analysis of sinuosity and channel bank erosion

3.1. Introduction

In the previous chapter the relationship between bank erosion and sinuosity over a time period of ~150 years (depending on the catchment) was analysed. It was noted this relationship was non-linear and there was a threshold value of sinuosity at which bank erosion rates were greatest. This chapter aims to analyse this relationship in greater detail and establish the value of such a threshold in sinuosity.

To enable estimation of change in bank erosion rates as a result of climate change it is important to consider changes in the river planform (such as sinuosity) over longer time periods. Channel sinuosity is expected to change with a change in climate, due to changing river discharge patterns as a result of changes to precipitation. Including the relationship between sinuosity and bank erosion within bank erosion models will allow the models to be used to assess the impact of climate change on sediment production from bank erosion processes.

In this chapter an existing meander migration model will be used to analyse the long-term relationship between channel sinuosity and bank erosion rate. Model outputs are used for this analysis as they are the only means of generating a data set covering a sufficiently long time period. The migration model chosen for the analysis is the Howard and Knutson (1984) model, which is a kinematic migration model where erosion rates are related to channel curvature (for further details see previous chapter). The model was run for a range of parameter values, corresponding to those of natural channels within the UK, and the relationship between channel sinuosity and bank erosion over long time scales (greater than 400 years) was analysed.

3.1.1. Aims and objectives

The objectives of this chapter are:

- Evaluate the performance of existing meander migration models when run for UK catchments.
- From meander migration model outputs, produce a long-term data set of channel sinuosity and bank erosion rates.
- Analyse the long-term relationship between sinuosity and bank erosion rate.
- Identify the existence of any threshold values of sinuosity influencing bank erosion rates.
- Provide a computationally efficient alternative to radius of curvature as a parameter for use in bank erosion models.

From the results in the previous chapter it is clear that the relationship between bank erosion rate and sinuosity is non-linear (similarly to that of radius of curvature and bank erosion rate). Therefore, this chapter aims to identify the presence of any sinuosity thresholds which may influence bank erosion rates.

The long-term relationship between sinuosity and bank erosion rate within river channels will be analysed. The results from the GIS data from the previous chapter cover a period of approximately 150 years and therefore are insufficient to provide a long-term relationship between sinuosity and bank erosion for the time-scale required. No observational data exists over time scales long enough for such an analysis. Therefore it is necessary to use model outputs to quantify any such relationship.

The performance of the Howard and Knutson meander migration model will be assessed using GIS data for catchments within England and Wales (taken from the previous chapter). If the model can successfully predict channel migration and bank erosion over a period of 150 years, it may be reasonable to assume that the model will produce reliable estimates of these variables over longer timescales.

The calculation of radius of curvature for a whole catchment would be a significant take in terms of the time required to do this manually. The overall aim of this project is to develop a bank erosion tool which can be coupled to existing sediment generation models for use throughout the UK at a catchment scale. Therefore calculation of radius of curvature within this model would be unsuitable. Calculation of channel sinuosity is more efficient in computational terms and if a relationship can be identified between channel sinuosity and bank erosion, this could be included within the bank erosion tool.

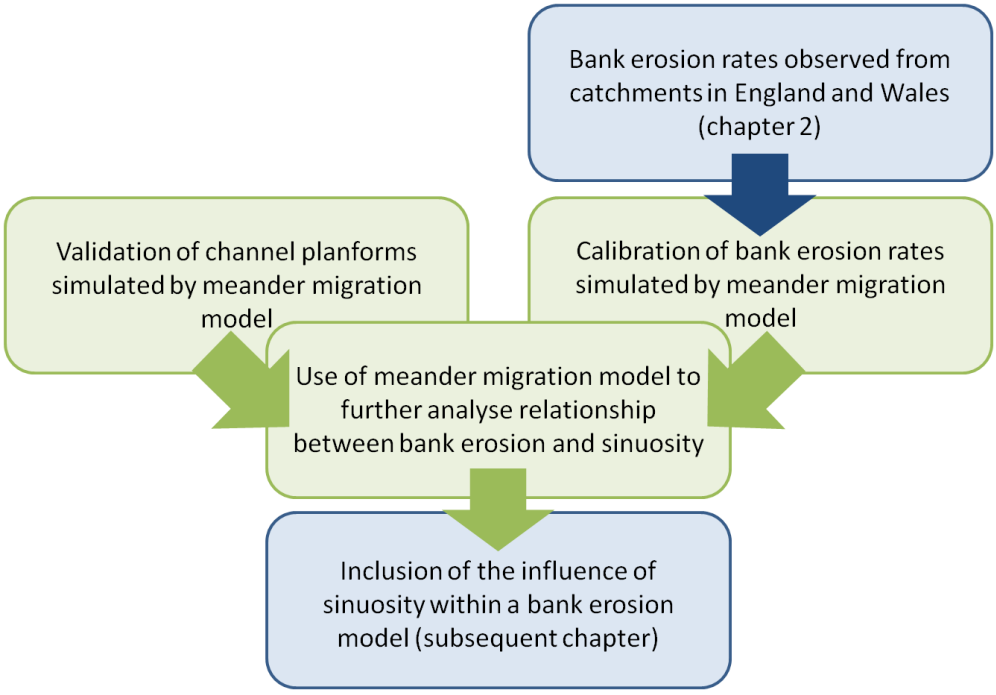

Figure 3.1: Schematic diagram indicating the objectives of this chapter, and how it links to the rest of this thesis.

3.1.2. Background

3.1.2.1. Channel sinuosity, radius of curvature, and bank erosion

Where little or no lateral erosion of channel banks occurs river channels remain relatively straight, whereas where lateral erosion of channel banks occurs channel sinuosity increases. As noted by Jansen *et al*, (2006) increasing sinuosity is a key mechanism by which river valleys widen downstream, or over time. Channel sinuosity induces changes to flow patterns within the river

channel; bends within the channel induce helical flow of water within the channel, which then focuses river energy on the outside of the river bend. The influence of sinuosity on bank erosion has been noted within many studies (Friedkin, 1945; Abam, 1993; Rosgen, 1994; Schilling and Wolter, 1999).

From the regression analysis within the previous chapter the correlation between bank erosion and sinuosity was found to be weak (Erosion in kg/ha/yr: R=0.397 p=0.01, Width averaged retreat rate: R=-0.214). On further analysis the relationship between sinuosity and bank erosion is non-linear (see Figure 3.2). From the data it appears that bank retreat rates are maximum with intermediate values of channel sinuosity (between 1.3-1.7). Where channel sinuosity increases/decreases outside this range the width averaged retreat rate appears to decline.

Crosato (2009) investigated the influence of radius of curvature, and sinuosity on migration rates using two models. The models used were the Ikeda *et al*, (1981) migration model, and the Crosato (1989) model as these represent both kinematic and dynamic model types respectively. Crosato (2009) found trends exist not only in migration rates and local radius of curvature, but also at a reach scale with sinuosity. In both models migration rates exhibited a maximum at a given value of channel sinuosity (see Figure 3.3).

An inverse relationship exists between radius of curvature and channel sinuosity: as radius of curvature/channel curvature ratio decreases, channel sinuosity increases. Therefore it is reasonable to assume that some non-linear relationship between bank erosion and sinuosity will also exist.

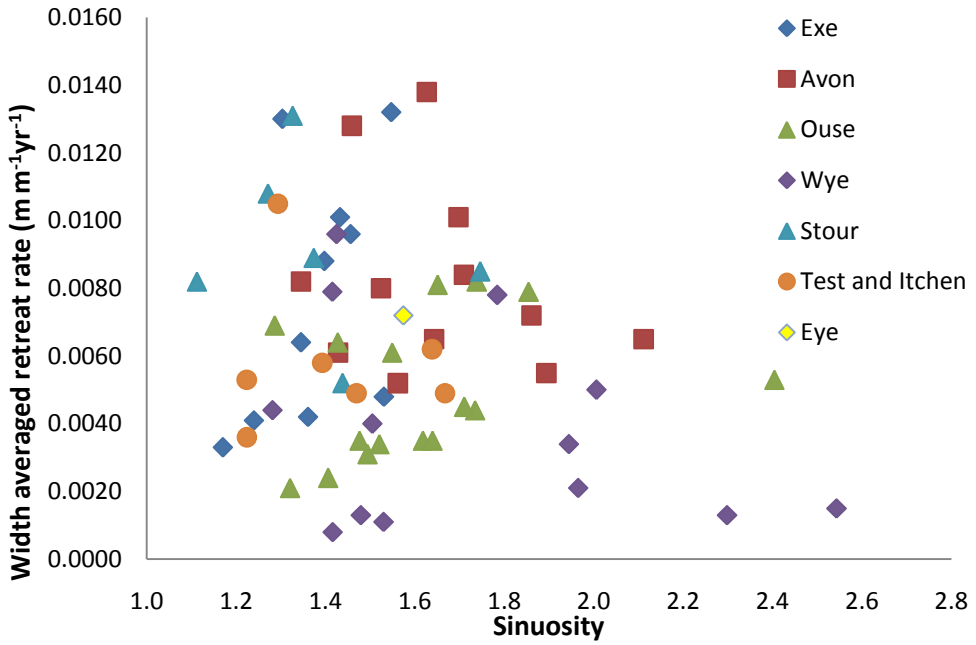

Figure 3.2: Scatterplot of channel sinuosity and width averaged retreat rate, taken from GIS data of 65 UK sub-catchments (see previous chapter).

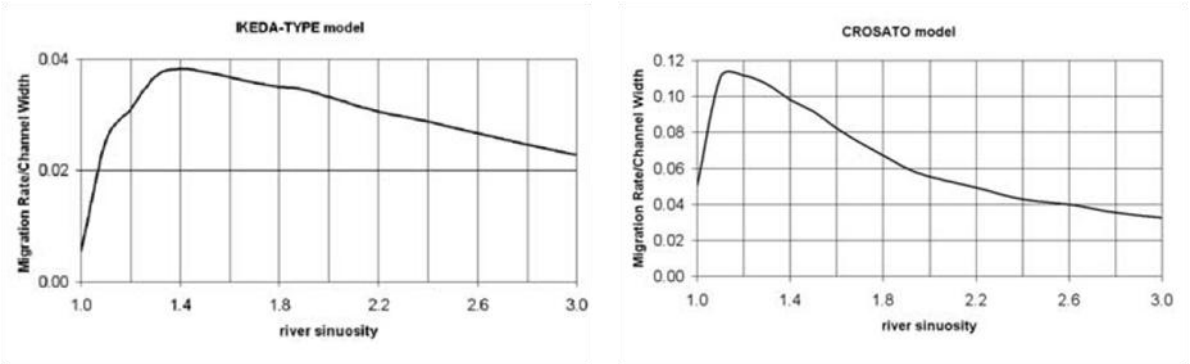

Figure 3.3: Reach-averaged migration rates and river sinuosity according to the kinematic Ikeda model (top) and the Crosato model (bottom). Note the different scales of Y-axis. Taken from Crosato (2009).

3.1.2.2. Secondary Flow

The non-linear relationship between radius of curvature and channel bank erosion rate was first noted by Hickin and Nanson (1975) on the Beatton river in Canada. They noted that as radius of curvature (or channel curvature ratio, calculated as radius of curvature normalised by channel width) decreased, the bank erosion rate increased until channel curvature ratio reached values of

approximately 3.0. Where channel curvature ratio decreased below 3.0 this resulted in a further decrease in bank erosion rates. A similar relationship has also been observed within several studies; Nanson and Hickin (1986), Biedenharn *et al*, (1989), Hooke (1997), Giardino (2011). The cause of this relationship can be explained by the variation of the positioning of the secondary flow within the channel, the formation of which is detailed in section 2.1.2.2. Secondary currents occur normal to the axis of primary flow. At meander bends, secondary currents result in fast surface water moving towards the outer bank and slow bed water towards the inner bank (see Figure 3.4). In straight channels there is little asymmetry in the channel cross section, and secondary circulation is weak. As the radius of curvature of the channel decreases, inertial forces result in an increase in flow asymmetry, with high shear acting on the concave bank. This is strengthened by intensifying helical flow. At the threshold radius of curvature value (observed to be ~3.0) the maximum velocity filament moves towards the convex bank, and bank erosion at the concave bank reduces. In bends of a low curvature ratio (<2.0) flow separation may occur (described below), and channel migration significantly decreases.

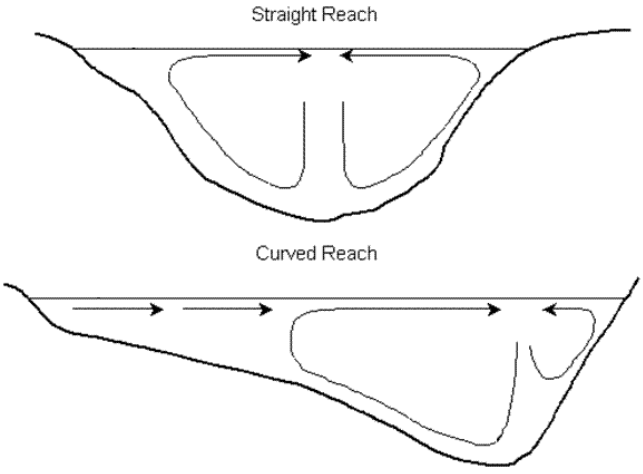

Figure 3.4: A channel cross-section illustrating secondary flow within a straight channel reach (top) and a curved channel reach (bottom).

In addition to the helical cell (sometimes termed centre-region cell) of secondary flow, some studies have observed the presence of an additional outer-bank cell of secondary flow in natural meander bends; in the river Dove,

Hey and Thorne (1975), in the river Severn, Bathurst *et al* (1977) and Thorne and Hey (1979) (see Figure 3.5). The outer-bank cell rotates in the opposite direction to the centre-region cell, and is normally relatively weak in comparison. Bathurst *et al* (1977) noted that the outer-bank cell seemed to depend on the form of the outer bank, occurring where the outer bank is steep. Mathematical modelling of flow in rectangular pipes (De Vriend, 1981) has shown that the outer-bank cell develops where the Dean number is >60. The Dean number (De) is calculated from the product of the Reynolds number (Re) and the square root of channel diameter (d) divided by the radius (R):

$$De = Re(\frac{d}{R})^{0.5}$$

where $Re = ud/v$

where u is the downstream velocity, and v is the viscosity of flow. The Dean number therefore increases as channel curvature ratio decreases (as sinuosity increases). Blanckaert (2002) noted the outer-bank cell widens and strengthens with increasing channel curvature ratio. Blanckaert and Graf (2001) noted the reduced level of turbulent activity in the region near the outer bank resulting in a protective effect on the outer channel bank. As the outward increase in downstream velocity from the centre-region cell does not extend to the outer-bank, the core of maximum flow velocity is located at the region of separation between the center-region and outer-bank cells. Therefore there is reduced shear stress acting upon the outer bank and reduced bank erosion. Additionally, it was noted that the strength of the outer-bank cell (and hence the reduction in shear stress at the outer-bank) increases with increasing channel curvature.

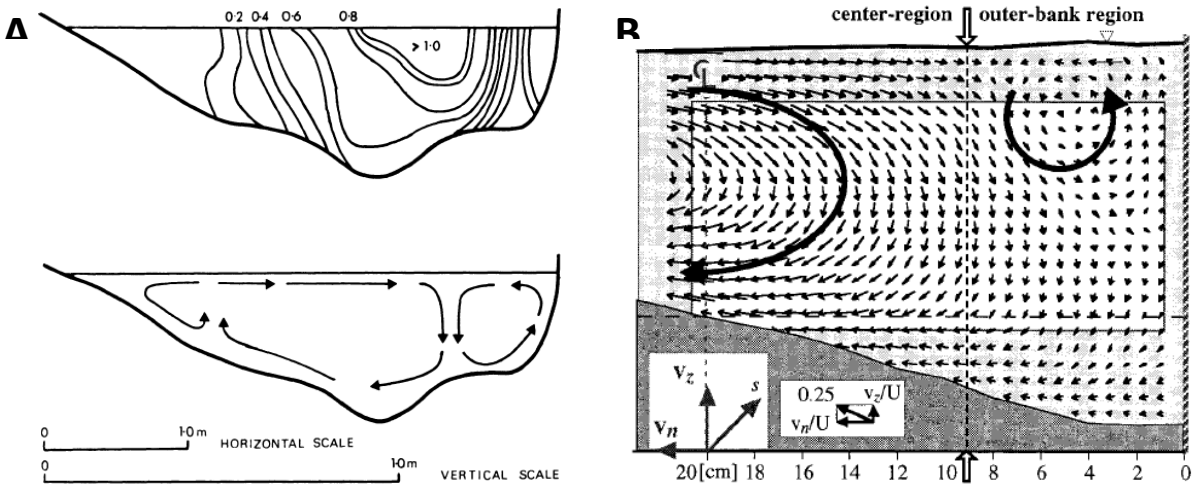

Figure 3.5: A) Velocity distribution and secondary flows at meander apex, River Dove. (radius of curvature = 62-5 m). Taken from Hey and Thorne (1975). Note the distortion of primary flow due to the presence of the outer-bend cell. B) Normalised depth averaged downstream velocity, taken from Blanckeart and Graf (2002).

De Vriend (1981) noted the influence of secondary flow on the main/primary flow within rivers (also illustrated in Figure 3.5 A). A feedback exists between the centre-region cell and the downstream velocity distribution; the centre-region cell flattens the downstream velocity distribution (i.e. the cell reduces the downstream velocity of waters high in the water column, and increases the downstream velocity of waters lower in the water column). Reducing the downstream velocity results in a weakening of the centrifugal force, this in turn weakens the centre-region cell, forming a negative feedback. As noted by Blanckeart and De Vriend (2004), in channels with high curvature, where the maximum velocity is found in the lower part of the water column due to this negative feedback mechanism, accurate computation of secondary flow circulation requires fully three-dimensional momentum equations including advective transport terms. They noted that in the outer-bank region the centrifugal force and cross-stream turbulent stresses contribute to the formation of the outer-bank cell. In this cell the sign of the centrifugal term in the vorticity equation complies with the rotation, meaning the centrifugal force enhances the outer-bank cell circulation.

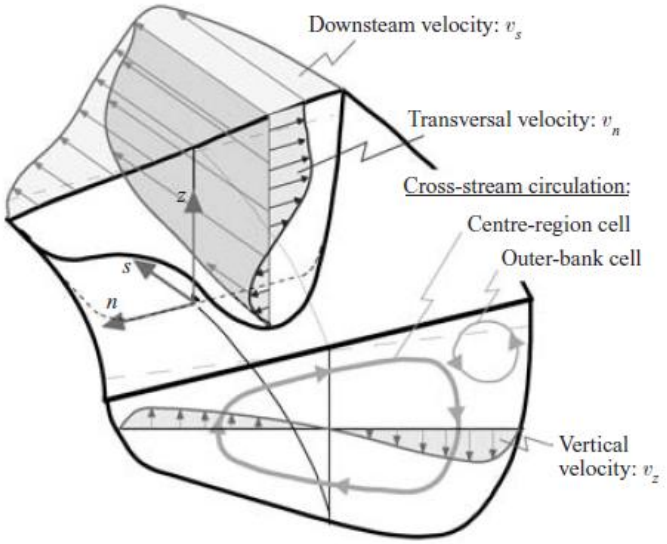

Figure 3.6: Curved open-channel flow and cross-channel circulation. Taken from Blanckeart and Vriend (2004).

Where channel curvature is sufficiently high, flow separation occurs and a second cell of secondary circulation develops (here termed an outer-bank cell). As channel curvature increases further, the centrifugal force increases, which increases the strength of the outer-bank cell and moves the positioning of the cell towards the centre of the channel. The high velocity core of flow is located at the separation between the centre-region and outer-bank cells and therefore the presence of the outer-bank cell moves the high velocity flow away from the outer channel bank. The reduction in the near bank flow velocity results in a reduction of shear stress acting on the outer bank, and bank erosion decreases. As channel curvature increases the positioning of the outer-bank cell moves further towards the centre of the channel, and the strength of the cell increases, therefore providing increased protection to the bank from erosion due to the reduction in shear stress from the flow. This explains the observed decrease in bank erosion above the threshold value of channel channel curvature ratio (~1.3).

3.1.1.1. Channel geometry

The importance of the influence of upstream channel geometry has been noted in several studies (Carson and Lapoint, 1983; Davies and Tinker, 1984; Furbish, 1991; Saminara *et al*, 2001; Zolezzi and Seminara 2001). Several models of meander migration include factors associated with channel planform geometry to predict channel migration rates. Kinematic channel migration models are based on empirical relationships derived from natural channels. The influence of radius of curvature, and upstream geometry of the channel has been incorporated into several kinematic meander migration models (Ikeda *et al*, 1981; Howard and Knutson, 1984; Meakin *et al*, 1996). The Howard and Knutson (1984) model uses channel curvature, and includes a lag distance between the bend apex and point of maximum bank shear stress. The influence of upstream channel geometry in their model is achieved using a weighting function. However, there is currently no inclusion of sinuosity within existing channel migration or bank erosion models.

The occurrence of chute cut-offs within channels has also been linked to the sinuosity of the channel (Stolum, 1996; Hooke and Yorke, 2010; Michelli and Larsen, 2011). These findings have been linked to the theory of self-organised critically (SOC): channel meandering is an autogenic process; as the channel develops, sinuosity increases over time until the supercritical sinuosity is reached, at which point chute cut-offs occur resulting in a decrease in sinuosity. This theory implies that channel sinuosity increases as the channel develops until reaching an equilibrium sinuosity state, at which point further increases in sinuosity are restricted by the occurrence of chute cut-offs. This produces a negative feedback mechanism; as channels develop, bank erosion rates are likely to vary due to changes in sinuosity, and then reach a constant rate, the magnitude of which is dependent on the equilibrium value of sinuosity. This also implies that any changes to the river system, such as climate change, which would result in changes to the magnitude and frequency of precipitation events and consequently changes to the river discharge regime, may result in a shift in the equilibrium state of the channel (and hence the sinuosity) which in turn would result in a change to bank erosion rates.

As noted by Schumm (1968) discharge has no direct influence on the sinuosity of river channels. Ebisemiju (1994) noted that the influence of discharge on sinuosity was largely dependent on the spatial scale being observed (see Figure 3.7); at low spatial scales the analysis would involve just individual bends, however with high spatial scales the variations in sinuosity will be lost. Therefore the mean value of sinuosity and range of sinuosity values will vary depending on the spatial scale chosen for analysis. Additionally it was noted that the influences of discharge on sinuosity were conflicting, between different studies, due to differences in additional influencing variables such as geology, climate, and river size.

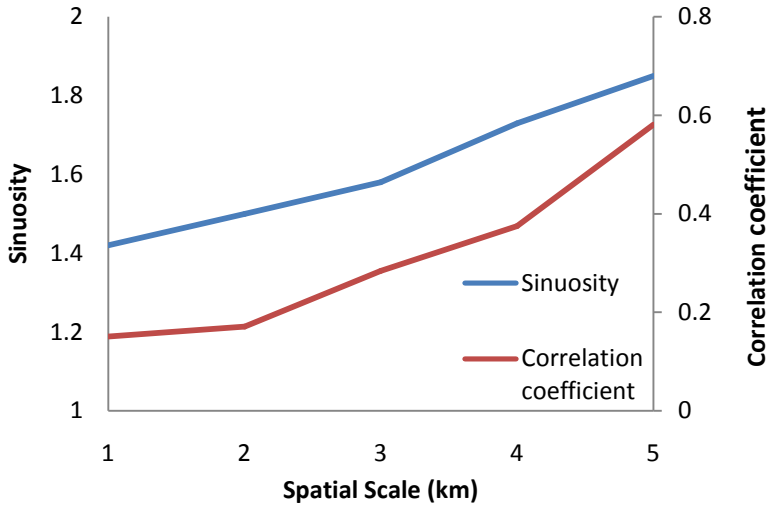

Figure 3.7: Affect of spatial scale on sinuosity, and correlation with stream discharge. Data taken from Ebisemiju (1994).

The influence of channel gradient on channel sinuosity was noted in flume experiments by Schumm and Khan (1972); sinuosity was found to increase with slope up to a point where channel braiding began to occur. At this point slope decreased slightly with increasing discharge. Aswathy *et al*, (2008) observed a similar relationship. As channel slope increases the flow velocity increases according to Manning's equation. Increased flow velocities create a greater shear force at the channel banks and providing greater energy for bank erosion. Therefore, whilst discharge may not show a clear direct influence on channel sinuosity due to the numerous additional variables controlling sinuosity,

it is clear that changes to channel discharge will at least indirectly influence channel sinuosity and therefore bank erosion. Therefore when calculating sediment generation in response to climate change it is necessary to consider changes in channel sinuosity.

3.2. Methodology

To identify any relationship between bank erosion and sinuosity data is required over a considerable time period (greater than 150 years). Observed bank erosion data is not available for such long time scales. Therefore this chapter will assess the ability of an existing meander migration model to predict channel planform change and bank erosion rates over timescales for which observed bank erosion data are available (from the digitised ordnance survey data used in the previous chapter). The model chosen for analysis was the Howard and Knutson model (1984). The model parameters were calibrated for several individual channels from the original data to identify a range of parameter values representative of 'natural' channels. If the model can represent channel migration over the time period observed (up to 150 years depending on catchment) it can be used to investigate the relationship between sinuosity and erosion rate over longer time scales.

The model will then be run from a straight line using several combinations of these parameter values to produce a sinuosity and bank erosion time series longer than that available from observed data. The relationship between sinuosity and bank erosion over longer time periods can then be examined and used to inform a bank erosion tool.

3.2.1. Howard and Knutson model

Howard and Knutson (1984) illustrated that channel migration rates estimated from a non-linear relationship with curvature alone produced unrealistic meandering patterns and indicated the importance of upstream channel geometry. In their model a spatial lag between bend geometry and maximum rates of shear stress and bank erosion are implemented.

In their model the channel centerline is represented by a series of equally spaced discrete points which the model repeatedly cycles through. At each node the nominal migration rate (R_0) is determined by the channel curvature (RW) and given a sign (positive for curvature in the clockwise direction and vice versa). Upstream channel geometry is accounted for through a weighting

procedure; the adjusted migration rate (R_1) is determined through weighting R_0 for present and upstream locations using the equation:

$$R_1(s) = \Omega R_0(s) + \left[\Gamma \int_0^x R_0(s-\xi)G(\xi)d\xi\right]\left[\int_0^x G(\xi)d\xi\right]^{-1}$$

Where s is the downstream distance, $R_0(s-\xi)$ is the nominal migration rate at distance ξ upstream from s, Ω and Γ are weighting parameters and $G(\xi)$ is an upstream weighting function (Howard and Knutson, 1984). The model assumes constant channel bank erodibility, uniform width-averaged bed sediment, and no anastomising within the channel.

The model performs well producing many features resembling those which naturally occur in channels as illustrated in Figure 3.8. As the authors noted, many similarities between the simulations and natural streams were observed:

- Low-amplitude meanders migrate rapidly downstream and as their amplitude increases the migrations decreases.
- As meander amplitude increases the meander loops are skewed upstream. This is partly as a result of the most rapidly migrating sections of the loops being located upstream from the centre of symmetry and partly due to upstream rotation of meander due to erosion of downstream portions of previous loop.
- When the path length through a meander is very long shorter meanders initiate on the straighter sections which initially migrate rapidly downstream.
- Cutoffs occur late in the development of a loop. When cutoffs do occur the sharp bend may rapidly enlarge to form a new loop.
- Patterns are not universal due to the dependency of local bank erosion on upstream channel geometry.

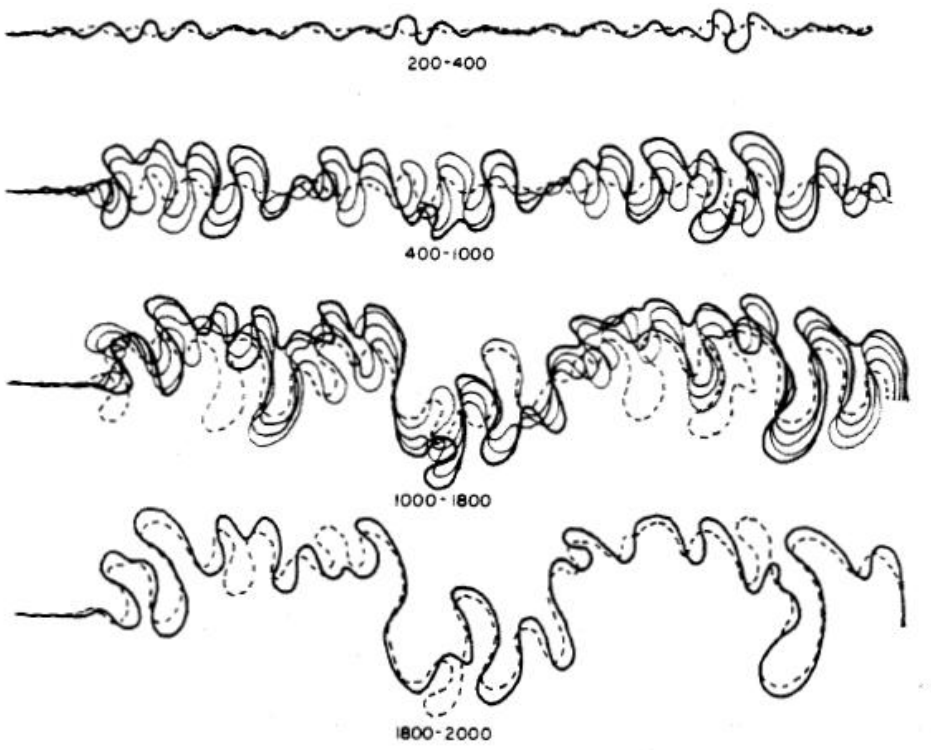

Figure 3.8: Successive centerlines of simulated streams, displayed in increments of 200 iterations. Downstream to right. The first centreline of each sequence is a dashed line and the last is bold. Taken from Howard and Knutson (1984).

3.2.2. Model Calibration

Firstly channel centerlines were digitised for a selection of WFD sub-catchments. The oldest base-map was used for each sub-catchment so the migration rate and pattern over the time period covered by the ordnance survey maps could be compared to that predicted by the migration model. The sub-catchment channel centerlines digitised and used for model calibration included channels with both low and high sinuosities. This enabled assessment of the model's ability to predict migration patterns and bank erosion of channels with varying degrees of sinuosity. Additionally, channels chosen showed changes over the time period observed by ordnance survey data. The sub-catchment channel centrelines digitised included the Nidd 35, Ouse 30, Ebble 6, East Stour 8. The average sinuosities of these channels were 2.40, 1.73, 1.49, and 1.11 respectively.

For each centerline x,y co-ordinates were generated along the line. Co-ordinate points were positioned equal distances apart, and this distance was set at the average channel width. The co-ordinates of the line were then input into the meander migration model and the model was run for the number of years for which ordnance survey data was available (Nidd 35: 150 years, Ouse 30: 150 years, Ebble 6: 120 years, East Stour 8: 135 years). The bank erosion rate from the model output was then calculated by overlaying channel centrelines from consecutive years in GIS to produce an area of erosion, and dividing this by the length of the channel to produce a bank retreat rate in m yr^{-1} (see Figure 3.9). This method was chosen as it was the most comparable to the method used in the GIS analysis of bank erosion rates from chapter 2 and therefore the most suitable for assessment of the model's ability to reproduce observed retreat rates.

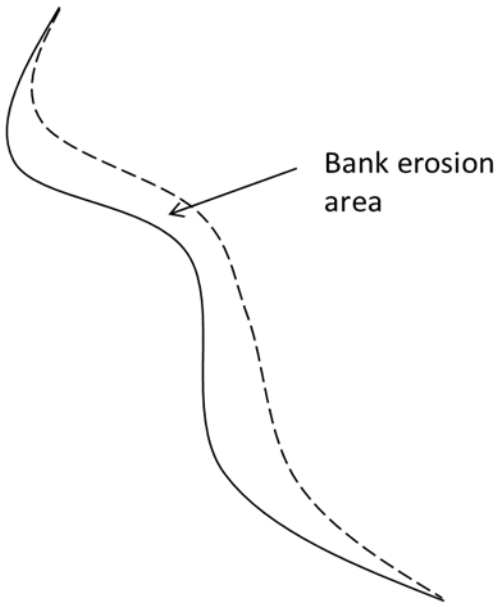

Figure 3.9: Hypothetical channel centrelines from two consecutive model outputs. The dashed line represents year 1, the solid line represents year 2, the area between the lines represents the bank erosion area. This area was divided by the length of the channel to provide a bank retreat rate in m yr^{-1}.

The parameters for the Howard and Knutson (1984) model include bank erodibility (E), alpha and gamma (α, Γ), which control the amplitude and wavelength of channels (see Figure 3.10 and Figure 3.11), and a chute cut-off

parameter. The chute cut-off parameter was included in a modified version of the model and controls the frequency of the occurrence of chute cut-offs within the channel. The cut-off parameter is effectively a threshold gradient advantage that must be exceeded for a chute cut-off to occur. In other words, if the parameter value is two then a chute cut-off will occur if two nodes on the channel are separated by a distance (along the channel centreline) that is at least twice the distance across the point bar. The model parameters were calibrated for individual sub-catchments so that values of annual bank retreat rate, and channel planform change were close to the values observed from the GIS data. The model was calibrated over the time period for which observed data were available. This then provided a range of parameter values observed within natural channels. It is important to calibrate these coefficients because, as noted by Crosato (2009), they can significantly affect the values of bank migration rates as they weight the intensity of the system response to perturbations, but not the type of dependency on curvature or sinuosity.

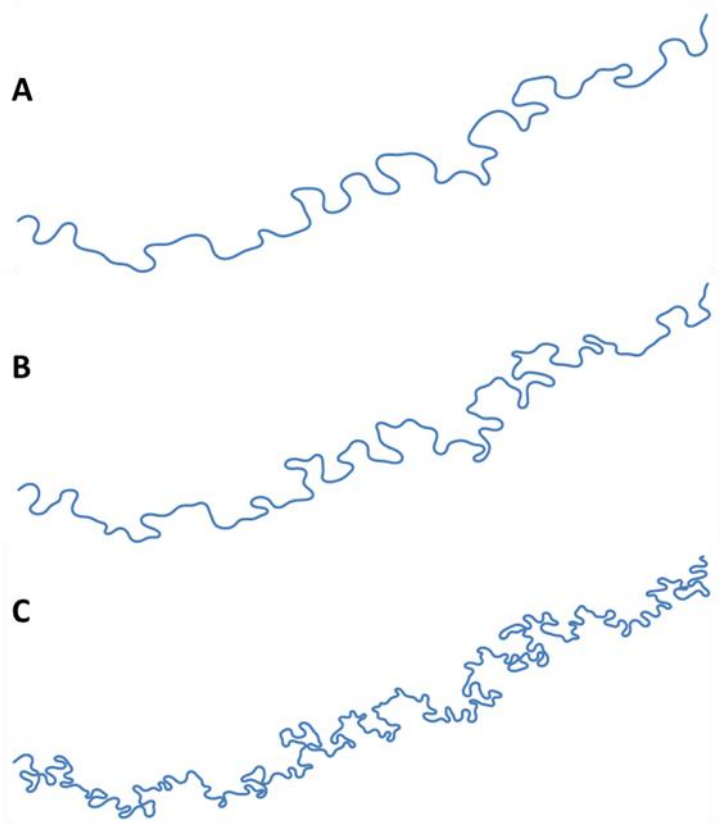

Figure 3.10: Influence of the value of the parameter alpha (α) on the Howard migration model output after 100 iterations. A: α=0.1, B: α=0.5, C: α=2.0.

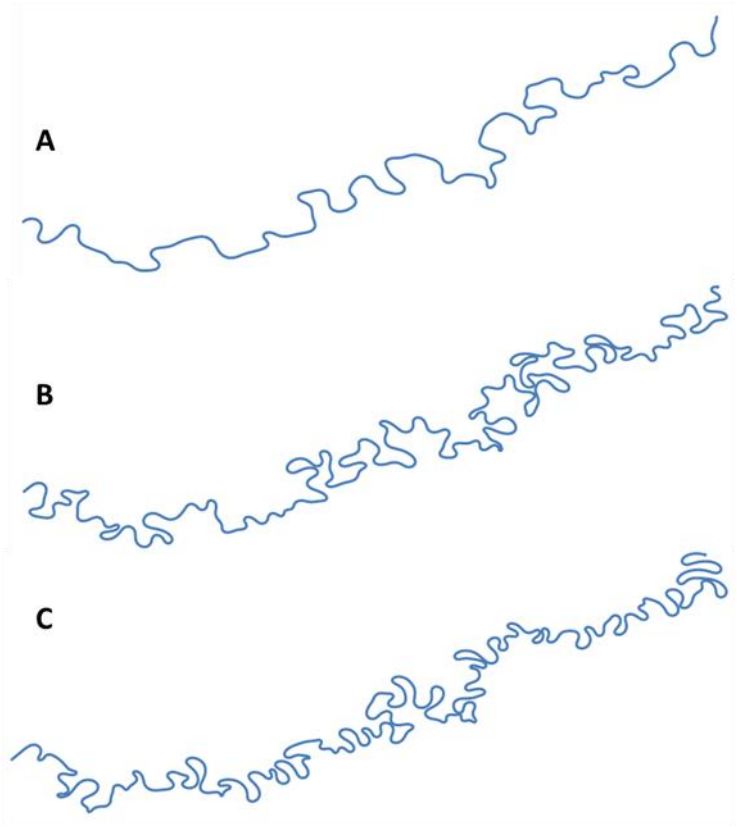

Figure 3.11: Influence of the value of the parameter gamma (Γ) on the Howard migration model output after 100 iterations. A: Γ=1.0, B: Γ=3.0, C: Γ=5.0.

3.2.3. Model Validation by comparison with measured bank erosion rates

To ensure the model could accurately represent channel bank erosion, validation statistics were calculated to compare the GIS derived bank retreat rates and the modelled bank retreat rates. The performance statistics used included the mean absolute error (MAE), root mean square error (RMSE), Nash-Sutcliffe efficiency (NSE), and percent bias (PBIAS). These statistics were chosen as it has been suggested that a combination of a dimensionless index (representing the ratio between the mean square error and the 'potential' error) and an absolute error index should be used (Legates and McCabbe, 1999).

MAE and RMSE are error indices calculated as:

$$MAE = \frac{\sum_{i=1}^{n}(Sim' - Obs')}{n}$$

$$RMSE = \sqrt{n^{-1}\sum(Sim' - \overline{Obs'})^2}$$

A MAE or RMSE value of 0 indicates a perfect fit. NSE (developed by Nash and Sutcliffe, 1970) is a normalised (dimensionless) statistic, which determines the relative magnitude of residual variance compared to the variance of the observed data. The statistic is calculated using the equation:

$$NSE = 1 - \left[\frac{\sum_{i=1}^{n}\left(y_i^{obs} - y_i^{sim}\right)^2}{\sum_{i=1}^{n}\left(y_i^{obs} - y^{mean}\right)^2}\right]$$

NSE ranges from 0-1, values between 0.0-1.0 are viewed as acceptable, values of <0.0 are unacceptable as this indicates the mean observed value is a better predictor than the simulated value (Moriasi *et al*, 2007).

PBIAS measures the average tendency of the simulated data to be larger or smaller than the observations. PBIAS is calculated as:

$$PBIAS = \left[\frac{\sum_{i=1}^{n}\left(y_i^{obs} - y_i^{sim}\right)\times 100}{\sum_{i=1}^{n} y_i^{obs}}\right]$$

Positive values indicate a tendency to underestimate the data and vice versa.

3.2.4. Model Validation by analysis of channel planform

Model validation using bank erosion rates due to meander migration alone are insufficient as they do not indicate if the model can accurately represent styles of channel planform change as observed in natural channels. Channel planform change was assessed qualitatively by comparing the planform of natural channels from GIS analysis, to that of channels from migration model outputs.

Lancaster and Bras (2002) derived a sinuosity-based method of analysing channel planform, by determining characteristic length-scales. They

noted that the value of channel sinuosity is largely dependent on the length and location of channel reach covered in the measurement. Their method measures the average sinuosity and the variance of sinuosity for a range of measurement lengths. This enables identification of particular channel lengths at which contributions to sinuosity are important. Average sinuosity should increase with increase in measurement length, and the rate of increase also increases as typical channel segments tend to curve back on themselves as measurement length increases. Once the measurement length reaches that of single bends, the rate of average sinuosity increase with further increase in measurement length decreases because some channel segments stop curving back on themselves. Therefore, the length of simple bends can be identified by this decrease in slope (as illustrated in Figure 3.12). As measurement length further increases reaches may include more than one bend, and some will include longer and very sinuous bends resulting in a larger variance in sinuosity for certain measurement lengths. This results in peaks in the variance of sinuosity at particular measurement lengths, possibly corresponding to inflections in mean sinuosity. The first peak represents the length of long simple or compound bends, and the second peak represents the length of multi-bend loops. Lancaster and Bras (2002) indicated that by plotting the mean sinuosity and sinuosity variance at each measurement length-scale (as shown in Figure 3.12) allowed identification of these characteristic length-scales and hence comparison of channel planform features. The measurement lengths were incremented by channel widths.

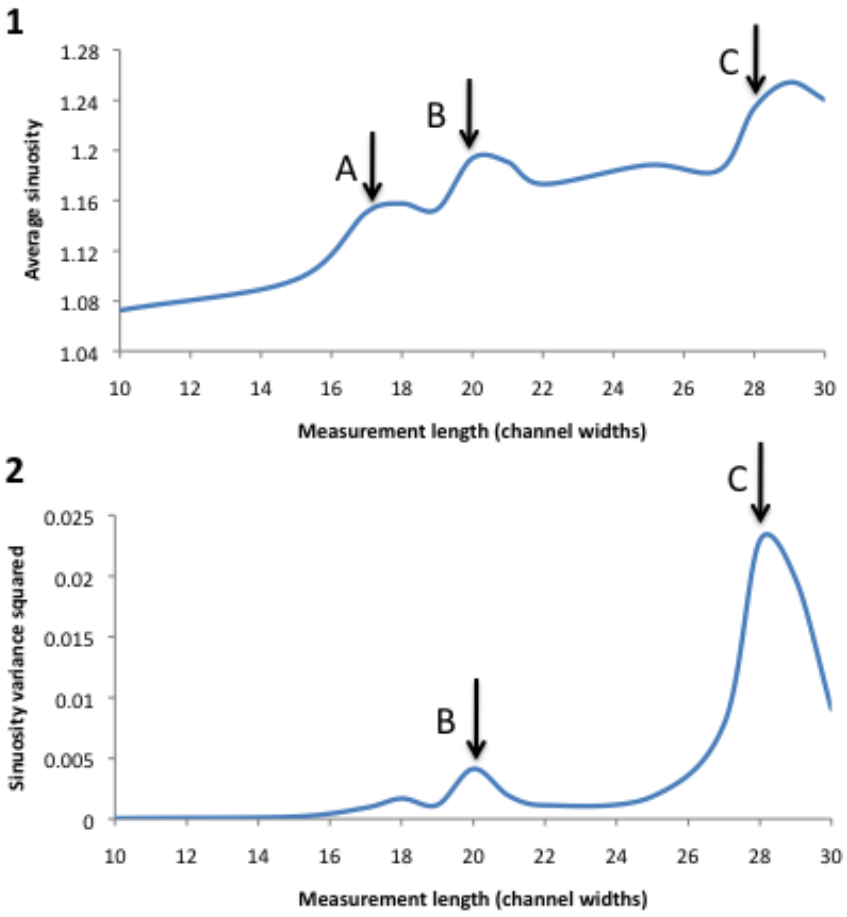

Figure 3.12: 1 - Change in sinuosity with increasing measurement length (as increments of channel widths). 2 - Change in the squared variance of sinuosity as measurement length increases. Point A1 mark where the rate of increase in average sinuosity with increase in measurement length reduces, and represents the typical bend length (in this case approximately 17 channel widths). Point B2 indicates the first peak in variance at 20 channel widths, and is equivalent to the length of long simple or compound bends. A corresponding inflection can also be seen in 1. Point C2 indicates the second peak in variance at 29 channel widths, and is equivalent to the length of multi-bend loops. A corresponding inflection can also be seen in 1.

Six channel reaches were analysed to determine characteristic length-scales (Ebble 6, Exe 18, Ouse 30, Swale 31, Nidd 35, East Stour 43). Channel centerlines were digitised in GIS. As the analysis used in Lancaster and Bras (2002), the channels selected were single-threaded and unconfined by valley

walls. In their study, Lancaster and Bras used intensely meandering channels within Alaska. The channels chosen within this study represent both highly sinuous UK channels, and UK channels of low sinuosity. The channel width for each of the reaches was calculated as shown in a previous chapter.

The same procedure was used to analyse the Howard and Knutson model output when run from initial co-ordinates of a straight line. The initial channel co-ordinates had slight perturbations from a straight line to allow the channel to initiate migration (as migration is dependent on radius of curvature, a completely straight channel will not migrate using the Howard and Knutson model). The model was run using parameter combinations observed in natural channels from the calibration procedure. Outputs from model iterations during the period when channel behaviour is characterised by dynamic equilibrium (or after the initial start up period of the model) as defined in the following section, were chosen for the analysis. As model simulations proceeded the upper section of the simulated channel becomes straight (because bends tend to translate downstream leaving an unperturbed channel upstream). Therefore the first 1000 points of the output channel were omitted from the simulated channel output to ensure the initial straight section of the channel was not included in later analysis. The number and positioning of breaks in average sinuosity and peaks in squared variance in both natural and simulated channels could then be compared. The dynamic equilibrium phase for this set of parameter values occurred after ~1400 iterations, therefore outputs were analysed at 1500, 1550, 1600, and 1650 iterations.

3.2.5. Relationship between sinuosity and erosion

Once the model parameters were calibrated and validation statistics had indicated the model's capability to reproduce observed channel bank retreat rates, the model was run from a straight line for 2000 iterations (years), in order to isolate the influence of sinuosity on channel planform geometry. As before, the initial channel co-ordinates were perturbed slightly from a straight line to allow the channel to initiate migration. The model was run with several parameter combinations, the values of which were taken from the range of

parameters identified to produce realistic channels during the calibration of the model.

As the model initially starts from a straight line, sinuosity increases from an initial value of 1 with the number of iterations of the model. Eventually chute cut-offs occur preventing further increase in sinuosity of the channel. At this point the sinuosity fluctuates with the occurrence of chute cut-offs. Erosion rate initially increases with sinuosity and when sinuosity begins to level-off due to chute cut-offs erosion rate does also. At this levelling off period, a dynamic equilibrium exists between the sinuosity, erosion rate, and chute cut-off occurrence causing sinuosity to remain within a particular range of values. To investigate the relationship between sinuosity and erosion rate the values of sinuosity and erosion must be taken from the model iterations within this period of dynamic equilibrium and should not include the initial period representing the initial start-up phase of the model. The number of iterations required to reach dynamic equilibrium varies depending on the parameter set chosen, and can be easily identified by plotting the time series of sinuosity and erosion from the model output as shown in Figure 3.13.

For each set of parameters used for a model run, the correlation between sinuosity and erosion rate (during the period of dynamic equilibrium) was calculated. Additionally, the average sinuosity and average erosion rate was calculated for this period.

A

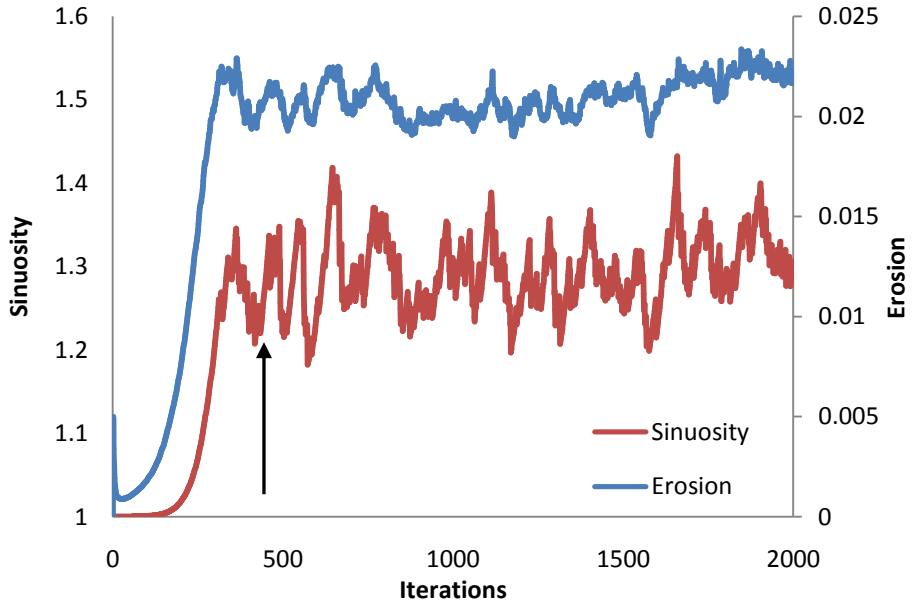

B

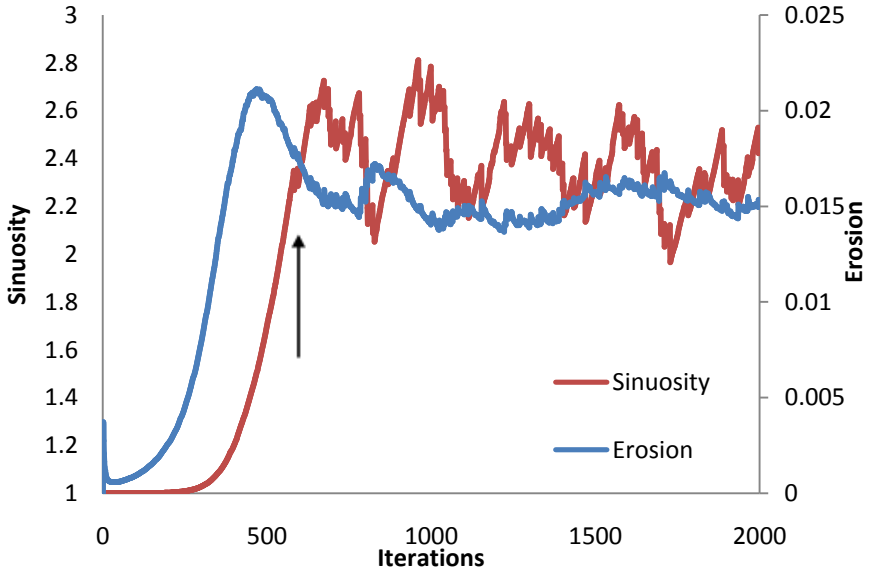

Figure 3.13: A: Howard and Knutson (1984) model output for 2000 iterations with parameters E:0.4, A:0.5, G:1.5, Cutoff:2. Dynamic equilibrium occurs at approximately 400 iterations (indicated by arrow). B: Howard model output for 2000 iterations with parameters E:0.4, A:0.6, G:1.5, Cutoff:9. Dynamic equilibrium occurs at approximately 700 iterations (indicated by arrow).

3.3. Results

3.3.1. Results of model calibration: Comparison of bank erosion rates

The results of the model calibration when comparing bank erosion rates of the Howard and Knutson (1984) model to the observed bank erosion rates are shown in Table 3.2. The calibration procedure of the Howard model indicated parameter values for natural river channels within the UK were within the following ranges:

- Erosivity: 0.3-0.5
- Alpha: 0.5-0.6
- Gamma: 1.5-2.0
- Chute cut-off: 2-9.

These values are similar to those used from previous studies; Howard and Knutson (1984) E=0.67, α=-1, Γ=2.5; Howard (1992) α=1, Γ=1.5; Finnegan and Dietrich α=-1, Γ=2.5. The validation statistics (see Table 3.1) indicated the model performed well when reproducing bank erosion rates (calculated as bank retreat rates) as observed from the GIS data for each sub-catchment for which the model was calibrated.

Table 3.1: Validation statics for individual sub-catchments used to assess model performance in comparison to GIS data.

Sub-catchment	MAE	RMSE	NSE	PBIAS (%)
East 8	-0.0030	0.0336	0.4256	0.0402
Ebble 6	0.0077	0.0198	0.0430	-0.0008
Ouse 30	-0.0005	0.0390	-0.0547	0.0000
Nidd 35	0.0015	0.0456	-0.1359	-0.0002
All	0.0014	0.0360	0.3909	-0.0001

Table 3.2: Results of model calibration

Channel	Erosivity	Alpha	Gamma	Chute cut-off	Observed bank erosion	Output 9-10 yrs	Output 49-50 yrs	Output 99-100 yrs	Output 119-120 yrs
Ebble 6	0.3	0.6	1.8	2.0	0.1104	0.1456	0.1099	0.1075	0.1091
East 8	0.5	0.6	1.6	8.0	0.0700	0.0592	0.0658	0.0746	0.0779
Ouse 30	0.3	0.6	2.0	6.0	0.1638	0.1666	0.1521	0.1511	0.1550
Nidd 35	0.3	0.5	1.5	9.0	0.0987	0.1279	0.1065	0.0956	0.0909

The optimal values of MAE and RMSE are zero and low values indicate accurate estimation. Singh *et al*, (2004) stated acceptable values of MAE and RMSE should be less than half the standard deviation of the observed data. The standard deviation of the observations of East 8, Ebble 6, Ouse 30, Nidd 35, and all observations are 0.0345, 0.0284, 0.0393, 0.0443, 0.0470 respectively, and therefore the half standard deviations are 0.0173, 0.0142, 0.0197, 0.0222, 0.0235. All values of MAE are lower than half the standard deviation, however all values of RMSE are higher. As values of MAE and RMSE are all close to zero it indicates the model has low error when reproducing observed bank erosion values.

The optimal value of NSE is 1, and values between 0.0-1.0 are viewed as acceptable (Morasi, 2007). All values of NSE are within or very close to this range, with the lowest value -0.1359. When the statistics were calculated for all simulations as a single NSE the value was 0.3909. Additionally, sub-catchments which produced validation statistics less than 0.0 produced statistics within an acceptable range for all others statistics calculated.

The optimal value of PBIAS is zero and low values indicate accurate estimation. The value of this statistic furthest from 0 is 0.0402. As all these values are close to zero it indicates the model does not consistently over/under predict bank erosion rates.

Figure 3.14 and Figure 3.15 show observed channel migration over 150 years, and calibrated model channel migration prediction over 150 iterations (equivalent to 150 years) for the Ouse 30 and Nidd 35 respectively. The grey square in Figure 3.14 indicates an area of large observed channel migration. In Figure 3.14 it is clear the model output does not indicate a similar migration pattern in this location. This is most likely due to the fact that the Howard and Knutson (1984) model calculates channel migration based on radius of curvature only; the observed migration pattern of the natural channel may be due to additional factors not considered in the model. Figure 3.14 and Figure 3.15 indicate the model produces similar channel planforms to those found in natural channels.

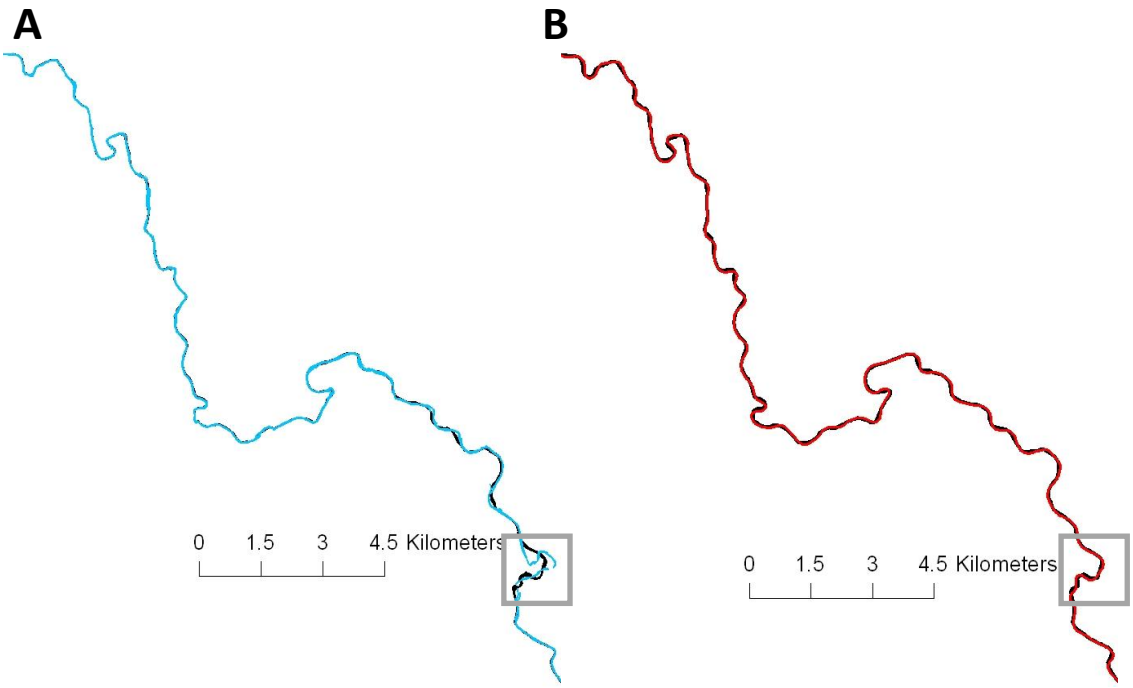

Figure 3.14: A - Observed channel migration of Ouse 30, black channel 1860, blue channel 2010. B - Model predicted channel migration, black channel 1 iteration, red channel 150 iterations.

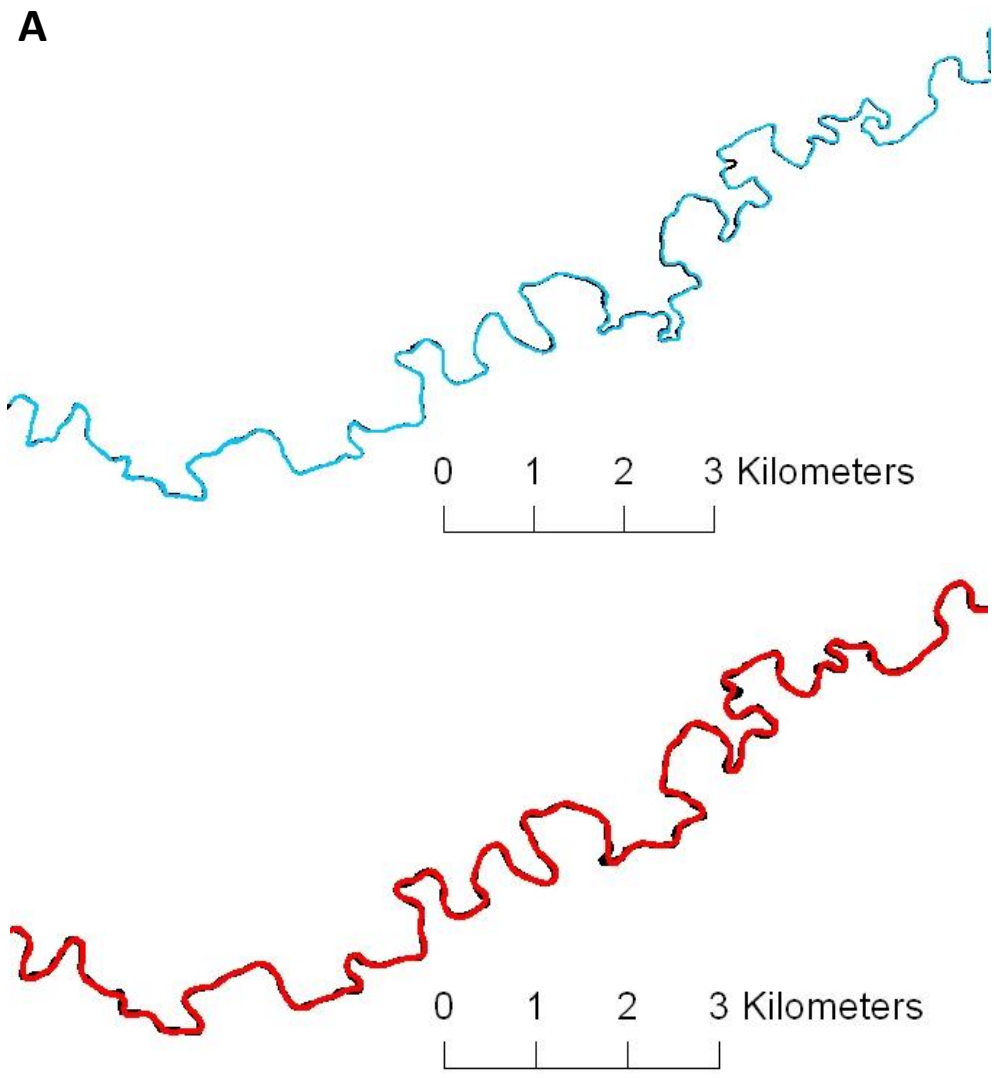

Figure 3.15: A - Observed channel migration of Nidd 35, black channel 1860, blue channel 2010. B - Model predicted channel migration, black channel 1 iteration, red channel 150 iterations.

3.3.2. Results of model calibration: Analysis of channel planform in natural channels

The natural channels used in the analysis are shown in Figure 3.16 and their characteristics are shown in Table 3.3. The results of the sinuosity analysis and characteristic length-scales; simple bend length (s'_{sb}), long simple/compound bends (s'_{v1}), and multiband loops (s'_{v2}) are shown in Table 3.4. The average sinuosity and variance are plotted against measurement length (in channel widths) in Figure 3.17.

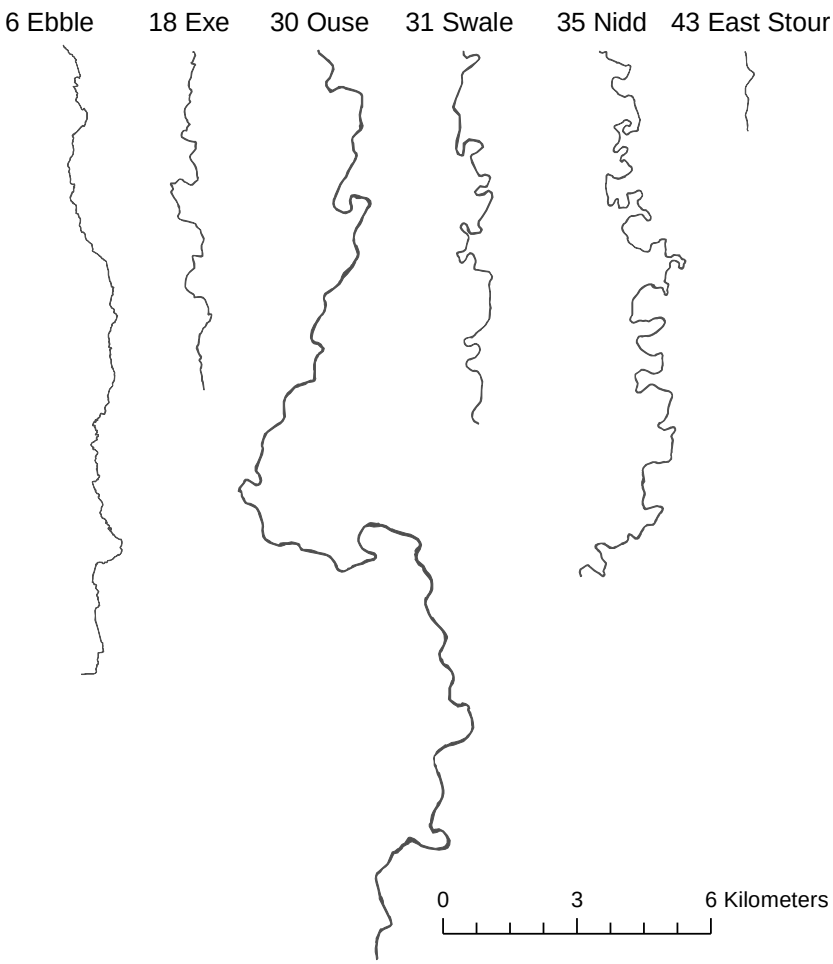

Figure 3.16: Meandering UK channels used for analysis. Flow is from top to bottom.

Table 3.3: Characteristics of natural meandering channels in UK used in validation analysis.

Number	Channel	Average Sinuosity	Channel Width (m)	Channel length (channel widths)
6	Ebble	1.46	9	2381
18	Exe	1.34	15	671
30	Ouse	1.73	37	955
31	Swale	1.71	22	654
35	Nidd	2.40	19	1521
43	East Stour	1.11	9	229

Table 3.4: Summary of natural channel analysis: characteristic length-scales (in channel widths) and mean sinuosities at those lengths (μ values). s'_{sb} the smallest length scale (corresponding to simple bends), s'_{v1} are compound bends, and s'_{v2} are multibend loops.

Channel reach	s'_{sb}	$\mu_s(s'_{sb})$	s'_{v1}	$\mu_s(s'_{v1})$	s'_{v2}	$\mu_s(s'_{v2})$
Ebble 6	10	1.11	15	1.14	29	1.17
Exe 18	20	1.16	37	1.23	45	1.28
Ouse 30	20	1.19	28	1.23	33	1.32
Swale 31	18	1.32	35	1.76	45	1.89
Nidd 35	19	1.28	30	1.56	45	1.81
East Stour 43	17	1.03	25	1.04	40	1.09

A) Ebble 6

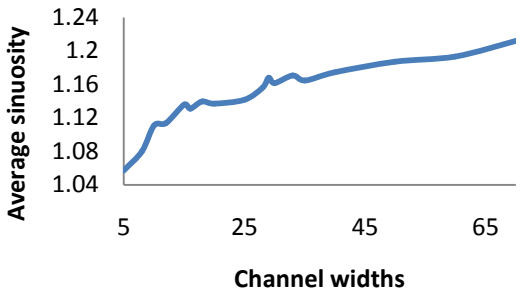

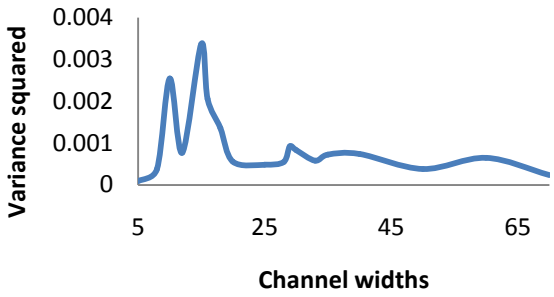

B) Exe 18

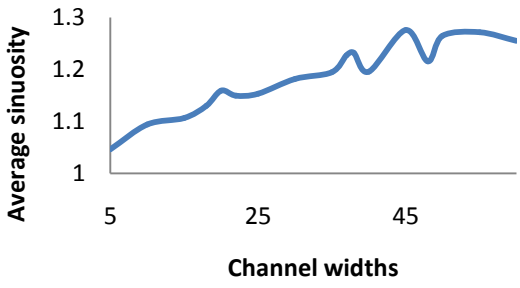

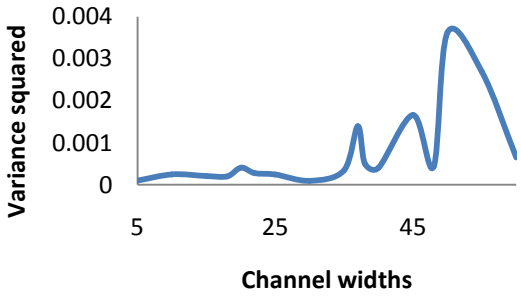

C) Exe 18

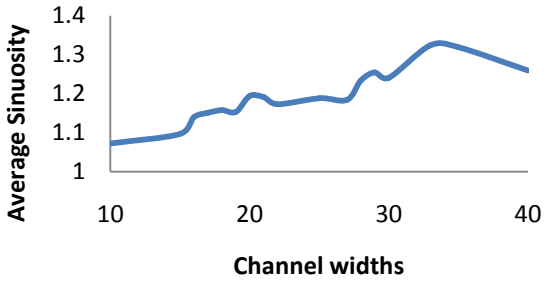

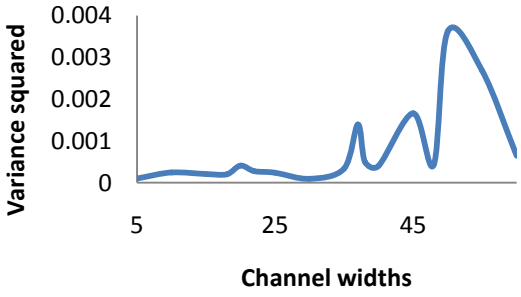

D) Swale 31

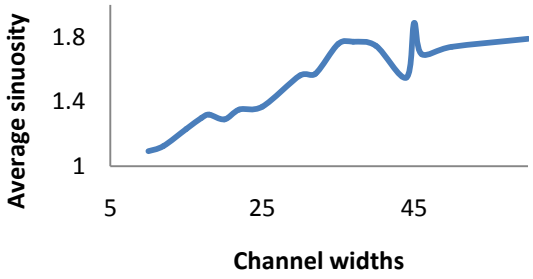

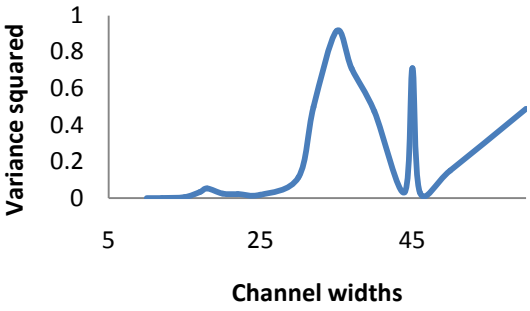

E) Nidd 35

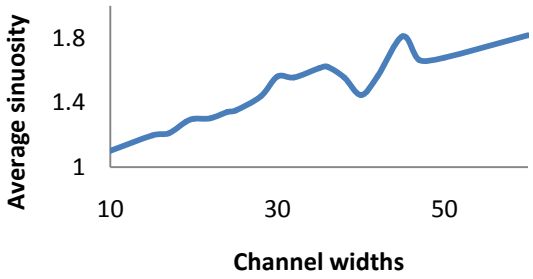

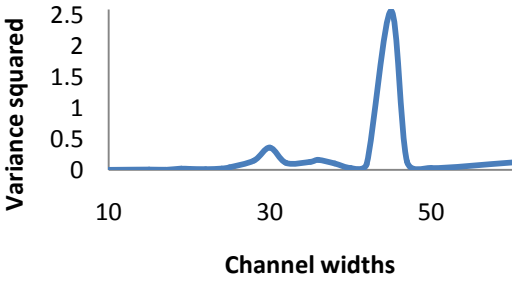

F) East Stour 45

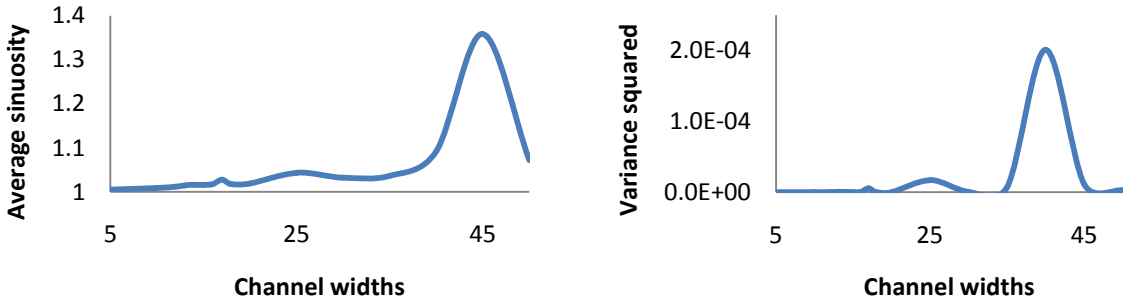

Figure 3.17: Sinuosity mean and variance versus normalized reach length for the meandering channels listed in Table 3.4 and shown in Figure 3.16.

As in the analysis of Alaskan streams by Lancaster and Bras (2002), there is an increasing average sinuosity with increasing reach length, and breaks or levelling off of average sinuosity often correspond to peaks in sinuosity variance. From the six channels considered in this study, the smallest length-scales (s'_{sb}) are most tightly clustered (channel widths 10-20, mean sinuosity 1.03-1.32). Intermediate lengths (s'_{v1}) are less tightly clustered (channel widths 15-37, mean sinuosity 1.04-1.76). The longest lengths (s'_{v2}) are the least tightly clustered (channel widths 29-45, mean sinuosity 1.09-1.89).

Figure 3.18 shows a section of the channel Nidd (number 19) and illustrates the representative parts of the channels to the lengths $s'_{sb,}$ $s'_{v1,}$ s'_{v2}. This indicates that s'_{sb} does correspond to the typical length of simple bends, s'_{v1} to the length of long often compound bends, and s'_{v2} to the length of multibend loops.

The relative importance of the contribution to sinuosity at the three length-scales varies among streams as shown in Figure 3.17. For example, as can be seen from Table 3.4 the average sinuosity at length s'_{v1} and s'_{v2} in the Ebble varies only slightly (1.14-1.17). Figure 3.17 A shows only a very small peak for s'_{v2}. As observed by Lancaster and Bras (2002) this is due to the significant natural variation in the importance of multibend loops to planform complexity.

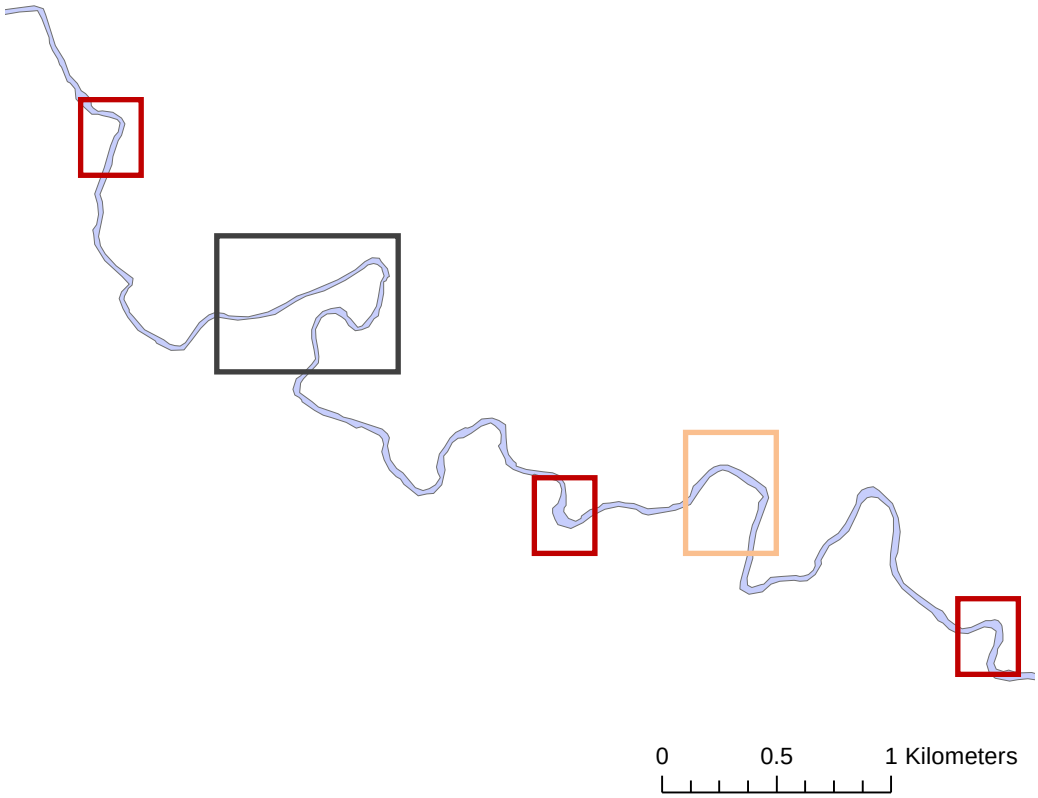

Figure 3.18: The forms represented by the three channel length-scales shown in Figure 3.17 and Table 3.4 from the channel Nidd 19. Red boxes indicate $s'_{sb,}$, orange s'_{v1}, and black s'_{v2}.

3.3.3. Results of model calibration: Analysis of channel planform in simulated channels

Channels simulated with the Howard and Knutson model are shown in Figure 3.19 and analysis of these channels is shown in Table 3.5 and Figure 3.20.

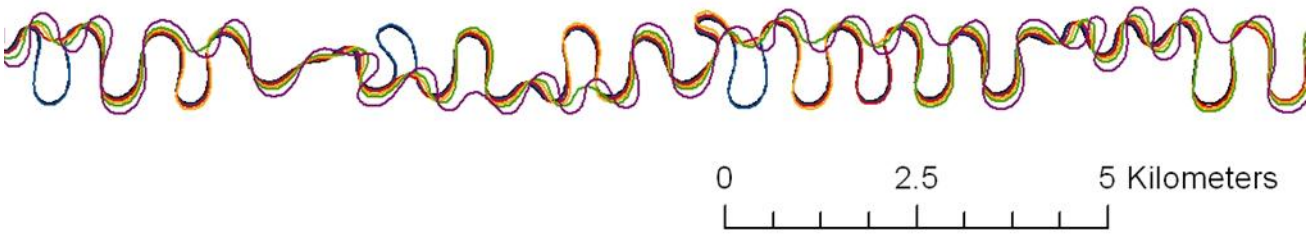

Figure 3.19: Simulated channels using the Howard and Knutson model when run from initial co-ordinates of a straight line, with parameter values the same as for the channel Ouse 30 (E:0.3, A:0.6:, G:2.0, C:6, and channel width 37m). Simulations shown are without the first 1000 channel points to remove straightened sections of channel. Simulations shown are within the dynamic equilibrium period; 1500 (black), 1525 (blue), 1550 (red), 1600 (orange), 1650 (green), and 1800 (purple).

Table 3.5: Analysis of channel planforms simulated with the Howard and Knutson model: measurement lengths in channel widths, and average sinuosities at those lengths.

Number of iterations	s'_{sb}	$\mu_s(s'_{sb})$	s'_{v1}	$\mu_s(s'_{v1})$	s'_{v2}	$\mu_s(s'_{v2})$
1500	33	2.11	47	2.41	55	2.48
1525	30	1.57	45	2.23	55	2.42
1550	35	1.84	45	2.06	55	2.34
1600	40	1.80	47	2.26	60	2.19
1650	30	1.69	43	1.82	60	2.21
1800	20	1.38	35	1.93	55	1.95

A) 1500

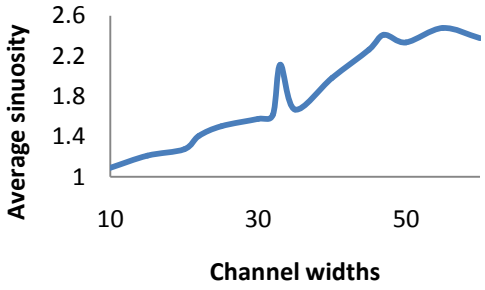

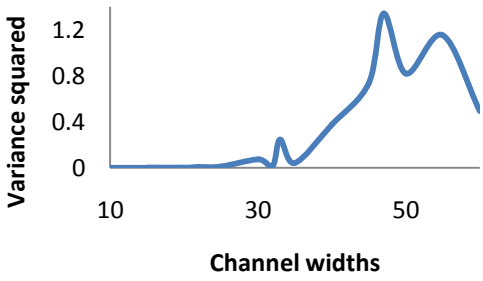

B) 1525

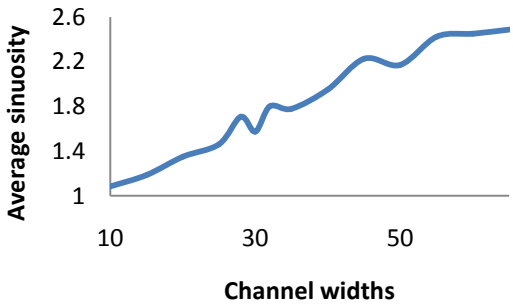

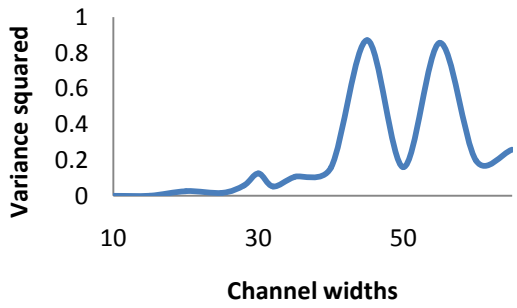

C) 1550

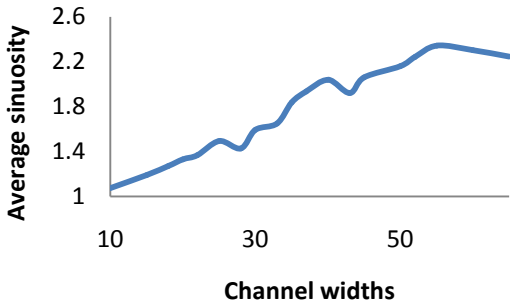

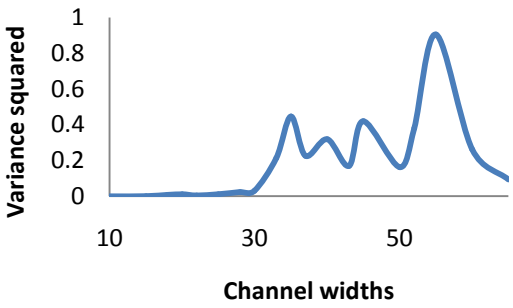

D) 1600

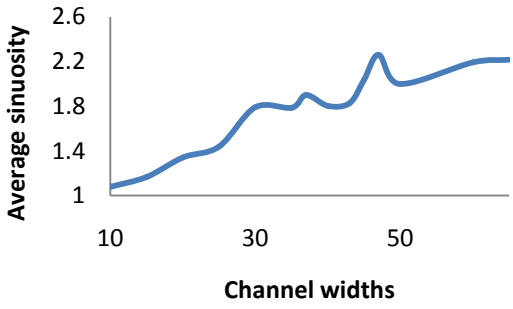

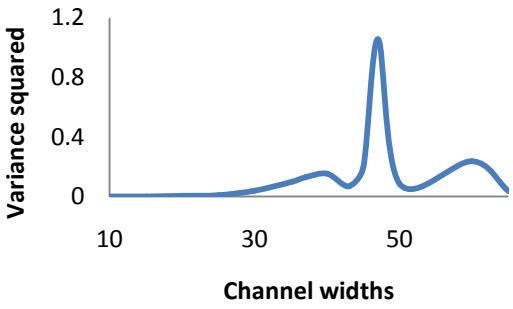

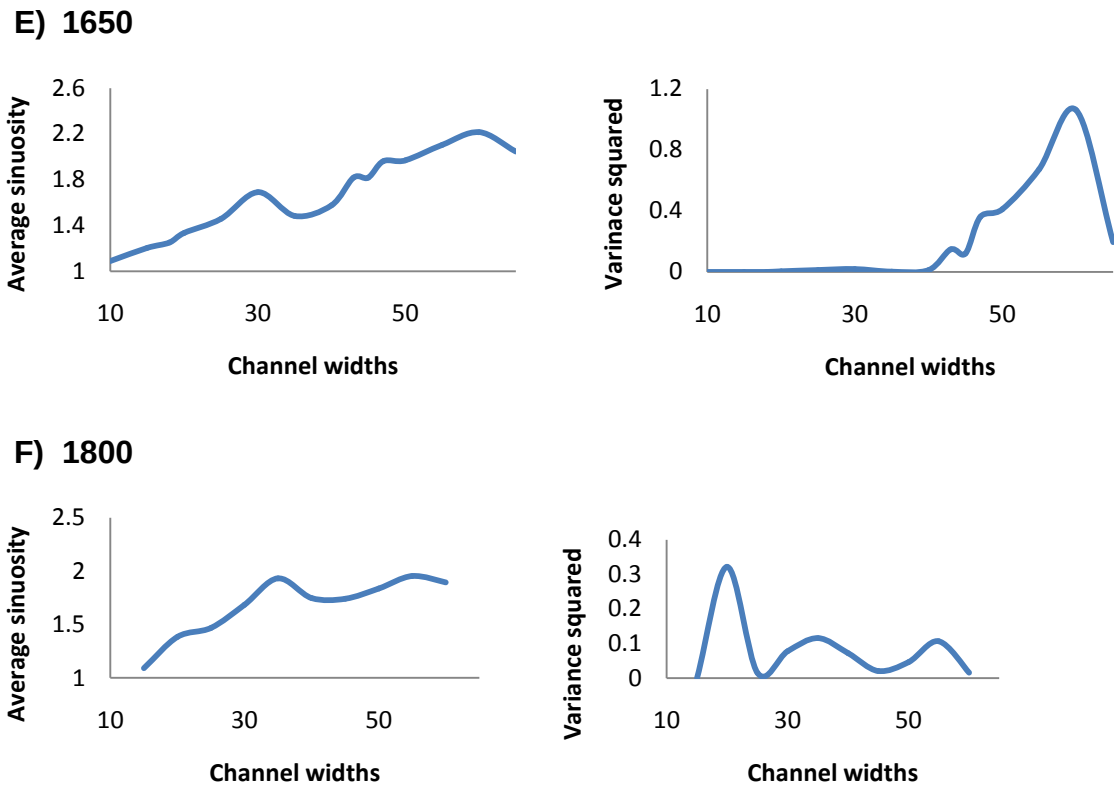

Figure 3.20: Sinuosity mean and variance versus normalized reach length for the simulated channels listed in Table 3.5 and shown in Figure 3.19.

The graphs in Figure 3.20 indicate breaks or levelling off of average sinuosity and correspond to peaks in sinuosity variance, similar to those of natural channels. Lancaster and Bras (2002) noted differences in model outputs for different simulations due to differing channel sinuosities caused by the frequency of channel cut-offs as a result of the stage of channel development. The outputs analysed in this study were all within the period of dynamic equilibrium, so are after the stage of initial channel development, and channel sinuosity fluctuates only a little around an equilibrium value.

The sinuosities at the length-scales for simulated channels are generally clustered as those in natural channels, with the exception that the largest length-scale is more tightly clustered. As in the findings of Lancaster and Bras (2002), the sinuosities at each of the length-scales are higher than those found in natural channels, with the difference being greater at larger length-scales (see Table 3.6). Lancaster and Bras (2002) explained this finding by the

difference in the nature of the channel planform generated by the model and that observed in natural channels; in the natural channels s'_{v2} was found to correspond to multi-loop and compound bends, whereas in model simulations s'_{v2} was found to correspond to very long sinuous bends. By comparison of the natural channel length-scales in Figure 3.18 and those from simulated channels in Figure 3.21, it can be seen that whilst the model does produce multi-loop bends, they are more regular and more sinuous than those from natural channels. However overall, the model does produce values to the data from natural channels.

Table 3.6: Difference between sinuosities at each of the three length-scale between natural and simulated channels.

	s'_{sb}	s'_{v1}	s'_{v2}
Average in natural channel	1.18	1.33	1.43
Average in simulated channel	1.73	2.12	2.27
Difference	0.55	0.79	0.84

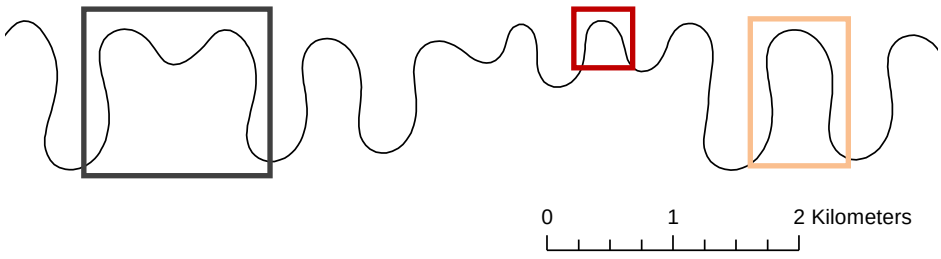

Figure 3.21: The forms represented by the three channel length-scales shown in Figure 3.19 and Table 3.5 from the output for iteration 1600. Red boxes indicate s'sb,, orange s'v1, and black s'v2.

3.3.4. Results of correlation between sinuosity and erosion

The model was then run from a straight line for 64 individual parameter sets (see Appendix B Table 84 for details of parameter sets used) taken from

the range of parameters estimated from the calibration procedure. Correlation analysis was performed on the model outputs from each of the 64 parameter sets to analyse the relationship between sinuosity and erosion. The results of these analyses are shown in Appendix B Table 84.

As can be seen from the results, the correlation between bank erosion rate and sinuosity is observed to be positive for some model parameter sets, and negative for others. Figure 3.22A, Figure 3.23A, Figure 3.24A, Figure 3.25A show a time series plot covering the period of dynamic equilibrium of the channel sinuosity (red) and bank erosion (blue) from individual model outputs obtained with different parameter sets. The scatterplots in Figure 3.22B, Figure 3.23B, Figure 3.24B and Figure 3.25B show channel sinuosity and erosion rate for the same model output data sets, also during the dynamic equilibrium period. As a result of the different parameter combinations used, the results shown in these figures represent channels of differing average channel sinuosity (averaged over the period of dynamic equilibrium).

A

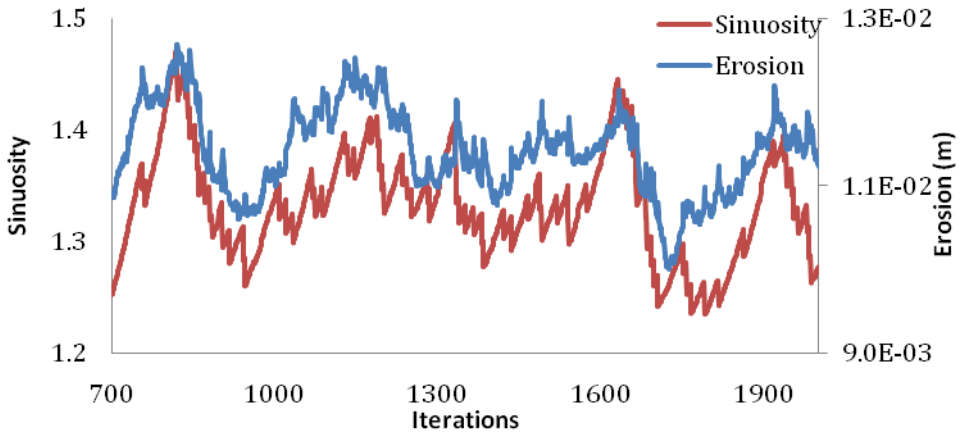

B

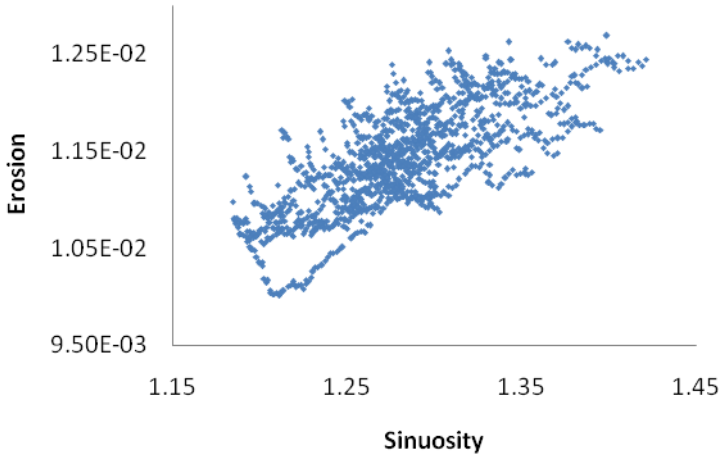

Figure 3.22: A: Time series plot of erosion and sinuosity during the dynamic equilibrium period, parameter values: E:0.3, A:0.5, G:2.0, CC:2. B: Scattlerplot of sinuosity vs. erosion for same parameter set, for the dynamic equilibrium period. Average channel sinuosity 1.28.

A

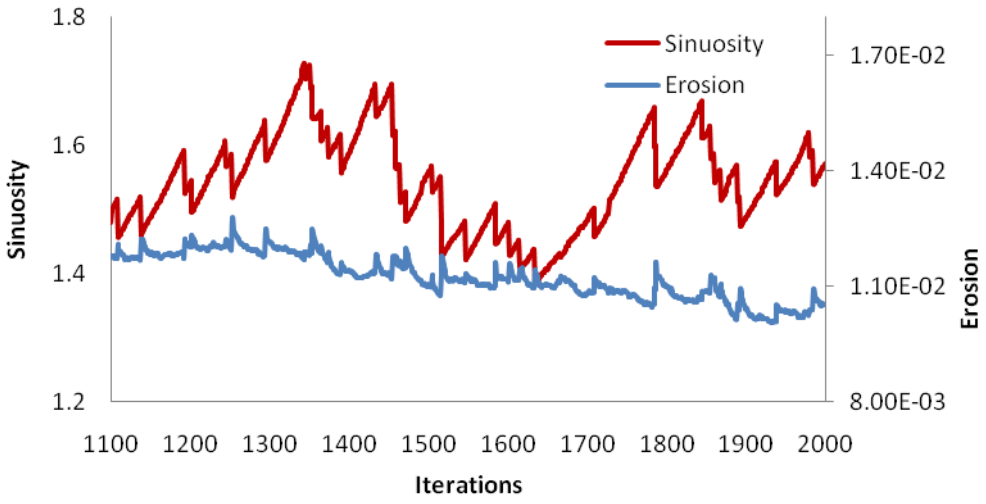

B

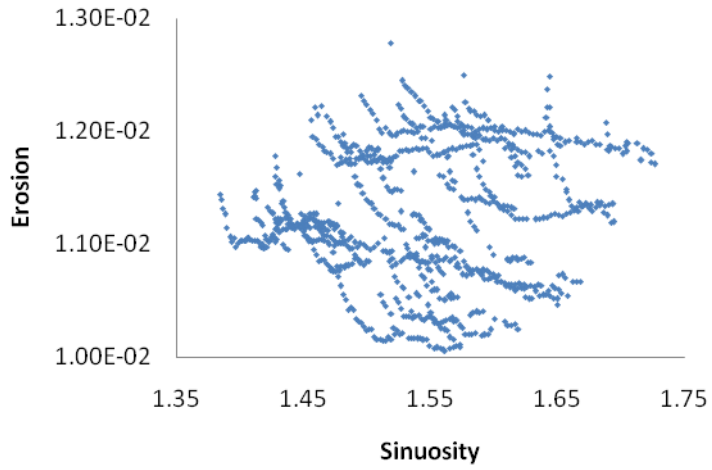

Figure 3.23: A: Time series plot of erosion and sinuosity during the dynamic equilibrium period, parameter values: E:0.4, A:0.6, G:2.0, CC:3. B: Scattlerplot of sinuosity vs. erosion for same parameter set, for the dynamic equilibrium period. Average channel sinuosity 1.54.

A

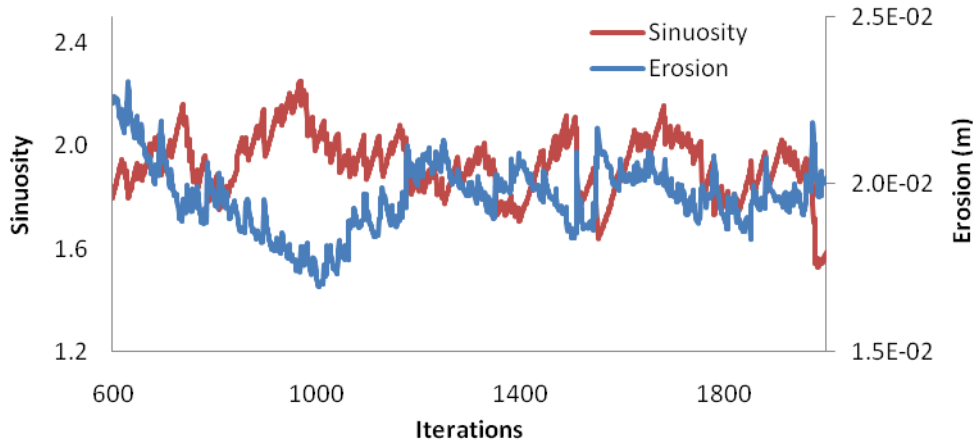

B

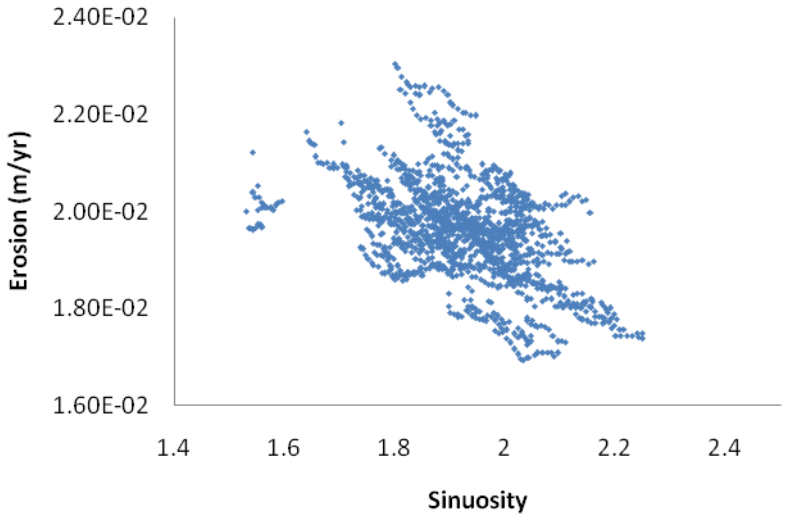

Figure 3.24: A: Time series plot of erosion and sinuosity during the dynamic equilibrium period, parameter values: E:0.4, A:0.5, G:1.5, CC:5. B: Scattlerplot of sinuosity vs. erosion for same parameter set, for the dynamic equilibrium period. Average channel sinuosity 1.93.

A

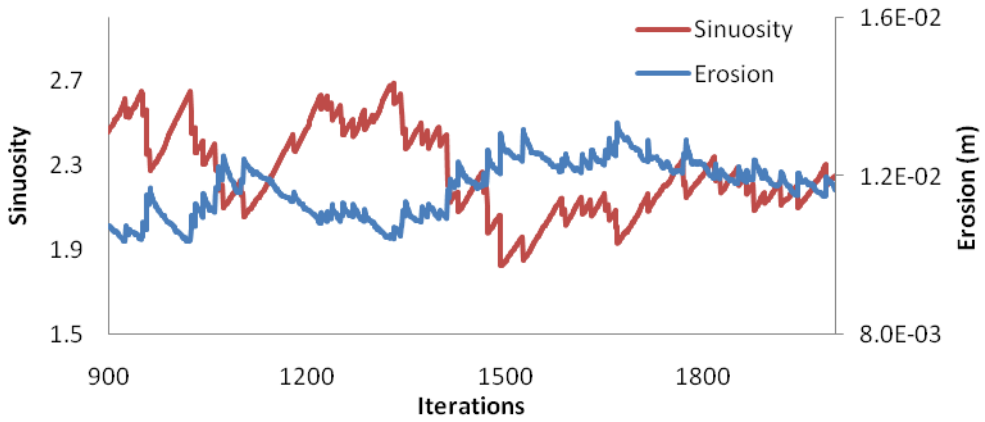

B

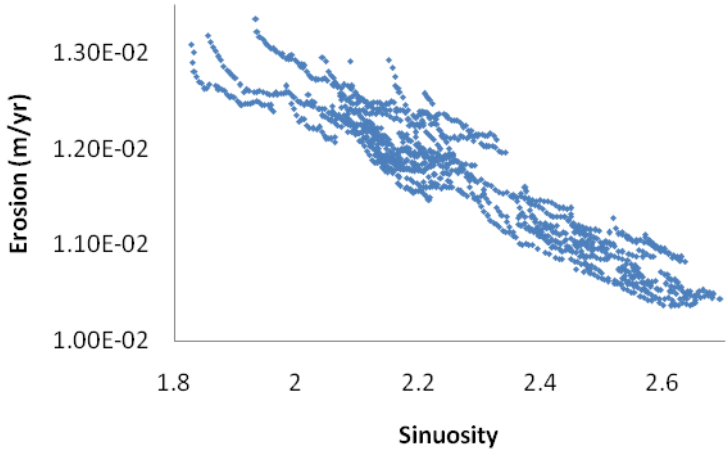

Figure 3.25: A: Time series plot of erosion and sinuosity during the dynamic equilibrium period, parameter values: E:0.3, A:0.6, G:2.0, CC:7. B: Scattlerplot of sinuosity vs. erosion for same parameter set, for the dynamic equilibrium period. Average channel sinuosity 2.27.

Figure 3.22 shows a positive relationship between sinuosity and bank erosion (R=0.754). The average sinuosity for the channel in this model output was 1.28. Figure 3.23 also shows a positive relationship between sinuosity and bank erosion (R=0.098), however this relationship is much weaker than that observed in example A. The average sinuosity for the channel in this model output was 1.54. Figure 3.24 shows a negative relationship between sinuosity and bank erosion (R=-0.492). The average sinuosity for the channel in this

model output was 1.925. Figure 3.25 also shows a negative relationship between sinuosity and bank erosion (R=-0.939), however this relationship is much stronger than that observed in example C. The average sinuosity for the channel in this model output was 2.27. Figure 3.26 shows a scatterplot of all four of these examples, with R^2 values and trendlines shown, indicating the changing strength and sign (positive or negative) of the relationship between erosion and sinuosity, depending on the parameter set chosen, and hence the average sinuosity of the simulated channel.

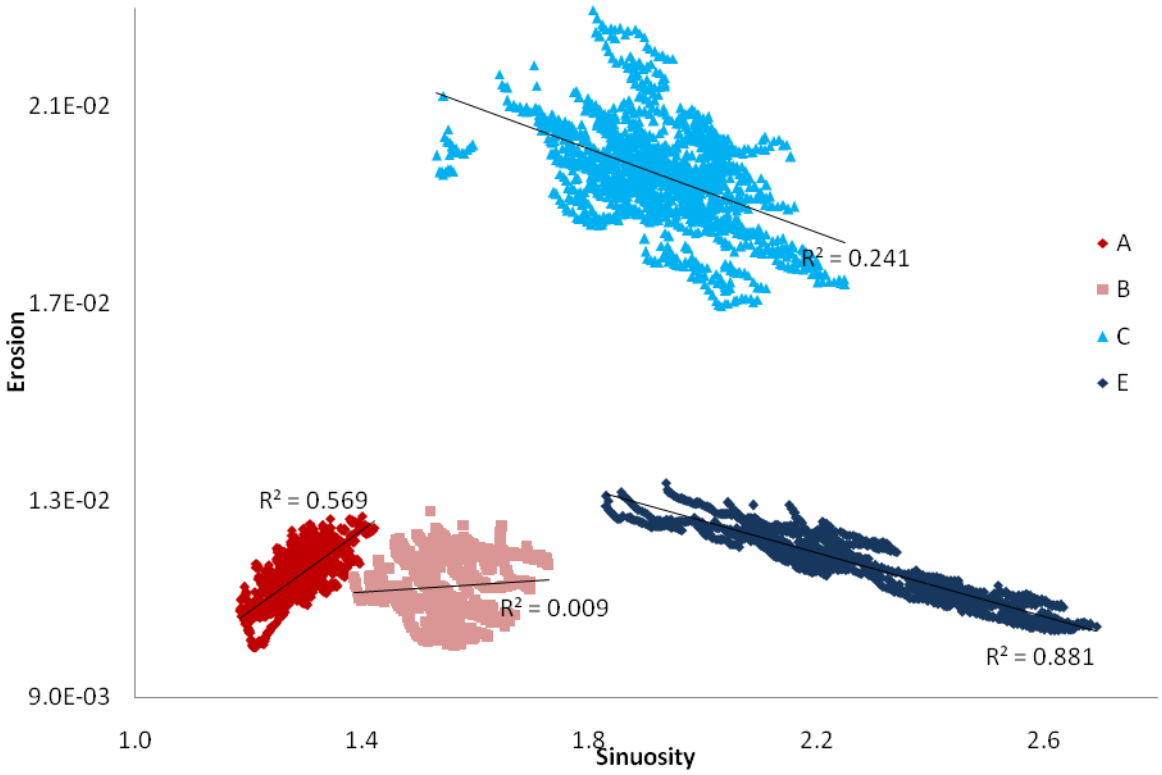

Figure 3.26: Scatterplot of four examples of model output with different parameter combinations: A:E0.3,A0.5,G2.0,CC2; B: E0.4,A0.6,G2.0,CC3; C: E0.4,A0.5,G1.5,CC5; D:E0.3,A0.6,G2.0,CC7. Trendlines and R^2 values are shown to illustrate the varying nature and strength of the relationship between erosion and sinuosity when the parameter set is changed, and hence average channel sinuosity is changed.

From this analysis it is clear that in channels of low sinuosity the relationship between bank erosion and sinuosity is positive. As the sinuosity of

the channel increases the positive relationship between bank erosion and sinuosity weakens, and eventually a threshold value of sinuosity is reached and the relationship becomes negative. As sinuosity increases further above this threshold value the negative relationship between sinuosity and bank erosion strengthens. Figure 3.27 indicates the relationship between average sinuosity and erosion rate for various values of channel sinuosity, (each point represents a different parameter set, as indicated in Appendix B Table 7.8) and indicates the switch from a positive to a negative relationship occurs at channel sinuosities of approximately 1.5.

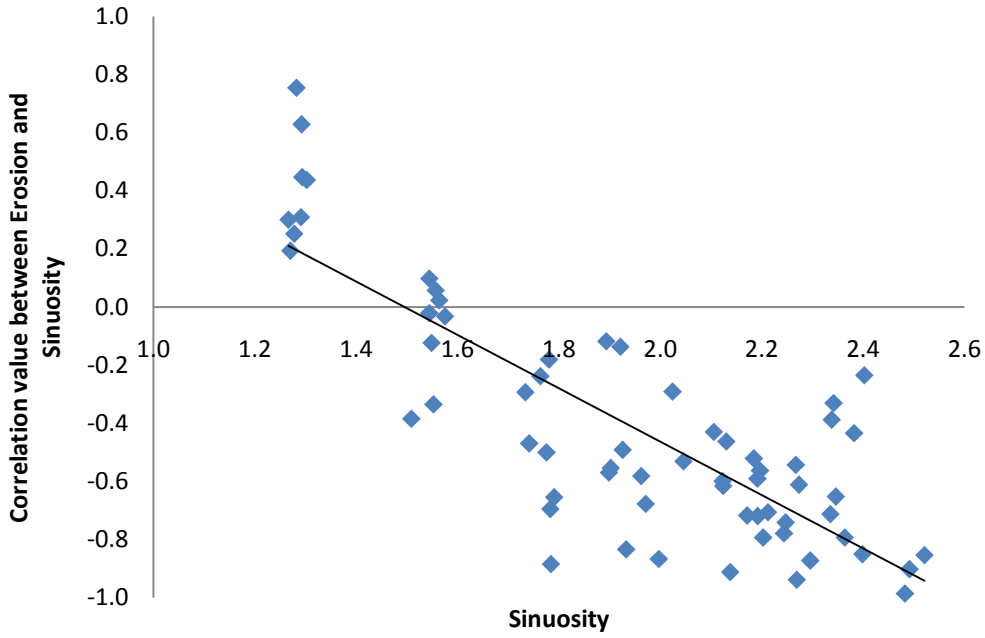

Figure 3.27: Relationship between sinuosity and correlation coefficient between average sinuosity and average erosion (averaged within the period of dynamic equilibrium). Each point represents a model simulation with a different parameter combination (see Appendix B Table 7.8). From the graph it can be seen that the relationship between sinuosity and erosion switches from positive to negative at sinuosities of ~1.5.

The influence of the chute cut-off parameter on the channel sinuosity can be seen in Figure 3.28. As the chute cut-off parameter decreases, the

frequency of chute cut-offs increases, thereby restricting the sinuosity of the channel.

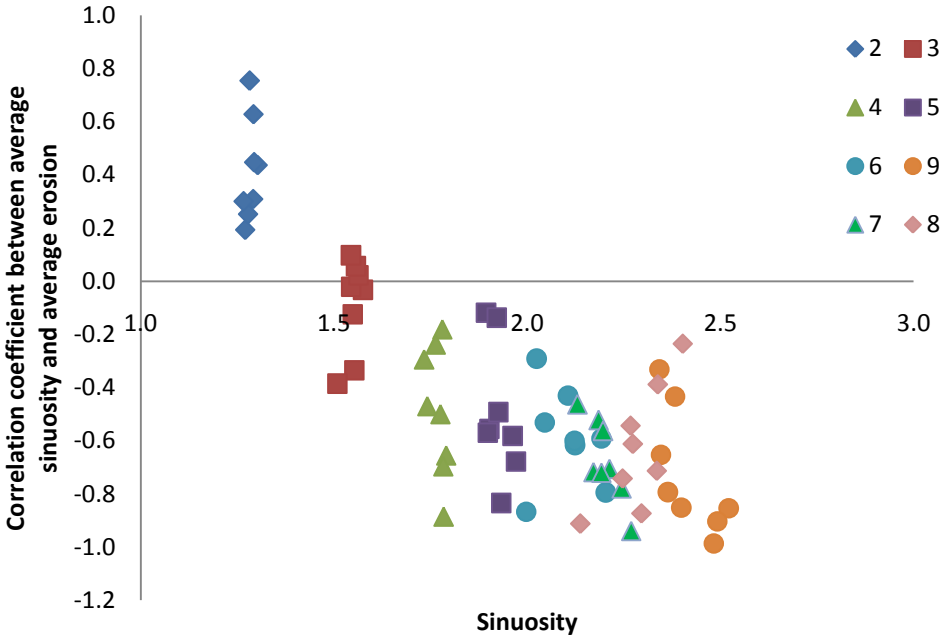

Figure 3.28: Scatterplot indicating the influence of varying the chute cut-off parameter on the sinuosity of the model output, and the correlation between sinuosity and erosion rate.

3.4.Analysis

The relationship between the average sinuosity over a simulation and average erosion rate for all model outputs from each of the 64 parameter combinations is shown Figure 3.29. From this scatterplot it is clear that there is a general decrease in erosion rate as sinuosity increases. As noted in Figure 3.27 at lower sinuosities there is a positive relationship between erosion rate and sinuosity, and erosion rate increases with increasing sinuosity. This is not clear in the graph in Figure 3.29 due to the small number of model runs with sinuosities below the observed threshold value of ~1.5 (only 8 of the 64 parameter combinations produced a model output with average sinuosity below 1.5).

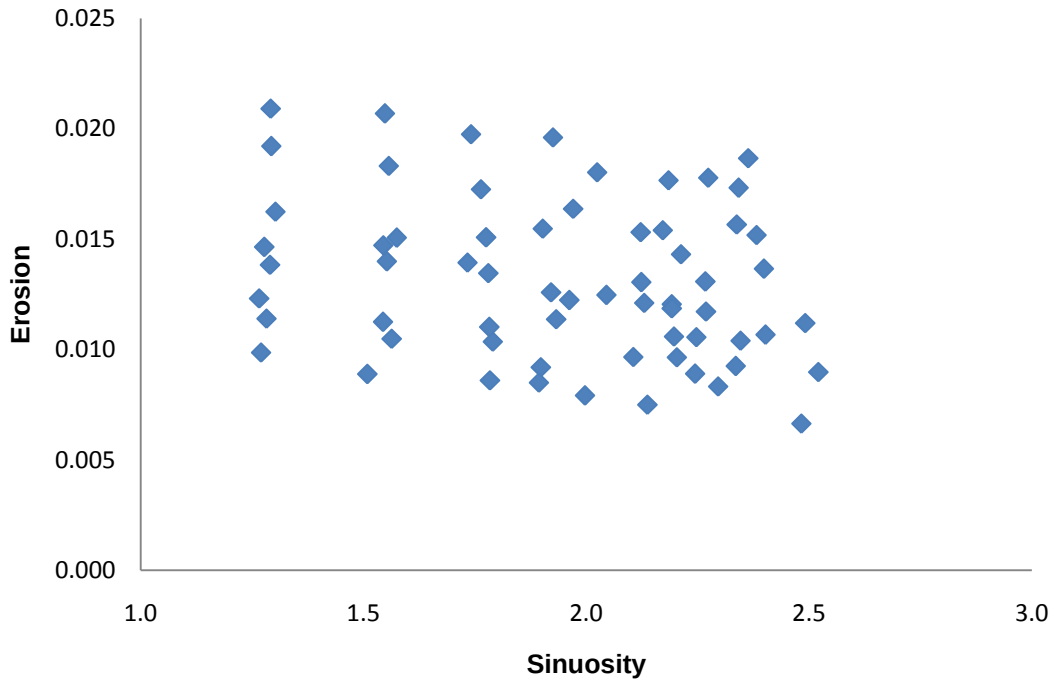

Figure 3.29: Relationship between average sinuosity and average erosion rate for model simulations using 64 parameter value combinations. The x-axis has been reversed (sinuosity decreases to the right) to allow comparison with the Nanson and Hickin style graph, because sinuosity decreases as radius of curvature increases.

From the original GIS data set covering selected UK river channels, only 2 channels within the 65 sub-catchments had sinuosities below 1.2 and had an average sinuosity of 1.57. Therefore, as the migration model was calibrated using this data, the model the outputs from all the 64 parameter combinations produced similar values of sinuosity, and no model output is associated with a sinuosity below 1.2. Therefore the model was run to produce channels with lower sinuosities, to investigate if the relationship between sinuosity and bank erosion at lower values of sinuosity is similar to the relationship between bank erosion and channel curvature ratio (for low channel curvature). This was achieved by lowering the chute cut-off parameter, which leads to a greater frequency of chute cut-off and reduces channel sinuosity (see parameter combinations used in Appendix B Table 7.9). The results from this are shown in Figure 3.30 with the results from the original 64 parameter combinations. With the additional data points from model outputs with a lower sinuosity, the relationship between sinuosity and erosion is clearly non-linear. For values of sinuosity lower than 1.5, bank erosion increases as sinuosity increases.

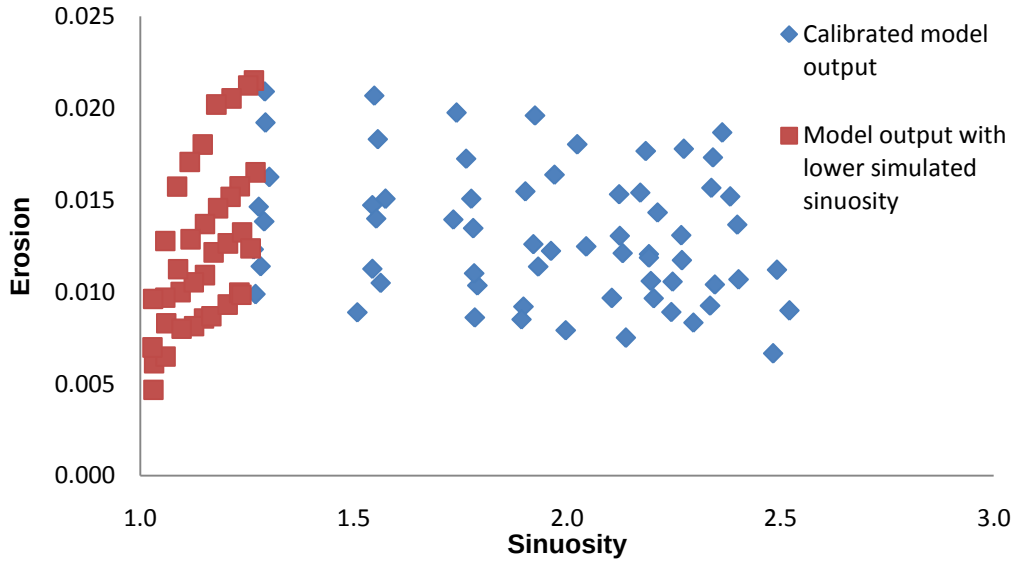

Figure 3.30: Scatterplot of average sinuosity and average erosion from calibrated model parameter sets, and from model outputs with lower simulated sinuosity by reducing chute cut-off parameter.

Additionally, as shown in Figure 3.31 the correlation coefficient between average erosion and average sinuosity becomes increasingly positive as channel sinuosity decreases.

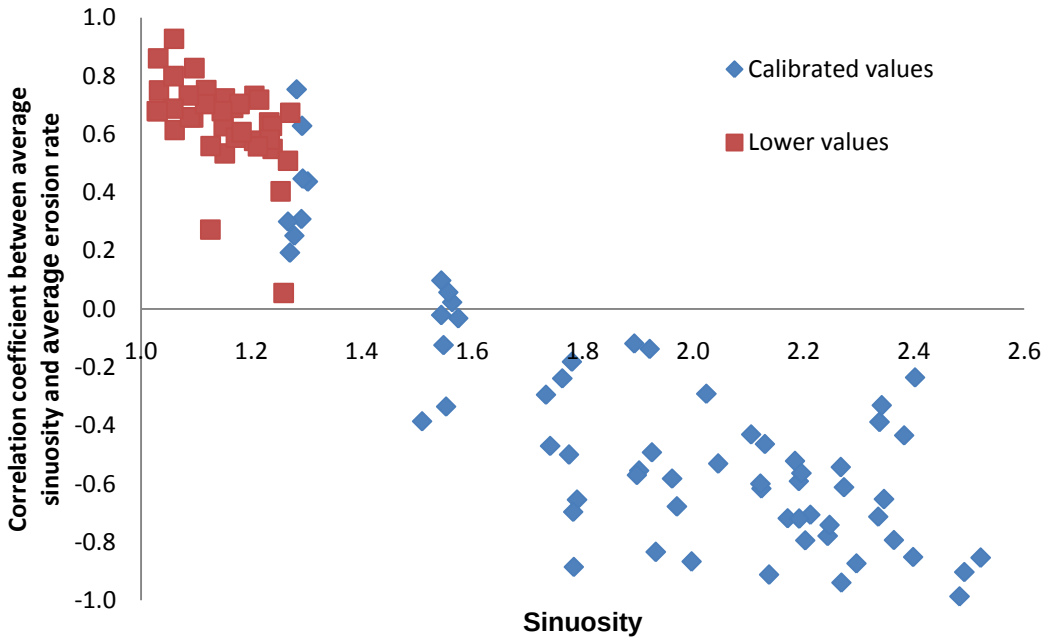

Figure 3.31: Scatterplot of average sinuosity and correlation coefficient between average sinuosity and average erosion rate. The points in blue indicate model outputs when parameter values are within the calibrated parameter value ranges, and data points in red indicate where parameter values have been modified to allow channels of lower sinuosities to develop.

The model results indicate that with low values of sinuosity (or high radius of curvature) bank erosion rates are low, and as sinuosity increases (or radius of curvature decreases) bank erosion rate increases up until a threshold value of sinuosity of approximately 1.5. As sinuosity increases above this threshold value (or radius of curvature decreases below this value) bank erosion rate decreases. This non-linear relationship between sinuosity and bank erosion is similar to the relationship between radius of curvature and bank erosion as observed in natural channels. The scatterplot of the calibrated model outputs alone only represents data for the end of the growth period and the termination stage of the Nanson and Hickin graph (see Figure 3.32) where

further increases in sinuosity (or decrease in radius of curvature) result in a decrease in bank erosion rate. When including the data from model outputs with lower channel sinuosity the resemblance to the relationship observed between radius of curvature and bank erosion as observed in natural channels is clearer.

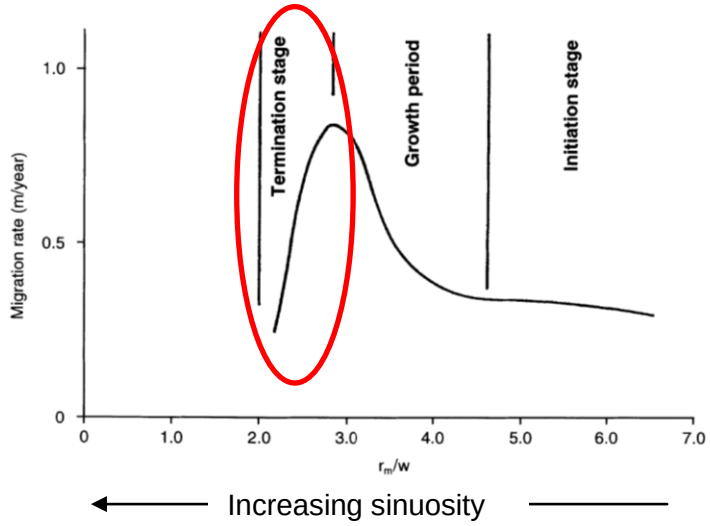

Figure 3.32: The Nanson and Hickin graph relating migration rate to channel curvature ratio, the red circle indicates the portion of this graph represented by the data from the model outputs for the 64 parameter sets used (adapted from Hooke, 2003).

As described in the previous chapter, radius of curvature can be calculated from a circular arc superimposed onto a meander channel centreline, with the radius of the arc being equal to the radius of curvature. As can be seen from Figure 3.33, as sinuosity of a channel increases the radius of curvature decreases. Therefore an inverse relationship exists between radius of curvature and sinuosity; as radius of curvature decreases sinuosity increases. Channel curvature ratio is calculated by dividing the radius of curvature by the channel width.

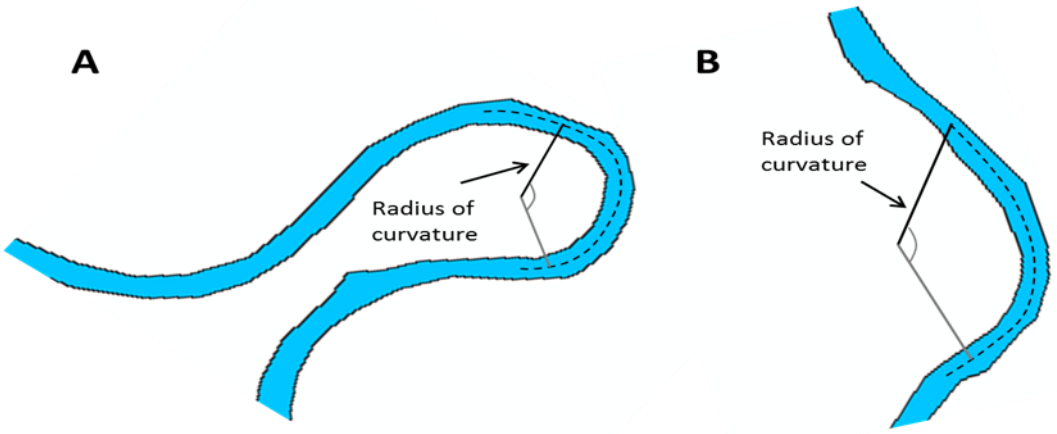

Figure 3.33: A - Channel with high sinuosity, radius of curvature is small. B - Channel of low sinuosity, with large radius of curvature.

The relationship between channel curvature ratio and erosion rate has also been detailed previously. High values of channel curvature ratio have been found to correspond to low bank erosion rate, and as channel curvature ratio decreases bank erosion rate increases until a peak value of radius of curvature/width of approximately 3.0. Therefore, due to the inverse relationship between radius of curvature/channel curvature ratio and sinuosity the results presented here are similar to those from natural channels found in previous studies investigating of the relationship between bank erosion and radius of curvature (Nanson and Hickin, 1986; Biedenharn *et al*, 1989; Hooke, 1997; Giardino, 2011). Where values of channel sinuosity are low (high channel curvature ratio) bank erosion increases with an increase in channel sinuosity, producing a positive correlation between bank erosion and sinuosity. Upon reaching a threshold value of sinuosity of approximately 1.5, any further increase in sinuosity results in a decrease in bank erosion rate, producing a negative correlation between bank erosion and sinuosity.

The physical explanation for the non-linear relationship between bank erosion and channel curvature ratio involves variation of the positioning and strength of the secondary flow within the channel. Changing flow patterns within the channel according to different values of channel curvature ratio result in

variation in the rate of bank erosion (as detailed in section 3.1.2.2). In channels that are relatively straight (low sinuosity and high radius of curvature) there is very little asymmetry in the channel cross-section and only a small portion of the velocity is distributed to the outer bank. Secondary circulation in the channel is weak. Bank erosion rates are therefore low. As channel curvature ratio decreases, asymmetry of the channel cross-section increases, resulting in more of the channel velocity being distributed to the outer bank and an increase in secondary circulation and the formation of helical flow. These three phases of meander development and migration in channels were defined by Hickin (1978) according to channel curvature ratio, channel asymmetry and flow structure as indicated in Figure 3.34. The high velocity core of secondary flow within the channel shifts according to the channel geometry, resulting in variation of channel bank erosion rates depending on channel sinuosity.

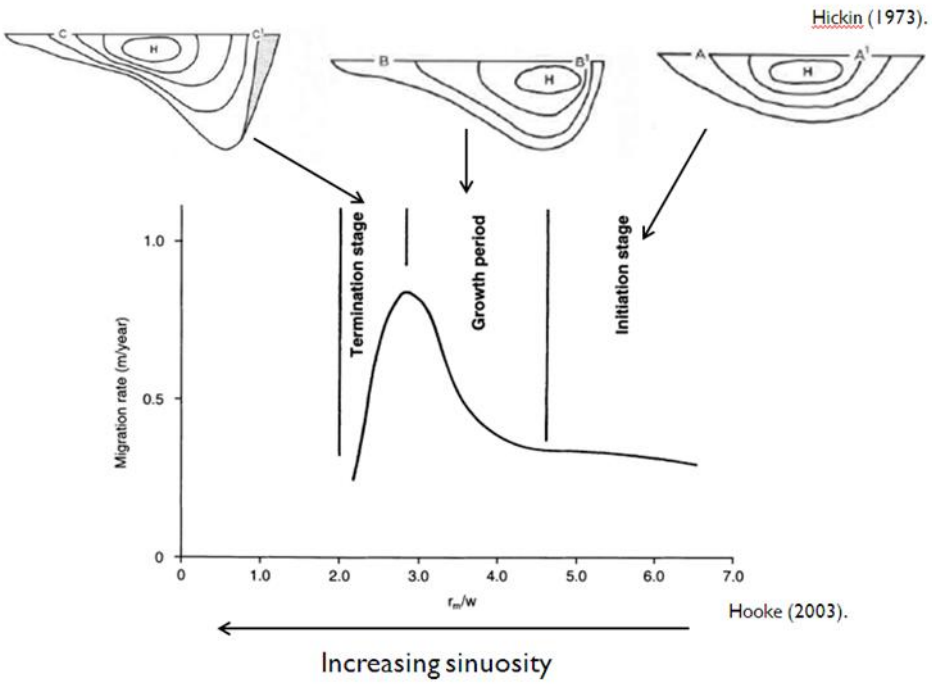

Figure 3.34: Model of non-linear relationship between rc/w and channel migration and the stages of meander development, adapted from Hooke (2003). The channel asymmetry and flow patterns resulting in this non-linear relationship with curvature were identified by Hickin (1973) and related to each of the 3 stages of the meander development model.

However, flow separation is not included within either the Howard and Knutson (1984) model or the Lancaster and Bras (2002) model and therefore cannot explain the observed relationship between sinuosity and bank erosion from the model outputs. Whilst the physical processes associated with secondary flow may explain the observed relationship between channel curvature ratio and bank erosion in natural rivers, and the relationship between sinuosity and bank erosion from both observations from natural channels and model outputs, there may be an additional causal factor to this phenomenon in natural channels.

As noted by Crossato (2009), the relationship between channel curvature ratio and bank erosion in moderately sinuous channels (i.e. with high values of channel curvature ratio) that is evident from model results can be explained by the local near-bank velocity excess which is driven by radius of curvature within kinematic models (in this case the Howard and Knutson model). However, the modelled decrease in migration rate with increasing sinuosity above ~1.5 (or as channel curvature ratio decreases below the threshold value of approximately 3.0) cannot be explained by the dependence of secondary flow on curvature. Crossato (2009) noted that the lag distance between near-bank velocity excess accounts for this effect. The lag effect within the Howard and Knutson (1984) models allows the incorporation of the influence of upstream channel geometry. This means that there is a lag distance between the effect of forcing (maximum curvature at the bend apex) and the point of maximum near-bank velocity. This effect has been noted in several studies; Furbish (1991), Meakin *et al*, (2006), Duan and Julien (2005), and is detailed in Figure 3.35.

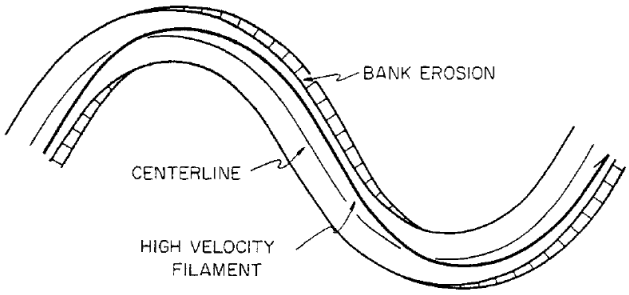

Figure 3.35: Position of high-velocity filament (dark line) within river channel and bank erosion (hatched area) within a sinuous channel. Near-bank velocity reaches a maximum downstream from channel apex. Taken from Furbish (1991).

In shorter and sharper bends the lag distance is large, and the location of maximum velocity moves further from the point of maximum curvature. Therefore these bends do not migrate and instead translate further downstream. This effect was noted by Furbish (1991) who observed the downstream migration of meanders, and that bends of small curvature disappear with iterations of the model. This means that the maximum rates of meander migration are downstream of the point of maximum curvature (bend apex) within the channel, resulting in the observed negative relationship between sinuosity and bank erosion at high values of sinuosity.

3.5. Conclusions

The relationship between sinuosity and bank erosion rate from the calibrated meander migration model output has been observed to be non-linear. Bank erosion increases with sinuosity until a threshold value of sinuosity of approximately 1.5, at which point any further increase in sinuosity results in a decrease in bank erosion rate. The physical explanation for the variation in bank erosion rate with channel curvature ratio is due to the relationship between channel curvature a, the strength of secondary flow circulation and the occurrence of flow separation within the channel.

Whilst the relationship between sinuosity and bank erosion produces a similar pattern to that of channel curvature ratio and bank erosion from observational data in natural channels, the explanation for this relationship from the model outputs is not the same as flow separation used to explain this relationship in natural channels is not accounted for within the migration models. The explanation for the increase in bank erosion with sinuosity up to the threshold value is the same as the physical explanation above, due to the dependence of bank erosion rates on channel curvature ratio within the model. However, the decrease in bank erosion rates above the threshold value of sinuosity observed in the model outputs is due to the lag effect, introduced by the weighting procedure within the model. With increasing values of sinuosity above the threshold value, the lag distance (i.e. the distance between the bend apex and point of maximum bank shear stress) increases. Therefore locations in the channel with high sinuosity, above the threshold value (low channel curvature ratio, below the threshold value) are not the locations with maximum bank erosion. Locations of maximum bank erosion within the channel are located further downstream. This follows observations in natural channels of downstream migration of meander bends.

The relationship between bank erosion and sinuosity has been analysed using output from the calibrated meander migration model as opposed to observational data. However, no observational data exists over time scales required for such an analysis. The model performance was validated against a data set covering approximately 150 years (depending on catchment) and validation statistics confirmed the model's capability to reproduce bank erosion rates over these time scales. Additionally, analysis of channel planform was

conducted, identifying characteristic length-scales in both natural and simulated channels, which indicate the model's ability to reproduce realistic channel planforms. Based on this it was assumed that the model's performance over time scales greater than 150 years would be acceptable.

The model has been calibrated using under present day conditions (over the last 150 years). Under future environmental change scenarios, both climate and land use changes may influence channel sinuosities and channel migration patterns. Rates of channel migration may be influenced by environmental changes as discussed in the literature review; increased bank erosion and channel migration may occur as a result of intensification of farming practices (arable intensification resulting in the removal of natural vegetation, destabilising channel banks, and pastoral resulting in increase bank destruction through trampling). Additionally increased urbanisation and bank protection will decrease channel migration rates. Climatic changes to rainfall across catchments may change both the volume of precipitation and magnitude of rainfall events, altering channel discharge and bank erosion rates. Therefore the model may not represent channel migration under future environmental scenarios with the same level of accuracy. However, the purpose of this work was to identify the nature of the relationship between bank erosion and sinuosity, resulting in the observation of a non-linear relationship and threshold value, which could then be incorporated within a bank erosion model. If the assumption that this relationship, and threshold value remains the same (or similar) under future environmental conditions is true, this should not influence the accuracy of the bank erosion model. This is a reasonable assumption as this relationship is due to the nature of water flow in meander bends, rather than environmental conditions.

The meander migration model used in this analysis (the Howard and Knutson model) is a kinematic model of meander migration; the model calculates migration rates based on an empirical relationship relating erosion to the channel curvature, and hence the model does not include simulation of secondary flow. As this kinematic model was found to be capable of accurately simulating channel migration in this study, the use of this model was preferable compared to a more complex alternative (such as a dynamic model, which involves solution of equations of flow within the channel).

The analysis between sinuosity presented in this chapter provides a basis for including sinuosity within a predictive tool for quantifying bank erosion model, rather than basing such predictions on measurements of radius of curvature. The benefit of this is that the sinuosity is much easier to calculate than channel curvature ratio. In the following chapters of this thesis, I aim to incorporate the non-linear influence of sinuosity on bank erosion rates into an existing bank erosion index.

4.Routing Model

4.1. Introduction

As noted previously this thesis aims to develop a bank erosion-modelling tool, which can be coupled to existing sediment generation models such as PSYCHIC. Currently PSYCHIC is being revised and will be succeeded by a new model known as the APT model (ADAS Pollutant Transfer model). This model does not currently include a channel routing component; overland sediment and water generation, and delivery to the channel network is estimated. This chapter aims to develop and test a simple routing procedure, which can be coupled to overland sediment generation models and used to route water and sediment through the catchment.

In this chapter, a routing model will be developed and validated for water routing within the Exe catchment, UK, using the APT model output as input data. In the following chapter sediment routing will be included within the model. The bank erosion index will also be incorporated within the routing model to enable inclusion of sediment contribution from bank erosion within the channel.

4.1.1. Background - Channel routing

Channel routing techniques can be classified as hydraulic or hydrologic. Hydraulic techniques are based on the solution of partial differential equations, such as the St. Venant or dynamic wave equations. Hydrologic routing is based on the solution of the continuity equation and a relationship between storage and discharge within a reach (Chow, 1959). The continuity equation can be written as:

$$I - O = \frac{\Delta S}{\Delta t}$$

Where *I* and *O* are inflow and outflow to the reach over time *Δt* respectively, and *S* is storage within the reach. The equation of conservation of mass is then used to define storage routing:

$$\frac{O_1 + O_2}{2} = \frac{I_1 + I_2}{2} - \frac{S_1 - S_2}{\Delta t}$$

The relationship between storage and discharge of a reach is not uniform during the passing of a floodwave. Figure 4.1 indicates that storage for a given discharge (and hence water surface slope) is greater on the rising limb of a floodwave than on the falling limb. Due to this looped relationship the application of hydrological routing methods is limited as the relationship between storage and discharge within hydrologic routing is typically single-valued.

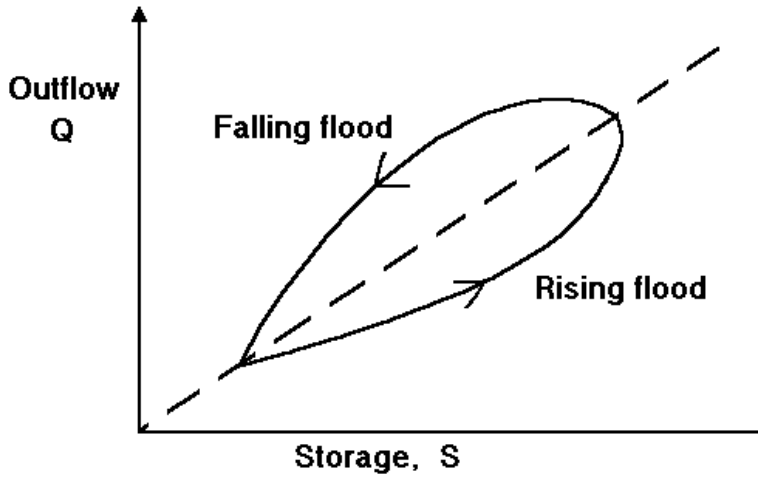

Figure 4.1: Looped storage-outflow relationship for river reach during a floodwave. Taken from US Army Corps of Engineers (1994).

Models can be described as lumped or distributed; lumped models compute flow as a function of time at one location, distributed models compute flow as a function of time at several cross-sections along the channel simultaneously. Lumped flow routing is simplistic compared to distributed methods. In addition, lumped methods neglect backwater effects and are not accurate for hydrographs with a rapid rising limb (Fread, 1992). Distributed models can allow representation of variation in flow rates, velocities and depth at cross-sections along the channel and therefore provide a more accurate representation of flow.

These models can also be sub-classified as kinematic or diffusion wave models. Kinematic models assume gravity and friction forces control the motion of the hydrograph along the channel. Uniform flow is therefore assumed in terms of momentum, meaning kinematic models cannot represent attenuation of the floodwave, hence diffusion does not occur . Flow disturbances can only propagate downstream in kinematic models, making them unsuitable where backwater effects are significant (Fread, 1992). Diffusion models include a pressure differential term, which allows for diffusion (attenuation) of the floodwave. Diffusion models are applicable to a wider range of hydrographs and bottom slopes than kinematic models (Fread, 1992).

Hydraulic routing methods have been shown to accurately represent discharge and floodwave propagation within river catchments (Connell *et al*, 2001; Hicks and Peacock, 2005; Nicholas and Mitchell, 2003). However, due to the high demand of computational power and quantity of input data (such as surveyed channel cross-sectional profiles and flow resistance data) their application at catchment scale is limited. Hydrologic methods of routing are less complex and have been found to provide satisfactory results in several applications (Bates and De Roo, 2000; Bell *et al,* 2007; Cole and Moore, 2009; Haltas and Kavvas, 2009; McMichael *et al*, 2006; Moramarco and Singh, 2000; US Army Corps Engineers, 1994).

The Muskingum methodology is a commonly chosen method of routing because of its simplicity in comparison to hydraulic methods; the parameters have a physical basis (such as channel slope, width and reach length) and are easily available. Koussis *et al*, 2012 compared the accuracy of the Muskingum methodology with hydraulic methods at a reach scale and found the models performed equally well, yet required much lower computational effort. Additionally, the methodology has been successfully applied to catchments in previous studies (Choudhury *et al*, 2002; Tewodle and Smithers, 2006; Takeuchi *et al*, 1999; Sadeghi and Singh, 2010).

The requirements of the routing methodology to be used within this study include: computational efficiency (so that it can be coupled to existing overland water and sediment generation models, and include further catchment sediment source and sink components which will be incorporated in the next chapter) and simplicity of implementation at a catchment scale (parameter values that are

easy to assess from available data). These requirements indicate the suitability of the Muskingum routing methodology for this study.

4.1.2.Muskingum method

The Muskingum method is a hydrologic method of routing, developed by McCarthy (1938), which accounts for the looped relationship illustrated in Figure 4.1. Storage within a reach is calculated as prism and wedge storage. Prism storage is storage under the steady-flow water surface profile, and wedge storage is the additional storage under the actual water surface profile.

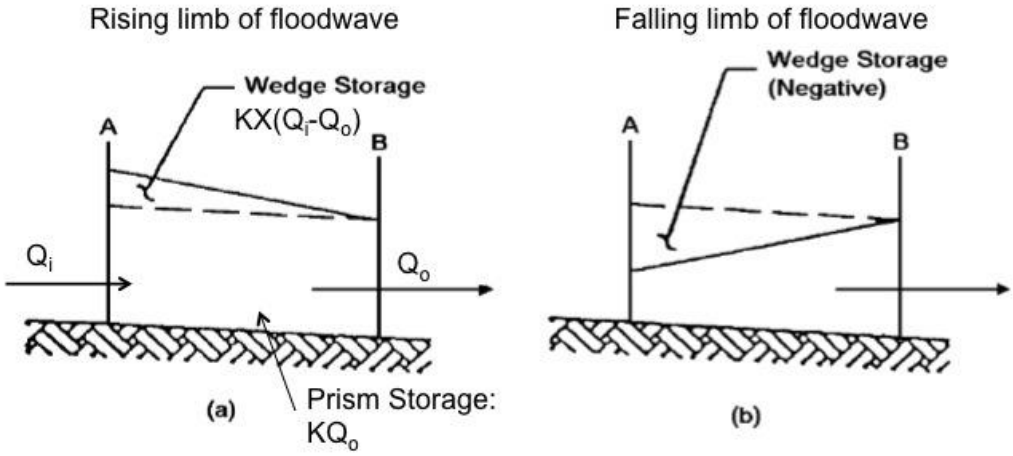

Figure 4.2: Muskingum prism and wedge storage concept. A: Rising limb of floodwave, positive wedge storage. B: Falling limb of floodwave, negative wedge storage Adapted from US Army Corps of Engineers (1994).

The Muskingum equation can then be derived as follows:

$$S = Prism\ storage + Wedge\ storage$$

$$S = KO + KX(I - O) \text{ or } S = K[XI + (1 - X)O]$$

Substituting this into the continuity equation produces:

$$O_2 = C_1 I_2 + C_2 I_1 + C_3 O_1$$

This equation is known as the Muskingum equation where K is a storage constant with a dimension of time, and X is a dimensionless weighting factor. K corresponds to the travel time of the floodwave through the reach. X determines the attenuation of the floodwave as it passes through the routing reach. The value of X varies between 0 and 0.5. A value of 0 results in maximum attenuation of the floodwave and 0.5 results in pure translation of the floodwave. For most river channels it usually varies between 0.2 and 0.4 (Chadwick *et al,* 2004).

The constants are calculated as:

$$C_1 = \frac{\Delta t - 2KX}{2K(I - X) + \Delta t}$$

$$C_2 = \frac{\Delta t + 2KX}{2K(I - X) + \Delta t}$$

$$C_3 = \frac{2K(I - X) - \Delta t}{2K(I - X) + \Delta t}$$

Where the sum of C_1, C_2 and C_3 should be equal to 1.0.

Within the standard Muskingum method the parameters *K* and *X* are determined from stream flow records, and related to flow and channel characteristics. Simultaneous measurements of inflow and outflow discharge are used to calculate parameters K and X by either 1) least-squares estimation; 2) graphical estimation; 3) method of moments; 4) method of cumulants; 5) direct optimization method (Singh and McCann, 1980). The determined values of K and X are valid only for the given reach and event used for the calibration procedure. The Muskingum-Cunge method was developed (Cunge 1969) involving simple parameter estimation based on flow and channel characteristics using the following equations:

$$K = \frac{\Delta x}{c}$$

$$X = 0.5 - \left(1 - \frac{Q_0}{BS_0 c\Delta x}\right)$$

where Δx is the reach length, Q_0 a reference flow from the inflow hydrograph (taken as midway between the base and peak flow, US Army Corps Engineers, 1991), and *B* is the surface width of the channel associated with Q_0. c is the floodwave celerity and is estimated for a wide rectangular channel using Manning's friction law as:

$$c = 1.67v_0$$

Where v_o is the velocity corresponding to the discharge Q. The Muskingum-Cunge method is a physically based alternative to the standard Muskingum method. Parameter estimation using these equations enables channel routing in un-gauged streams with reasonable accuracy (Franchini *et al*, 2011; Mekawi, 2010; Tewolde and Smithers, 2006).

Ponce and Yevjevich (1978) then expressed the routing parameters of the Muskingum-Cunge in terms of the Courant (C) and Reynolds (D) numbers:

$$C = \frac{c\Delta t}{\Delta x}$$

$$D = \frac{q_0}{S_0 c\Delta x}$$

where q_0 is the flow per unit width and can be calculated based on the peak discharge (Ponce, 1994). The routing coefficients are then determined as:

$$C_0 = \frac{-1 + C + D}{1 + C + D}$$

$$C_1 = \frac{1 + C - D}{1 + C + D}$$

$$C_2 = \frac{1 - C + D}{1 + C + D}$$

And the routing equation is:

$$Q_{j+1}^{n+1} = C_0 Q_j^{n+1} + C_1 Q_j^n + C_2 Q_{j+1}^n$$

Or

$$Q_j^n = C_0 Q_{j-1}^n + C_1 Q_{j-1}^{n-1} + C_2 Q_j^{n-1}$$

where j is a spatial index and n a temporal index.

Within both the Muskingum and Muskingum-Cunge approaches, the parameter values and routing constants remain the same at each reach for all iterations. This is also known as linear mode, or constant parameter Muskingum-Cunge. A further development of the model has been proposed in some papers named the Variable Parameter Muskingum-Cunge (VPMC) where the parameter values are re-calculated during each iteration. This method is non-linear and results in a small loss of flow volume. Ponce (1982) stated that the differences in the level of accuracy between constant and VPMC are more marked over very long reaches and where wide variations in flow levels exist.

The temporal resolution of the Muskingum-Cunge method must be small enough to represent the shape of the hydrograph. The temporal resolution should be less than 1/5 of the rising limb of the hydrograph, and is also constrained by the following equation:

$$2KX < \Delta t \leq K$$

Ideally *K* should be equal to ***Δt*** (US Army Corps Engineers, 1994). Within the hydrological model TR-20, Merkel (2002) used inflow hydrographs to determine the time interval used in the routing. Where there are less than ten intervals to the peak of the hydrograph, the hydrograph is then interpolated to provide ten intervals.

Kumar *et al* (2011) investigated the sensitivity of the time interval used on the computed outflow hydrograph. Time intervals of 24,18, 12 and 6 hours were simulated and the outflow hydrographs are shown in Figure 4.3. The mean relative error of estimated outflow predicted by the model decreased with decreasing time interval (24hr=23.3%, 18hr=17.4%, 12hr=15.9%, 6hr=9.1%).

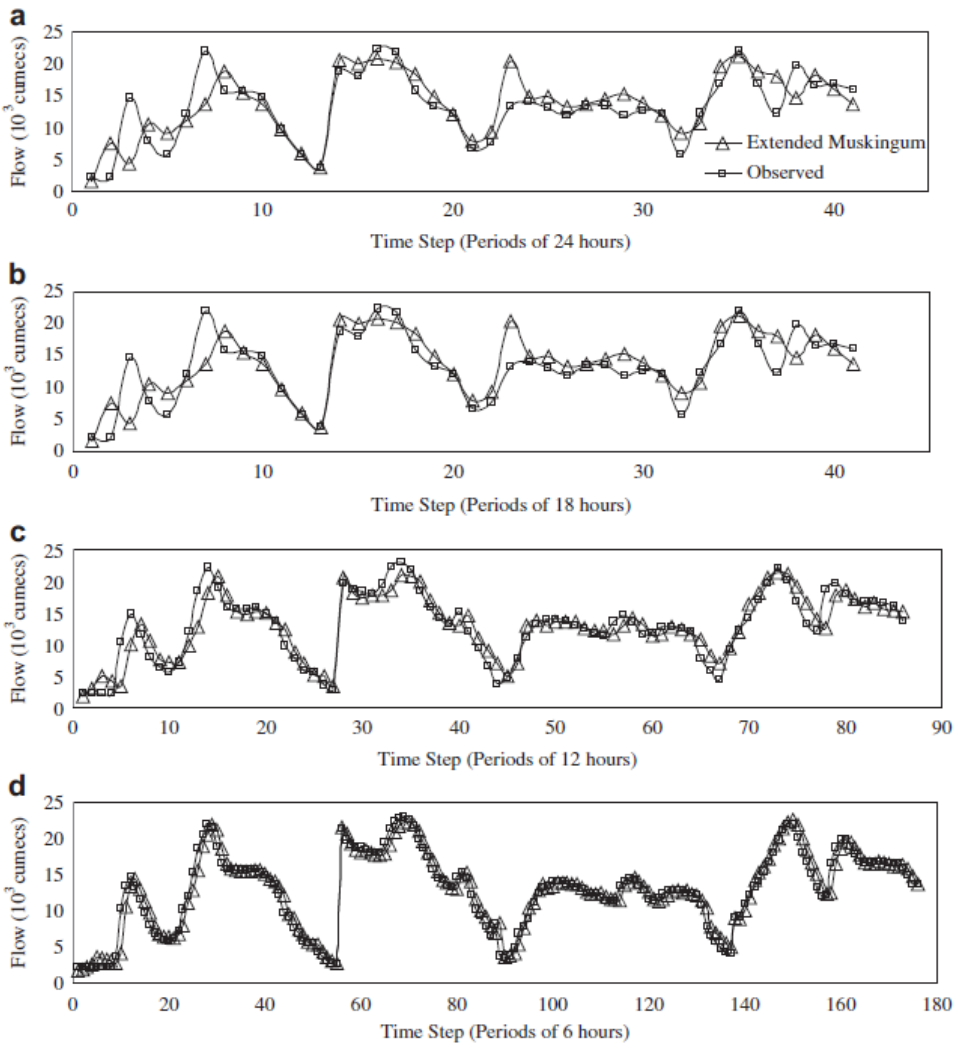

Figure 4.3: Performance of different temporal routing intervals. A: 24hours, B: 18hours, C:12hours, D:6hours. Taken from Kumar *et al*, (2011).

Merkel (2002) indicated the reach length within the routing procedure should not be significantly smaller than the distance travelled by the flood wave during a single time step. The suitability of the spatial resolution can also be determined through summing the Courant and Reynolds numbers (which are inversely related to reach length):

$$C + D \geq 1$$

If the Courant number is kept close to 1, dispersion in the hydrograph output is minimised (Cunge, 1969 and Ponce, 1994). Ponce and Chaganti (1994) noted one advantage of using the Muskingum-Cunge method was that the routing

results were independent of spatial and temporal resolution when numerical dispersion is minimised.

Barry and Bajracharya (1995) indicated the accuracy of the Muskingum-Cunge model depends on the ratio of the spatial and temporal resolution used. As can be seen from the previous equation, the Courant number is essentially a ratio between the spatial and temporal resolutions. Optimal results from the Muskingum-Cunge model were observed when the Courant number =0.5.

The ability of the Muskingum-Cunge methodology to accurately represent channel discharge when applied at a variety of spatial scales has been noted in several previous studies; Ponce *et al*, (1996) compared peak outflow and travel times from the Muskingum-Cunge model to those from outputs derived from the theory of linear stability. Two wave periods were used: 48 and 96 hours, and the spatial and temporal resolution of modelling for these were 6.25 miles and 1.5 hours, and 12.5 miles and 3 hours respectively. It was concluded that the Muskingum-Cunge routing accurately simulates flood wave propagation.

Mekawi (2010) used the constant parameter method to route floodwater along the Blue Nile, Sudan. The accuracy of the model was assessed within 3 separate reaches between 1969-2000. The mean coefficient of determination for these simulations when compared to observational data was 0.91. It was noted in one reach the simulated flows were under-estimated by the model due to lack of inclusion of lateral inflows.

Franchini *et al*, (2011) assessed the accuracy of the Muskingum-Cunge method with constant parameter values within 3 reaches of the Tiber river, Italy. The time intervals used were 4.9, 3.4 and 9.2 hours with spatial interval 40.23, 30.83, 71.06 km respectively. The model was simulated with lead times of 1,2,3,4 and 5 hours. The mean values of Nash-Sutcliffe and Mean square error were mutually consistent indicating the model reproduces both rising and falling limbs of the hydrograph. An increase in accuracy was observed with decreasing lag time. Additionally, it was noted the model may not be suitable for highly non-uniform reaches with significant overbank flooding due to marked damping effects, and in such instances non-linear mass conservative routing methods are more appropriate, although more computationally demanding. However the

model has successfully been applied to reaches with overbank flooding; Perumal *et al*, 2001 applied a variable parameter Muskingum method to 3 river reaches in Australia and assumed a constant channel width and floodplain width for each reach. It was noted that whilst this representation of the channel was crude, it was also unavoidable given the lack of cross-sectional channel and floodplain data. The model was found to accurately represent discharge during flood events where overbank flow occurred. Garbrect and Brunner (1991) also used the Muskingum method of flow routing to represent overbank flow by routing main channel and overbank flow separately and simulated hypothetical events. Both magnitude and timing of event peaks were compared to a hydraulic routing model output and differences were within 4%.

Tewolde and Smithers (2006) assessed the accuracy of the Muskingum-Cunge method in three sub-catchments of the Thukila catchment in KwaZulu-Natal, South Africa, using observational data. The spatial intervals used were 4, 21 and 54km, with temporal resolutions 0.5, 1.5, and 2.5 hours respectively. The model output outflow volume, peak discharge, timing of peak flow and shape of the hydrograph were similar to those from observational data. Statistical analysis showed low values of RMSE (<7.4), coefficient of efficiency close to 1 (all >0.82), and low volume error (all <12%).

Permual (1992) tested the VPMC Muskingum-Cunge method over a 40km reach for three different spatial resolutions; 40km, 5km and 1km. For each spatial resolution four different channel configurations were used, with varying bed slope and manning's roughness coefficient. The same inflow hydrograph was used for each simulation and was compared to the corresponding St.Venant solution. The results showed the reproduction of the St Venant outflow hydrograph was better when using multiple reach routing as oppose to single reach, however there was very little difference between the resolution from 5km to 1km. It was also noted that for all channel types the reduced outflow was produced at the beginning of the hydrograph but as the number of reach sub-divisions increased this effect was minimised.

Ponce and Chaganti (1994) used five Muskingum-Cunge techniques to model a flood wave with 96-hour period within a 500 mile reach. Each method was simulated using two levels of spatial and temporal resolution; 25 miles and 6 hours, and 12.5 miles and 3 hours. The five methods used were as follows;

- Constant-parameter method, CMPC: routing parameters C and D are same for all cells.
- Three-point variable-parameter, VPMC3: routing parameters C and D computed for each cell based on average unit-width discharge and celerity at three known grid points.
- Four-point variable-parameter, VPMC4: routing parameters C and D computed for each cell based on average unit-width discharge and celerity at four known grid points.
- Modified three-point variable-parameter, MVPMC3: routing parameters C and D computed for each cell based on average unit-width discharge and at three known grid points, and average celerity is calculated based on the average unit width discharge of the three points.
- Modified four-point variable-parameter, MVPMC4: routing parameters C and D computed for each cell based on average unit-width discharge and at four known grid points, and average celerity is calculated based on the average unit width discharge of the four points.

It was noted all five methods gave approximately the same peak outflow and time to peak. The constant parameter method conserved mass exactly whilst the variable parameter methods were subject to a small loss of mass, with the loss of mass greater for three-point than four-point methods. Additionally the loss of mass was greater for the conventional VPMC3 and VPMC4 compared to the modified MVPMC3 and MVPMC4.

The previous examples indicate the successful application of Muskinugm-Cunge methodologies (both constant and variable parameter methods) at a range of spatial and temporal scales. Both the Muskingum and Muskingum-Cunge methods are limited to diffusion waves. Additionally, in constant parameter versions of the model the influence of flow non-uniformity is omitted, yet with variable parameter versions there is some mass loss within the model. The method is suitable for channel routing in streams where there are no significant backwater effects.

The advantages of the Muskingum-Cunge approach include its simplicity in comparison to alternative diffusion wave models. The model can be

implemented where gauged data is sparse and channel geometry does not need to be defined in detail. The previous examples indicate that the Muskingum method accurately represents channel discharge at both reach and catchment scale.

4.1.3.Justification and aims

The aims of this chapter include to:

- Develop a computationally efficient catchment water routing model
- Include input water from surface runoff within the routing methodology
- Ensure the methodology conserves mass throughout the routing procedure
- Validate the accuracy of the model using gauging station data from the catchment

The overland sediment generation model PSYCHIC is outlined in the introduction chapter. The model does not include a channel routing component. In order to couple the model to a bank erosion tool a routing model should be developed. The routing model should be computationally efficient to enable integration within a larger model (i.e. a sediment budget model). To enable the routing model to be coupled to overland water and sediment generation models (such as PSYCHIC) input of water from overland flow should be included within the routing procedure. Sediment routing and input will be included in a subsequent chapter.

The accuracy of the routing methodology used will be validated by comparison of model outputs, and observational channel discharge data taken from gauging stations. The model should be able to predict the volume and timing of discharge with a reasonable degree of accuracy, which can be assessed quantitatively using validation statistics. The routing methodology chosen should also conserve mass as in natural systems; water input should equal water output.

4.2. Methodology

This section will outline how the output from the APT model was used as input data for a catchment routing model. The APT model provides data of both sediment and water delivery to the channel network. This chapter will use the water delivery data only. The model was applied to the Exe catchment, UK from 1991-2010.

The Muskingum-Cunge variable parameter method (VPMC) was chosen for the routing methodology. As outlined in the previous section, the Muskingum methodology is computationally efficient in comparison to hydraulic methods of channel routing, and accurate when applied at catchment scale (Biftu and Gan, 2004; Orlandi and Rosso, 1998; Tewolde and Smithers, 2006; Shrestha *et al*, 2007). Model performance in this study was assessed using daily flow data recorded at several gauging stations.

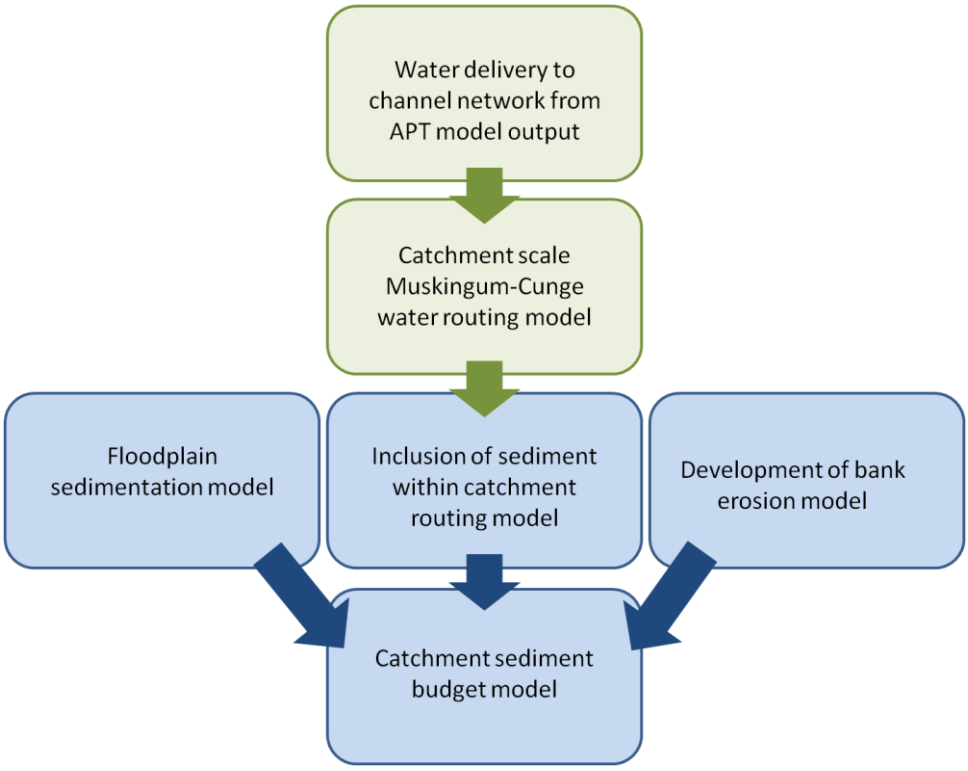

Figure 4.4: Schematic diagram to indicate how the routing model developed in this chapter will be used within this thesis. Green boxes indicate work in this chapter and blue boxes indicate work in the following chapter.

4.2.1. Routing data

The input data used for the routing model simulations were generated from the output of the updated APT model and provided by ADAS. This model succeeds the model PSYCHIC, and generates both overland sediment and water loads. In this chapter only the water data will be used.

The hydrological component of the APT model is based on the ADAS IRRIGUIDE model (Bailey and Spackman, 1996). Weather station meteorological data series are used as input for the model. These data are then interpolated between stations using a weighting interpolation function to provide meteorological data across the catchment. Four flow pathways are then quantified; surface runoff, rapid flow through soil, slow flow through soil, and deep seepage towards groundwater. The model uses a curve number approach to estimate runoff (smaller curve number indicating a greater risk of runoff) and curve numbers are approximated using the HOST classification (Boorman *et al*, 1995). A soil water storage capacity parameter is used to account for various soil surface conditions: moisture deficit, crop cover, trampling and poaching, capping, and tramlines. This parameter determines the proportion of rainfall that becomes surface runoff. Re-infiltration of surface flow is estimated from slope, field length, and the storage capacity parameter.

The APT model generates data over a $1km^2$ grid with a daily temporal resolution (see Figure 4.5 A). The data generated by the model and used here covers a period of 20 years (from October 1st 1991 – September 30th 2010). The channel network within the catchment is divided into a series of stretches. Thiessen polygons are used to define the land area contributing to each stretch, and the proportion of each $1km^2$ grid cell that is contained within each polygon. The channel network is then overlaid on a $500m^2$ grid (see Figure 4.5B) and the proportion of each stretch within each grid cell is determined. Mapping from the $1km^2$ grid to the $500m^2$ grid cells using the stretches provides the load for each $500m^2$ grid cell of the river network.

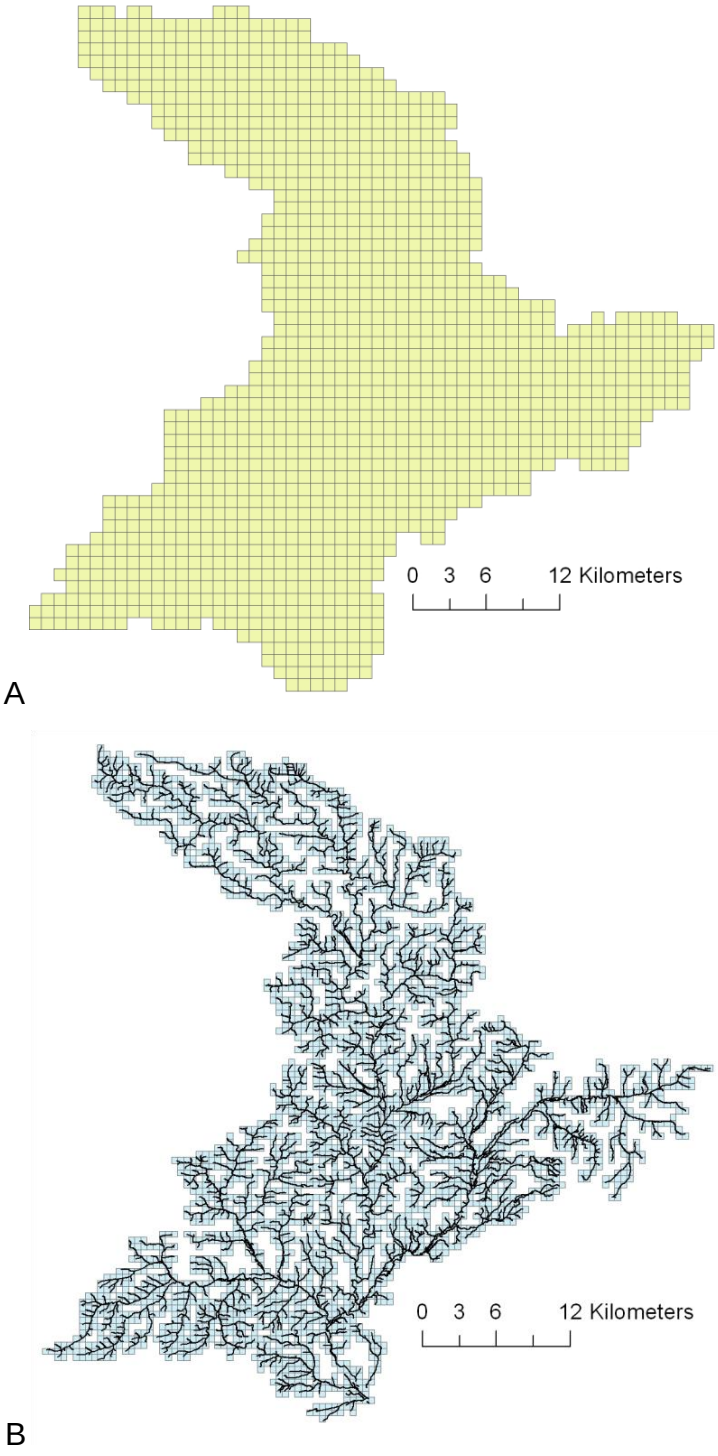

Figure 4.5: A - 1km^2 grid cells used for generation of APT model output data over the Exe catchment. B – 500m^2 grid cell data and catchment network overlay.

The channel network within the Exe catchment is divided into 15,506 individual stretches. These stretches were used to establish how the grid cells

linked together. Each stretch of river contains information on the stretch it flows to, the length of the stretch, and the grid cell the stretch occupies. Some stretches cover more than one grid cell. GIS was used to calculate the x and y co-ordinates of the upstream end of each of the stretches. This information was then used to establish the following details:

- Total number of stretches upstream of each stretch – used to calculate the order of each channel stretch.
- Number of stretches directly upstream of each stretch, and the stretch ID for each of these upstream stretches – required for the routing methodology, as discharge at each location is dependent on discharge at the channel stretch(s) directly upstream.
- Total number of grid cells each stretch flows through, and the grid cell(s) ID for each of these – used to calculate the total water (and sediment) delivery to each stretch.
- Total length of channel within each grid cell – used to calculate the proportion of water (and sediment) delivery to each stretch from gridcells which contain more than one stretch.
- Length of each stretch within individual grid cell(s) - used to calculate the proportion of water (and sediment) delivery from each grid cell to a stretch.
- Proportion of channel length within each grid cell - used to calculate the proportion of water (and sediment) delivery to each stretch from gridcells which contain more than one stretch.
- Channel order number of each stretch – required for the routing procedure.

Due to the varying length of stretches (0.01-250m) the stretches from the raw data could not be used as reaches for the routing model. Therefore the stretches were used to generate links within the channel network. Links were defined by stretch(es) that were bounded at the up and downstream ends by a junction in the channel network (2 or more stretches).

After doing this there was still considerable variation in the length of links. It was also noted that several links were made up of just one stretch, resulting in several short links. Many of these short links were caused by small tributaries that created junctions. Adjacent links were then combined to ensure the

minimum link length exceeded a threshold distance of 3km. After combining links, link lengths varied between 3000 and 8800m.

4.2.2. Selection of model parameters

Channel slope, velocity of flow, peak discharge and wave celerity are held constant for all reaches throughout the VPMC routing process. The channel slope is required for estimating the Reynolds number (*D*) and was calculated in GIS; using Land-Form PROFILE contours that were obtained from Digimap providing 5m vertical intervals. At 3000m intervals along the channel the slope was estimated using these data, and an average slope for the reaches calculated.

The mean velocity of flow (*v*) is required to calculate the wave celerity (*c*), and was calculated using Manning's equation. Channel and floodplain roughness coefficients of 0.028 and 0.04 were used and estimated by averaging values from the (Fisher and Dawson, 2003; Hey and Thorne, 1986; Nicholas and Mitchell, 2003; Thomas and Nisbet, 2007). An average of the two velocities was calculated.

Wave celerity (*c*) is required to calculate the Courant number (*C*) and was calculated as the velocity multiplied by 1.67 (Ponce, 1994) and the courant and Reynolds numbers, and the routing coefficients were calculated as per equations in the previous section.

Flow per unit width (q_0) is required to calculate the Reynolds number (*D*) and was calculated as peak discharge divided by peak flow width of the channel (similarly to Ponce, 1994). Peak flow width was estimated as from the floodplain width, which was estimated using Environment Agency flood maps (identical to those used in chapter two to calculate floodplain width). Floodplain width was measured at 3000m intervals along the channel and an average value was taken. The peak discharge was calculated by multiplying the velocity and the total channel and floodplain area. Floodplain area was estimated by multiplying floodplain width by floodplain depth. Floodplain depth was estimated from the Land-Form PROFILE contours; the difference in contour height at the channel and at the edge of the floodplain provided the height difference over the floodplain width. The average discharge per unit width of the channel (q_0) was calculated by dividing the peak discharge by the floodplain width.

4.2.3. Spatial and temporal resolution

The data provided from the APT model was of daily resolution, and this was interpolated to provide 1.5 hourly data, which allowed the use of a higher spatial resolution in the routing model without causing numerical dispersion. A further increase in temporal resolution would have greatly increased the computational resources required by the model.

Merkel (2002) noted that spatial resolution should not be significantly smaller than the distance travelled by the flood wave in one time step. Ponce and Theurer (1982) noted the following upper and lower limits on spatial resolution of the methodology:

$$\text{Upper limit: } \Delta x \leq \frac{c\Delta t}{2X}$$

$$\text{Where: } X = 0.5\left(1 - \frac{q_0}{S_0 c \Delta x}\right)$$

$$\text{Lower limit: } \Delta x \geq \frac{q_0}{S_0 c}$$

According to this the spatial resolution of the model should be between 248 and 5520m, indicating the chosen resolution of minimum reach length of 3000m is suitable. As noted in the previous section the channel reach lengths within the model range between 3000 and 8800 m. Running the model with this range of reach lengths results in model error; for reach lengths that exceed 5300m the routing parameter C_1 becomes negative resulting in mass creation. Therefore within channel reaches greater than 5200 m the routing procedure was split into two separate reaches of equal length (resulting in a minimum reach length 2605 m which is also within the range of acceptable spatial resolution noted above). The variable parameter Muskingum-Cunge routing methodology used within the model accounts for the varying reach lengths within the catchment network and different routing times through each reach as routing parameters C, D, C_1, C_2 and C_3 (which are dependent on routing reach length) are calculated at each individual reach.

There is no requirement of an upper or lower limit of the temporal resolution, however previous studies (Boroughs and Zagona, 2002; Ponce and Theurer, 1982; Ponce and Chaganti, 1994; Ponce et al, 1996) have noted numerical dispersion is minimized by keeping the Courant number (C) equal to

or slightly greater than one. As noted previously, the courant number is calculated as the product of flood wave celerity, and the ratio of time and distance resolution of the routing model. Therefore to minimise the numerical dispersion of the model, both time and space resolution must be considered. The Courant number varied at each reach (due to the dependence of the Courant number on reach length) and ranged between 1 and 1.9 and therefore meets this criterion.

Ponce (1994) indicated the sum of the Courant and Reynolds number should be greater than or equal to one as this avoids negative values of C_1. The sum of courant and Reynolds for the routing parameters used is 1.73, and assuming a reach length of 3000 m C_1 is 0.265. The C_3 coefficient is negative, however Ponce (1994) indicates that negative values of C_2 and C_3 do not have an adverse effect on the model.

4.2.4. Model testing

The model was run using a temporally constant water input to establish the duration of the start-up period. This was calculated as the time taken for the discharge at the catchment outlet to become constant. To check the mass conservation of the model the total input discharge was calculated (when using temporally constant input) and compared to the discharge at the catchment outlet after the start-up period (when a constant value was established). Previous studies have noted when using the variable parameter Muskingum-Cunge method some mass loss is inevitable (Perumal and Sahoo, 2008; Ponce and Chaganti, 1994; Tang et al, 1999).

The speed of the flood-wave through the catchment was calculated using a temporally varied (though spatially uniform) water input. The constant input was adjusted over 2 days (after the start-up period) by increasing the (constant) input by an order of magnitude. The flood-wave travel time was calculated as the time of input peak to the peak at the catchment outlet. The maximum distance of routing was divided by the travel time to calculate flood-wave speed. The travel time of the flood-wave peak was compared with the length of the start-up period of the model as these time periods should be similar.

4.2.5. Calibration

Whilst the model parameters have specific values, a period of calibration was used to ensure the input data values (from the APT model output) were realistic; the pattern of flow hydrographs and discharge values should be similar to observed gauging station flow.

Daily gauging station data from the National River Flow Archive (NRFA) from the Centre for Ecology and Hydrology (CEH) were used for both calibration and validation of the routing model, with different years used for each process. The location of the gauging stations over the channel network is shown in Figure 4.6. Stations 45001, 45002 and 45009 provided data for the Exe at Thorverton, Stoodleigh, and Pixton respectively, 45003 the river Culm at Wood Mill, and 45012 the river Creedy at Cowley. The routing model reach corresponding with each gauging station was used to compare the model simulated discharge and the discharge from the observed data (45001:Reach no.150, 45002:Reach no. 366, 45003:Reach no. 359, 45009:Reach no.194, 45012:Reach no.130).

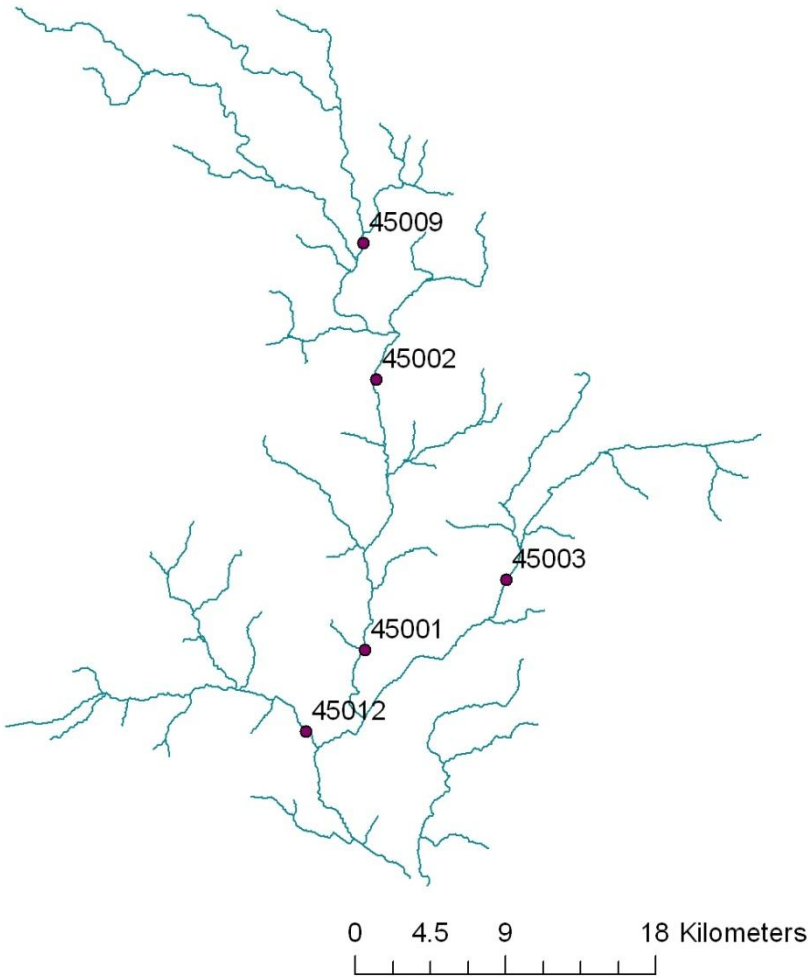

Figure 4.6: Exe catchment network data and NRFA gauging station location.

The NRFA data at each gauging station provides a daily mean value of observed discharge. As the routing model output calculates discharge every 1.5 hours, a daily average, maximum, and minimum discharge was calculated at each reach to enable comparison with NRFA daily data. The first five days of routing output were discarded from the validation as these were within the model start-up phase.

The statistics calculated to compare model output and NRFA data included Root mean square error (RMSE), Mean absolute error (MAE), Nash Sutcliffe efficiency (NSE), Percent bias (PBIAS), coefficient of determination (R^2), Persistence model efficiency (PME) and Peak value error. RMSE, MAE, NSE and PBIAS have been defined in the previous chapter (see Migration model chapter). The R^2 value is the proportion of variance in the observed data

that is explained by the model, ranging from 0 to 1 (1 being a perfect model). Values greater than 0.5 are considered acceptable (Morassi *et al*, 2007; Santhi *et al*, 2001; Van Liew *et al*, 2003). PME is a normalised validation statistic that quantifies the relative magnitude of the residual variance (or 'noise') to the variance of errors obtained by the use of the simple persistence model. The simple persistence model assumes the best estimate of streamflow at the next time step is given by the observed flow at the current time step (Gupta et al, 1999). The value ranges from -1 to 1, with 1 being the optimal value and 0.0 indicating minimal acceptable performance. PME is calculated using the equation:

$$PME = 1 - \sum_{t=1}^{N} \left(q_t^{sim} - q_t^{obs}\right)^2 / \sum_{t=1}^{N} \left(q_t^{obs} - q_{t-1}^{obs}\right)^2$$

One of the weather stations on the west side of the catchment used as input data for the ADAS APT model provided input meteorological data for the years up to 2001 (see Figure 4.7). The rainfall input to the catchment estimated by the APT model is calculated by interpolating recorded rainfall values from weather station data. Inclusion/exclusion of a station will influence the spatial pattern of rainfall predicted over the catchment by the model. The accuracy of the rainfall estimation is likely to vary between these two periods. Therefore rather than simply using the first 4 years of data NRFA data and model output for model calibration and the remaining 16 for validation, the first 2 years and the 11th and 12th years were used for 2 separate periods of model calibration; calibration period 1: 01/10/1991-30/9/1993 and validation period 1: 1/10/1993-30/9/2001 with the additional weather station, and calibration period 2: 01/10/2001-30/9/2003 and validation period 2: 1/10/2003-30/09/2011 without the additional weather station.

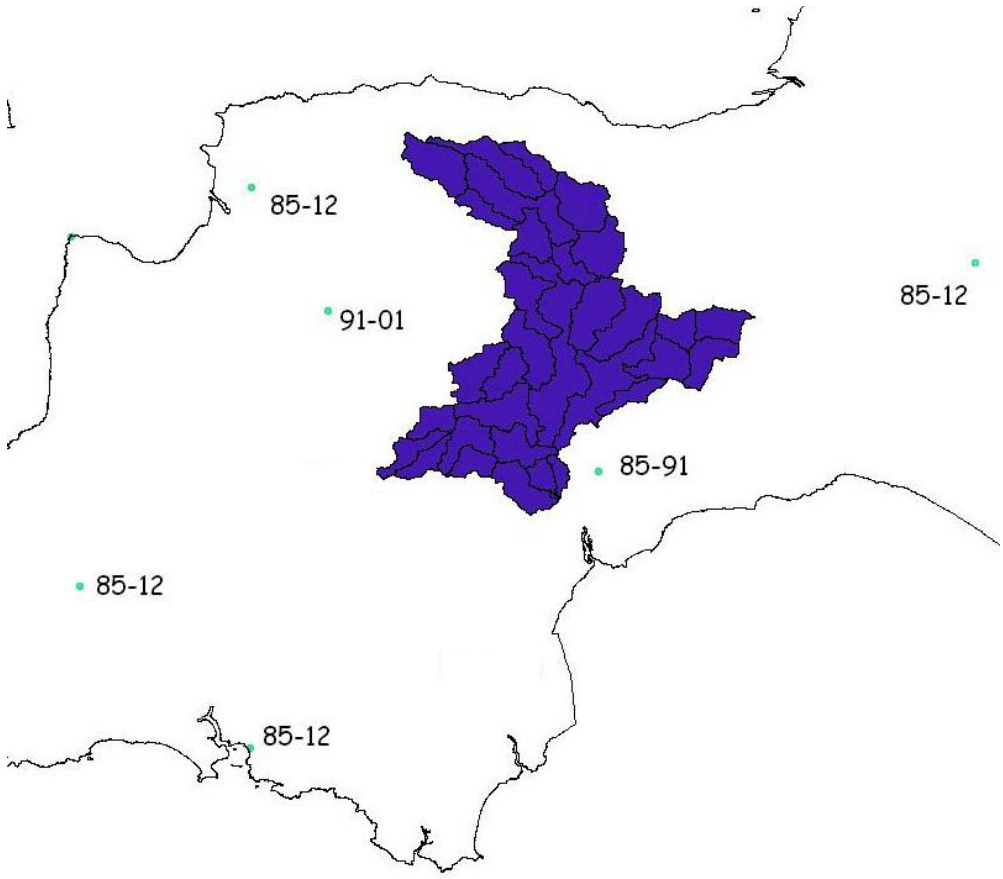

Figure 4.7: Positioning of weather stations used to generate ADAS APT model output, and the years for which data was available. The Exe catchment is highlighted in purple.

4.2.6. Validation

As for the calibration period, the statistics RMSE, MAE, NSE, PBIAS and PME were calculated for both the validation periods (validation period 1: 1/10/1993 – 30/09/2001 and validation period 2: 1/10/2003 – 30/09/2011). Additionally, flow duration curves and hydrographs of the observed and simulated flows were also plotted to enable comparison and assess the ability of the model to replicate variations in discharge. Flow duration curves indicate the model's ability to replicate discharge at various magnitudes, thus illustrating difficulties with predicting extreme values. Hydrographs also indicate the ability of the model to replicate the timing of discharge peaks.

A peak-over-threshold analysis was used (similarly to Hurkmans *et al*, 2008; Prudhomme *et al*, 2002) to analyse high magnitude event prediction. This was used to establish the 24 largest events at each gauging station during each of the validation periods. Peaks were a minimum of 6 days apart to ensure

independency of peaks; 6 days is a mid-range value from those reported in the literature to allow for independency between peaks (Hurkmans *et al*, 2008; Prudhomme *et al*, 2002). These were compared to the corresponding peak in the simulated discharge time series and percentage error in peak, and peak timing error statistics were calculated for each of the 24 events. Peak value error was calculated as a percentage error in estimation of the magnitude of the maximum discharge peak:

$$Error\ Peak\ volume = \frac{q_{sim}^{peak} - q_{obs}^{peak}}{q_{obs}^{peak}} \times 100$$

$$Error\ Peak\ time = t_{sim}^{qpeak} - t_{obs}^{qpeak}$$

Positive values indicate that the simulated peak is earlier than the observed and vice versa. The corresponding peak in simulated discharge was calculated as the highest magnitude discharge during the 3 days preceding, and following the day of the event from the observational data. Two of these events from each of the validations periods were compared to the corresponding simulation period. Statistics RMSE, MAE, NSE, PBIAS and PME were generated. Hydrographs for 11-day periods covering the event were also produced and analysed to assess the model's ability to predict the timing and variation of discharge during the period of the event. The events were chosen based on a distinguishable peak at all gauging station locations.

Lower RMSE and MAE values indicate better model fit, and Singh *et al* (2004) noted that RMSE and MAE values less than the half of standard deviation of observations can be considered low. The RMSE –observations standard deviation ratio (RSR) as formulated by Morassi *et al* (2007) is a ratio of the RMSE and standard deviation of observations:

$$RSR = \frac{RMSE}{STDEV_{obs}}$$

The RSR standardises RMSE using the standard deviation of observations and ranges from optimal values of 0 to large positive values. Lower RSR (and RMSE) indicates better model performance, and values ≤ 0.7 considered

acceptable model performance (Morassi *et al,* 2007).

4.2.7. Sensitivity analysis

A sensitivity analysis to assess the influence of varying parameter values on the model was conducted. As indicated previously, the model parameters slope, peak flow width, and both the temporal and spatial resolution had been determined from catchment characteristics in GIS and the available datasets for model input and therefore these were not changed in the sensitivity analysis. The model was run using both an increased and decreased velocity parameter, which in turn alters the wave celerity and discharge per unit width. These values then alter the Courant and Reynolds numbers, which are used to calculate the routing constants (C_1, C_2 and C_3). Validation statistics (as indicated in the previous section) were calculated when using the varied velocity parameters, and hydrographs at the catchment outlet were compared to assess the influence of this parameter on model output.

4.3. Results and Analysis

4.3.1. Channel network

The modified channel network is compared to the actual channel network data in Figure 4.8. The modified network ensures channel reaches are 3000m or more in length. This modification was necessary to provide longer reaches for the routing methodology; as noted in the previous section the ratio between space and time resolution of the routing model influences the Courant number, which should have a value equal to or slightly greater than 1 to ensure minimal numerical dispersion of the model. A finer spatial resolution than 3000m results in a Courant number that is too large when used with a 1.5 hour temporal resolution. Increasing the temporal resolution was not beneficial as the resolution of gauging station data was daily; validation of the model output at a resolution finer than 24 hours is not possible. Additionally above hourly results in an increase the computational power.

Figure 4.8 indicates the modified channel network is an adequate representation of the Exe catchment network. Reasons for differences between the actual and modified channel networks in Figure 4.8 include the representation of the channel network within the APT model; as shown in Figure 4.5B, the channel network representation used within the APT model includes many very small tributaries, that are not represented by the actual channel network shown in Figure 4.8. The modified channel network in Figure 4.8 incorporates these small tributaries within larger channel reaches, leading to some distortion within the visual channel network representation.

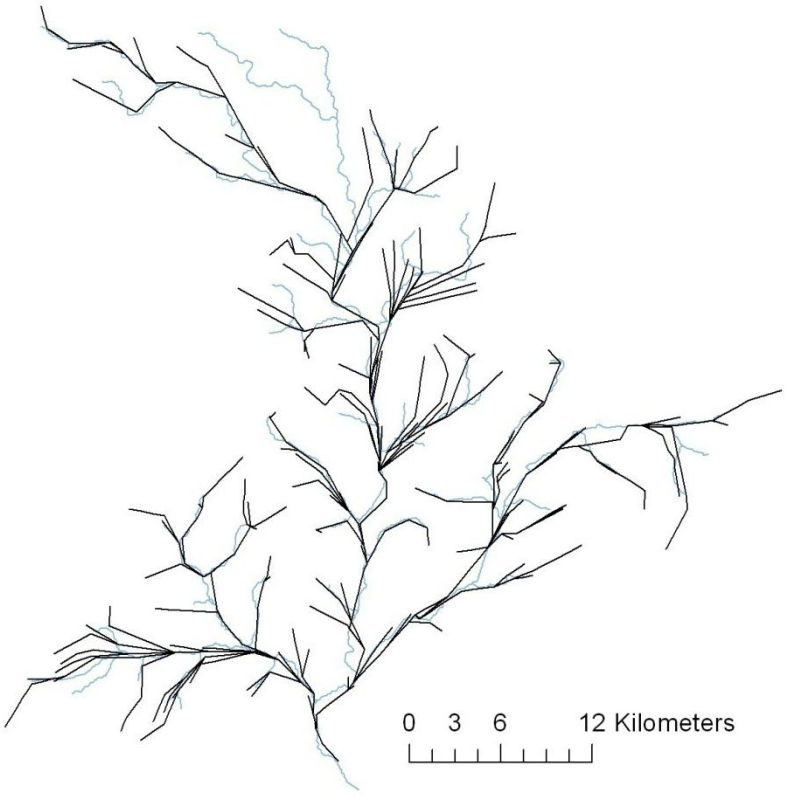

Figure 4.8: The modified channel network (black) used for the routing model and the actual channel network (blue).

4.3.2. Mass conservation

To check the mass conservation within the routing model, the input to the channel network was held constant and the total input for a single time-step across the whole network was calculated. Once a constant discharge at the catchment outlet was reached (on the 3rd day at the 15th timestep/ 94.5 hours) and the output was compared with the total input. The total input and discharge at the catchment outlet would be identical in the case of perfect mass conservation within the model. The results indicated a small mass loss throughout the routing process. As noted previously, mass loss is inevitable when using the variable parameter Muskingum-Cunge method. The error in mass conservation is small it will not significantly affect the routing model results, and the mass conservation of the model considered adequate.

4.3.3. Calibration results

The model was run using channel water delivery data from the ADAS ATP model output for 2 separate calibration periods; period 1 1/10/1991 – 30/09/1993, and period 2 1/10/2001 – 30/09/2003. The routing model output was compared with the data NRFA of the corresponding periods for each of the 5 gauging stations with NRFA data. The routing reach number in which each NRFA gauging station was located was used for comparison. Table 4.1 and Table 4.2 indicate the values of the calibration statistics for each of these stations, for both calibration periods.

Table 4.1: Calibration statistics for first calibration period (1/10/1991 - 30/9/1993).

Station	R^2	NSE	MAE	RMSE	STDEV obs	RSR	PME	PBIAS (%)
45001	0.54	0.49	2.92	10.43	14.68	0.71	-1.04	21.21
45002	0.52	0.45	2.46	8.23	11.07	0.74	-1.43	22.46
45003	0.38	0.35	0.48	2.69	3.34	0.81	0.25	16.19
45009	0.41	-0.04	0.49	4.10	4.02	1.02	-6.48	-12.90
45012	0.47	0.40	0.57	2.95	3.82	0.77	-0.22	-21.72

Table 4.2: Calibration statistics for the second calibration period (1/10/2001 - 30/9/2003).

Station	R^2	NSE	MAE	RMSE	STDEV obs	RSR	PME	PBIAS (%)
45001	0.89	0.65	6.40	12.10	20.34	0.59	-0.49	39.60
45002	0.90	0.76	3.55	6.63	13.55	0.49	0.06	32.17
45003	0.71	0.58	1.43	3.14	4.81	0.65	0.33	35.61
45009	0.78	0.76	0.79	2.58	5.24	0.49	-0.17	18.17
45012	0.80	0.71	0.77	2.69	5.01	0.54	0.27	22.90

The initial calibration results indicate the accuracy of model performance varies within the catchment. Moriasi *et al*, (2007) indicates model simulation can be judged as satisfactory if NSE>0.5 and R^2>0.5. According to these limits, the second calibration phase provides acceptable results at all locations. From the

first phase stations 45001 and 45002 fulfill the R^2 requirement and values of NSE are borderline. Values of MAE for all stations and for both calibration periods are less than half the standard deviation of observations indicating good model accuracy. For the first validation period the RMSE values indicate poor model performance, particularly at station 45009 as the RMSE is greater than the standard deviation of observations. For the second validation period RMSE indicates good model accuracy (although stations 45009 and 45012 are just over half the standard deviation). The RSR values indicate for the first calibaration period none of the stations fulfill the criteria (≤0.7) of acceptable model performance, however for the second calibration period all stations fulfill this criteria indicating acceptable model performance.

The PBIAS statistics for the first calibration period indicate at stations 45001, 45002, and 45003 discharge is under-estimated by the model, whilst at 45009 and 45012 there is a slight over-estimation. During the second calibration period discharge is under-predicted at all locations (by a minimum of 18% and maximum of 39%). As the model has been checked for mass conservation this error is caused by underestimation of the runoff input to the channel network from the APT model. Therefore, the model was re-run with a calibrated input by increasing the water input for both calibration periods by various amounts. The optimum values were found to be an increase of 5% for the first calibration period, and an increase of 30% for the second calibration period. The statistics when the model was run with a calibrated input are shown in Table 4.3 and Table 4.4.

Table 4.3: Calibration statistics for calibration period 1 with input increased by 5%.

Station	R^2	NSE	MAE	RMSE	STDEV obs	RSR	PME	PBIAS (%)
45001	0.54	0.50	2.38	10.36	14.68	0.71	-1.01	17.27
45002	0.52	0.45	2.03	8.22	11.07	0.74	-1.43	18.60
45003	0.38	0.35	0.23	2.70	3.34	0.81	0.25	7.81
45009	0.41	-0.15	0.71	4.31	4.02	1.07	-7.24	-18.54
45012	0.47	0.37	0.74	3.04	3.82	0.80	-0.29	-27.81

Table 4.4: Calibration statistics for calibration period 2 with input increased by 30%.

Station	R^2	NSE	MAE	RMSE	STDEV obs	RSR	PME	PBIAS (%)
45001	0.89	0.82	3.47	8.74	20.34	0.43	0.22	21.48
45002	0.90	0.89	1.30	4.52	13.55	0.33	0.56	11.83
45003	0.71	0.69	0.65	2.69	4.81	0.56	0.51	16.29
45009	0.78	0.71	0.28	2.80	5.24	0.53	-0.38	-6.38
45012	0.80	0.80	0.01	2.25	5.01	0.45	0.49	-0.23

For the first calibration period the calibrated input has no effect on any of the R^2 values and little effect on NSE values. MAE decreases for 45001, 45002 and 45003 when using calibrated input indicating reduced error in model prediction. PBIAS error values decrease when using the calibrated input; the only PBIAS value exceeding 20% error after calibration is 45012 (overestimated by 27%). For the second calibration period the R^2, NSE and PME values increase, whilst RMSE and MAE decrease (with the exception of station 45009) indicating increased accuracy of the model. Additionally PBIAS decreases; from a maximum of 39% to 21%. Some PBIAS values become negative (indicating model over-estimation) but the magnitude of over-estimation is small (<7%).

4.3.4. Validation statistics

The model was then run for both the validation period using the calibrated input values; validation period 1 (1/10/1993-30/9/2001) with a 5% increase in runoff input, and validation period 2 (1/10/2003-30/9/2011) with a 30% increase in runoff input. The reason these two validation periods were chosen is due to the formation of the input data as noted previously; APT model (used as the runoff input to the routing model) has different input data for the periods 1991-2001 and 2001-2011. Rainfall gauging station was interpolated to provide rainfall input to the APT model, and from 1991-2001 there was an additional weather station data used to generate the model input. This will affect the accuracy of the rainfall input estimation, and hence the runoff generation by the APT model and therefore it is necessary to calibrate (and validate) these two simulation periods separately. The routing model output from was

compared with discharge records from NRFA corresponding to the same periods. Table 4.5 and Table 4.6 indicate the values of the validation statistics for each of these.

Table 4.5: Validation statistics for validation period 1.

Station	R^2	NSE	MAE	RMSE	STDEV obs	RSR	PME	PBIAS (%)
45001	0.80	0.65	5.85	13.40	22.79	0.59	-0.36	31.24
45002	0.80	0.69	4.41	9.07	16.19	0.56	-0.28	30.88
45003	0.69	0.66	1.21	3.22	5.58	0.58	0.39	27.70
45009	0.66	0.64	0.50	3.76	6.24	0.60	-0.75	9.45
45012	0.69	0.66	0.17	3.76	6.49	0.58	0.41	-4.27

Table 4.6: Validation statistics for validation period 2.

Station	R^2	NSE	MAE	RMSE	STDEV obs	RSR	PME	PBIAS (%)
45001	0.83	0.80	3.23	8.10	18.22	0.44	0.14	22.14
45002	0.86	0.86	1.63	4.54	12.34	0.37	0.32	15.62
45003	0.60	0.57	0.68	2.71	4.14	0.65	0.43	19.75
45009	0.70	0.55	0.18	2.89	4.33	0.67	-1.99	-4.44
45012	0.68	0.71	0.13	2.57	4.74	0.54	0.35	-4.40

The validation results for all stations, for both validation periods indicate good model accuracy; all R^2 and NSE values are above 0.5, and all MAE values are less than half of the standard deviation of observations. The RMSE values for the first validation period are all slightly larger than half of the standard deviation of observations, as are the values for 45003, 45009, and 45012 for the second validation period, but these values indicate an improvement of model accuracy compared to validation periods. Additionally the RSR values are all ≤0.7 for both validation periods (indicating adequate model accuracy as according to the criteria as defined by Morassi *et al*, 2007).

The PME statistics for the first validation period are negative except for stations 45003 and 45012, yet for the second validation period only 45009 is negative. Negative values indicate the simple persistence model (assuming the

discharge at the next time-step is given by the observed flow at the current time-step) is a better estimate of discharge. PME is calculated as a ratio between the error of model prediction and the difference between observed values of current and previous time-step. When the dataset includes more than one hydrograph peak and periods of relatively constant discharge, (which is true in this case where a 10-year period of discharge has been analysed) the sum of differences between observed values of discharge at current and previous time-step is increased. This then results in a lower value of the PME statistic, as observed. Moramarco et al, (2006) observed a similar effect on the PME statistic when using the Muskingum method to forecast discharge in the River Tiber, Italy; 75% of PME statistics were greater than 0.6 and the lower PME values were observed for events characterised by multiple flood peaks. Therefore as these data sets cover long time periods (10-years) with several hydrograph peaks as opposed to single events, it is unsurprising that the PME statistic would produce unacceptable values (<0.0 according to the definition by Gupta *et al*, 1999). It is encouraging that 6 of the 10 values produce acceptable values (above 0.0). This statistic will be used to analyse a selection of individual flood events.

PBIAS statistics for both validation periods indicate the model under-predicts discharge at stations 45001, 45002, and 45002 (and 45009 during the first validation period). For the second validation period all PBIAS statistics are <25% and therefore the model performance is considered satisfactory (Morasi et al, 2007). The statistic indicates slight over-prediction (<5%) at stations 45012 for this period (and station 45009 for the second validation period) that is not considered significant. Under/over-estimation of discharge is also shown in the flow duration curves (Figure 4.11 and Figure 4.12).

These results indicate the model performs with greater accuracy during the second validation period (1/10/2003 – 30/09/2011). The PBIAS statistics for the first validation period indicate under-prediction of discharge at 4 of the 5 gauging stations, and by up to 31% for station 45001. This value of under-estimation by the model for the first validation period is considerably higher than the under-estimation during the first calibration period (17%, see Table 4.3). To investigate the cause of the observed difference in model accuracy between the first calibration and validation periods, the observation data for the period of

01/10/1991-30/09/2001 (the first calibration and validation period) were analysed. Figure 4.9 shows the mean, median, minimum and maximum discharge observed at gauging station 45001 for the first 10 years. This plot indicates both the average and maximum discharge observed at this location for the first 2 years (the 1st calibration period) was lower than most of the following 8 years (the 1st validation period); the average discharge for the first 2 years was 13.7m^3s^{-1}, but for the following 8 years was 18.7m^3s^{-1}. Year one has the lowest recoded annual maximum and mean discharge (97.3m^3s^{-1} and 12.17m^3s^{-1} respectively) of the first 10 years of observation. The values of annual minimum and annual median discharge do not differ significantly between the two periods. This suggests the model has difficulty predicting high magnitude flows, and under-estimates peak discharges. The under-estimation of higher magnitude flows during the first validation period is indicated in the flow duration curves (see Figure 4.11). This will be discussed in more detail in a later section analysing individual events.

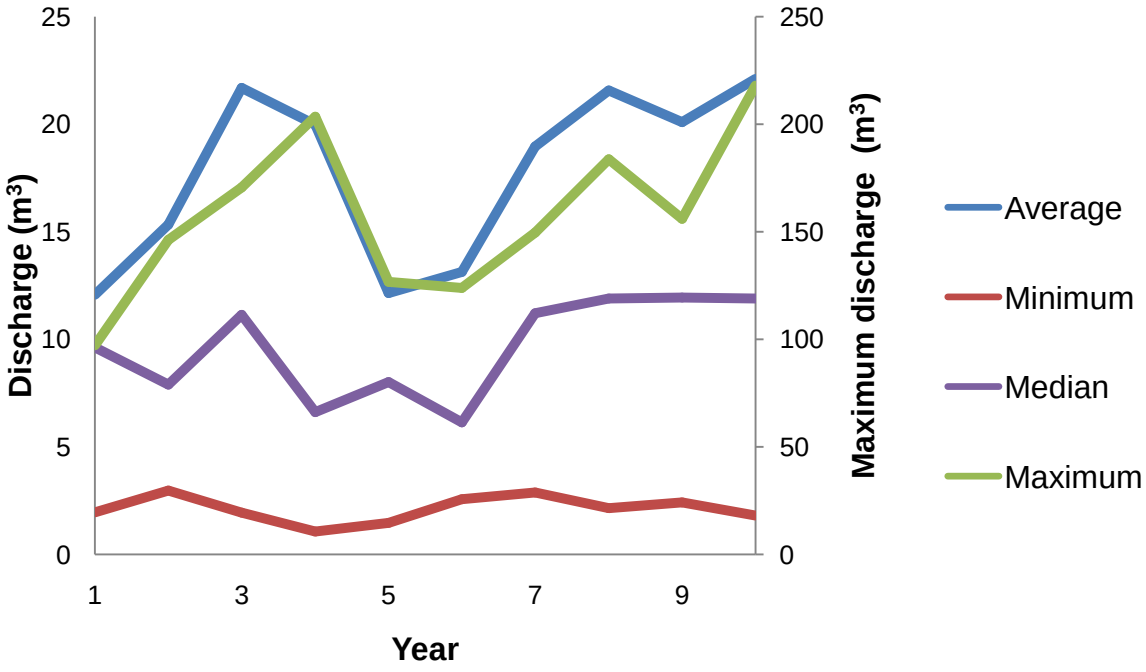

Figure 4.9: Plot showing mean, minimum and median discharge (left axis) and maximum discharge (right axis) for the first 10 years of observational data (1/10/1991 – 30/09/2001) for gauging station 45001 (Exe at Thorverton).

With the exception of under-estimation during the first validation period, the results indicate satisfactory model performance for all gauging stations. Station 45009 (River Exe at Pixton) has the lowest R^2, NSE and PME values in validation period 1, and the lowest NSE, and PME for validation period 2, and the highest values of RSR for both validation periods. The PBIAS statistic for this station is low for both validation periods (indicating the model does not consistently under/over-predict discharge at this location). This gauging station is the most upstream gauging station located on the Exe, with the highest station level (128m). The contributing area of this gauging station includes Exmoor, where precipitation is highly spatially variable (see Figure 4.10). It is possible that due to the low number of meteorological stations in the area used to generate the input data the interpolation of rainfall data does not fully capture the spatial variation of rainfall in this area to the same level of accuracy as other areas in the catchment.

The magnitude of flow is more accurately represented at station 45009 (and also at gauging station 45012, Creedy) than at other gauging stations (as indicated by a lower PBIAS statistic). A possible explanation for this is the inverse weighting interpolation method used to estimate the rainfall across the catchment from the weather station data (see Silgram et al, 2007) which was then used as input data to the APT model. It can be seen from the positioning of the weather stations used to generate the input data (see Figure 4.7) that the weather station closest to gauging stations 45001, 45002 and 45003 (Exe at Thorverton, Exe at Stoodleigh and Culm respectively) is located on the east side of the catchment. The spatial variation of the rainfall in the catchment (Figure 4.10) indicates this weather station is located in an area that receives less rainfall than the sub-catchments of gauging stations 45001, 45002, and 45003. As this weather station will heavily influence the rainfall estimates over these sub-catchments this could explain the variation in under-estimation throughout the catchment.

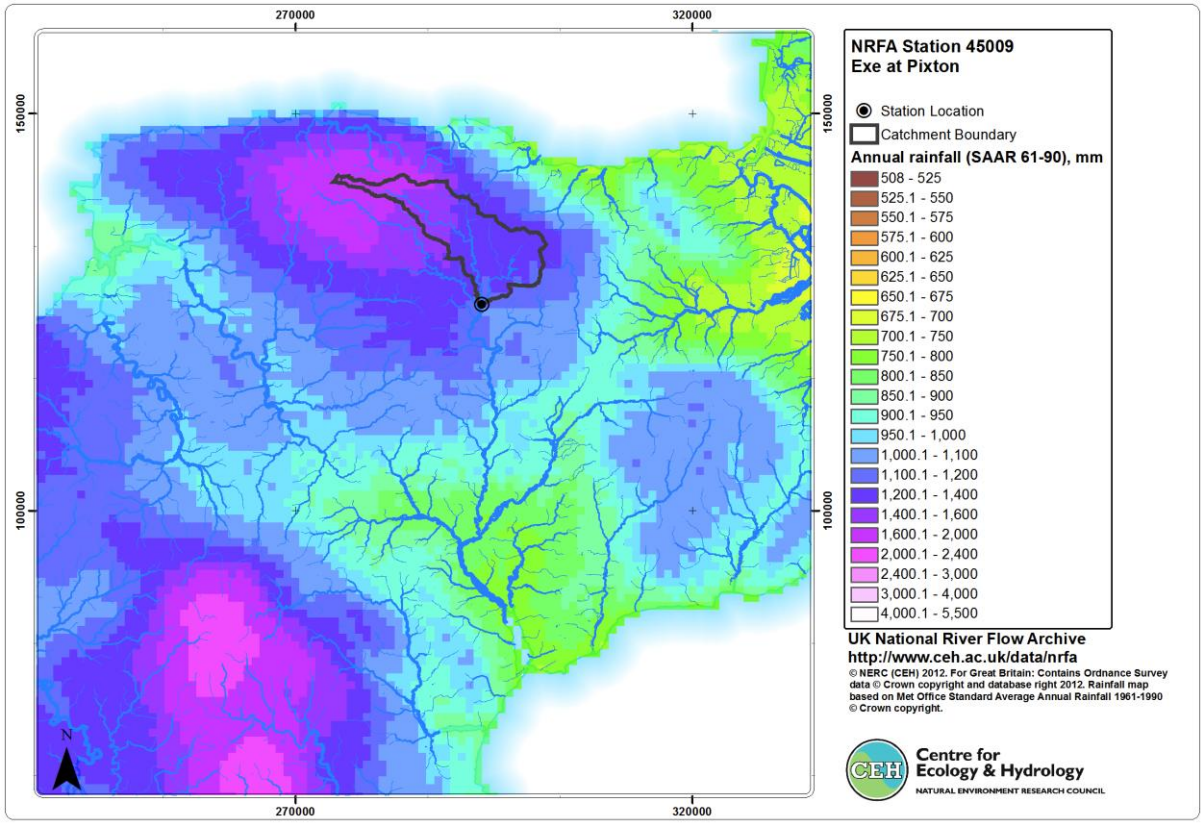

Figure 4.10: Annual rainfall over the Exe catchment, with NRFA gauging station 45009 and contributing area indicated. Data from Met Office 1960-1990, image from CEH website (2013).

The flow duration curves for the first validation period are shown in Figure 4.11. As indicated by the PBIAS statistic, for the gauging stations 45001, 45002, 45003 and 45009 the model under-predicts flows of all magnitudes. At 45001 the level of under-prediction is slightly greater for high magnitude flows; the average under-prediction for the quartile of highest magnitude discharges (largest 25% of observed flow magnitudes) was 51%, compared to the quartile of lowest discharges (lowest 25% of observed flow magnitudes) 20%. At stations 45003 and 45009 under-prediction is slightly greater for low magnitude flows (average under-prediction for the quartile of highest magnitude discharges 21% and 8%, compared to the quartile of lowest discharges 71% and 35% respectively). At station 45002 the level of under-prediction is relatively constant. At station 45012 the model slightly under-estimates high magnitude flows and low magnitude flows, and slightly over-estimates mid-range

magnitude flows. However, as noted in the PBIAS statistic, the average total error in flow magnitude estimation is <5%.

The positioning of weather stations used to generate the rainfall input data to the APT model is the likely cause of the under-prediction errors within the routing model. The small number of weather stations used for the interpolation of rainfall across the catchment will result in inaccuracies in the spatial variation of rainfall. Additionally as some of the weather stations are located some distance from the catchment this will result in errors in the magnitude of rainfall estimated within the catchment. Errors within the rainfall estimation across the catchment will result in errors of the predicted runoff delivery to the catchment by the APT model, which have been used as input data for this routing model. For example, the positioning of the weather station to the west of the catchment (see Figure 4.7) will heavily influence the rainfall estimated (and hence runoff delivery) within the sub-catchment of gauging station 45003 on the river Culm due to the interpolation method used. Figure 4.10 indicates the average annual rainfall in the area of this weather station is significantly lower than the average annual rainfall within the west of the Exe catchment, resulting in an under-estimation of the rainfall within the Exe catchment.

In this study it has been deemed appropriate to calibrate the input data by increasing the runoff delivery to the catchment as a whole (by a given percentage) as it is possible to calculate the magnitude of under-estimation of water delivery to the catchment due to the mass conservation of the model, and the existence of daily gauging station data at several locations within the catchment. As indicated by the flow duration curves in Figure 4.11, after calibration of the input data the simulated discharge is still under-estimated, and the level of under-estimation varies spatially within the catchment, and also varies depending on the magnitude of flow. It was not appropriate to vary the calibration of runoff input data spatially as there is insufficient data to justify or validate any such calibration as the spatial resolution of gauging station is too coarse for such a calibration. The temporal resolution of the gauging station data is daily and any further calibration to the runoff delivery is likely to be at a finer temporal resolution than this; errors estimating peak event flow are likely to be associated with under-estimation of rainfall events that may be less than a

24-hour duration. Additionally, there will be a time delay between rainfall events and observed peak flows and the gauging station data alone are insufficient to provide information on timing of rainfall events and hence runoff delivery to the catchment. Whilst it may be possible to obtain rainfall data to the catchment at a finer temporal and spatial resolution this data this data would be used to calibrate the APT model, which then estimates the runoff delivery to the catchment. Calibrating the runoff delivery using rainfall data would therefore not be suitable as this would not take into account any factors influencing the delivery of water to the channel such as storage, interception, evapotranspiration, and abstraction.

Therefore, errors within the discharge prediction of the routing model as a result of errors within the runoff input data have been minimised as best as is possible through the calibration of input data. Further calibration of the runoff input to the model was not viable within this study due to lack of data to support any such calibration.

A

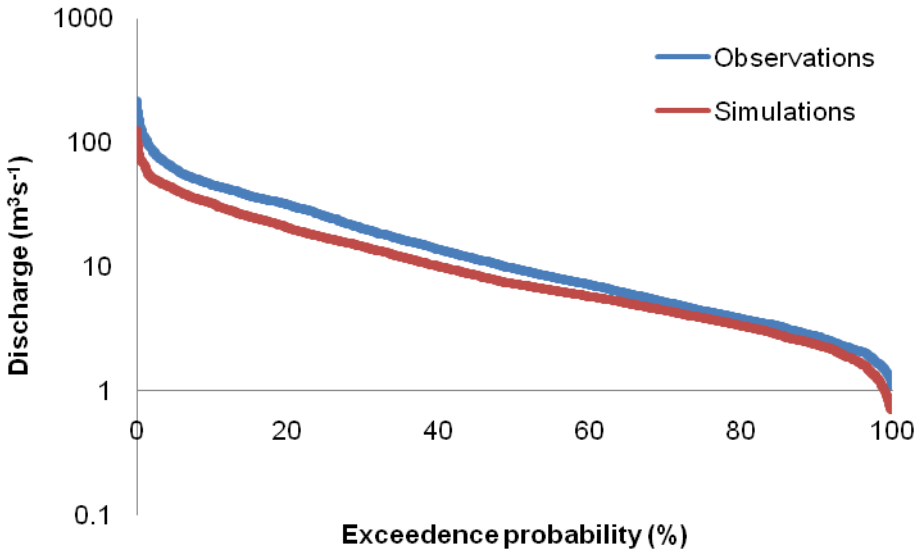

B

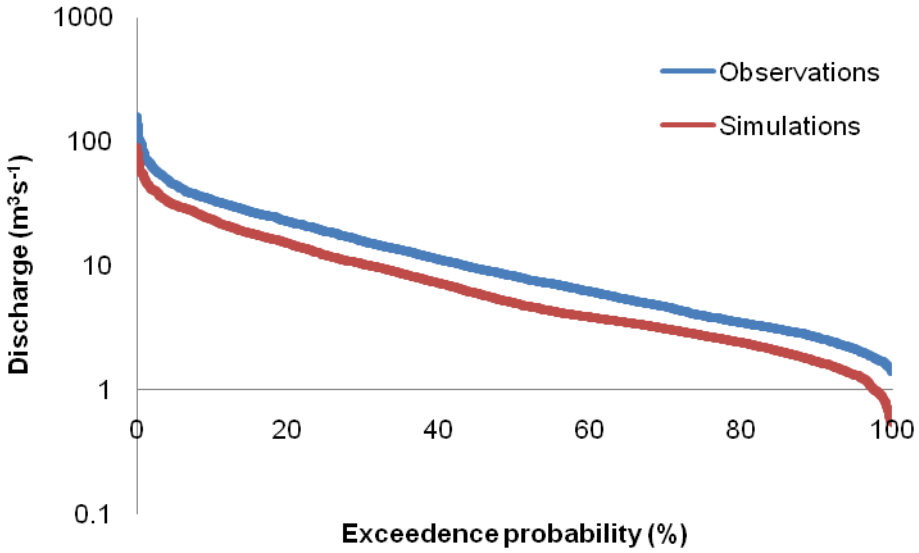
1000
100
10
1
0.1
0
20
40
60
80
100
Discharge (m³s⁻¹)
Exceedence probability (%)
Observations
Simulations

C

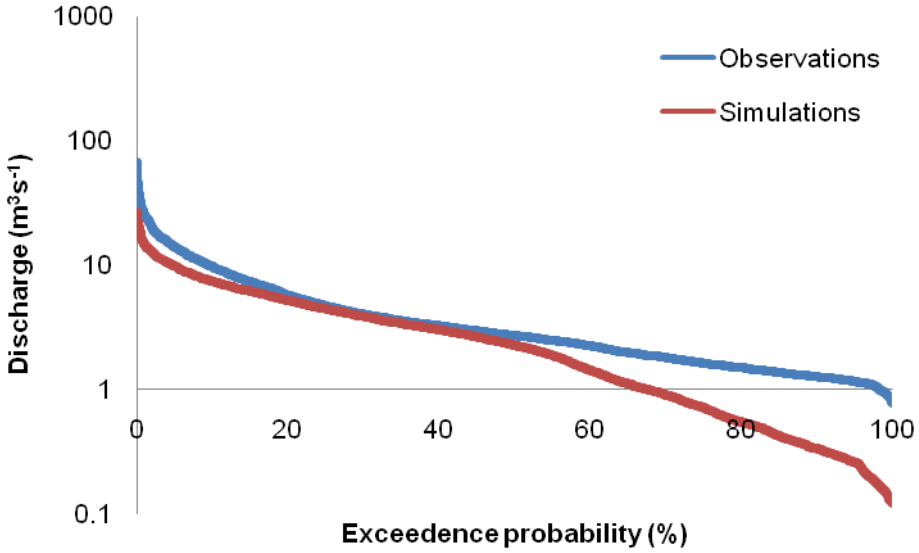
1000
100
10
1
0.1
0
20
40
60
80
100
Discharge (m³s⁻¹)
Exceedence probability (%)
Observations
Simulations

D

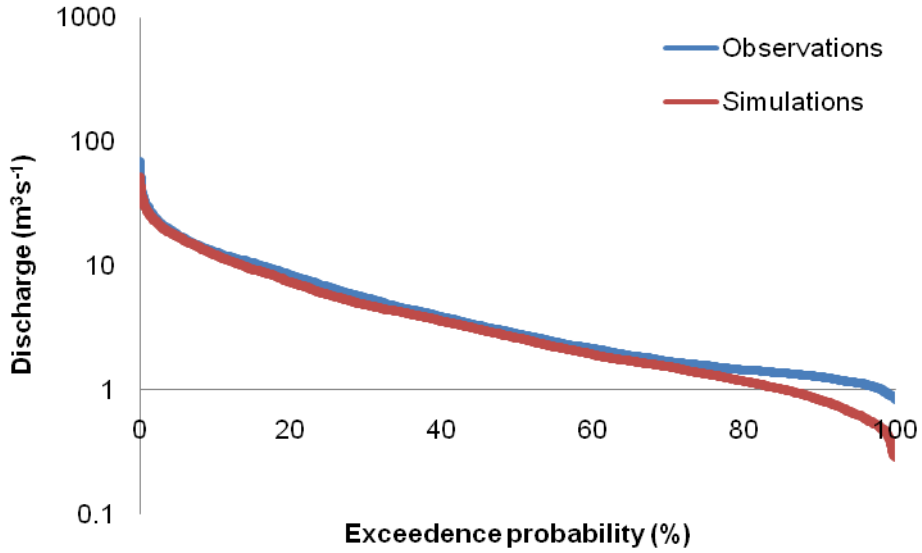

E

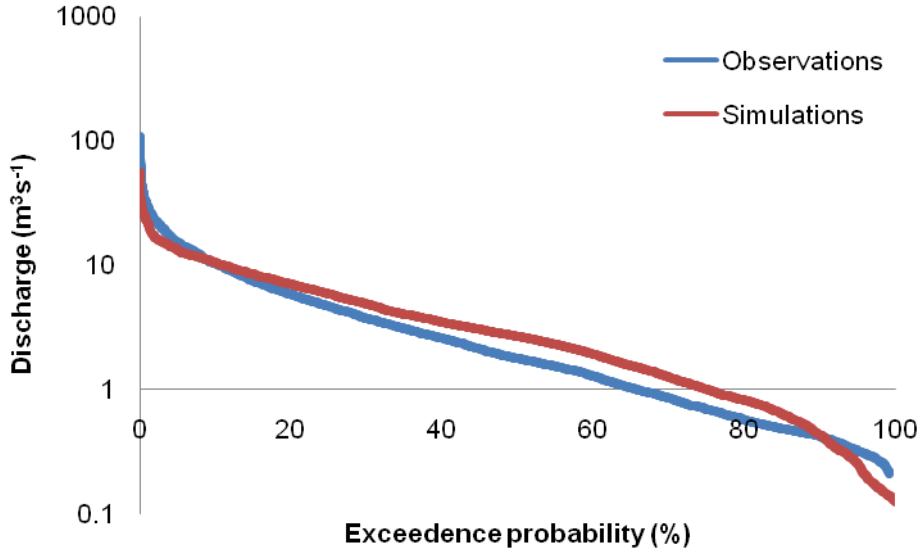

Figure 4.11: Flow duration curves for the first validation period (1/10/1993-30/09/2001) for gauging stations A-45001, B-45002, C-45003, D-45009, E-45012.

The flow duration curves for the second validation period are shown in Figure 4.12. As indicated by the PBIAS statistic, for the gauging stations 45001,

45002 the model under-predicts flows of all magnitudes. At both these locations the level of under-prediction is fairly constant for flows of all magnitudes, however there is a slight increase in the level of under-prediction at low magnitude flows (the average under-prediction for the quartile of highest magnitude discharge was 22% and 12%, compared to the quartile of lowest discharge 25% and 30% respectively). At station 45003 the PBIAS statistic indicates average model under-prediction of <20%. The flow duration curve (Figure 4.12 C) indicates the level of under-prediction increases for low magnitude flows (upper quartile of discharge magnitudes 10%, lower quartile 73%). Some mid-range flows at this location are slightly over-predicted by the model. Both 45009 and 45012 show a variation in model over/under-estimation, with slight increase in under-estimation for low magnitude flows, however the PBIAS statistic for both these locations was <5% indicating the magnitude of error is not significant.

A

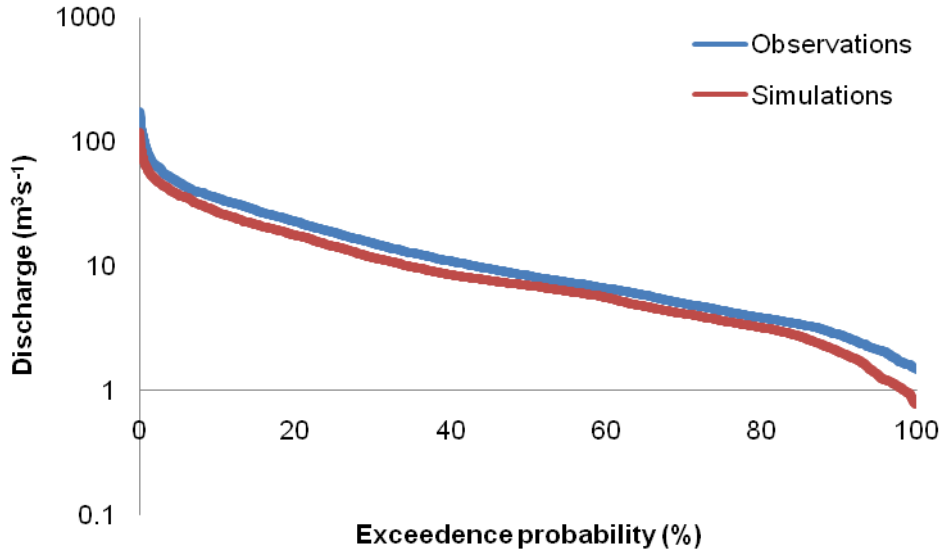

B

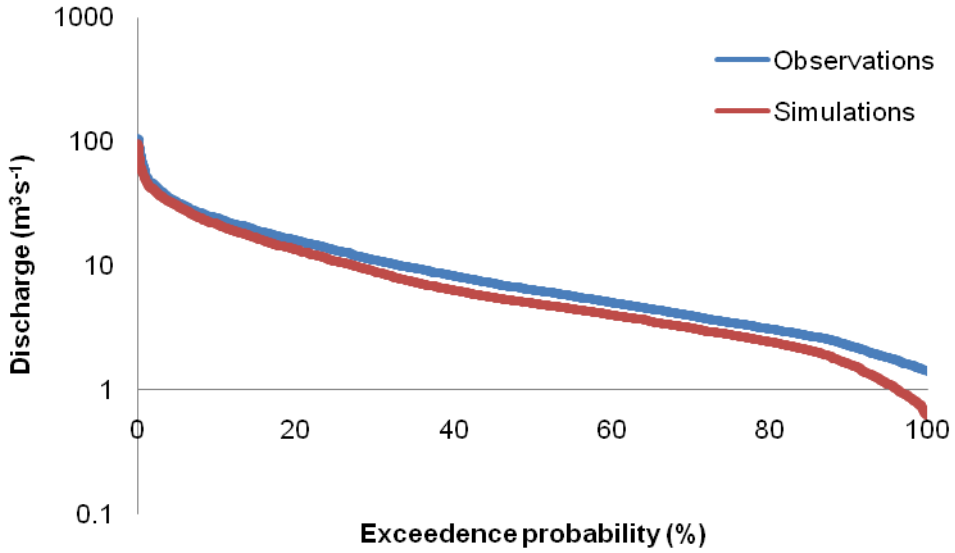
1000
100
10
1
0.1
0
20
40
60
80
100
Discharge (m³s⁻¹)
Exceedence probability (%)
Observations
Simulations

C

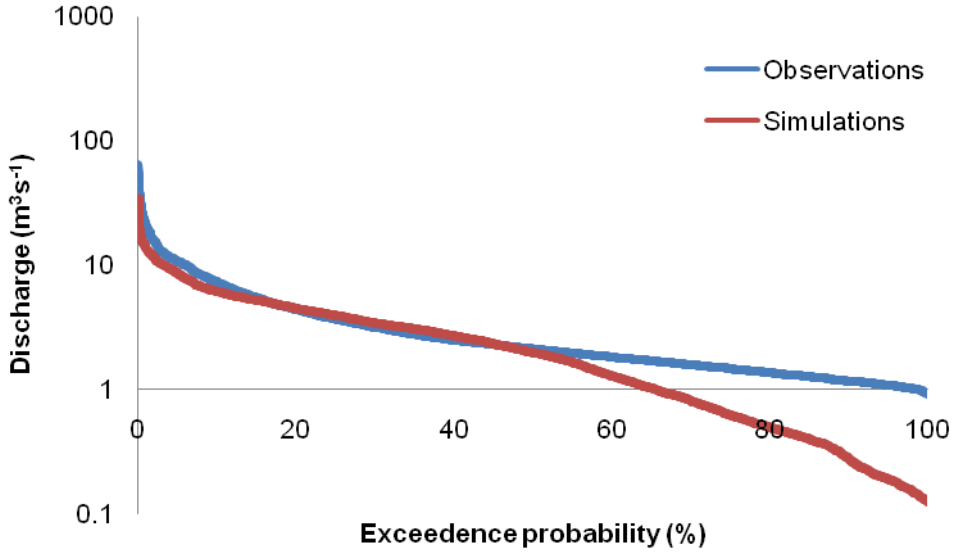
1000
100
10
1
0.1
0
20
40
60
80
100
Discharge (m³s⁻¹)
Exceedence probability (%)
Observations
Simulations

D

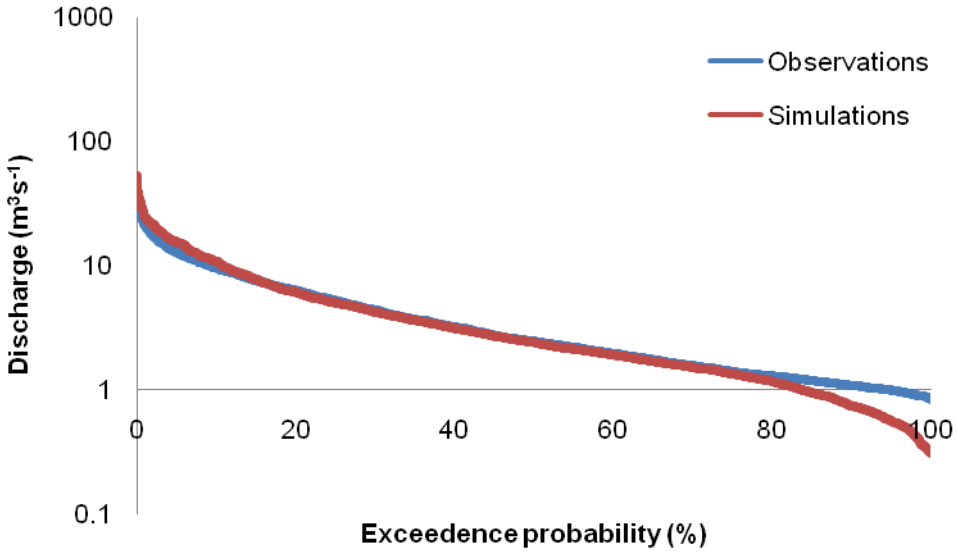

E

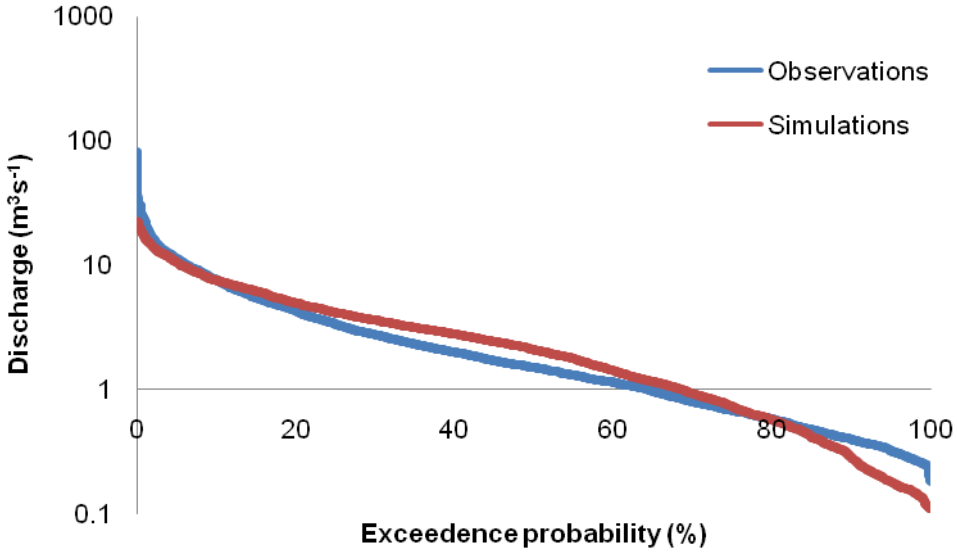

Figure 4.12: Flow duration curves for the second validation period (1/10/2003-30/09/2011) for gauging stations A-45001, B-45002, C-45003, D-45009, E-45012.

4.3.5.Analysis of peak flows

The 24 largest discharge events recorded for each of the two validation periods, for each gauging station were identified from the NRFA data. The corresponding simulated peak was then compared to this value and a percentage error of estimate (similar to PBIAS, but by comparing only 2 values rather than a whole data set), and date error was calculated for each event. The results from this analysis are shown in Table 4.7 - Table 4.16. The average error in prediction of all 48 events was calculated for each validation period at each gauging station, these values are shown in Table 4.17. With the exception of station 45009, for all gauging stations and validation periods the average error percentage is negative indicating the model under-estimates the peak discharge for these events (as was previously indicated from the flow duration curves in Figure 4.11 and Figure 4.12). For all gauging stations the magnitude of average percentage error is lower for the second validation period than the first. This is likely due to the increased calibration of input (30% increase) for the second period compared to the first period (5% increase).

Similarly to the previous section, the magnitude of peak flows predicted at station 45009 (Exe at Pixton) is more accurate than other locations. As noted in the previously, this is likely to be due to the positioning of weather stations used to generate the rainfall input to the APT model (see Figure 4.7) and the magnitude of rainfall is more accurately reproduced within this sub-catchment area.

Table 4.7: Event analysis statistics for largest 24 events during validation period 1 (1/10/1993-30/9/2001) at gauging station 45001 (Exe at Thorverton).

Event number	Obs Day	Obs Q	Sim Day	Sim Q	Error %	Day error
1	2587	218	2587	134.3	-38.4	0
2	454	203.5	454	118.3	-41.9	0
3	1857	183.7	1858	81.4	-55.7	-1
4	395	174.1	396	124.9	-28.3	-1
5	1850	172.2	1851	66.7	-61.3	-1
6	81	170.7	81	91.2	-46.6	0
7	2625	160	2626	87	-45.6	-1
8	2278	156	2278	82.1	-47.4	0
9	1556	149.7	1556	75.8	-49.4	0
10	484	143	485	98.3	-31.3	-1
11	2270	143	2271	111.2	-22.2	-1
12	2263	138	2263	79.6	-42.3	0
13	813	126.8	814	72.8	-42.6	-1
14	1231	124	1232	52.6	-57.6	-1
15	1937	122	1934	63.9	-47.6	3
16	1619	118.5	1619	47.6	-59.8	0
17	2593	114	2588	124.9	9.5	5
18	1913	112.9	1914	58.2	-48.4	-1
19	97	111	97	78.2	-29.5	0
20	1366	104.6	1366	31.5	-69.8	0
21	73	103.7	74	56	-46	-1
22	1520	103	1520	63.6	-38.2	0
23	1979	102	1981	49.2	-51.7	-2
24	405	96.4	406	78.2	-18.9	-1

Table 4.8: Event analysis statistics for largest 24 events during validation period 2 (1/10/2003-30/9/2011) at gauging station 45001 (Exe at Thorverton).

Event number	Obs Day	Obs Q	Sim Day	Sim Q	Error %	Day error
1	1802	174	1803	127.5	-26.7	-1
2	1530	150	1531	98.1	-34.6	-1
3	2662	148.3	2662	94.8	-36.1	0
4	74	140	74	111.6	-20.3	0
5	1744	121	1745	69.2	-42.8	-1
6	768	116	768	47.2	-59.3	0
7	104	115	104	97.9	-14.9	0
8	1568	109	1569	64	-41.3	-1
9	1152	105	1152	88.8	-15.4	0
10	2129	105	2130	82.2	-21.7	-1
11	1524	101	1529	80.1	-20.7	-5
12	2250	97.4	2252	77.4	-20.5	-2
13	2300	92.4	2301	39	-57.8	-1
14	1959	92.3	1960	57.4	-37.8	-1
15	1574	85.2	1569	64	-24.9	5
16	395	82.7	395	65.5	-20.8	0
17	1901	79.3	1901	58.2	-26.6	0
18	1253	79.2	1253	67.1	-15.3	0
19	1941	77.8	1942	65.3	-16.1	-1
20	1198	74.2	1198	67.2	-9.4	0
21	1779	73.1	1778	52	-28.9	1
22	795	71.5	796	51.6	-27.8	-1
23	2599	71	2601	42.7	-39.8	-2
24	446	69.5	446	72.4	4.2	0

Table 4.9: Event analysis statistics for largest 24 events during validation period 1 (1/10/1993-30/9/2001) at gauging station 45002 (Exe at Stoodleigh).

Event number	Obs Day	Obs Q	Sim Day	Sim Q	Error %	Day error
1	453	157.9	454	104.8	-33.6	-1
2	1857	137.6	1858	75.4	-45.2	-1
3	395	134.8	396	116.5	-13.6	-1
4	2587	132.6	2587	124.5	-6.1	0
5	1850	125.9	1851	60.8	-51.7	-1
6	81	108.5	81	73.6	-32.2	0
7	1556	103.9	1558	64.6	-37.9	-2
8	484	99.8	485	82.8	-17	-1
9	1618	99.3	1619	43	-56.7	-1
10	1231	98	1231	47.5	-51.5	0
11	2263	97.6	2263	67.1	-31.3	0
12	2278	97.6	2278	64.3	-34.1	0
13	2625	97.4	2626	76.3	-21.7	-1
14	2270	94.8	2271	99.1	4.6	-1
15	813	89.7	813	60.5	-32.5	0
16	1937	85.1	1934	57.1	-32.9	3
17	1913	82.6	1913	51.1	-38.2	0
18	1979	81.7	1980	39.4	-51.8	-1
19	1366	79.3	1366	28.5	-64.1	0
20	73	73.7	74	47.7	-35.2	-1
21	97	72.2	96	62.7	-13.1	1
22	1520	70.2	1520	56.1	-20.1	0
23	2593	69.9	2588	52.3	-25.3	5
24	185	69.3	186	83.4	20.4	-1

Table 4.10: Event analysis statistics for largest 24 events during validation period 2 (1/10/2003-30/9/2011) at gauging station 45002 (Exe at Stoodleigh).

Event number	Obs Day	Obs Q	Sim Day	Sim Q	Error %	Day error
1	1802	105	1803	117.6	12	-1
2	74	102.7	74	107	4.2	0
3	2662	101.8	2662	83.6	-17.8	0
4	1530	97.4	1531	87.1	-10.5	-1
5	104	77.5	104	87.5	12.9	0
6	768	77.2	768	42.9	-44.5	0
7	1744	76	1745	65.3	-14.1	-1
8	1151	70.1	1152	82.2	17.2	-1
9	2250	69.1	2251	60.5	-12.4	-1
10	1568	68.2	1568	51	-25.2	0
11	1524	66.6	1529	69	3.6	-5
12	2129	64.6	2130	79.9	23.7	-1
13	1574	61.9	1569	45	-27.4	5
14	1197	58.9	1198	57.3	-2.8	-1
15	2300	53.1	2300	29.7	-44.1	0
16	395	51.5	395	52.7	2.3	0
17	2599	51.3	2601	38.6	-24.7	-2
18	1253	50.8	1252	50.6	-0.3	1
19	1941	50.2	1941	52.2	4	0
20	501	47.8	501	51.3	7.4	0
21	1208	47.3	1206	43.7	-7.6	2
22	1779	47	1778	48.1	2.3	1
23	755	46.1	756	44.9	-2.6	-1
24	124	45.6	129	57.3	25.7	-5

Table 4.11: Event analysis statistics for largest 24 events during validation period 1 (1/10/1993-30/9/2001) at gauging station 45003 (Culm at Wood Mill).

Event number	Obs Day	Obs Q	Sim Day	Sim Q	Error %	Day error
1	2625	66.5	2625	42.2	-36.5	0
2	81	56.9	80	28.1	-50.6	1
3	2587	56.1	2586	35.2	-37.3	1
4	405	48.7	404	22.3	-54.2	1
5	2278	45.3	2277	27.4	-39.4	1
6	2270	43.8	2270	26.1	-40.4	0
7	2593	43.1	2588	8.4	-80.5	5
8	1406	37.5	1405	11.2	-70.2	1
9	813	37.2	812	16.1	-56.8	1
10	1850	37	1850	8.9	-76	0
11	2377	36.8	2376	6.5	-82.4	1
12	1857	34	1857	13.9	-59.2	0
13	484	33.7	484	25.3	-24.8	0
14	1556	31.8	1557	20.1	-36.8	-1
15	97	31.4	96	24.2	-23.1	1
16	1937	29	1937	15.7	-45.7	0
17	1510	28.9	1509	13.9	-52	1
18	126	27.9	125	16.1	-42.3	1
19	2180	27.5	2179	20.7	-24.9	1
20	2031	27.4	2030	14.9	-45.6	1
21	830	26.9	830	21.4	-20.5	0
22	1520	25.6	1519	15.4	-39.8	1
23	1146	25.2	1145	7.4	-70.8	1
24	453	25.1	453	18.2	-27.6	0

Table 4.12: Event analysis statistics for largest 24 events during validation period 2 (1/10/2003-30/9/2011) at gauging station 45003 (Culm at Wood Mill).

Event number	Obs Day	Obs Q	Sim Day	Sim Q	Error %	Day error
1	1959	64	1959	26.6	-58.4	0
2	1857	53.4	1856	61.7	15.6	1
3	794	51.4	793	23.6	-54.1	1
4	1901	42.1	1900	25.4	-39.6	1
5	1530	39.3	1530	20.2	-48.6	0
6	1568	36.4	1567	18.6	-48.8	1
7	1802	36.3	1802	9.9	-72.8	0
8	104	35.5	103	18.4	-48.3	1
9	1251	34.4	1252	22.5	-34.7	-1
10	2300	31.8	2305	17.3	-45.7	-5
11	2605	29.9	2605	10.6	-64.7	0
12	768	27.2	767	6.4	-76.4	1
13	446	26	447	9.1	-65.2	-1
14	1703	25.3	1703	7.5	-70.3	0
15	1868	24.3	1868	19	-21.8	0
16	395	23.9	393	20.2	-15.7	2
17	1744	23.4	1744	4.5	-80.7	0
18	2246	22.8	2251	19.6	-13.9	-5
19	1623	21.5	1628	18.5	-14.2	-5
20	124	21.4	128	19.7	-7.8	-4
21	2333	21.2	2332	7.6	-64.2	1
22	2259	20.5	2258	17.8	-13.3	1
23	2306	20.5	2305	17.3	-15.7	1
24	1232	20.1	1232	14.7	-26.7	0

Table 4.13: Event analysis statistics for largest 24 events during validation period 1 (1/10/1993-30/9/2001) at gauging station 45009 (Exe at Pixton).

Event number	Obs Day	Obs Q	Sim Day	Sim Q	Error %	Day error
1	454	68.9	454	60.9	-11.6	0
2	2586	59.6	2586	66.5	11.6	0
3	395	50.6	395	61.5	21.5	0
4	1850	49.9	1850	35.6	-28.7	0
5	1857	49.2	1858	43.8	-10.9	-1
6	484	41	485	43.8	6.8	-1
7	80	40.6	80	37	-8.9	0
8	2625	38.2	2626	40.7	6.7	-1
9	1366	37.6	1366	14.8	-60.7	0
10	1558	37.4	1555	34.3	-8.2	3
11	1619	37.4	1619	27.2	-27.3	0
12	1913	34.4	1913	34.8	1.3	0
13	1231	32.4	1236	32.8	1.4	-5
14	1980	30.6	1980	21	-31.3	0
15	2277	30.5	2277	30.1	-1.4	0
16	2263	29.5	2263	40.1	35.9	0
17	1937	29	1934	35.6	22.9	3
18	813	28.1	813	32.8	16.6	0
19	97	26.7	96	30.4	13.9	1
20	2271	26.6	2270	54.4	104.4	1
21	2631	25.4	2626	40.7	60.4	5
22	2593	24.6	2590	18.2	-26	3
23	1922	24.3	1920	27.1	11.6	2
24	2346	23.3	2346	25.2	8.3	0

Table 4.14: Event analysis statistics for largest 24 events during validation period 2 (1/10/2003-30/9/2011) at gauging station 45009 (Exe at Pixton).

Event number	Obs Day	Obs Q	Sim Day	Sim Q	Error %	Day error
1	1802	40.6	1802	64.9	59.8	0
2	2662	34.5	2662	48.1	39.5	0
3	1530	34.4	1531	47.8	39	-1
4	1573	31.2	1568	28.2	-9.5	5
5	74	29.7	74	67.6	127.7	0
6	1152	27.6	1152	51.1	85.3	0
7	104	26.9	104	49.6	84.2	0
8	2250	25.9	2246	30.8	18.9	4
9	768	24.5	768	26.7	8.8	0
10	1524	24.2	1529	41	69.4	-5
11	1198	22.9	1198	31.5	37.6	0
12	1253	21.4	1252	26.5	24	1
13	2599	20.6	2604	22.5	9.4	-5
14	395	19.6	390	31.3	59.6	5
15	2129	19.6	2130	51.4	162.3	-1
16	1208	19.5	1206	24.6	26.1	2
17	1942	19.4	1941	29.1	50	1
18	125	18.2	129	31.2	71.7	-4
19	2300	17.5	2300	16.4	-6.4	0
20	1744	17	1744	41.3	142.9	0
21	1629	16.8	1629	42.6	153.5	0
22	1162	16.5	1167	25	51.3	-5
23	1168	15.8	1168	25.4	60.6	0
24	1565	15.7	1568	28.2	79.8	-3

Table 4.15: Event analysis statistics for largest 24 events during validation period 1 (1/10/1993-30/9/2001) at gauging station 45012 (Creedy at Cowley).

Event number	Obs Day	Obs Q	Sim Day	Sim Q	Error %	Day error
1	505	516	502	16.5	-96.8	3
2	499	504	502	16.5	-96.7	-3
3	2614	108	2609	17.8	-83.5	5
4	2259	89	2262	36.5	-59	-3
5	2576	71.4	2571	8.7	-87.8	5
6	81	70.7	80	30.6	-56.7	1
7	2267	61.8	2270	73.9	19.6	-3
8	2582	53.6	2586	46.7	-12.9	-4
9	1846	51	1850	18.8	-63.1	-4
10	126	47.3	125	16.4	-65.4	1
11	482	42.8	481	32.2	-24.8	1
12	2597	39.4	2595	13.6	-65.4	2
13	1547	38.5	1547	12.4	-67.9	0
14	819	38.4	814	18.5	-51.9	5
15	2717	35.2	2720	6.2	-82.3	-3
16	454	34.6	453	49.3	42.6	1
17	2661	34.1	2656	9.1	-73.4	5
18	97	32.7	96	26.8	-18.2	1
19	1815	31.9	1810	1.4	-95.6	5
20	802	31.8	798	4.2	-86.9	4
21	146	31.7	148	22.9	-27.7	-2
22	434	29.3	433	18	-38.6	1
23	1839	28.7	1842	6.9	-76.1	-3
24	1926	28.4	1921	14.1	-50.4	5

Table 4.16: Event analysis statistics for largest 24 events during validation period 2 (1/10/2003-30/9/2011) at gauging station 45009 (Creedy at Cowley).

Event number	Obs Day	Obs Q	Sim Day	Sim Q	Error %	Day error
1	1959	81.1	1959	31.6	-61	0
2	2300	46.6	2305	15.1	-67.5	-5
3	1901	41.2	1900	24.6	-40.3	1
4	795	37.3	793	14.6	-60.8	2
5	1228	33.8	1232	18.5	-45.3	-4
6	480	32.3	480	8.7	-73	0
7	445	32	445	14.2	-55.7	0
8	1253	31.1	1252	22.9	-26.4	1
9	1802	29.9	1802	25.6	-14.5	0
10	395	29.6	394	18.4	-37.7	1
11	2252	26.9	2251	25.5	-5.2	1
12	2246	26	2251	25.5	-1.9	-5
13	768	25.9	767	9.8	-62.2	1
14	1154	25.5	1151	21.5	-15.6	3
15	2237	24.9	2236	17.3	-30.5	1
16	1568	24.8	1567	21.7	-12.6	1
17	1530	24.5	1530	25.8	5.2	0
18	2282	24.3	2282	14.9	-38.7	0
19	100	24	103	27.6	14.9	-3
20	2662	23.6	2661	23.7	0.1	1
21	124	23.2	128	22.1	-4.9	-4
22	1628	22.3	1628	18.2	-18.3	0
23	1160	22.1	1155	10.1	-54.3	5
24	1364	21.8	1369	4.3	-80.4	-5

Table 4.17: Average of percentage error estimate of model simulation for 24 largest discharge events compared to observational NRFA data. The standard deviation of peak error prediction is shown in brackets.

Station number	Average peak error % for period 1	Average peak error % for period 2
45001	-42 (±16)	-27 (±15)
45002	-30 (±20)	-5 (±19)
45003	-47 (±18)	-41 (±26)
45009	5 (±33)	60 (±48)
45012	-55 (±36)	-33 (±27)

The percentage error of peak flow estimation for some events is large (up to 96%). Instances where event magnitude is poorly represented by the model are likely to be caused by the rainfall input to the APT model not capturing localised high magnitude rainfall events due to the positioning of weather stations, the low number of weather stations, and the interpolation method used (as discussed previously). Under-estimation of rainfall to the APT model, and omission of heavy rainfall events within the input data to the APT model will result in under-estimation and omission of peak runoff delivery events to the catchment, and hence under-estimation of peak flow events within the routing model. As noted previously, any further calibration of the input data (temporally varying the calibration of runoff delivery to the catchment) could not be justified due to lack of data to validate any such calibration. The timing of peak flow events predicted by the model is generally good (34% and 38% of simulated events occurring on the same day as observed in validation periods 1 and 2 respectively). The magnitude of the error in estimation of peak flows has been minimised as best possible by calibrating the input data by increasing the rainfall runoff input values.

Additionally, the influence of the curve number parameter within the APT model will strongly influence the accuracy of peak flow prediction; low curve numbers are representative of areas with low runoff potential. Where less runoff is simulated by the model the time taken for water delivery to the channel network will increase, and the volume of water delivery will decrease, thereby decreasing predicted peak flow magnitudes, and attenuating hydrograph peaks.

The APT model output used here is from an un-calibrated model output, and therefore optimum values of the curve number may not have been selected. It is possible that some of the inaccuracy in peak flow prediction is due to lack of calibration of parameters within the APT model, such as the curve number.

4.3.5.1. Individual event analysis

Two individual events from each validation period were analysed using the same validation statistics as before, and plotting hydrographs to compare observed and simulated 1.5 hourly discharge at each gauging station. Events chosen were observed within the largest 10 magnitude events at all gauging stations. The 10 days prior to, and after the day of observed peak discharge were included in the analysis.

The hydrograph in Figure 4.13 shows the observed and simulated discharge at gauging stations from NRFA data for the period 20/10/2000 – 09/11/2000. Table 4.18 shows the validation statistics for this event. The shape of the simulated hydrograph is similar to the observed hydrograph. However the hydrographs and the PBIAS statistics indicate the model under-estimates the event discharge at all locations. Based on the statistics for the event (Table 4.18 – all but one of the R^2 and NSE values >0.5, MAE<half of the standard deviation of observations, and RSR<1) the overall model estimation of the event is satisfactory.

The event period illustrated in Figure 4.13 includes two hydrograph peaks; the first larger than the second. The magnitude of the first peak is replicated at stations 45002 (Exe at Stoodleigh), 45009 (Exe at Pixton), and 45012 (Creedy). However, the peak magnitude is under predicted at both 45001 (Exe at Thorverton) and 45003 (Culm). The spatial variation in accuracy of event peak prediction throughout the catchment is likely to be caused by the positioning of the weather stations and interpolation method used for generating rainfall input for the APT model, and the spatial variability of the accuracy of rainfall estimates across the catchment. The second (smaller) peak in the event period is not captured in the model simulation at any locations. This could be due to parameterisation within the APT model, such as low curve number values causing a lower runoff potential in parts or all of the catchment. This

would decrease the catchment sensitivity to rainfall events, and result in the omission of smaller event discharges in simulations. As the PBIAS values shown in Table 4.18: Validation statistics for validation period 1 (1/10/1993 - 30/9/2001) for event 1: 20/10/2000 - 09/11/2000. are calculated from the whole period shown (rather than just an error of the peak magnitude prediction) these values are high when compared to the magnitude of error shown in Figure 4.13: Hydrograph of observed (dashed lines) and simulated (solid lines) discharge for all gauging stations from 20/10/2000 - 9/11/2000.

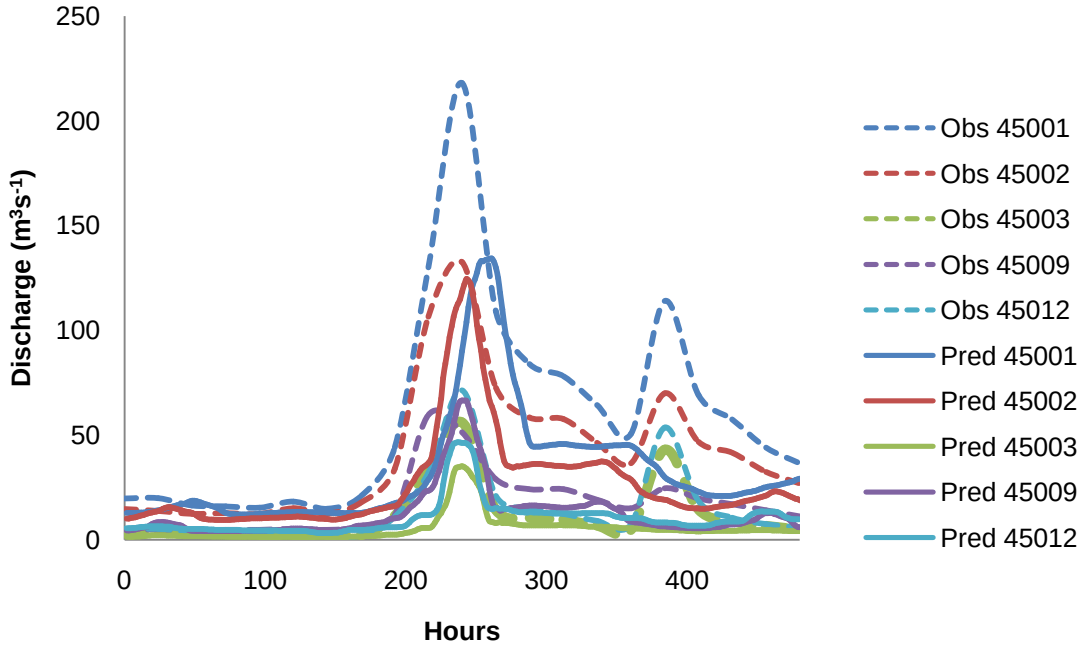

Figure 4.13: Hydrograph of observed (dashed lines) and simulated (solid lines) discharge for all gauging stations from 20/10/2000 - 9/11/2000.

Table 4.18: Validation statistics for validation period 1 (1/10/1993 - 30/9/2001) for event 1: 20/10/2000 - 09/11/2000.

Station	R^2	NSE	MAE	RMSE	STEV obs	RSR	PME	PBIAS (%)
45001	0.74	0.47	26.21	38.08	52.30	0.73	0.31	44.35
45002	0.77	0.79	15.58	21.24	46.68	0.46	-0.12	37.41
45003	0.59	0.97	6.43	12.22	65.44	0.19	0.09	54.27
45009	0.77	0.98	5.07	8.08	60.29	0.13	0.47	29.41
45012	0.44	0.95	4.09	14.11	63.75	0.22	0.25	28.45

The hydrograph in Figure 4.14 shows the observed and simulated discharge at gauging stations from NRFA data for the period 18/12/1994 - 07/01/1994. Table 4.19 shows the validation statistics for this event. The shape of the simulated hydrograph is very similar to the observed hydrograph, as indicated in the R^2 and NSE statistics. However the hydrographs and the PBIAS statistics indicate the model under-estimates the event discharge at all locations except 45012 where the model slightly over-estimates the discharge. Based on the statistics for the event (Table 4.19 – all of the R^2 and NSE values >0.5, MAE<half of the standard deviation of observations, and RSR<1) the overall model estimation of the event is satisfactory.

Similarly to the previous example, the magnitude of peak prediction is reasonably accurate at station 45009 (Exe at Pixton). At station 45012 (Creedy) the model slightly over predicts the peak discharge. At all other stations the model under predicts discharge. The variability of the magnitude of error between locations is likely to be caused by the variability of rainfall estimation within the APT input data throughout the catchment.

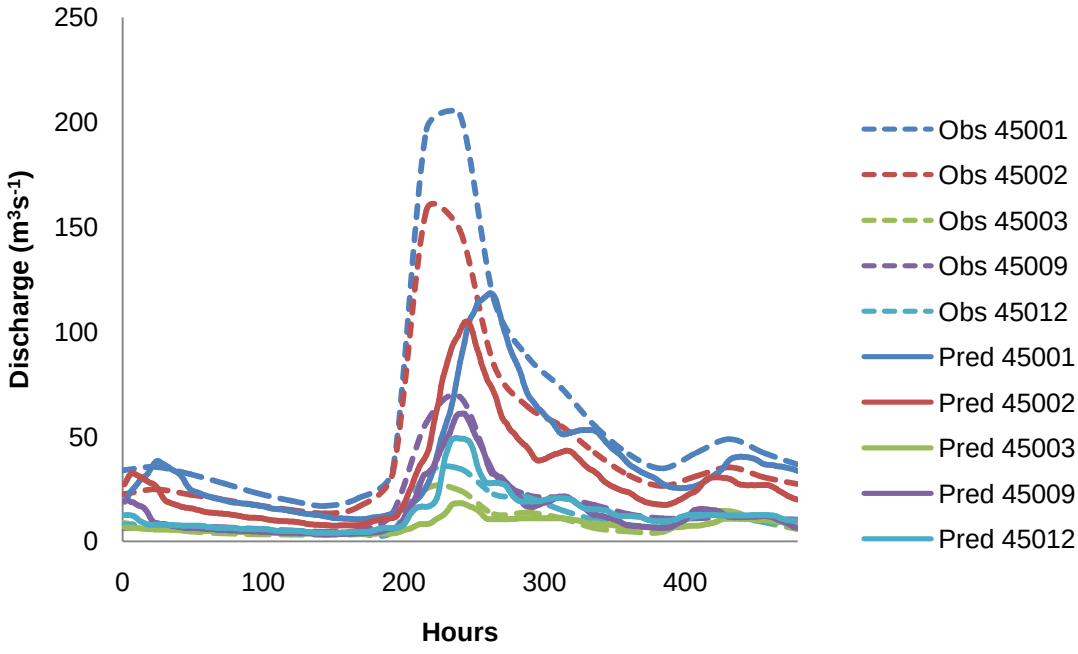

Figure 4.14: Hydrograph of observed (dashed lines) and simulated (solid lines) discharge for all gauging stations from 18/12/1994-07/01/1994.

Table 4.19: Validation statistics for validation period 1 (1/10/1993 - 30/9/2001) for event 2: 18/12/1994 - 07/01/1994.

Station	R^2	NSE	MAE	RMSE	STEV obs	RSR	PME	PBIAS (%)
45001	0.66	0.48	21.19	39.08	54.39	0.72	-0.13	36.46
45002	0.85	0.76	15.26	24.77	50.69	0.49	0.24	34.93
45003	0.79	1.00	1.29	3.83	67.16	0.06	0.47	14.65
45009	0.84	0.99	2.70	6.45	61.42	0.10	0.61	16.33
45012	0.87	1.00	1.78	2.48	65.01	0.04	0.85	-15.79

The hydrograph in Figure 4.15 shows the observed and simulated discharge at gauging stations from NRFA data for the period 26/08/2008 – 15/09/2008. Table 4.20 shows the validation statistics for this event. The shape of the simulated hydrograph is very similar to the observed hydrograph, as indicated in the R^2 and NSE statistics. However the hydrographs and the PBIAS statistics indicate the model over-estimates the event discharge at 45009 and 45012, and very slightly at 45002. Based on the statistics for the event (Table 4.20 – all but one of the R^2 and NSE values >0.5, MAE<half of the standard deviation of observations, and RSR<1) the overall model estimation of the event is satisfactory.

The hydrographs from the observed data in Figure 4.15 show several smaller peaks on the rising limb of the hydrograph, whereas the predicted hydrographs show a smooth rising limb. Similarly to the first example, this could be due to parameterisation within the model (particularly curve number estimation) and the sensitivity of the catchment to smaller rainfall events.

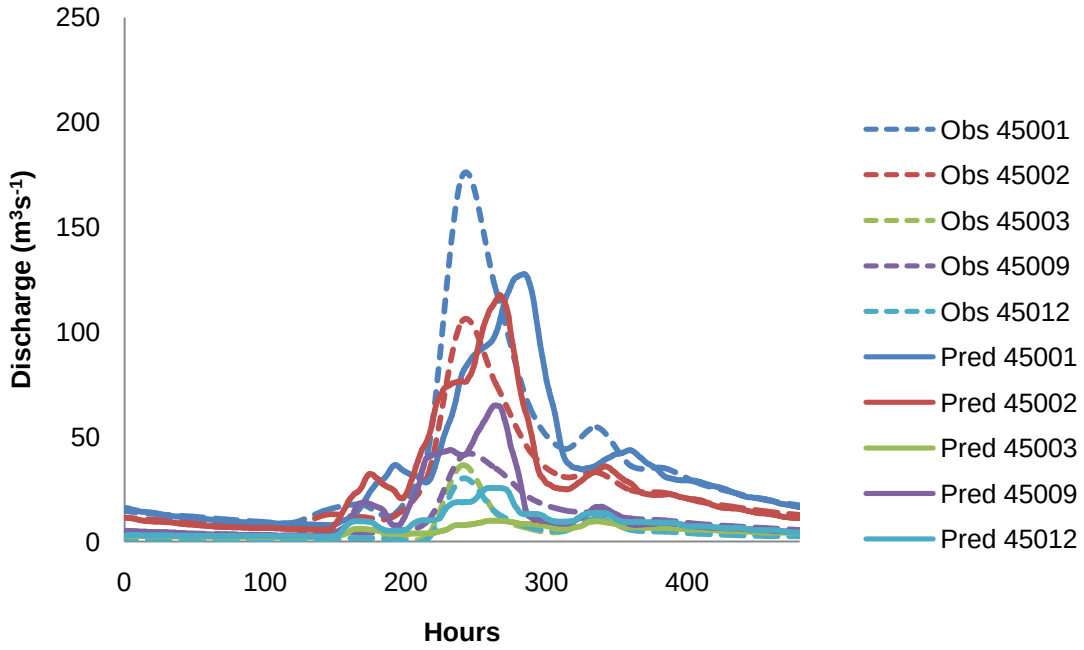

Figure 4.15: Hydrograph of observed (dashed lines) and simulated (solid lines) at all gauging stations from 26/08/2008-15/09/2008.

Table 4.20: Validation statistics for validation period 2 (1/10/2003 - 30/9/2011) for event 2: 26/08/2008 - 15/09/2008.

Station	R^2	NSE	MAE	RMSE	STEV obs	RSR	PME	PBIAS (%)
45001	0.72	0.88	3.59	19.48	55.58	0.35	0.64	9.75
45002	0.74	0.96	2.18	11.26	56.20	0.20	0.62	-8.80
45003	0.44	0.99	1.28	6.29	69.92	0.09	0.37	20.77
45009	0.55	0.98	2.52	9.22	66.00	0.14	-0.48	-24.07
45012	0.62	1.00	3.10	4.82	71.23	0.07	0.47	-65.07

The hydrograph in Figure 4.16 shows the observed and simulated discharge at gauging stations from NRFA data for the period 28/11/2007 – 18/12/2007. Table 4.21 shows the validation statistics for this event. The shape of the simulated hydrograph is very similar to the observed hydrograph, as indicated in the R^2 and NSE statistics. However the hydrographs and the PBIAS statistics indicate the model under-estimates the event discharge at all locations except 45012. Based on the statistics for the event (Table 4.20 – all of the R^2 and NSE values >0.5, MAE<half of the standard deviation of observations, and

RSR<1) the overall model estimation of the event is satisfactory. Similarly to previous examples, the accuracy of the model to simulate peak discharge varies throughout the catchment, and the shape of the hydrograph is not fully captured by the model (smaller peaks are not always represented).

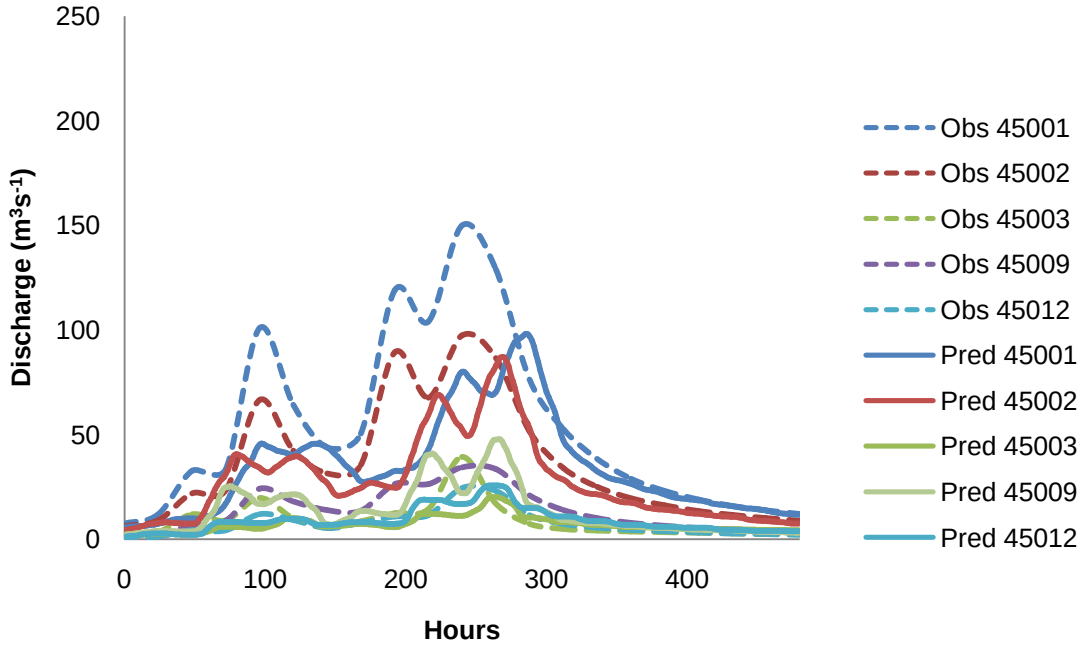

Figure 4.16: Hydrograph of observed (dashed lines) and simulated (solid lines) discharge at all gauging stations from 28/11/2007-18/12/2007.

Table 4.21: Validation statistics for period 2 (1/10/2003 - 30/9/2011) for event 2: 28/11/2007 - 18/12/2007.

Station	R^2	NSE	MAE	RMSE	STEV obs	RSR	PME	PBIAS (%)
45001	0.69	0.55	19.83	31.71	47.47	0.67	-0.20	36.94
45002	0.76	0.89	9.44	16.23	48.19	0.34	0.36	25.78
45003	0.58	0.99	1.92	6.33	67.30	0.09	0.21	21.48
45009	0.75	1.00	0.58	4.42	62.74	0.07	0.47	4.25
45012	0.80	1.00	1.18	2.50	68.45	0.04	0.70	-15.64

4.3.6. Sensitivity analysis

The model was run with increased (0.75) and decreased (0.35) velocity parameter values. These velocity values are appropriate are they are within the range of reasonable velocity parameter values based on the possible range of Manning's roughness coefficients used to estimate the velocity of flow (DEFRA, 2003; Hey and Thorne, 1986; Nicholas and Mitchell, 2003; Thomas and Nisbet, 2007). The validation statistics for the model when run with these parameter values are shown in Table 4.22 for the first validation period and Table 4.23 for the second. These statistics indicate varying the velocity parameter has very little influence on the validation statistics; all statistics only vary very slightly, if at all. The accuracy improves at some locations and diminishes at others.

Table 4.22: Validation statistics for period 1 (1/10/1993 - 30/9/2001) when using velocity parameter 0.35 and 0.75.

Station	R^2	NSE	MAE	RMSE	STDEV obs	RSR	PME	PBIAS (%)	
45001	0.72	0.58	6.03	14.70	22.79	0.65	-0.64	32.22	
45002	0.81	0.68	4.55	9.21	16.19	0.57	-0.32	31.87	
45003	0.66	0.64	1.19	3.29	5.58	0.59	0.36	27.24	v = 0.35
45009	0.66	0.64	0.64	3.72	6.24	0.60	-0.72	12.05	
45012	0.67	0.65	0.19	3.85	6.49	0.59	0.38	-4.69	
45001	0.82	0.66	6.11	13.31	22.79	0.58	-0.34	32.62	
45002	0.80	0.67	4.62	9.29	16.19	0.57	-0.35	32.30	
45003	0.69	0.66	1.21	3.22	5.58	0.58	0.39	27.60	v = 0.75
45009	0.64	0.61	0.64	3.87	6.24	0.62	-0.86	11.98	
45012	0.69	0.66	0.17	3.77	6.49	0.58	0.41	-4.23	

Table 4.23: Validation statistics for period 2 (1/10/2003 - 30/9/2011) when using velocity parameter 0.35 and 0.75.

Station	R^2	NSE	MAE	RMSE	STDEV obs	RSR	PME	PBIAS (%)	
45001	0.75	0.74	3.40	9.36	18.22	0.51	-0.14	23.27	
45002	0.87	0.87	1.75	4.50	12.34	0.36	0.34	16.83	
45003	0.59	0.56	0.67	2.74	4.14	0.66	0.41	19.38	v = 0.35
45009	0.72	0.61	0.06	2.71	4.33	0.63	-1.64	-1.42	
45012	0.66	0.69	0.14	2.62	4.74	0.55	0.33	-4.69	
45001	0.85	0.81	3.46	7.91	18.22	0.43	0.18	23.68	
45002	0.85	0.85	1.80	4.71	12.34	0.38	0.28	17.33	
45003	0.59	0.56	0.68	2.74	4.14	0.66	0.42	19.68	v = 0.75
45009	0.67	0.54	0.06	2.95	4.33	0.68	-2.11	-1.53	
45012	0.67	0.70	0.13	2.58	4.74	0.54	0.35	-4.24	

Similarly to the previous section, the error in peak estimate of the 24 highest magnitude events at each gauging station were calculated. The results from this analysis are shown in Appendix C Tables 86-95. The average error in prediction of all 24 events was calculated for each validation period at each gauging station, these values are shown in Table 4.24. The results indicate that varying the velocity parameter has only a very small influence on the peak discharge magnitude. The hydrographs in Figure 4.17 and Figure 4.18 show the model output at gauging station 45001 over 2 flood events (one from each of the validation periods) and these also indicate the peak magnitude is not influenced greatly but the change in velocity, but the timing of the flood wave peak is earlier with increased velocity parameter. The change in timing of peak discharge is considered insignificant to model performance; the observational data used for comparison has daily temporal resolution, and the influence of varying the velocity parameter on the timing of the peak discharge is less than 24 hours.

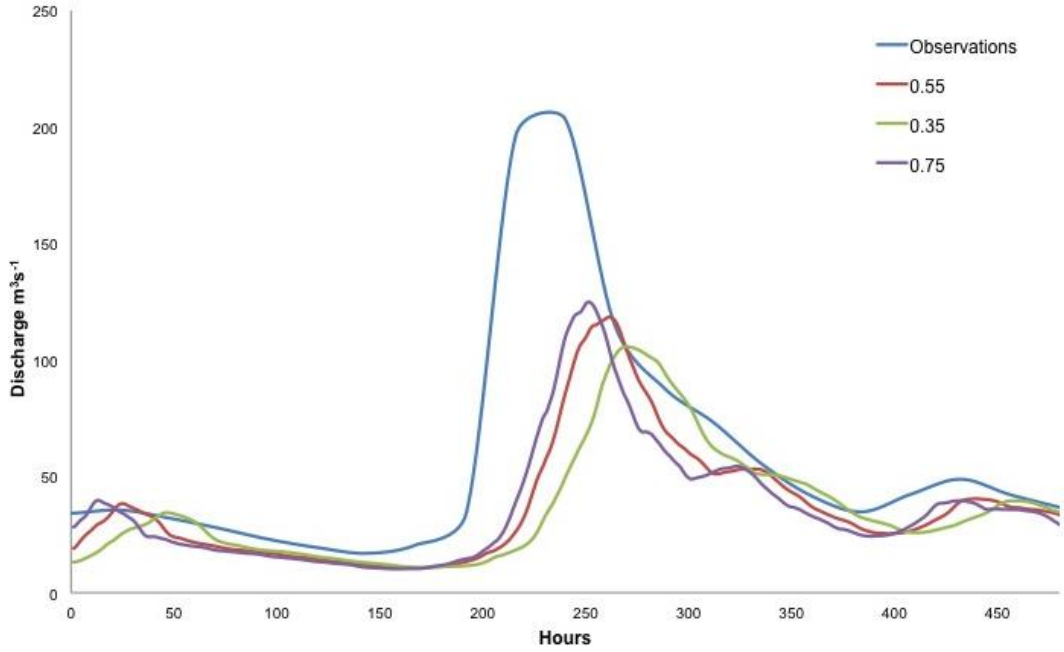

Figure 4.17: Hydrograph of observed discharge from 18/12/1994 - 07/01/1991 and model outputs over the same period for various velocity parameters at station 45001.

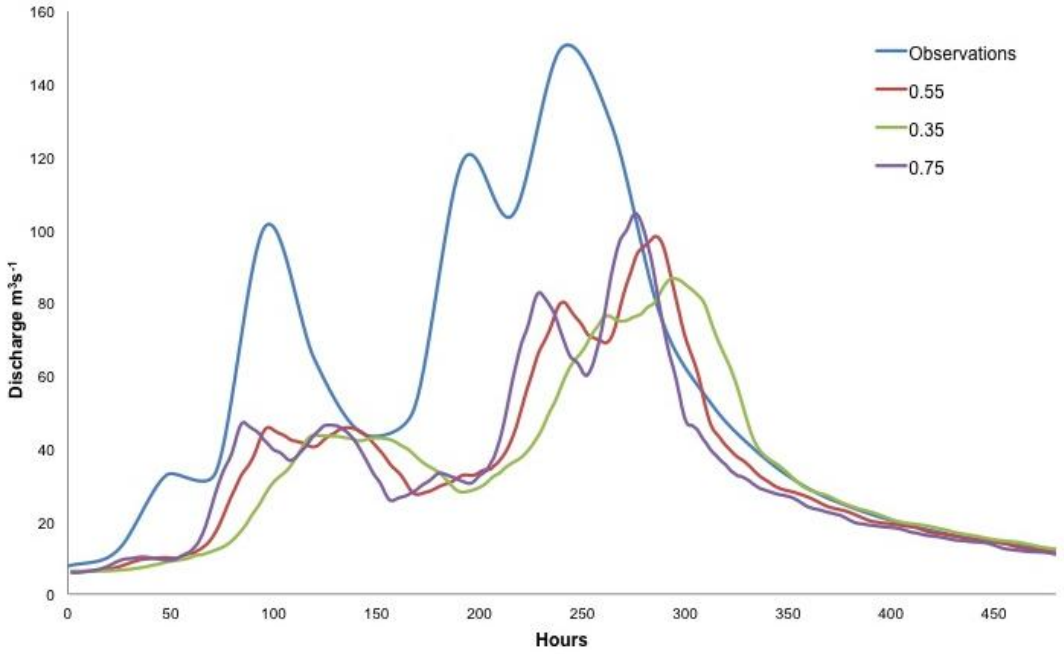

Figure 4.18: Hydrograph of observed discharge from 28/11/2007 - 18/12/2007 and model outputs over the same period for various velocity parameters at station 45001.

Table 4.24: Average of percentage error estimate of model simulation for 24 largest discharge events compared to observational NRFA data when the model is run using varied velocity parameter value.

Station	Average peak error % period 1	Average peak error % period 2	Velocity parameter
45001	-50	-36	
45002	-37	-15	
45003	-49	-45	v = 0.35
45009	-2	44	
45012	-55	-34	
45001	-41	-25	
45002	-28	-3	
45003	-47	-41	v = 0.75
45009	3	57	
45012	-55	-33	

4.4. Conclusions

The routing model developed in this chapter provides a computationally efficient methodology for routing catchment discharge. The model has been tested for a period of 20 years from 1/10/1991 – 30/09/2011 for the river Exe catchment, Devon. The model output has been compared to gauging station data from the catchment to assess model accuracy.

The model was shown to under-predict discharge at some locations in the catchment; stations 45001, 45002 and 45003 (Exe at Thorverton and Stoodleigh, and the river Culm respectively). This was attributed to under-estimation of water delivery to the catchment by the input data. The location and small number of weather station data available will have resulted in errors when estimating rainfall over the catchment (possibly an under-estimation of rainfall) within the ATP model. This would result in errors in rainfall-runoff delivery to the catchment by the APT model, which is observed in under-estimation of discharge within the routing model. The input data was calibrated accordingly as a result by increasing the runoff delivery to the catchment. After calibration the model still under-predicts discharge at several locations however this error has been minimised as best possible by the input data calibration and calibration statistics indicate overall acceptable model performance; R^2 values and NSE consistently are consistently above 0.5, and RMSE and MAE values are low (mostly below half of the standard deviation of observations), and RSR values less than 1.

Further calibration of the input data is not possible; there is inadequate data to justify any spatial variation of calibration of input data. This would require more detailed gauging station data across the catchment. Additionally, temporally varying the input data is not practical due to the daily resolution of the gauging station data as errors within the runoff delivery data are likely due to occurrence of rainfall events with a timescale of less than 24 hours.

The model under-estimates high-magnitude discharge peaks with the exception of station 45009 (Exe at Pixton). This could be due to the positioning of weather station data and the interpolation methodology; localised rainfall events over the catchment may not be captured fully by weather station data

available. Additionally, smoothing of the data by the interpolation method used may also contribute to this under-estimation. The majority of peak events were captured by the model (and hence input data) as indicated in the hydrographs showing both model and observed discharge, yet the simulated magnitude of peak discharge was under-estimated, most likely due to errors in rainfall under-estimation. The hydrographs indicate the model replicates the timing of the peaks with a good degree of accuracy (several of the high magnitude flow events are simulated on the same day as observed).

As in previous studies (Ponce and Chaganti, 1994), the results indicate there is some mass loss in the routing procedure. However, the magnitude of the mass loss is small and is not considered to significantly influence the model output.

Limitations of the model include the parameter estimation; the velocity parameter remains constant for the whole catchment, estimated using the Manning's equation. Due to the format of the input data (from the ADAS APT model output) routing reach lengths are variable. The influence of both these limitations is minimised through use of a variable parameter method, as the spatial resolution for each routing reach varies according to reach length, which in turn varies the Courant and Reynolds numbers, and the routing coefficients (C_1, C_2 and C_3) for all routing reaches. The value of the velocity parameter is based on Manning's equation calculated from a range of values estimated in the literature, and the sensitivity analysis indicates when the model is run using a range of alternative reasonable values there is very little difference to the validation statistics and/or hydrographs.

Whilst the Muskingum-Cunge routing methodology has been shown to accurately simulate catchment discharge at several locations in previous studies, in this study the model is tested and validated for one catchment. It would be beneficial to analyse the accuracy of this methodology in other catchments also, particularly when combined with the ADAS APT model input and the described catchment modification required for the routing procedure. The catchment network modification was analysed visually, by comparison with the natural channel network. From this it was assumed the catchment modification was acceptable.

The routing model developed in this chapter will be used in the following chapter and sediment input from the ADAS APT model will be incorporated within the model. The bank erosion model from previous chapters will provide an estimation of bank eroded sediment input, and a simplistic floodplain sedimentation component will also be included to enable estimation of the catchment sediment budget.

5. Sediment budget model

5.1. Introduction

This chapter aims to develop a catchment sediment budget model, including representations of sediment generation through bank erosion and sediment loss through floodplain sedimentation. Existing APT (ADAS Pollution Transport) model outputs estimate net water and sediment delivery to the channel network. The findings of the chapters two and three will be used to create a bank erosion index, and floodplain sedimentation will be accounted for using a power law relationship developed from a previous study (Nicholas *et al,* 2006). Both the bank erosion and floodplain sedimentation components will be calibrated individually using observational data and will then be incorporated within the routing model developed in the previous chapter. The model will be applied to the Exe catchment, UK for a 20-year period (1991-2011) and will provide an estimate of the catchment sediment budget.

The model will be an advance on existing methodologies due to the inclusion of sediment generated by bank erosion, which is currently not included within many widely-used models, including PSYCHIC (Davison *et al*, 2008), RUSLE (Renard *et al,* 1997), WEPP (Laflen *et al,* 1991), and CREAMS (Knisel, 1980). Catchment and channel characteristics such as channel confinement and channel sinuosity are not included within existing representations of bank erosion. The inclusion of these factors should improve the accuracy of predictions, with minimal increase in input data requirements and computation time. Additionally, floodplain sedimentation is not currently included within the existing PSYCHIC/APT model. Inclusion of this process within the model will provide a more complete representation of the catchment sediment budget. The sediment budget model created here may be a useful tool for catchment management, and improve understanding of catchment response and sensitivity to changes in land-use and climate change.

5.1.1. Aims and Justification

The importance of sediments as a source of diffuse pollution and their influence on both the chemical and ecological aspects of rivers has been outlined in chapter one. Additionally, regulation of sediments is required by EU policies, specifically the Water Framework Directive (WFD). Due to the numerous sources and sinks of sediment within catchments it is essential to consider the catchment as a whole when considering potential mitigation strategies. Walling and Collins (2008) indicate the value of the sediment budget concept for the management and control of sediment, particularly for considering the effects of upstream mitigation strategies on downstream fluxes. Additionally, the approach allows identification of key sediment sources, sinks and transfer pathways, which are of particular relevance for management purposes.

The sediment budget concept provides an effective means of improving understanding of catchment response to various land-use and climate change scenarios (Walling and Collins, 1998). Current scientific evidence projects changes in the hydrological cycle as a result of increasing temperatures. Whilst there is still great uncertainty surrounding these estimates, it is expected that climate change is likely to increase the average annual precipitation (IPCC, 2007), and the intensity of extreme precipitation events in much of the UK. The impact of these changes on sediment generation in the catchment will be estimated within this chapter.

As noted in the chapter one, the model PSYCHIC developed by ADAS estimates overland runoff and sediment generation and delivery to river catchments. Currently the model (and its successor the APT model, which is still in development stages) does not include a channel routing component. In the previous chapter a water routing methodology using the Muskingum method was applied to the Exe catchment. This chapter aims to include sediment within this routing methodology, enabling routing of both water and sediment generated from overland sources through the river catchment.

The ability of existing bank erosion representations within sediment generation models to accurately predict the variation of bank erosion rates within river catchments is limited. Additionally, the influence of channel sinuosity

should be considered when estimating bank erosion rates over longer time scales, for example when estimating the influence of climate and land-use changes.

As noted from the findings in chapter two and in the literature (Bull 1997; Carter *et al,* 1993; Walling *et al,* 2005 etc.) bank erosion is a significant sediment source within UK catchments, and rates of bank erosion vary significantly both spatially and temporally due to the number of influencing factors. Using data from chapters two and three, this chapter aims to develop an existing ADAS bank erosion index by incorporating some of the physical factors observed to influence channel bank erosion rates in UK catchments. These factors include channel confinement (by valley sides) and channel sinuosity. The inclusion of these factors should improve the physical realism and ability to represent spatial variation in bank erosion rates within the model. Additionally, inclusion of sinuosity makes the model more suitable for estimations of changes to sediment generation over longer time-scales.

As noted in several previous studies (Walling *et al,* 1998; Walling *et al,* 1999a; Walling and Owens, 2003, Nicholas *et al*, 2006) floodplain sedimentation is a significant sediment sink within UK catchments and therefore representation of this within models is necessary for accurate estimation of catchment sediment budgets. Physically-based floodplain sedimentation models have the ability to represent spatial variability of floodplain sedimentation and provide an estimate of sediment storage on floodplains at a reach scale (e.g. Nicholas and Walling, 1998). However, the high computational demands of such methodologies limit their application over larger areas, and therefore they are not suitable for integration with catchment sediment budget models. One of the limitations noted of the existing PSYCHIC model and bank erosion index was the lack of representation of floodplain sedimentation (Collins *et al,* 2009).

The power law model developed by Nicholas *et al,* (2006) provides a computationally efficient representation of floodplain sedimentation within catchments. Additionally, the input data requirements for this methodology are minimal in comparison to distributed models. Therefore this approach to representing sediment deposition on floodplains is more suitable for incorporation into a sediment budget model.

Therefore, the aim of this chapter is to build on recent advances in floodplain sedimentation modelling (Nicholas *et al*, 2006) and the progress made within this study in characterisation of bank erosion, to develop and apply a fully coupled catchment-scale sediment budget model. This requires the following objectives to be addressed:

- To develop a bank erosion model incorporating findings from the previous chapters of this thesis within an existing bank erosion index.
- Incorporate sediment routing within the routing model developed in the previous chapter.
- Incorporate the bank erosion model and a floodplain sedimentation model (based on the power law equation of Nicholas *et al,* 2006) within this sediment routing model to form a catchment sediment budget model.
- Apply this model to the Exe catchment, Devon, UK.
- Investigate the influence of climate change on sediment generation, through increased precipitation scenarios.

5.1.2. Background

5.1.2.1. Existing bank erosion components within sediment models

Chapter one outlined a selection of existing sediment generation models. Several of these do not currently include any representation of sediment generated through bank erosion (RUSLE, WEPP, PSYCHIC, CREAMS). Some models that include a representation of bank erosion were also outlined within this section (SedNet, SHETRAN, INCA-P, and ADAS bank erosion index). However, these existing representations include limitations such as lack of inclusion of several factors known to influence bank erosion rates. This will limit the accuracy of the estimates of sediment generation derived using these models, and also prevent representation of the spatial variability of sediment generation within the catchment. A further limitation of the ADAS bank erosion index is that it estimates the amount of bank eroded sediment that reaches the catchment outlet, rather than the total volume of sediment generated through bank erosion within the catchment.

5.1.2.2. Floodplain sedimentation

Several studies have included estimates of the magnitude of floodplain sedimentation as a percentage of the catchment sediment budget (see Table 5.1). The magnitude of these estimates demonstrates the importance including floodplain deposition when modelling catchment sediment budgets. Additionally, the importance of floodplains as sinks of sediment associated pollutants such as Phosphorus has been observed (Walling *et al*, 2000). Previous studies have also quantified the high degree of spatial variability that characterises floodplain sedimentation rates and highlighted some factors that control this variability. For example numerous studies have observed a decrease in floodplain sedimentation rates with distance from the main channel (Simm and Walling, 1998; Swanson *et al,* 2008; Walling *et al,* 1996; Walling and He, 1997, Walling and He, 1998). This observation is known as the diffusion effect and is partly explained by the preferential deposition of coarser sediment during overbank flow, due to its higher settling velocities. Additionally this observation reflects the ease of sediment transport from the main channel to these areas.

The influence of floodplain topography on floodplain sedimentation rates has also been observed from both sediment trap data and radionuclide analysis (Asselman and Middelkoop, 1995; Middelkoop *et al,* 1998, Lambert and Walling, 1987, Simm, 1995, Walling and Bradley, 1989, Walling and He, 1997). The timing and duration of inundation varies across the floodplain and influences the spatial distribution and magnitude of sediment deposition. Simm (1995) observed deposition rates for 14 flood events using sediment trap data over a section of the river Culm and observed average deposition for all floods to vary from 1625 g m^{-2} (8.1 mm yr^{-1}) on levee backslopes and 15 g m^{-2} (0.1 mm yr^{-1}) on flat sections of floodplains. High sediment deposition rates in depression areas reflect the increased depth of floodwaters during inundation due to surface ponding, resulting in a greater availability of sediment for deposition.

Table 5.1: Magnitude of floodplain sedimentation in several catchments, represented as a percentage of the catchment sediment budget.

Catchment	Percentage of annual sediment budget deposited on floodplain	Reference
Culm, UK	28	Lambert and Walling (1987)
Severn, UK	23	Walling and Quine (1993)
Swale, UK	47	Walling and Owens (2003)
Aire, UK	26	"
Ouse, UK	39	Walling *et al*, (1998)
Wharfe, UK	49	"
Tweed, UK	40	Walling *et al*, (1999a)
Dragonja, Sloveneia	26.6	Keestra *et al*, (2009)
Waal, Netherlands	19 (in one flood event)	Middelkoop and Asselman (1998)
Strickland, Papua New Guinea	13	Swanson *et al*, (2008)
Fly, Papua New Guinea	19	"
Ganges-Brahmaputra, India	39-71	Allison *et al*, (1998)
Veduga Creek, Russia	45	Golosov *et al*, (1992)
Little Kolysheley River, Russia	54	"

Valley width has also been observed to influence floodplain deposition rates; flood waters are constricted within narrow valleys resulting in increased flow depths and velocities, and therefore increase sediment transport capacities. The reverse is true for wide valleys, resulting in sediment deposition. Leece (1997) noted that valley width accounted for 57% of the variance in post-settlement alluvium in the Blue river, Wisconsin, USA.

Other physical catchment characteristics that have been observed to influence floodplain sedimentation rates spatially include hydraulic connectivity of the channel network; Swanson *et al,* (2008) observed the extensive channel network of the river Fly, Papua New Guinea provided an efficient means of transporting sediment to the floodplain. Sedimentation rates have also been observed to increase downstream (Leece, 1997). This correlation reflects the increase drainage area with distance downstream, and the increased quantity of sediment delivered through overland sediment generation processes.

The magnitude of sedimentation may also vary temporally. Blake *et al,* (2002) calculated floodplain deposition rates using beryllium-7 (^{7}Be) isotope analysis on the river Culm, Devon during two flood events in October 1998. The magnitude of mean deposition over the study area for the two events (0.24 g cm^{-2}) was found to be comparable to mean annual deposition rates observed from previous studies. This was attributed to the timing of the floods; these were the first flood flows from the autumn/winter so were likely to have higher sediment concentrations than subsequent flows. This also indicates the importance of sediment load within overbank flows. Simm (1995) observed different magnitudes of variability of sediment deposition between floods at different locations. This was due to the influence of the frequency of inundation, and the location of preferential flow routes that promote scouring (and removal) of sediment.

5.1.2.3. Models of floodplain sedimentation

Numerical models have also been used to quantify and account for spatial variability in floodplain sedimentation. For example, Pizzuto (1987) tested a model including diffusion processes only, accounting for the movement of sediment from areas of high concentration (near the channel) to low concentration (across the floodplain). As flow velocities and transport capacities over the floodplain decrease deposition occurs. Deposition was modelled as:

$$DR = \left(V_s^{\,2}/e_z\right)\zeta$$

where V_s is the settling velocity of sediment, and e_z the vertical sediment diffusivity. ζ is calculated as:

$$\zeta = \int_0^D C(z)dz$$

where D is the depth of the floodplain flow and $C(z)$ is the sediment concentration at height z above the floodplain. The model was found to underestimate the ability of floodwaters to transport sediment away from the channel due to the omission of other transporting processes (such as suspension, and bedload transport). Additionally the spatial variability of

sediment deposition is not represented due to the exclusion of floodplain topography.

Complex hydrodynamic models used to represent overbank inundation can be coupled with simplistic sediment transfer models to provide more detailed representation hydrological controls on sedimentation rates. For example, Middelkoop and Van Der Perk (1998) used outputs from an existing 2-dimensional hydrodynamic model (WAQUA) and coupled this to a simple GIS-based mathematical model of floodplain sedimentation (SEDIFLUX). Water flow was calculated over a 50 m x 50 m raster grid with input data of river bed and floodplain topography and hydraulic roughness. The sediment model was based on sediment balance per cell, determined by fluxes in and out of each cell. Sediment flux was calculated based on the sediment concentration, settling velocities, and applied shear stress by water flow. The model was applied to 3 reaches in the lower River Rhine, Netherlands and predicted deposition over the entire study area of each reach agreed with observed values (model errors ranging from 10 to 60%). Similarly, Nicholas and Walling (1998) used simplified hydraulic equations to represent overbank flow over complex floodplain topography represented using a finite difference grid. They noted the complex sequence of floodplain inundation, with overbank flow initially concentrated in low-lying drainage ditches and depressions, indicating the influence of floodplain topography on the frequency of inundation. The predicted decrease in suspended sediment concentration with distance from the main channel was found to be highly spatially variable as these are controlled by local flow conditions. The model was applied at a local scale (in a 600 m reach) and was found to represent observed patterns of spatial variability. The model required detailed input data relating to channel and floodplain topography (obtained from ground surveys) to represent complex floodplain geometry, making this unsuitable for use at a catchment scale.

The complexity of overbank flow patterns and the importance of floodplain topography have also been successfully illustrated by more complex flow models (Nicholas and Mitchell, 2003; R^2 predicted flow depth and unit discharge were 0.55 and 0.49 respectively). Output hydrographs from the latter study were used by Sweet *et al,* (2003) at 8 sites along the river Culm and were coupled to a sediment deposition model. The results of this work illustrate the

importance of small-scale topography as a control on sediment transport and deposition.

5.1.2.4. Influence of climate change

Current projections of climate change from the IPCC (2007) suggest temperatures will increase by 0.2°C per decade, with an increase of 0.6-4.0°C by 2080 depending on the CO_2 emissions scenario considered (see Figure 5.1 A). Changes in surface temperature will influence evaporation rates, and the water holding capacity of the atmosphere increases by 7% for every 1°C increase in temperature. These changes will influence the amount, frequency, and intensity of precipitation. Figure 5.1 B shows projected changes to mean annual precipitation across Europe as a result of climatic changes, indicating an increase in mean annual precipitation in the UK by 0-10%.

Climate simulations indicate further increased water vapour in the atmosphere will lead to more intense precipitation events, even in areas where the total precipitation is reduced. Palmer and Ralsanen (2005) estimate the probability of occurrence of wet winters in the UK will increase by a factor of 5 over the next 50-100 years. Fowler and Ekstrom (2009) estimate extreme precipitation over the UK to increase by 5-30% depending on region between 2070-2100. Christensen and Christensen (2006) noted an overall decrease in precipitation over much of Europe during July-September from 2071-2100 compared to 1961-1990, yet an increase in mean 5-day precipitation events, indicating the intensification of summertime precipitation across much of Europe.

Prudhome *et al,* (2003) analysed 25,000 climate scenarios from a range of model outputs and emission scenarios and couple these to a conceptual hydrological model. An increase in flood frequency and magnitude was observed, although the uncertainty range of estimates was noted to be high, with magnitude changes varying up to a factor of 9. Kay *et al,* (2006) used a regional climate model to estimate change in flood frequency for 15 UK catchments between 1970s and 2080s and observed decreases in annual rainfall in 14 catchments, yet 8 showed an increase in flood frequency at most

return periods. Catchments in the North and West of the UK showed an increase in flood peak at the 50-year return period of over 50% in some cases. Overall a marked change in the distribution of rainfall was observed.

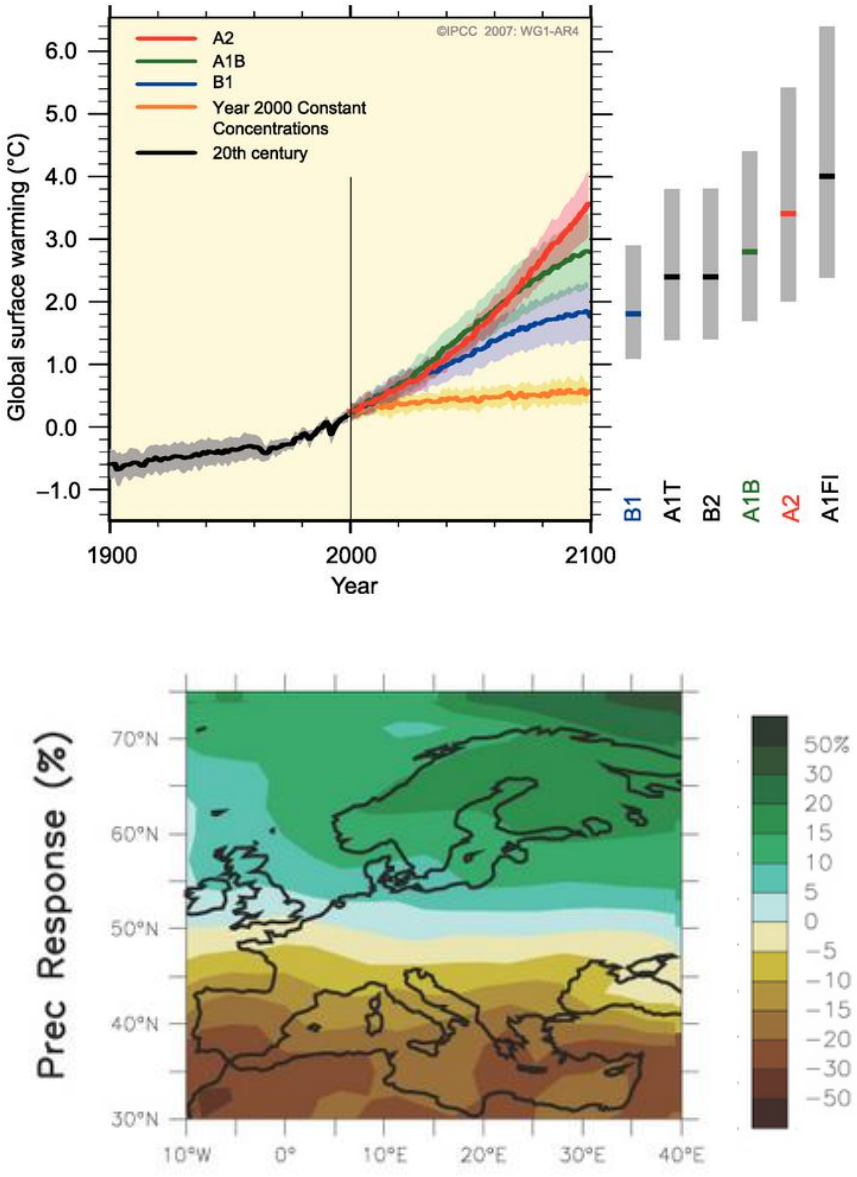

Figure 5.1: A - Projected mean surface temperature increase over the next 100 years. Solid lines represent multi-model averages for scenarios, shading denotes ±1 standard deviations. Temperature change is shown relative to 1980-1999. The grey bars indicate the best estimate (solid line) and the likely range. B – Projected mean annual precipitation changes across Europe between 1980-1999 and 2080-2099. Taken from IPCC (2007).

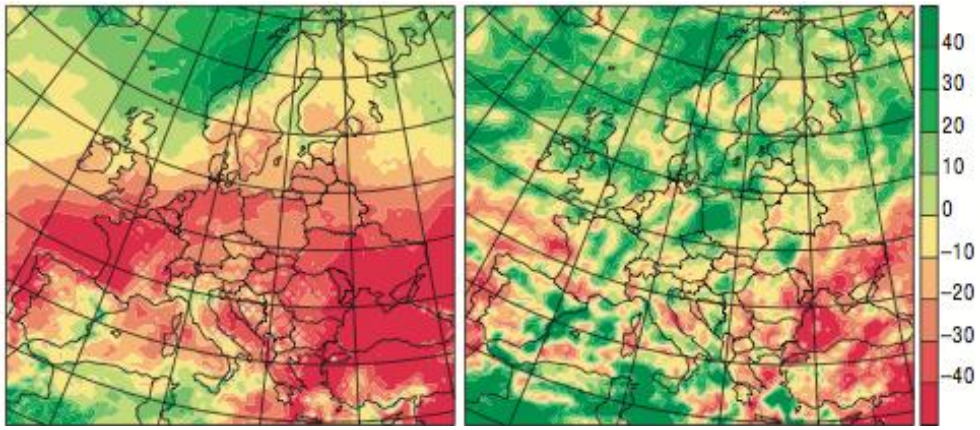

Figure 5.2: Relative percent change in precipitation in July-September 2071-2100 to present day. A shows the seasonal mean change, and B shows the 5-day mean. Taken from Christensen and Christensen (2006).

Both the magnitude and frequency of precipitation events influence overland sediment generation, and changes to catchment discharge will result in changes to channel bank erosion and floodplain sedimentation rates. Longfield and Macklin (1999) analysed the long-term variation in frequency and magnitude of flooding events in the Ouse basin, North Yorkshire, and the likely effects on the fluxes of fine sediment within the catchment. It was noted over the study period (1876-1996), the years 1978-1996 had experienced the highest flood frequencies and magnitudes, with cyclonic weather patterns generating the majority of floods. Field observations noted bank erosion generated a significant volume of sediment during several high magnitude flood events. Additionally, it was noted sediment supply was likely to have increased during this period due to increase grazing stocking densities. This research indicates with an increased frequency of cyclonic weather patterns, sediment fluxes within the catchment are likely to increase.

Tucker and Slingerland (1997) used the GOLEM landscape evolution model to investigate the response of a watershed in Pennsylvania, USA to nine different climatic scenarios. As expected, denudation rates were observed to increase with increasing runoff. Additionally, it was noted small variations in runoff and surface resistance can result in significant changes to denudation rates and hence sediment flux, and the time scale over which these changes

can occur is shorter than other catchment responses to climatic perturbations (such as basin relief).

5.2. Methodology

This section will detail the methodology used to create the catchment sediment budget model, incorporating bank erosion and floodplain sedimentation components within a catchment sediment routing model.

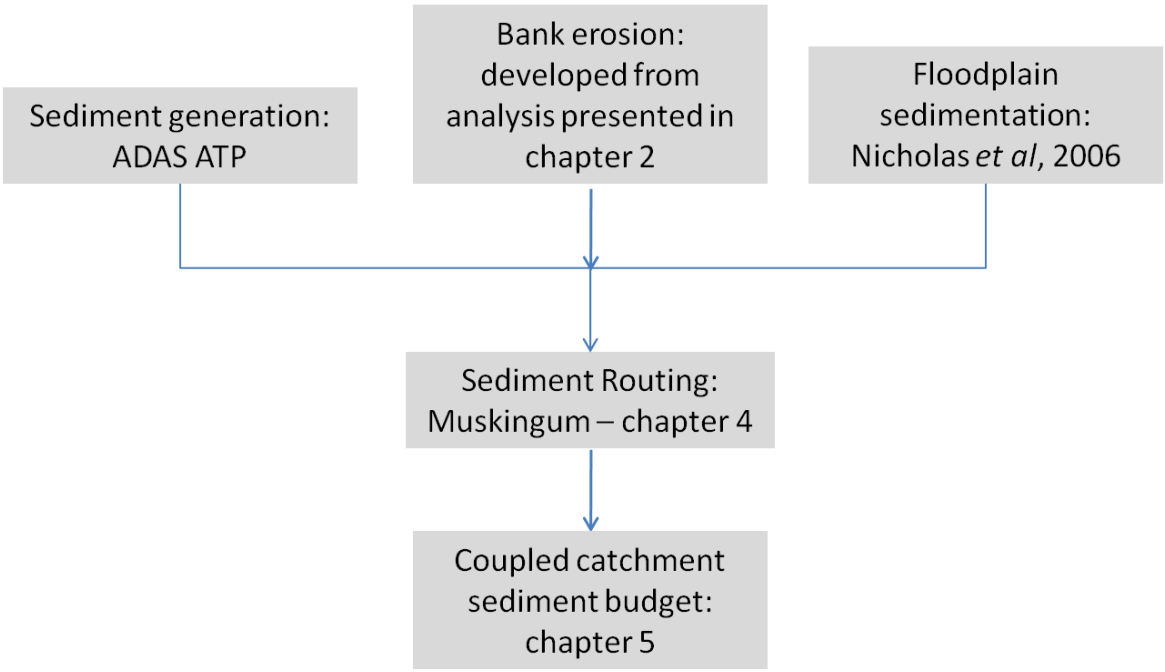

Figure 5.3: Elements of the coupled catchment sediment budget model to be developed in this chapter.

The second chapter of this thesis used GIS to estimate channel bank erosion rates over time periods of approximately 150 years and find statistical relationships between bank erosion and some of the physical factors influencing bank erosion rates. This analysis indicated the influence of channel confinement on bank erosion rates within UK catchments. In chapter two a non-linear relationship between bank erosion and sinuosity was identified with a threshold value of sinuosity of 1.5. The bank erosion module developed within this section will incorporate the findings from the first two chapters of this thesis within an existing ADAS bank erosion index.

A floodplain sedimentation component has been incorporated based on a power-law relationship identified by Nicholas *et al,* (2006). Finally, sediment routing is incorporated within the catchment routing methodology developed in the previous chapter. Input data of sediment delivery to the channel network from the ADAS ATP model for the Exe catchment is used, for the period of 1991-2011. Both the bank erosion and floodplain sedimentation components are included within the sediment routing model to enable estimation of the catchment sediment budget. The influence of climate change on the river catchment is examined by a systematic increase to the magnitude of water and sediment delivery from the catchment to the channel.

5.2.1. Bank erosion model

A similar approach to the ADAS bank erosion index (detailed in section 1.2.3.7) is used to represent bank erosion within the model. In chapters two and three additional factors observed to influence bank erosion rates included channel confinement (within the floodplain) and sinuosity. This model is a development of the ADAS approach as it will also incorporate the influence of these factors.

Bank erosion is simulated when the shear stress of the flow acting on the channel bank exceeds the critical shear stress of the flow required for erosion using the same methodology as the existing ADAS bank erosion index (Collins *et al,* 2009). The ADAS national bank erosion index estimates the percentage of the year in which the critical shear stress is exceeded by the flow, and from this estimates an annual value of sediment production. The model developed here simulates bank erosion at each time step where flow exceeds the critical shear stress.

The ADAS bank erosion index is represented by the following equation:

$$B = 0.0225\left(\frac{D.L.H}{A}\right)^{1.58}$$

where B is the catchment area averaged bank erosion rate (kg ha^{-1}), D is the percent duration of excess shear stress, L is the river channel length, H is the bankfull depth (m), and A is the total area of the catchment (km^2). As one of the

objectives of the model to be developed in this chapter is to estimate the total sediment generated through bank erosion the equation will be modified so catchment area is not used in the estimation. Additionally, channel length was removed as bank erosion is calculated at each reach, not at a catchment scale. Within the representation of the catchment by the routing model reaches are all of a similar length. Bankfull depth was removed from the equation as the influence of channel bank height on was not fully investigated within this study, and also detailed bank height data at a reach scale was not available. Therefore, bank erosion in the new model is estimated by the equation:

$$BE = a(log_{10}E \times (CCF + SF)) \qquad where\ \tau > \tau_c$$

where E is excess shear stress at the channel bank ($\tau - \tau_c$), CCF is a channel confinement factor and SF is a channel sinuosity factor. The parameter a was calibrated using observed values of bank erosion (Ashbridge, 1995; Collins *et al,* 1997; Collins *et al,* 1997b; Hooke, 1997).

5.2.1.1. Sinuosity factor

The sinuosity factor is intended to capture the influence of sinuosity on bank erosion rates. As noted in chapter three, bank erosion increases with sinuosity up to a threshold value of approximately 1.5 and above this value bank erosion decreases with further increase in sinuosity.

Figure 5.4 shows average values of bank erosion and channel sinuosity from several model outputs of the Howard and Knutson meander migration model from chapter three. The chute cut-off parameter was varied between model runs to provide channel formations of different average sinuosities. Each series (and line of best fit) plotted on the graphs represents a group of model outputs with other parameter values (E – erodibility, A – alpha, and G – Gamma) held constant. Figure 5.4A shows model outputs with average channel sinuosities below 1.5, and Figure 5.4B equal or greater than 1.5. The equations of the lines of best fit are shown in Table 5.2 and Table 5.3.

Average values of the gradient and y-intercept were taken from these two sets of equations (sinuosity <1.5 and ≥1.5). The reason average values were used is because the sets of parameters used within Howard and Knutson

model to generate these outputs were taken from a range of parameter values found to represent UK channels (see 3.3.1). This produced the following equations for each:

$$BE = (Si_i \times 0.0295) - 0.0215 \quad where\ Si_i < 1.5$$

$$BE = (Si_i \times -0.003125) - 0.019 \quad where\ Si_i \geq 1.5$$

where Si_i is the measured value of sinuosity at reach i. The y values were then multiplied by a constant (parameter c in the equations above) to provide a sinuosity factor of 1 when sinuosity = 1, and therefore has no influence on channel bank erosion, and a sinuosity factor of 2 where channel sinuosity results in a doubling of channel bank erosion. Finally, a bank erosion sinuosity factor was derived such that the value of SF is proportional to the influence on the bank erosion rate:

$$SF = [(Si_i \times 0.0295) - 0.0215] \times 125 \quad where\ Si_i < 1.5$$

$$SF = [(Si_i \times -0.003125) - 0.019] \times 125 \quad where\ Si_i \geq 1.5$$

Figure 5.5 shows the influence of the sinuosity factor on bank erosion as predicted by the model.

A

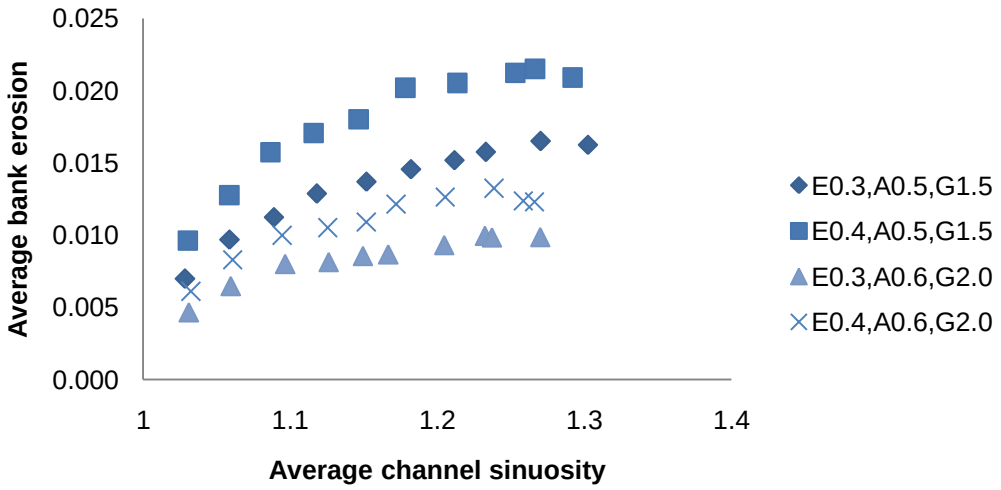

B

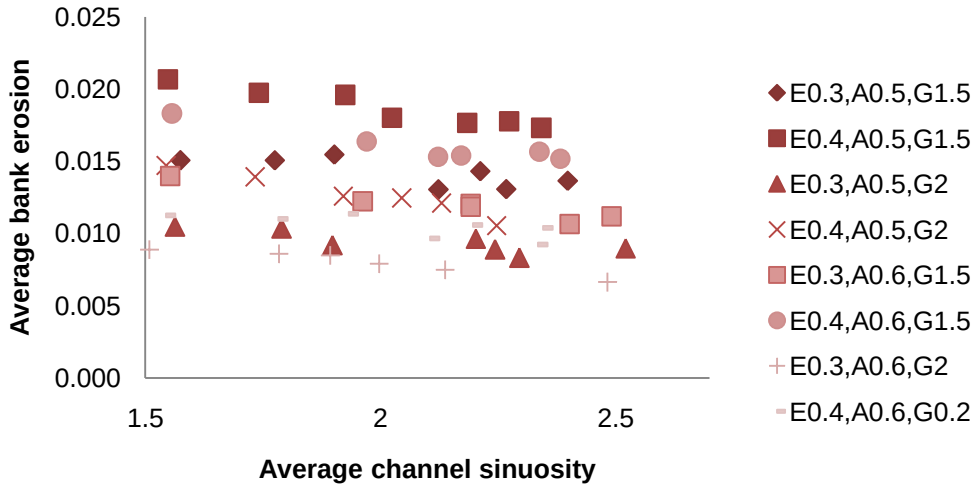

Figure 5.4: Average channel sinuosity and bank erosion of simulated channels from Howard and Knuston model outputs. A – model outputs with channel sinuosity <1.5, B – model outputs ≥ 1.5.

Table 5.2: Equation of line of best fit for each model output parameter set for channels with sinuosity less than 1.5.

Parameter set	Equation	R^2
E=0.3,A=0.5, G=1.5	$y=(Si_i \times 0.033)-0.025$	0.879
E=0.4,A=0.5, G=1.5	$y=(Si_i \times 0.041)-0.029$	0.873
E=0.3,A=0.6, G=2.0	$y=(Si_i \times 0.020)-0.015$	0.887
E=0.4,A=0.6, G=2.0	$y=(Si_i \times 0.024)-0.017$	0.775

Table 5.3: Equation of line of best fit for each model output parameter set for channels with sinuosity less than 1.5.

Parameter set	Equation	R^2
E=0.3,A=0.5, G=1.5	$y=(Si_i \times -0.033)+0.019$	0.566
E=0.4,A=0.5, G=1.5	$y=(Si_i \times -0.004)+0.027$	0.920
E=0.3,A=0.5, G=2.0	$y=(Si_i \times -0.002)+0.013$	0.640
E=0.4,A=0.5, G=2.0	$y=(Si_i \times -0.005)+0.023$	0.942
E=0.3,A=0.6, G=1.5	$y=(Si_i \times -0.003)+0.019$	0.921
E=0.4,A=0.6, G=1.5	$y=(Si_i \times -0.004)+0.024$	0.868
E=0.3,A=0.6, G=2.0	$y=(Si_i \times -0.002)+0.013$	0.944
E=0.4,A=0.6, G=2.0	$y=(Si_i \times -0.002)+0.014$	0.521

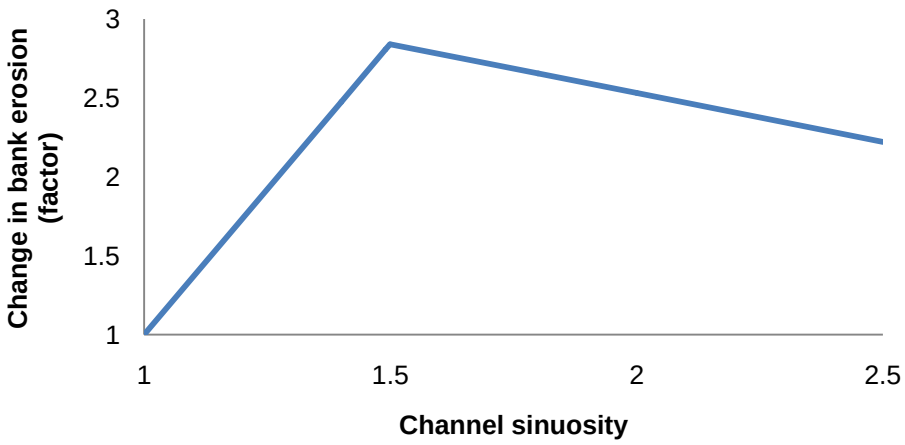

Figure 5.5: Influence of the sinuosity factor on bank erosion within the model. The y axis shows the change in bank erosion represented as a factor (i.e. 1=no influence on bank erosion, 2=doubled rate of bank erosion).

5.2.1.2. Channel confinement factor

The channel confinement factor is intended to capture the influence of channel confinement on bank erosion rates. Figure 5.6 shows values of bank erosion in relation to channel confinement (version 4) from the GIS analysis in chapter two. In chapter two, four methods of channel confinement estimation were used and that using the meander belt width as estimated by Williams (1986) produced the strongest correlation with bank erosion and was, therefore, used for this analysis. As the distribution of the channel confinement variable was not normal, the values were transformed using the logarithm to the base 10 before performing regression analysis (see chapter two for details).

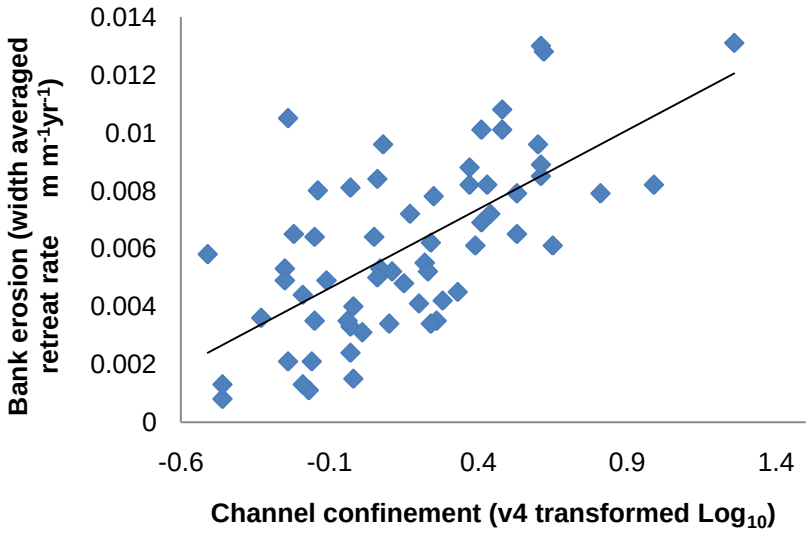

Figure 5.6: Relationship between channel confinement and bank erosion (from results of chapter two).

As for the calculation of the sinuosity factor, the value of bank erosion estimated due to channel confinement was scaled to provide a channel confinement factor, the values of which are proportional to the influence of confinement on bank erosion rates and a value of 1 equates to no effect on bank erosion rates. The equation used to calculate channel confinement factor was:

$$\mathrm{CCF} = [(\log_{10} CC_4 \times 0.00546) + 0.00517] \times 193.424$$

5.2.1.3. Catchment area

The analysis in chapter 2 identified upstream catchment area as an influential factor on bank erosion and this was noted to be due to the relationship with this variable and channel discharge. As the model simulates the discharge at each reach the exceedence of bank critical shear strength was used in the model equation rather than the upstream area. The values of exceedence of critical shear strength were transformed using the logarithm to the base 10 (as shown in the formula). Without transforming the input in this way high flow events resulted in unrealistically high values of sediment produced from bank erosion, with annual bank eroded sediment ranging from 7.16×10^{15} t yr^{-1} to infinite values. The requirement for this transformation and the impact on the values of bank erosion predicted by the model are related to the distribution of flow magnitudes; as flow magnitudes are not normally distributed without transformation of the data, high magnitude flows which greatly exceed the shear stress of the bank produce an unrealistically high mass of sediment.

5.2.1.4. Implementation of the bank erosion model

For many parameters within the bank erosion model, single values were calculated to represent each WFD sub-catchment (see Figure 5.7). All model reaches were assigned to a sub-catchment and used this set of parameter values. Channel sinuosity was measured using GIS every 5km along the channel and average values of sinuosity were calculated for each sub-catchment (similarly to chapter two) and applied to reaches. Channel width was estimated using River Habitat Survey (RHS) data. Bankfull discharge was estimated using channel bank heights and widths from RHS data (similarly to chapter two).

The critical shear stress of channel banks is defined as the magnitude of shear stress exerted by the flow required for entrainment of bank sediment. As outlined in chapter one, shear stress is calculated using the equation developed

by Guo and Julian (2005). Flow depth (required for estimation of shear stress acting on the channel bank) was estimated from modelled discharge (Q) within the reach

$$h = \frac{Q}{v}/b$$

where v is the flow velocity and b is channel width. Where discharge is greater than bankfull discharge, the depth of flow was estimated as bankfull depth. Critical shear stress is calculated using the equation developed by Julian and Torres (2006) (see section 1.2.3.7) and requires a value of silt-clay content of channel banks. This was estimated for sub-catchments (and all reaches within each sub-catchment) using data from previous studies (see Table 5.4).

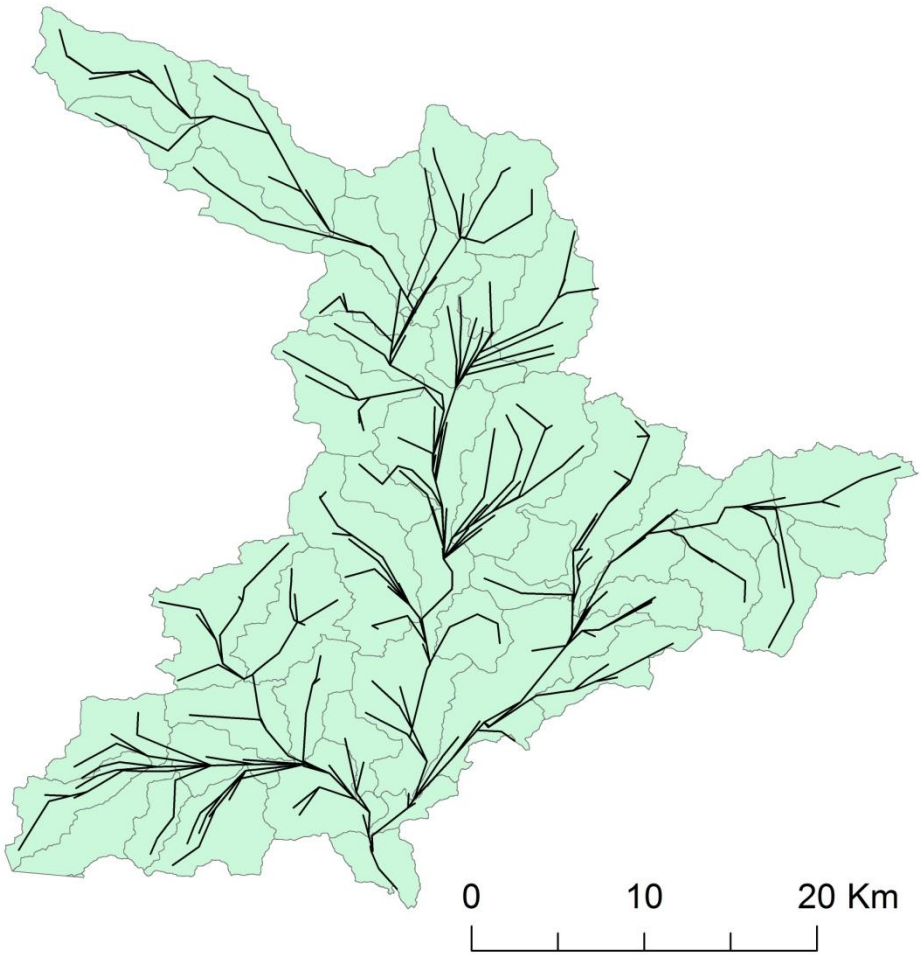

Figure 5.7: Sub-catchments of the Exe catchment, Devon and the channel network as represented by the routing and sediment budget model.

Table 5.4: Observed silt-clay content of channel banks within the Exe catchment from previous studies.

Channel	Silt-clay content (%)	Reference
Exe	46.1-51.1	Hooke (1980)
Creedy	65.4	"
Culm	58.5-60	"
Culm	50.98	Ashbridge (1995)

5.1.1. Floodplain sedimentation model

Nicholas *et al,* (2006) used output from a spatially-distributed model of floodplain processes to develop a power law equation to estimate floodplain sedimentation at a catchment scale. The starting point for their analysis was a simple conceptual model of floodplain sedimentation, which assumed that the frequency distribution of floodplain elevation could be represented by the floodplain geometry shown in Figure 5.8.

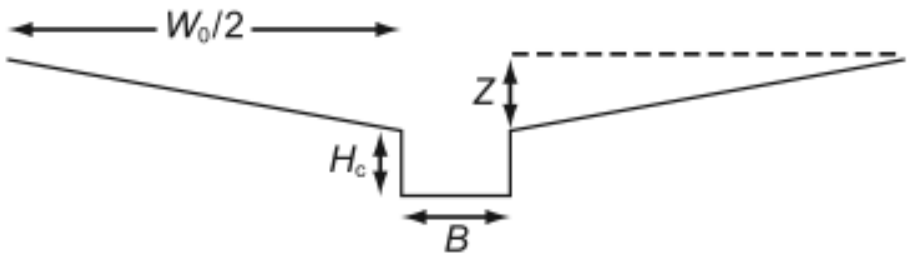

Figure 5.8: Simplified representation of floodplain cross-section geometry as used in the theoretical model of Nicholas *et al,* (2006).

Nicholas *et al,* (2006) argue that sedimentation rates are proportional to the extent of floodplain inundation (W) and the sediment content of floodwaters (given by the product of flow depth, H and sediment concentration, C) and inversely proportional to overbank flow velocities (V). Overbank sedimentation rates for the length of the reach (D) are thus estimated as:

$$D = \frac{WHC}{\propto V^{\beta}}$$

where $\propto$ and β are constants. The inundation width (W) is calculated as:

$$W = \frac{2W_0 H}{Z} \quad for\ 2H < Z$$

where W_0 is maximum floodplain width, and z is topographic relief. Overbank flow velocity for a given average flow depth and overbank discharge (Q_F) is calculated as:

$$V = \frac{Q_F}{WH}$$

The parameters $\propto$ and β are assumed to be 1, and in the range of 1-2, respectively. The relationship between overbank discharge and water level can be determined using Manning's equation.

This simple model was then used to estimate the overbank sedimentation rate per unit valley floor length per unit sediment concentration (D/C) as a function of discharge in excess of bankfull, for several reaches of the river Culm, Devon. Model results (see Figure 5.9) indicate the relationship between D/C and discharge (in excess of bankfull) can be approximated by the power law of the form:

$$D/C = \Gamma(Q - Q_{BF})^{\Lambda}$$

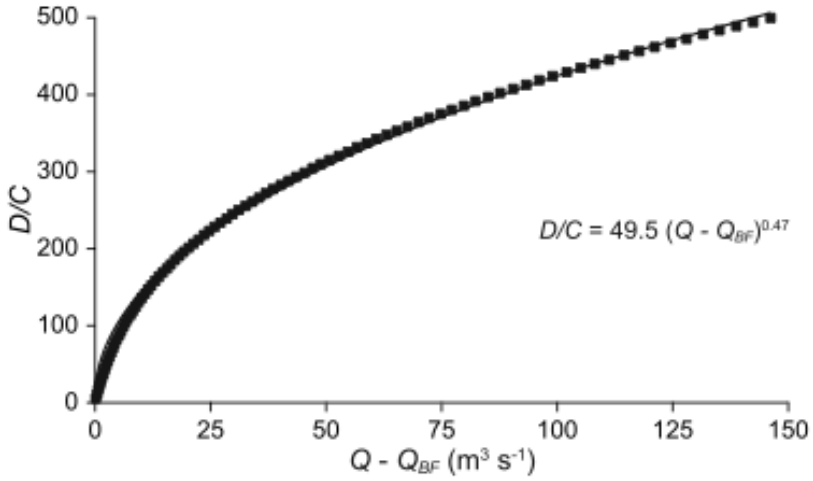

Figure 5.9: Relationship between sedimentation rate per unit valley length per unit sediment concentration and discharge in excess of bankfull. Taken from Nicholas *et al,* (2006).

The best-fit constant and exponent Γ and Λ were found to be largely dependent on floodplain width and β, which is thought to represent vegetation characteristics. The value of $\Lambda = 0.5$ was found to produce accurate results when Γ is estimated as:

$$\Gamma = \mu W_o^{\theta}$$

where μ and θ are a power law constant and exponent, which within the study were found to range between 0.001-0.1, and 0.2-0.7 respectively.

The high-resolution physically based flow model mentioned previously (Nicholas and Mitchell, 2003) and a suspended sediment transport model and deposition model were then used to assess the suitability of the power-law equation. This equation was tested at 22 sites along the rivers Axe, Culm and Exe. Integration of spatially-distributed sedimentation rates from the physically-based model was used to estimate sedimentation rate per unit valley floor length per unit sedimentation concentration for any given discharge. Figure 5.10 shows sedimentation rates from the power law relationship derived from the simple theoretical model and the distributed flow model, indicating the suitability of the power law relationship.

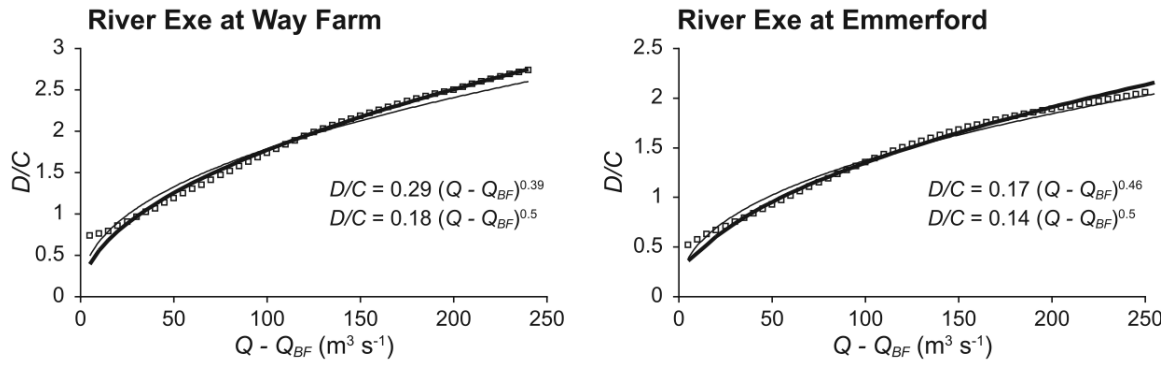

Figure 5.10: Relationship between sedimentation rate per unit valley length per unit sedimentation concentration and discharge in excess of bankfull at two sites on the river Exe. Symbols indicate results from spatially distributed flow and sediment models, thin lines and equations represent best fit power law, and thick lines indicate power law when exponent is set to 0.5. Taken from Nicholas *et al,* (2006).

The analysis of Nicholas *et al,* (2006) suggested that the following simple power law equation provides a means of estimating overbank sedimentation within catchment sediment budget models:

$$D_Q = \mu W_o^{\theta} \sqrt{Q - Q_{BF}} C_Q$$

where D_Q is deposition rate per unit valley floor length, μ and θ are parameters, W_0 is the floodplain width, and C_Q is the mean sediment concentration. This equation was then applied to estimate the annual floodplain sedimentation rate within the 3 catchments (Axe, Culm, and Exe) and compared model estimates against actual sedimentation rates derived from ^{137}Cs core analysis. Figure 5.11 shows the modelled and measured sedimentation rates (measurements were derived from ^{137}Cs data) and indicates the derived equation is capable of reproducing the observed sedimentation rates, and the spatial variability between reaches in the catchment.

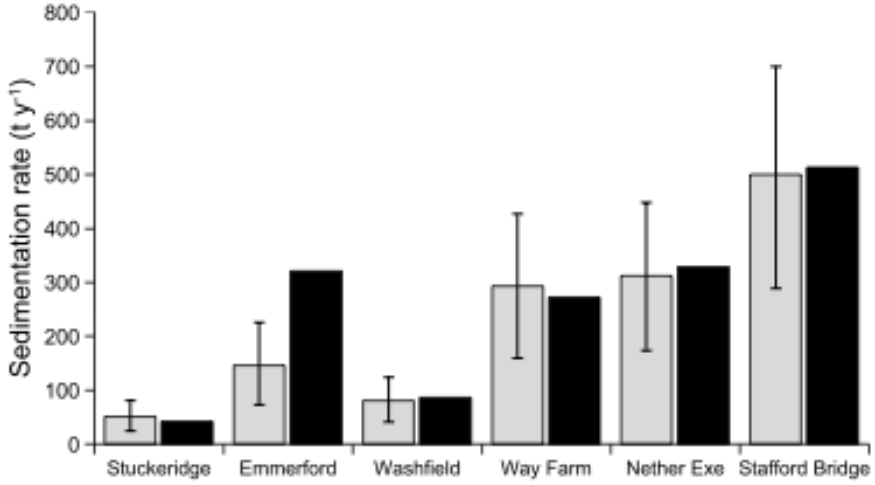

Figure 5.11: Total mean annual floodplain sedimentation rate at Exe sites. Upstream (left) to downstream (right). Black bars are ^{137}Cs derived rates, grey bars are modelled rates. Vertical lines indicate 5th and 95th percentiles of 20,000 model runs of varied parameter sets. Taken from Nicholas *et al,* (2006).

Values of floodplain width were measured using EA floodplain maps in ArcGIS. Floodplain width was measured every 5km along the channel and an average value for each sub-catchment was calculated. All channel reaches within those sub-catchments were assigned the same value (similarly to section 5.2.1.4). As indicated in Figure 5.7, there are 45 sub-catchment and 366 reaches and therefore variability of floodplain width within the whole catchment is represented within the model. Whilst floodplain width varies at a finer spatial scale than sub-catchment, for the purpose of a simplistic and computationally efficient sediment budget model higher resolution of input data would not fit the remit of this model. The concentration of sediment is calculated within the model (as both discharge and sediment load are known).

Bankfull discharge for each channel reach was calculated using the width and depth of the channel and the velocity of flow. Where flow simulated by the model (discharge values as generated by the routing model in chapter four) exceeded bankfull discharge, overbank flow occurs and floodplain sedimentation was calculated. Nicholas *et al,* (2006) defined the parameter ranges of β and θ for the Exe catchment (see Table 5.5).

Table 5.5: Values of parameters μ and θ with used in the floodplain sedimentation model best-fit relationship from Nicholas *et al,* (2006).

	μ	θ
River Axe	0.0044	0.62
River Culm	0.0120	0.46
River Exe	0.0260	0.30
All 22 sites	0.0120	0.45

5.2.2. Sediment routing

Sediment was incorporated into the routing model using the same storage concept as the water routing. Singh *et al,* (1987) used the standard Muskingum approach to calculate sediment routing and assumed the effect of sediment discharge on the momentum of water routing was negligible:

$$\frac{dS}{dt} = I_s - Q_s + BE - D_Q$$

$$S = K\left[X(I_s + BE) + (1 - X)\left(Q_s + D_Q\right)\right]$$

where S is the reach sediment load, I_s and Q_s are the sediment input and output from the channel reach (kg) per unit time, BE is sediment input generated from bank erosion (kg) per unit time, and D_Q is the sediment deposited on floodplains (kg) per unit time. K and X are the Muskingum routing constants, (as defined in the previous chapter). Sediment input to each reach is calculated by summing the output of sediment from all reaches directly upstream of the reach from the previous time-step.

As the Muskingum-Cunge variable parameter method was used in this study, routing constants were calculated using Courant and Reynolds numbers. The sediment routing equation used was defined as:

$$Q_{s_j}^{\ n} = C_0 Q_{s_{j-1}}^{\ n} + C_1 Q_{s_{j-1}}^{\ n-1} + C_2 Q_{s_j}^{\ n-1} + C_0 E_j^n - D_{Q_j}^{\ n}$$

where j and n are spatial and temporal time-steps respectively.

5.2.3. Sediment budget model

The full sediment budget model (incorporating water and sediment routing, bank erosion and floodplain sedimentation components) was run using a range of parameter values. For both the bank erosion and floodplain sedimentation components a set of minimum, mid-range and maximum parameter values were established based on the calibration results (detailed in the following section). The model was then applied with several different combinations of these parameter values. Additionally, for each set of parameter combinations the model was run using six different sediment input scenarios (the details of which are outlined in the following section).

5.2.3.1. Input data

The input data used for the sediment budget model in this chapter is an un-calibrated/un-validated output from the APT model. Analysis of these data showed that several grid cells at certain dates produce extremely high values of sediment delivery, with concentrations exceeding realistic values.

In the previous chapter after comparison of modelled discharge values against gauging station data it was noted that the input data from the APT model output underestimates the volume of water input to the catchment. The water input to the routing model was then modified by way of an increase (between 5 and 30% depending on time period). Sediment generation through the APT model is heavily dependent on rainfall and will not show a simple linear relationship, however it would be expected that as the model is showing an underestimation of water delivery (due to an underestimation of rainfall) across the catchment, the sediment generation and delivery across the catchment would also be underestimated. Therefore it was assumed that the concentration of sediment input (from the APT output) would remain the same, and therefore sediment inputs were increased by 5 or 30%, as per the increase to water input as detailed in chapter 4.

Due to the scarcity of sediment data a comparison of modelled sediment discharge with observational data was not possible. Therefore six different sediment input scenarios were created by modification of the APT model output

to account for this uncertainty. Firstly minimum, maximum, and mid-range estimates of annual bank erosion and floodplain sedimentation for the whole catchment were estimated (see Table 5.6) based on observations from previous studies (shown in Table 5.12 and Table 5.13, in a later section of this chapter). From the estimates of bank erosion and floodplain sedimentation in Table 5.6, a minimum, mid-range, and maximum estimate of annual sediment delivery to the catchment was calculated by assuming sediment load at the catchment outlet was approximately 22,500 t yr^{-1} as observed by Nicholas *et al*, 2006. These are shown in Table 5.7.

Table 5.6: Minimum, maximum and mid-range estimates of catchment based annual bank erosion, floodplain sedimentation for the Exe catchment.

	Bank erosion (t yr^{-1})	**Floodplain sedimentation (t yr^{-1})**
Minimum	1100	18000
Mid-range	4500	24000
Maximum	8000	28000

Table 5.7: Minimum, maximum, and mid-range estimates of catchment based annual sediment delivery to the Exe catchment.

	Sediment input (t yr^{-1})
Minimum	~28000
Mid-range	~33000
Maximum	~42000

For the three input data scenarios the APT model input was modified by applying 3 different sediment concentration limits. These concentration limits were varied to produce similar average annual minimum, maximum, and mid-range catchment sediment delivery estimates as shown in Table 5.7.

For the other three input datasets a more realistic sediment concentration limit was applied (of 100 kg m^3) and then the sediment input was multiplied to provide similar values of annual sediment delivery to the minimum,

maximum and mid-range estimates. All of the six scenarios accounted for the correction of rainfall estimation and sediment concentration before any other modification was made. The input data scenarios are shown in Table 5.8.

Table 5.8: Input data scenarios and data adjustments.

Input scenario	Average annual catchment sediment delivery (t yr^{-1})	Data adjustment
1	29,600	Limit conc' 350 kg m^{-3}
2	39,500	Limit conc' 450 kg m^{-3}
3	47,800	Limit conc' 650 kg m^{-3}
4	33,700	Limit conc' 100 kg m^{-3} and x sediment input 3
5	39,400	Limit conc' 100 kg m^{-3} and x sediment input 3.5
6	50,700	Limit conc' 100 kg m^{-3} and x sediment input 4.5

5.2.3.2. Parameter values for sub-catchments

As indicated in section 5.2.1.4, for each of the 45 sub-catchments of the Exe (see Figure 5.7) values of channel width, bank height (channel depth), sinuosity, silt-clay content and channel confinement were estimated (see Table 5.9). Each channel reach within the model was assigned to a sub-catchment and the parameter values of the sub-catchment were applied to the reach.

Table 5.9: Sub-catchment parameter values for the Exe catchment. Table is continued onto next page.

FID	Sub-catchment name	Channel width (m)	Channel depth (m)	Silt-clay content (%)	Sinuosity	CC4
0	Exe (Creedy to Estuary)	32	2.2	48.5	1.2	0.928
1	Exe (Culm to Creedy)	22	2.1	48.5	1.4	1.893
2	Lower Creedy	15	2.4	65	1.4	2.336
3	Jackmoor Brook	3	0.7	65	1.2	4.278
4	Middle Creedy	6	1.8	65	1.5	3.983
5	Shobrooke Lake	3.5	0.6	65	1.2	3.599
6	Weaver	4	0.7	56	1.2	1.653
7	Culvery River	6.5	1.6	65	1.2	1.439
8	Ford Brook (EXE)	3.4	1.6	65	1.2	0.991
9	Upper Yeo (Creedy)	7	1.6	65	1.2	0.662
10	Troney	5	0.6	65	1.2	1.448
11	Lower Yeo (Creedy)	8	0.6	65	1.2	3.803
12	Colebrook	6	0.6	65	1.2	0.918
13	Ben Brook	2.5	0.7	48.5	1.2	1.399
14	Upper Batherm	5	0.7	48.5	1.2	1.770
15	Burn (Exe)	2.5	1	48.5	1.4	1.399
16	Ken Stream	2.5	1.2	56	1.3	1.749
17	Fulford Water	2	1.2	56	1.2	1.796
18	Holly Water	3.5	1	65	1.2	1.920
19	Upper Creedy	2	0.7	65	1.2	1.347
20	Madford River	2	0.7	56	1.2	7.185
22	Sheldon Stream	2	0.6	56	1.1	8.084
23	Halberton Stream	2	0.7	56	1.2	2.695
24	Lower Culm	11	2.1	56	1.4	3.044
25	Middle Culm	5	1.3	56	1.3	4.083
26	Calverleigh Stream	6	0.7	48.5	1.2	0.787
27	Upper Culm	3	0.9	56	1.3	4.848
28	Dart (Exe)	6.5	0.8	48.5	1.3	0.960

FID	Sub-catchment name	Channel width (m)	Channel depth (m)	Silt-clay content (%)	Sinuosity	CC4
29	Spratford Stream	2	0.9	56	1.3	3.593
30	Lowman	5.5	0.9	48.5	1.2	2.314
31	Iron Mill Stream	6.5	0.7	48.5	1.2	0.960
32	Exe (Barle to Culm)	25	1.8	48.5	1.5	1.411
33	Exe (Haddeo to Barle)	22	1.8	48.5	1.2	1.601
34	Lower Batherm	6.5	1	48.5	1.4	1.439
35	Brockey River	3	0.8	48.5	1.2	1.711
36	Lower River Haddeo	4	1	48.5	1.2	1.240
37	Lower Barle	15	1	48.5	1.2	0.329
38	Danes Brook	3	0.6	48.5	1.2	1.996
39	Sherdon Water	5	0.6	48.5	1.2	1.127
40	Middle Barle	10	1.4	48.5	1.3	0.518
41	Upper Barle	7	0.6	48.5	1.2	0.552
42	Exe (Quarme to Haddeo)	18	1.8	48.5	1.3	1.111
43	Upper River Haddeo	2.5	0.6	48.5	1.2	2.448
44	Pulham	4	0.7	48.5	1.2	3.099

5.2.4. Calibration

5.2.4.1. Bank erosion model

The bank erosion model was run initially without the floodplain sedimentation component for calibration purposes. The bank erosion model was calibrated by adjusting the parameter *a*. The total mass of sediment over the 20-year simulation period was calculated for each of the simulations, and from this an average mass of sediment per year.

The values of bank erosion estimated by the model were compared to observed values of bank erosion from the literature (Table 5.12) to assess which parameter values produce magnitudes of bank erosion similar to the minimum, mid-range and maximum estimates (Table 5.6). The values of parameter *a* chosen and the average annual bank erosion over the 20-year simulation are shown in Table 5.10.

Table 5.10: Parameter values used for minimum, mid-range and maximum bank erosion estimations (based on average annual bank erosion over 20-year simulation).

	a	Average annual bank erosion (t yr^{-1})
Minimum	0.3	1134
Mid-range	1.2	4537
Maximum	2.1	8000

5.2.4.2. Floodplain sedimentation

For calibration purposes, the floodplain sedimentation model was initially simulated without the bank erosion model, and with a single sediment input scenario (mid-range scenario, with sediment concentration limit of 450 kg m^3). The floodplain sedimentation model was calibrated by varying parameters μ and θ. The range of parameter values was initially based on those observed by Nicholas *et al,* (2006) for the Exe catchment during model development (see Table 5.5). However these initial parameter values were obtained using a different catchment model. Additionally, the model presented here includes a more complete treatment of water and sediment routing and is driven by different input data (APT model output) the floodplain sedimentation parameters may require recalibration. Therefore the model was also applied with a wider range of these parameter values and combinations (see Table 5.11).

The parameter values were calibrated by comparing values of annual sedimentation predicted by the model to observational data (see Table 5.13). Values of sedimentation were converted from g cm^{-2} yr^{-1} to total catchment sedimentation per year by assuming for the Culm the area of inundation is 5.1 km^2 (based on an estimate used by Lambert and Walling, 1987). For the Exe catchment an area of inundation of 12 km^2 was assumed based on analysis of Environment agency flood maps.

Table 5.11: Average annual floodplain sedimentation predicted by the model when using different combinations of parameters μ and θ.

μ	θ	Average annual floodplain sedimentation (t yr^{-1})
0.0044	0.3	782
0.0044	0.62	3635
0.012	0.45	4075
0.012	0.46	4263
0.025	0.7	15972
0.025	0.75	17593
0.025	0.8	19066
0.025	0.85	20393
0.025	0.93	22264
0.025	0.96	22899
0.026	0.3	4141
0.026	0.62	13428
0.03	0.93	23038
0.035	0.93	23688
0.039	0.93	24155
0.04	0.93	24267
0.045	0.7	19519
0.045	0.75	20823
0.045	0.8	22005
0.045	0.93	24804
0.045	0.96	25618
0.045	1.08	37250
0.05	0.96	26384
0.05	0.98	27328
0.052	1.24	29240
0.055	0.7	20580
0.055	0.96	27246
0.055	0.98	28445
0.45	0.85	23087

Table 5.12: Values of bank erosion from the literature.

Observed bank erosion value	Methodology	Bank erosion t yr^{-1}	Reference
5.3% of budget Exe	Sediment fingerprinting	1305-1444	Collins et al, (2007)
3500 t yr^{-1} on Culm only	Erosion pins	3500+	Ashbridge (1995)
10% of Culm budget	Sediment fingerprinting	750+	Walling and Woodward (1995)
12% of Culm budget	Sediment fingerprinting	900+	He and Owens (1995)

Table 5.13: Observed rates of floodplain sedimentation from previous studies.

Study area	Methodology	Annual sedimentation ($t^{-1}yr^{-1}$)	Reference
Exe catchment	Modelled rates	23797	Nicholas et al, (2006)
Exe catchment	^{137}Cs	37,200-51,600	He and Walling (1996)
Culm	Suspended sediment loads	1750-2500	Walling and Bradley (1989)
"	Sediment traps	117-70,492	"
"	^{137}Cs	7,650-76,500	"
Culm	Sediment traps	434-11,475	Simm and Walling (1998)
Culm	Sediment traps	2,499	Lambert and Walling (1987)
Culm	^{137}Cs	3,060-30,600	Walling and He (1993)
Culm	^{137}Cs	11,949	Simm (1995)
Culm	^{137}Cs and ^{210}Pb	4,590-40,800	Walling et al, (1996)
Culm	Modelled rates	5,100-25,500	Sweet et al, (2003)

The values shown in Table 5.11 were compared to observed values of floodplain sedimentation (Table 5.13) to assess which parameter values produce magnitudes of floodplain sedimentation similar to the minimum, mid-range and maximum estimates (Table 5.6). The values of the parameters μ and θ chosen and the average annual floodplain sedimentation over the 20-year simulation are shown in Table 5.14 .

Table 5.14: Parameter values used for minimum, mid-range and maximum floodplain sedimentation estimations (based on average annual bank erosion over 20-year simulation).

	μ	θ	Average annual floodplain sedimentation (t yr^{-1})
Minimum	0.025	0.8	19066
Mid-range	0.035	0.93	23688
Maximum	0.055	0.98	28445

5.2.5. Comparison with literature values

Validation of sediment models is limited due to lack of data availability both spatially and temporally. The model was validated by applying the model with different parameter values and input data sets (see Table 5.8). For each of the six input data sets the model was run nine times using a combination of bank erosion and floodplain sedimentation parameters which aimed to represent a minimum, mid-range and maximum estimate of these processes (see Table 5.6). Estimates of bank erosion, floodplain sedimentation, and sediment load at the catchment outlet from previous studies were compared against modelled values to assess accuracy. Therefore the model was run 54 times and data from previous studies used to assess which parameter combination are able to reproduce observed bank erosion, floodplain sedimentation, and catchment yield. This provides a fairly limited validation of the model, yet indicates the model's ability to provide a reasonable estimation of catchment sediment processes. The results of this will be shown in section 5.3.

5.2.6. Influence of climate change

A range of parameter value combinations from the previous section found to reproduce observed annual values of bank erosion, floodplain sedimentation, and sediment load at the catchment outlet were then used to apply the model to various climate change scenarios. As indicated in the previous section, climate change is likely to result in an overall increase to the annual precipitation over the UK and increased magnitude of extreme events and flooding within UK catchments. Varied input data from the ADAS APT model was not available so instead this change was represented in the model by increasing the magnitude of annual water delivery to the catchment by 5-10%. These values of increase were chosen as a representative estimated average increase in precipitation from the literature (Fowler and Ekstrom , 2009; Kay *et al,* 2009; Prudhomme *et al,* 2003; IPCC, 2007).

The resulting changes to the magnitude of sediment generated by overland processes were represented by increasing sediment delivery. Due to the uncertainty in the magnitude of the increase in sediment in response to increased precipitation the model was applied using a range of scenarios, shown in Table 5.15. Resulting changes to bank eroded sediment and floodplain sedimentation was also analysed.

Table 5.15: Climate change scenarios simulated based on precipitation and water delivery change, and result sediment delivery scenarios.

Precipitation increase (%)	Sediment input increase (%)
5	5
5	10
5	15
10	10
10	20
10	30

5.3. Results

5.3.1. Bank erosion model

The results presented in this section are from simulations of the full sediment budget model (including sediment routing, bank erosion, and floodplain deposition). The values of parameter *a* chosen to represent the possible range of total bank erosion within the catchment are shown in Table 5.10. The annual bank eroded sediment for each of the 20-years for each parameter value is shown in Table 5.16 and Figure 5.12. As bank erosion is dependent on the magnitude of shear stress acting on the channel banks sediment concentration of flow does not influence bank erosion. Therefore the modelled bank erosion rate using the same parameter value for *a* are the same when the model is run using different sediment input scenarios and floodplain sedimentation parameters.

The estimates of bank erosion from previous studies shown in Table 5.12 indicate a large range of uncertainty in values of annual mass of sediment generated from bank erosion, which is unsurprising given the temporal and spatial variation of bank erosion rates as observed in chapter 2. Fingerprinting studies estimate the percentage of bank-eroded sediment that reaches the catchment outlet, and erosion pin methodologies estimate the total bank eroded sediment. As much the bank-eroded sediment may not reach the catchment outlet (due to deposition on floodplains/in the channel), sediment fingerprinting will under estimate the magnitude of total bank eroded sediment. This partly explains the difference in magnitude of bank erosion estimates between fingerprinting and erosion pin methodologies studies.

It is difficult to convert observed bank retreat rates from previous studies to a mass of eroded sediment due to the nature of the retreat measurements (at single points along the channel bank, rather than an average retreat rate for a given length of channel) and the need for bank height and sediment density data. Whilst estimations from retreat rates in the literature (see Table 2.6 in chapter 2) are not detailed here for these reasons, it is clear that this data also indicates annual mass of bank-eroded sediment for the Exe catchment would be towards the higher end of this estimate.

Table 5.16: Modelled annual bank eroded sediment (t yr^{-1}) over 20-year simulation for range of x parameter values.

Simulation year	*a*=0.3	*a*=1.2	*a* =2.1
1	676	2704	4732
2	1281	5123	8965
3	1712	6849	11986
4	1433	5732	10031
5	972	3890	6807
6	675	2699	4722
7	1128	4513	7897
8	1190	4760	8329
9	1301	5204	9108
10	1528	6113	10698
11	1120	4478	7837
12	1317	5270	9222
13	888	3552	6217
14	864	3458	6051
15	798	3190	5583
16	1457	5828	10198
17	1336	5345	9353
18	1195	4780	8366
19	1112	4449	7785
20	701	2805	4909

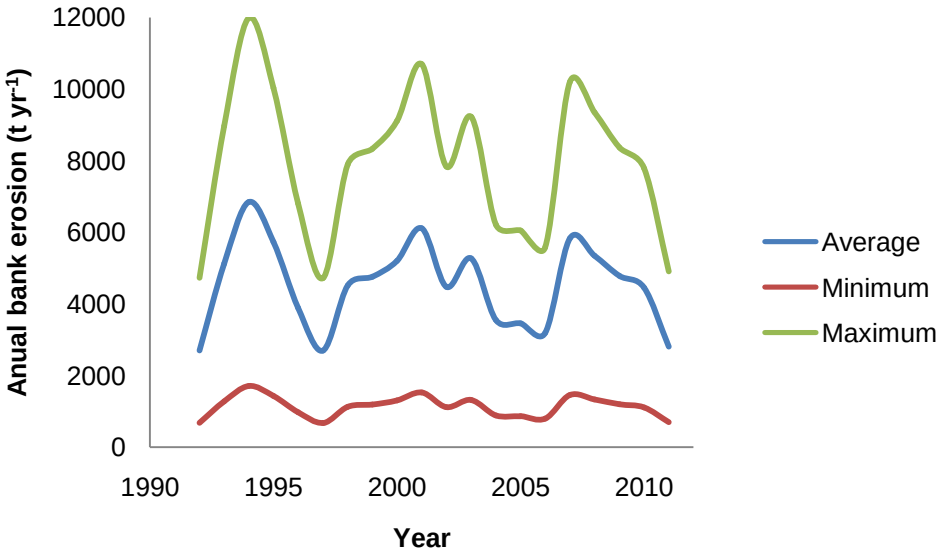

Figure 5.12: Range of predicted bank erosion values for all 20 years of model simulation. The blue line represents the average estimate, green is the maximum and red the minimum for all simulations.

The magnitude of bank erosion as predicted by the model for the range of parameters chosen is 675-11,986 t yr^{-1}. Several of these estimates are within the range of bank erosion estimates for the catchment as indicated in Table 5.12 (approximately 3,500-5,500 t yr^{-1}). The range of possible values of parameter *a* results in a large range of uncertainty in predicted bank erosion values, and the range of annual bank erosion predicted by the model is greater than the range of observed values.

Figure 5.13 shows the predicted bank erosion when using various values of parameter *a*. This indicates a linear relationship between the magnitude of bank erosion and the value of parameter *a*, and the equation relationship is also shown. Based on this equation, and assuming annual catchment bank eroded sediment generation is approximately between 3,500 and 5,500 t yr^{-1}, a plausible range of values of parameter *a* under present day conditions in 1.0-1.4.

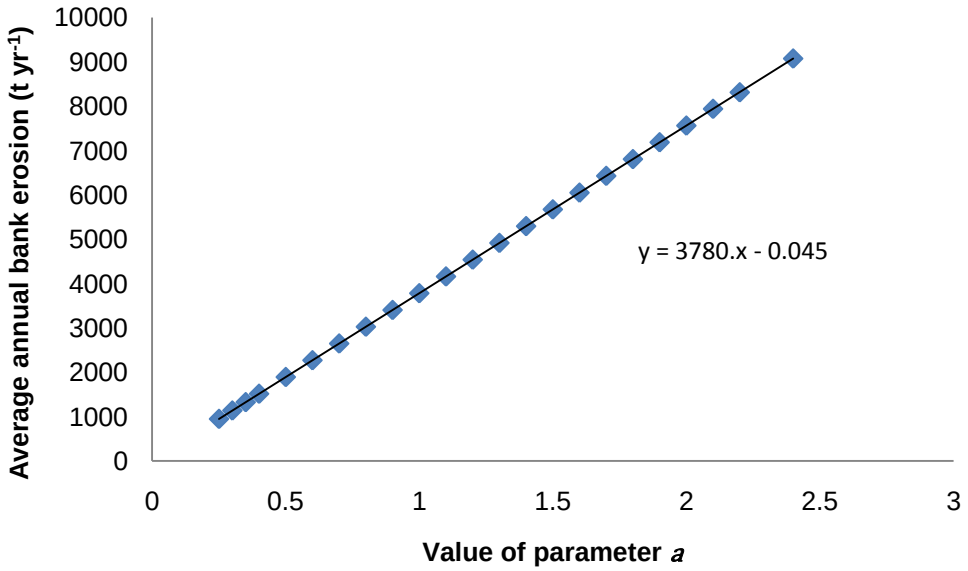

Figure 5.13: Variation of modelled bank erosion with parameter *a*.

5.3.2. Floodplain sedimentation model

The results presented in this section are from simulations of the full sediment budget model (including sediment routing, bank erosion, and floodplain deposition). The range of values of the parameters μ and θ chosen for model simulations are shown in Table 5.14 (note that these results are based on the calibration analysis, where the model was run without bank erosion and using only one mid-range sediment input scenario). The average annual floodplain sedimentation for all 54 model simulations is shown in Table 5.17, and the range of annual floodplain sedimentation for each year over the 20-year simulation period is shown in Figure 5.14.

Table 5.17: Average annual floodplain sedimentation over 20-year simulation period for all model simulations. Sediment input scenarios can be found in Table 5.8. Table continues onto next page.

Simulation number	Sediment input scenario	a	μ	θ	Average floodplain sedimentation (t yr^{-1})
1	1	0.3	0.025	0.8	14258
2	1	1.2	0.025	0.8	15795
3	1	2.1	0.025	0.8	17332
4	1	0.3	0.035	0.93	17619
5	1	1.2	0.035	0.93	19674
6	1	2.1	0.035	0.93	21729
7	1	0.3	0.055	0.98	21195
8	1	1.2	0.055	0.98	23744
9	1	2.1	0.055	0.98	26016
10	2	0.3	0.025	0.8	17541
11	2	1.2	0.025	0.8	19066
12	2	2.1	0.025	0.8	20591
13	2	0.3	0.035	0.93	21635
14	2	1.2	0.035	0.93	23689
15	2	2.1	0.035	0.93	25744
16	2	0.3	0.055	0.98	25898
17	2	1.2	0.055	0.98	28445
18	2	2.1	0.055	0.98	31000
19	3	0.3	0.025	0.8	23588
20	3	1.2	0.025	0.8	25114
21	3	2.1	0.025	0.8	26639
22	3	0.3	0.035	0.93	28756
23	3	1.2	0.035	0.93	30810
24	3	2.1	0.035	0.93	32864
25	3	0.3	0.055	0.98	34194
26	3	1.2	0.055	0.98	36740
27	3	2.1	0.055	0.98	39291
28	4	0.3	0.025	0.8	12746
29	4	1.2	0.025	0.8	14272
30	4	2.1	0.025	0.8	15797
31	4	0.3	0.035	0.93	16032
32	4	1.2	0.035	0.93	18087
33	4	2.1	0.035	0.93	20143
34	4	0.3	0.055	0.98	19452
35	4	1.2	0.055	0.98	22004
36	4	2.1	0.055	0.98	24561
37	5	0.3	0.025	0.8	14786
38	5	1.2	0.025	0.8	16311
39	5	2.1	0.025	0.8	17837

Simulation number	Sediment input scenario	a	μ	θ	Average floodplain sedimentation (t yr^{-1})
40	5	0.3	0.035	0.93	18590
41	5	1.2	0.035	0.93	20645
42	5	2.1	0.035	0.93	22700
43	5	0.3	0.055	0.98	22553
44	5	1.2	0.055	0.98	25104
45	5	2.1	0.055	0.98	27660
46	6	0.3	0.025	0.8	18050
47	6	1.2	0.025	0.8	19575
48	6	2.1	0.025	0.8	21100
49	6	0.3	0.035	0.93	22683
50	6	1.2	0.035	0.93	24737
51	6	2.1	0.035	0.93	26792
52	6	0.3	0.055	0.98	27514
53	6	1.2	0.055	0.98	30063
54	6	2.1	0.055	0.98	32618

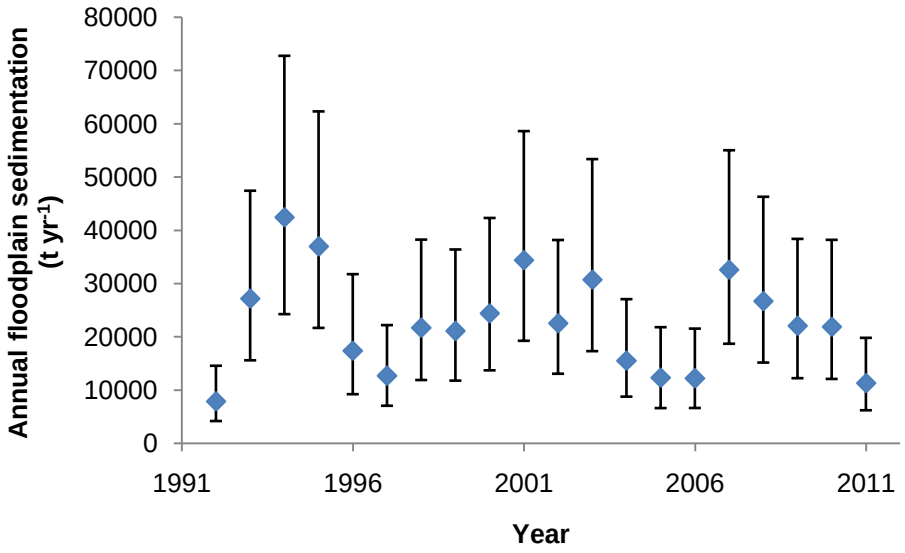

Figure 5.14: Range of model estimated total catchment annual floodplain sedimentation for each of the 20 years of model simulation. Blue points indicate the average value from model outputs and the bars indicate the range of output values.

Table 5.13 indicates values of annual floodplain sedimentation within the Exe catchment observed from previous studies. This data indicates floodplain sedimentation accounts for approximately 23,000 t yr^{-1} within the Exe

catchment, and accounts for between at least 20 and up to 60% of the sediment load (Nicholas *et al*, 2006). However there is a large degree of uncertainty surrounding this estimate, and some of these figures are derived from modelled estimates of floodplain sedimentation. Additionally there is a lack of observational data estimating the total floodplain sedimentation for the whole of the Exe catchment. The average annual floodplain sedimentation predicted by the model ranges from 12,746 to 39, 291 t yr^{-1}. Due to the range of model parameters used the level of uncertainty within the model predictions is high (as illustrated in Figure 5.14). Comparison of model estimates with observational data suggests estimates of modelled floodplain sedimentation are high, and account for between 35 and 88% of the sediment load.

Figure 5.15 and Figure 5.16 illustrate the sensitivity of the model to sediment concentration within overbank flow. As shown in Figure 5.15, with constant values of parameters μ and θ, as sediment concentration increases (sediment input scenarios 3 and 6, or increasing the bank erosion through changes in parameter a) average annual floodplain sedimentation increases significantly. Additionally, with the same set of parameters μ and θ and the same sediment input scenario the model indicates a range of average annual sedimentation due to the variation of parameter a; higher values of parameter a result in increased bank erosion predicted by the model, which results in a slight increase to sediment concentrations within overbank flows and therefore increased floodplain sedimentation. The uneven pattern in Figure 5.16 is due to the different treatment of maximum sediment concentration within each of the sediment input scenarios (see Table 5.8).

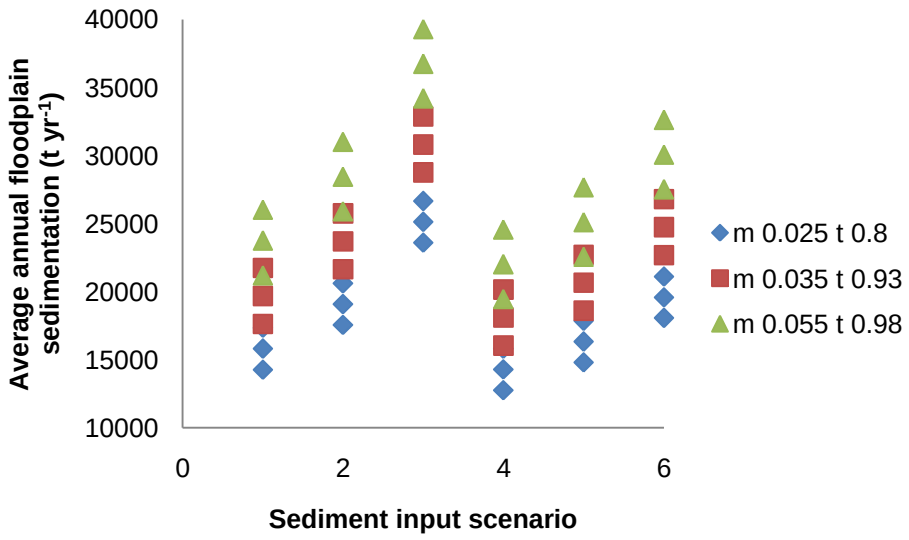

Figure 5.15: Average annual floodplain sedimentation (t yr^{-1}) predicted by the model for each sediment input scenario, and each parameter set of μ (m) and θ (t).

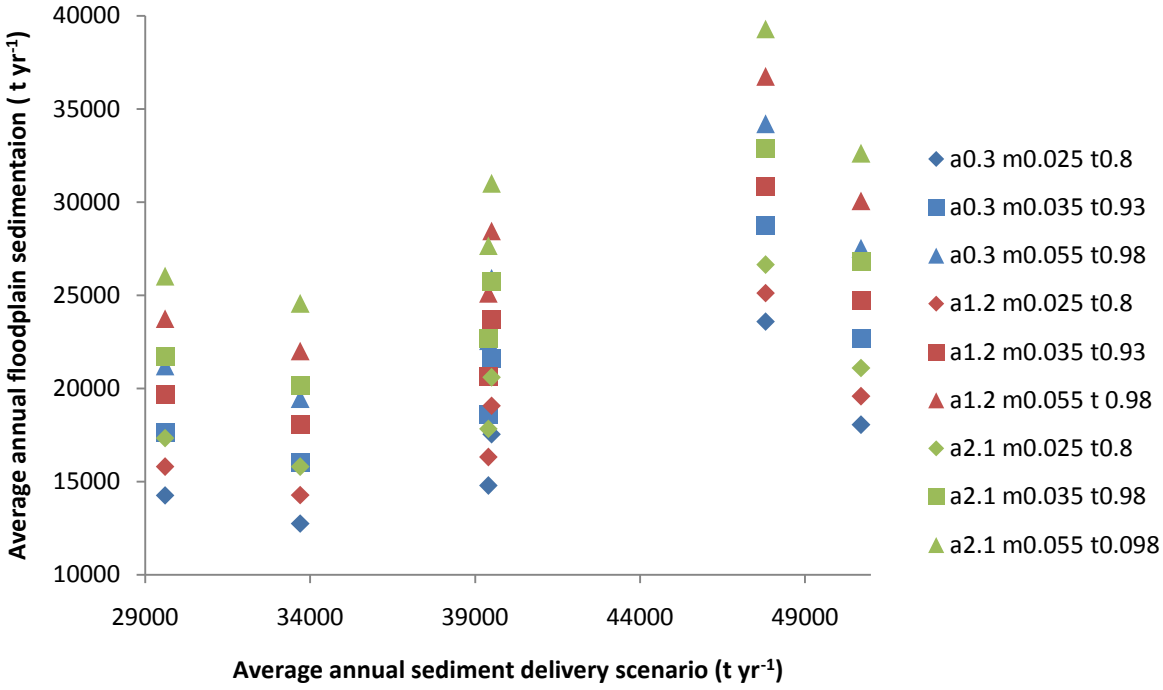

Figure 5.16: Average annual floodplain sedimentation (t yr^{-1}) and average annual sediment delivery (t yr^{-1}) for each set of parameter combinations.

Figure 5.17 indicates the model sensitivity to the parameters μ and θ taken from Table 5.11. The values of parameters μ for this analysis were varied

over a greater range than θ; μ values ranged from 0.0044-0.45 (equivalent to 10227% increase) and θ values ranged from 0.3-1.24 (equivalent to 413% increase). Figure 5.17 indicates the model is much more sensitive to changes in values of θ than μ as indicated by the R^2 values from the relationships between the parameter values and estimated floodplain sedimentation (θ R^2 =0.870, μ R^2 =0.050).

A

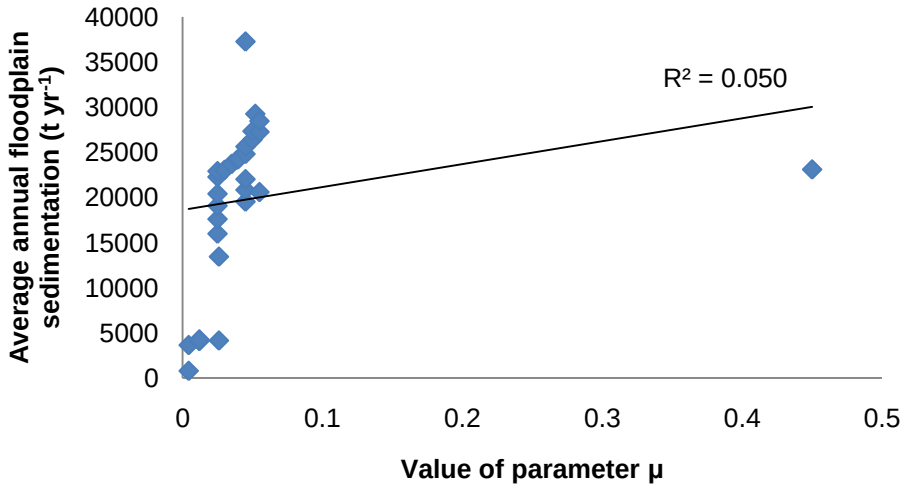

B

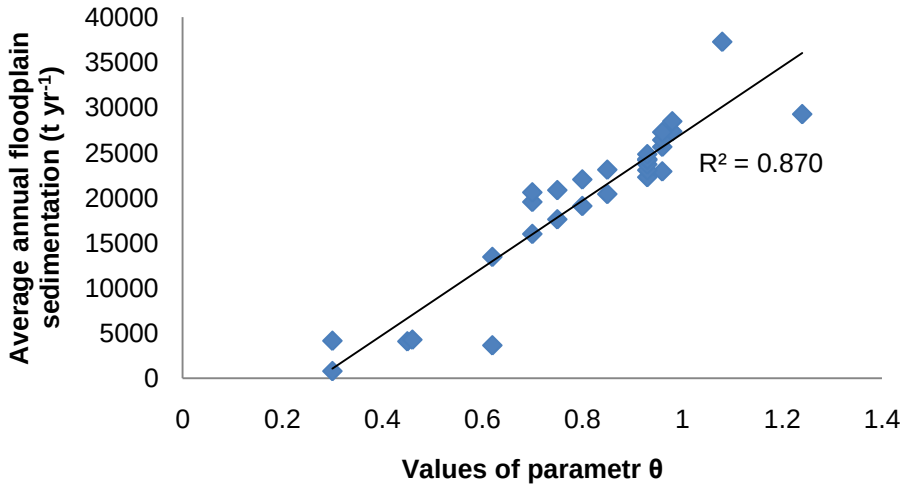

Figure 5.17: A - Average annual floodplain sedimentation predicted by the model with varying values of parameter μ. B - varying values of parameter θ . Both of these graphs show model outputs from simulations of floodplain sedimentation only.

A regression analysis was performed on this data with both parameter values of μ and θ used as dependent variables (and floodplain sedimentation as independent). The modelled floodplain sedimentation is compared to that predicted by the regression equation in Figure 5.18A. The t statistic from the regression output indicated the variable μ had little significance to the regression equation. Therefore the regression analysis was re-run with only θ as a dependent variable (see Figure 5.18B). The R^2 value when inputting both μ and θ as dependent variables is only slightly higher than when only θ is used (R^2=0.875 and R^2=0.870 respectively). These results also indicate the model is much more sensitive to changes in values of parameter θ than μ.

As noted previously, whilst the range of values of average floodplain sedimentation predicted by the model are within the range of observed values, the upper estimates of modelled floodplain sedimentation are high. Therefore the range of plausible model parameter values for floodplain sedimentation under present day conditions are likely to be smaller than the range used within this analysis. Assuming floodplain sedimentation accounts for between 30 and 60% of the sediment generated within the catchment, based on the two mid-range scenarios the model results suggest that values of μ=0.025-0.055 and θ=0.8-0.98 are acceptable.

A

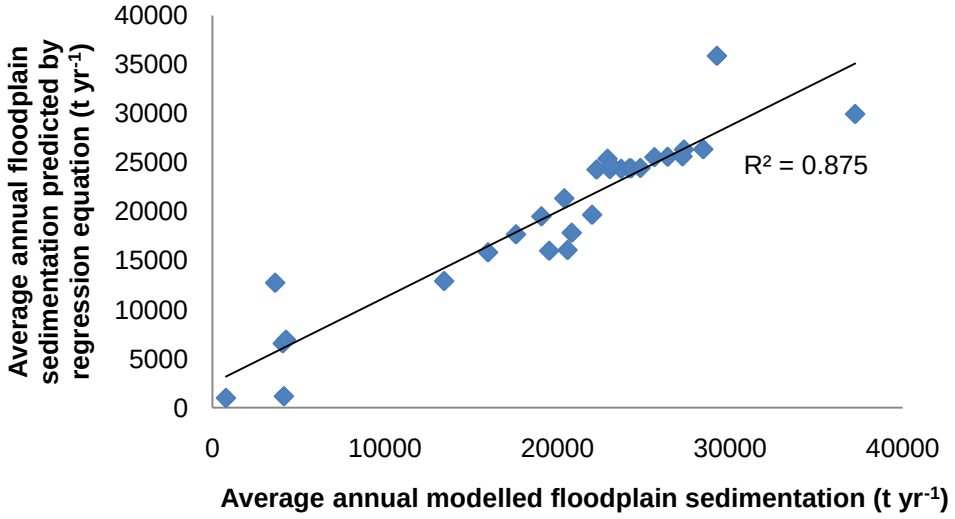

B

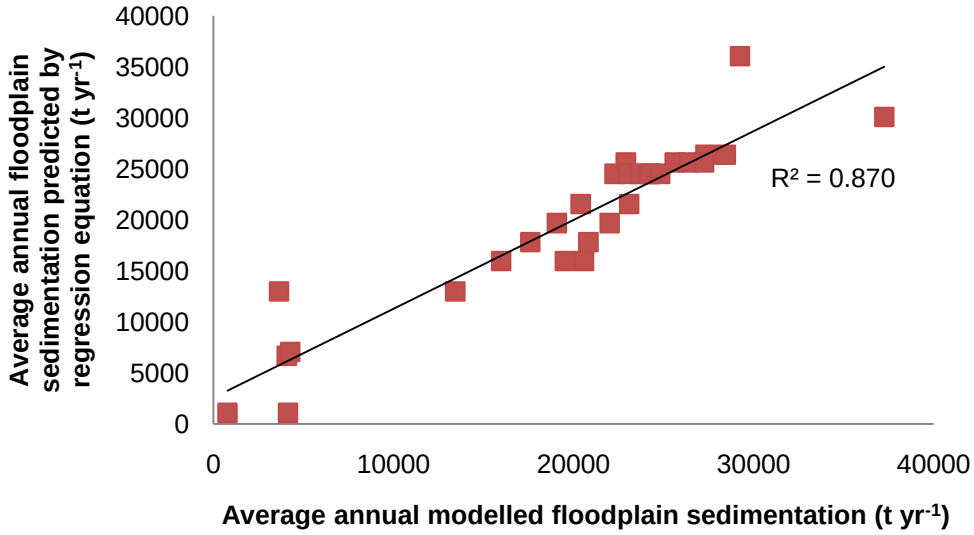

Figure 5.18: Modelled average annual floodplain sedimentation for a range of values of parameters μ and θ, and as predicted by regression equations. A - Regression equation including both m and t as independent variables. B - Regression equation with only t as an independent variable.

5.3.3. Sediment budget model

The full sediment budget model (including the bank erosion and floodplain sedimentation components) was ran 54 times, each with different

combinations of sediment input scenarios, bank erosion and floodplain sedimentation parameter values. The average annual sediment load at the catchment outlet for each of the simulations is shown in Table 5.18. Figure 5.19 shows the range of predicted annual sediment loads at the catchment outlet for all model simulations. This figure highlights the wide range of model estimates, which is due to the uncertainty associated with the range of possible parameter values chosen for the bank erosion parameter a the two floodplain sedimentation parameters μ and θ, and the sediment input scenario.

The mean of all 54 model simulation values of average annual sediment load at the catchment outlet is 14,339 t yr^{-1} and the minimum and maximum predicted sediment loads at the catchment outlet are 8,215 and 24,118 t yr^{-1} respectively. The sediment load at the Exe catchment outlet has been observed in previous studies (Nicholas *et al,* 2006 and Walling *et al,* 2004) as 22,500-27,240 t yr^{-1}, which is within the range of some of the model estimates. Several of the model outputs indicate sediment load at the catchment outlet that is low when compared to observational values. This is partly due to the over estimation of sediment deposited on floodplains (as indicated in the previous section).

Table 5.18: Average annual sediment load at catchment outlet for 20-year simulation period. Results from all 54 model simulations. Table continues onto next page.

Simulation number	Sediment input scenario	a	μ	θ	Sediment load at catchment outlet (t yr^{-1})
1	1	0.3	0.025	0.8	12395
2	1	1.2	0.025	0.8	14172
3	1	2.1	0.025	0.8	15949
4	1	0.3	0.035	0.93	9488
5	1	1.2	0.035	0.93	10811
6	1	2.1	0.035	0.93	12134
7	1	0.3	0.055	0.98	8215
8	1	1.2	0.055	0.98	9311
9	1	2.1	0.055	0.98	10285
10	2	0.3	0.025	0.8	13991
11	2	1.2	0.025	0.8	15778
12	2	2.1	0.025	0.8	17566

Simulation number	Sediment input scenario	a	μ	θ	Sediment load at catchment outlet (t yr^{-1})
13	2	0.3	0.035	0.93	10455
14	2	1.2	0.035	0.93	11777
15	2	2.1	0.035	0.93	13100
16	2	0.3	0.055	0.98	9015
17	2	1.2	0.055	0.98	10111
18	2	2.1	0.055	0.98	11208
19	3	0.3	0.025	0.8	16430
20	3	1.2	0.025	0.8	18217
21	3	2.1	0.025	0.8	20005
22	3	0.3	0.035	0.93	11983
23	3	1.2	0.035	0.93	13305
24	3	2.1	0.035	0.93	14628
25	3	0.3	0.055	0.98	10316
26	3	1.2	0.055	0.98	11413
27	3	2.1	0.055	0.98	12509
28	4	0.3	0.025	0.8	14512
29	4	1.2	0.025	0.8	16300
30	4	2.1	0.025	0.8	18088
31	4	0.3	0.035	0.93	11656
32	4	1.2	0.035	0.93	12979
33	4	2.1	0.035	0.93	14302
34	4	0.3	0.055	0.98	10351
35	4	1.2	0.055	0.98	11447
36	4	2.1	0.055	0.98	12543
37	5	0.3	0.025	0.8	16831
38	5	1.2	0.025	0.8	18619
39	5	2.1	0.025	0.8	20407
40	5	0.3	0.035	0.93	13525
41	5	1.2	0.035	0.93	14848
42	5	2.1	0.035	0.93	16171
43	5	0.3	0.055	0.98	12015
44	5	1.2	0.055	0.98	13111
45	5	2.1	0.055	0.98	14207
46	6	0.3	0.025	0.8	20542
47	6	1.2	0.025	0.8	22330
48	6	2.1	0.025	0.8	24118
49	6	0.3	0.035	0.93	16516
50	6	1.2	0.035	0.93	17839
51	6	2.1	0.035	0.93	19162
52	6	0.3	0.055	0.98	14677
53	6	1.2	0.055	0.98	15774
54	6	2.1	0.055	0.98	16870

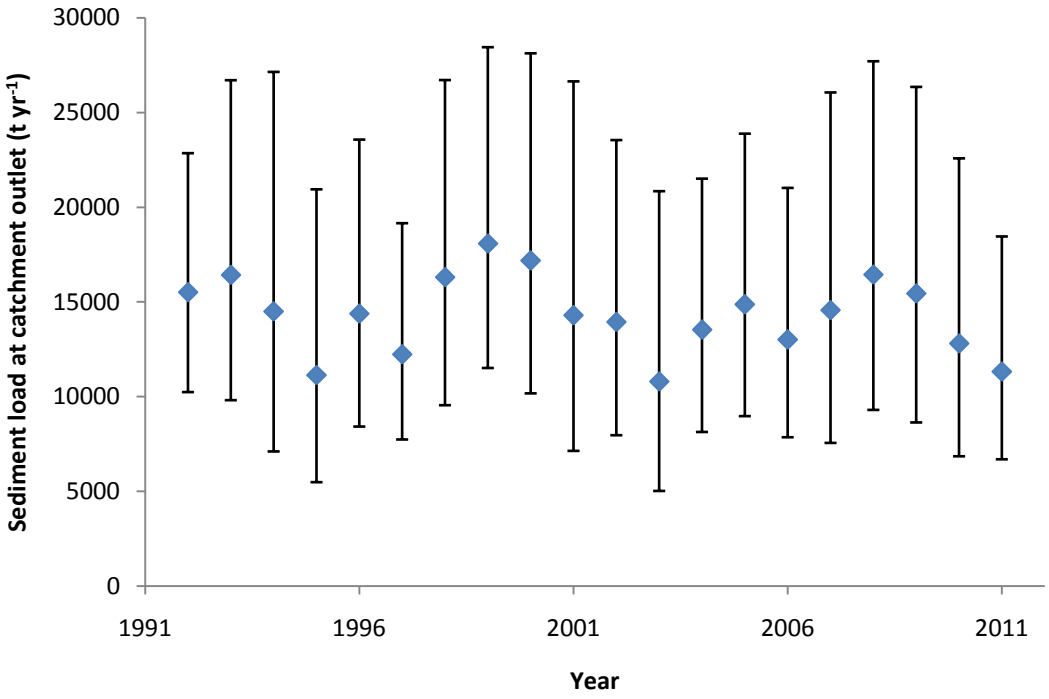

Figure 5.19: Range of predicted annual sediment loads at the catchment outlet for each of the 20 years of simulation, from all model outputs.

Figure 5.20A shows the average annual floodplain sedimentation and B shows the average annual sediment load at the catchment outlet for the two mid-range input scenarios. As bank erosion parameter increases the magnitude of both floodplain sedimentation and sediment load at the catchment outlet increases, which is to be expected as increased values of parameter a result in increased sediment generated through bank erosion. Changes to parameter a appear to have little to no effect on the proportioning of sediment between the floodplain and catchment outlet.

Figure 5.21 illustrate the influence of parameters μ and θ to the average annual sediment load at the catchment outlet. As indicated in section 5.3.2 the parameter θ has a greater influence on the magnitude of floodplain sedimentation within the model, therefore it is unsuprising that increasing this parameter has a greater influence on the sediment load at the catchment outlet (as θ increases, the proportion of sediment deposited on floodplains increases and the sediment load at the catchment outlet decreases).

A

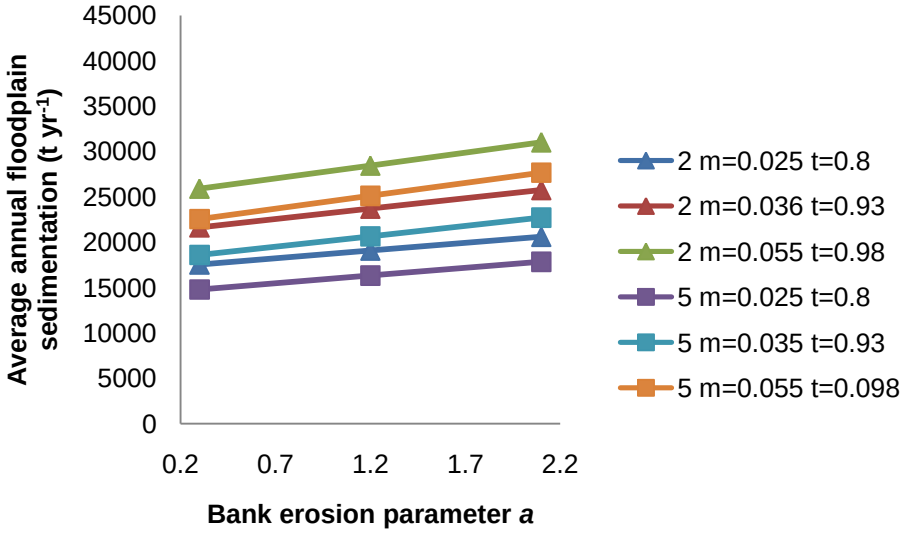

B

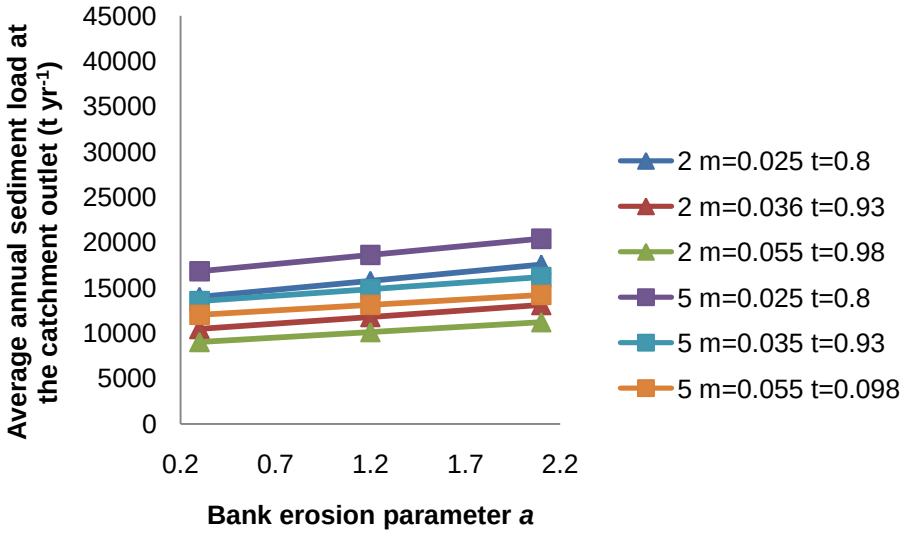

Figure 5.20: A - Average annual floodplain sedimentation for both mid-range scenarios for the range of bank erosion parameters a. B - Average annual sediment load at the catchment outlet for both mid-range scenarios for the range of bank erosion parameters a.

A

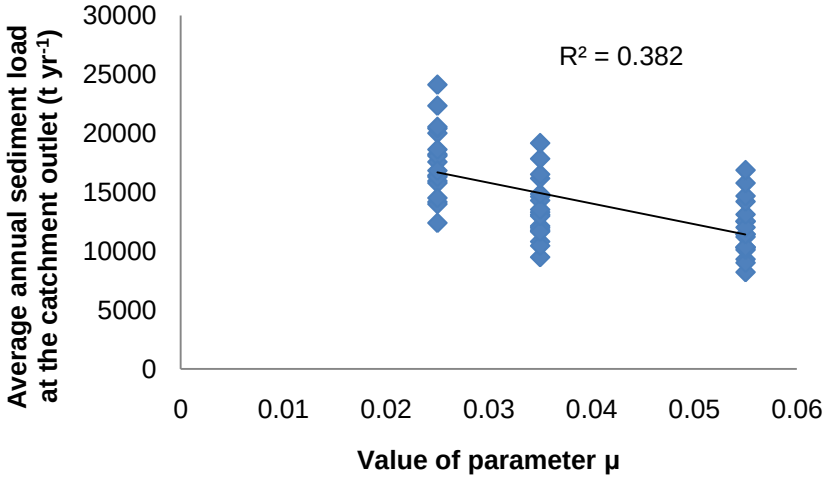

B

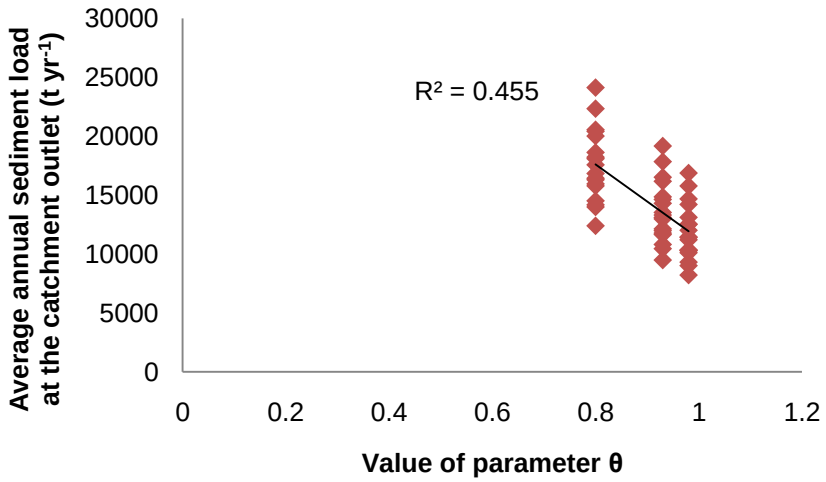

Figure 5.21: Model predicted sediment load at the catchment outlet (t yr^{-1}) and A - model parameter μ, and B - model parameter θ.

5.3.4. Climate change scenarios

The impact of an average annual increase in precipitation was examined, by increasing the water and sediment delivery to the catchment. The scenarios of climatic change (precipitation change) and varying levels of sediment delivery change to the catchment (in response to precipitation changes) are shown in Table 5.15. Initial sediment input used for these simulations was a mid-range sediment scenario from the previous section (input scenario 2) and climatic

change scenarios were applied to this data set. For each of the six climate change scenarios shown in Table 5.15, the sediment budget model was ran 9 times using different combinations of bank erosion and floodplain sedimentation parameters (see Table 5.19). The range of parameter values chosen were taken from a range of plausible values (as indicated in the previous sections). The range of parameter values was more limited than those used in the previous section (for simulations under present day climatic conditions). The reason for this is from the analysis of results in the previous section the range of plausible parameter values was refined by comparison of the model estimates with literature values of sediment processes. In particular, several of the parameter sets used in the previous section overestimated floodplain sedimentation, and therefore the range of parameter values has been refined here to allow a more realistic (lower) estimation of floodplain sedimentation by the model.

Table 5.19: Parameter value combinations used for climate change scenarios.

	a	***μ***	***θ***
1	1	0.030	0.90
2	1	0.035	0.93
3	1	0.040	0.93
4	1.2	0.030	0.90
5	1.2	0.035	0.93
6	1.2	0.040	0.93
7	1.4	0.030	0.90
8	1.4	0.035	0.93
9	1.4	0.040	0.93

5.3.4.1. Bank erosion

The changes to bank erosion rates in response to climate change are shown in Figure 5.22. These results indicate an increase in precipitation results

in an increase in annual sediment generated through bank erosion, which is to be expected, as the magnitude of shear stress acting on channel banks will increase with increasing discharge. Figure 5.22 illustrates the increase in uncertainty of bank erosion predictions for years with greater total bank erosion. This is due to years with increased frequency of flow events with the potential to initiate bank erosion, and therefore more bank erosion events allow the difference in bank erodibility (represented by parameter *a*) to become more apparent.

Through comparison of average bank erosion rates under present day conditions and climate scenarios, the model indicates a 5% increase in precipitation will result in a 6% increase in average annual bank erosion, and 12% increase with 10% increase in precipitation. It should be noted that the range of bank erosion parameters used for the simulations of climate change were taken from a range of plausible value estimated for present day conditions. Therefore there is further uncertainty within the model estimates due to the assumption that these values are applicable to future scenarios.

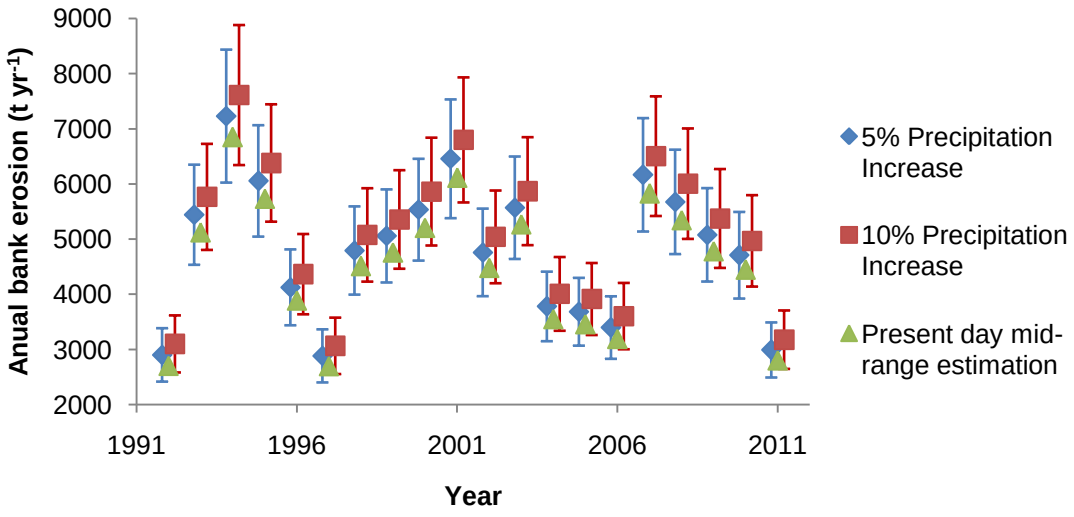

Figure 5.22: Annual predicted bank erosion for 20 years under climate change scenarios. Blue and red show results of 5% and 10% increase in precipitation respectively. Points indicate averages and bars show the range of outputs for various parameter values. Green points indicate present day mid-range model output.

The increase in precipitation represented in the climate change scenarios here increase all water inputs of the model by 5 or 10%. In reality precipitation changes are likely to also result in magnitude variation of precipitation events, particularly with increased frequency of higher magnitude events (Ekström *et al,* 2005). These changes have not been represented by the climate scenarios in this study, but this would result in a greater variation of annual bank erosion rates predicted by the model between different years. Additionally the model does not account for changes to bank erodibility as a result of climate change. Mechanism of change to bank erodibility due to climate change include high magnitude events resulting in changes to the channel morphology and sinuosity, changes to vegetation cover, changes to types and rates of weathering processes acting on channel banks.

Climatic change would result in variation of the seasonal erodibility of channel banks due to changes in vegetation growth as a result of precipitation and temperature changes. Additionally, high magnitude events may result in the removal of vegetation on channel banks thereby increasing channel erodibility for subsequent flows. A further development of the model could involve temporal and/or spatial variation of the parameter for a to account for the seasonal influence of vegetation.

5.3.4.2. Floodplain sedimentation

The changes to floodplain sedimentation rates in response to climate change scenarios are shown in Figure 5.23. These results indicate an increase in precipitation result in an increase in annual floodplain sedimentation which is to be expected, as frequency of overbank flow events will increase. The uncertainty range associate with the model outputs are due to uncertainty to changes in overland sediment generation in response to climate change (the possible scenarios used for model input are shown in Table 5.15) and uncertainty of the bank erosion parameter x. Both of these factors will alter the sediment concentration of overbank flows, and hence floodplain sedimentation rates.

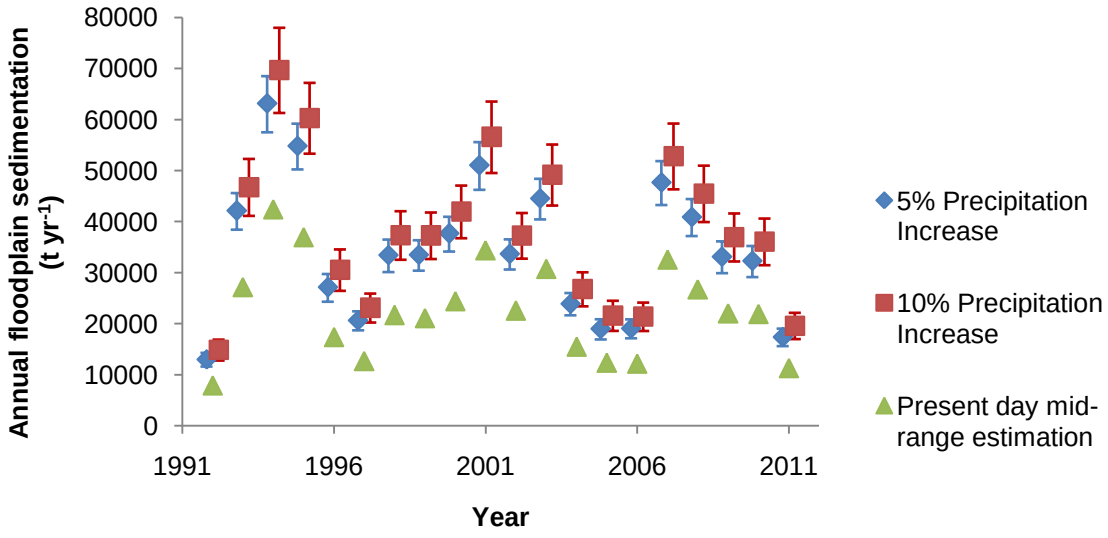

Figure 5.23: Annual predicted floodplain sedimentation for 20 years under climate change scenarios. Blue and red show results of 5% and 10% increase in precipitation respectively. Points indicate averages and bars show the range of outputs for various parameter values. Green points indicate model estimation of present day under mid-range scenario.

Through comparison of average annual floodplain sedimentation under present day conditions and climate scenarios, the model indicates a 5% increase in precipitation will result in a 53% increase in average annual floodplain sedimentation, and 71% increase with 10% increase in precipitation. It should be noted that the range of floodplain sedimentation parameters used for the simulations of climate change were taken from a range of plausible value estimated for present day conditions. Therefore there is further uncertainty within the model estimates due to the assumption that these values are applicable to future scenarios.

As noted in the previous section, the climate scenarios considered here do not account for changes to the variation in magnitude of precipitation events. This will impact floodplain sedimentation as higher magnitude events will result in wider inundation of the floodplain and hence greater sedimentation. Additionally, changes to the rainfall events such as longer dry periods and higher intensity precipitation events will result in temporal changes to overland sediment generation that have not been represented here. Changes to

floodplain vegetation associated with climate change, and potential land-use changes would not only influence overland sediment generation and delivery to the catchment, but also floodplain sediment trapping and deposition rates and the erodibility of channel banks. These effects are also neglected by the model.

5.3.4.3. Sediment budget model

Figure 5.24 shows the range of predicted annual sediment loads at the catchment outlet for all climate change model simulations. This figure highlights the range of model estimates, which is due to the uncertainty associated with the range of possible parameter values chosen for the bank erosion parameter a, and the two floodplain sedimentation parameters μ and θ, and also the changes to overland sediment generation in response to increased precipitation. The average annual sediment load at the catchment outlet for each of the simulations is shown in Table 5.20 and Table 5.21.

Compared to the simulations of present day scenarios of the same input scenario (i.e. sediment input scenario 2, as this was the sediment and water input scenario that was modified to account for climatic changes) the average annual sediment load at the catchment outlet predicted by the model increases by 11% and 18% under 5% and 10% precipitation increase respectively. This estimate is bounded by a level of uncertainty as illustrated in Figure 5.24.

As noted in the previous sections, the climate change scenarios illustrated here do not consider changes to the frequency and timing of precipitation events, which would influence both bank erosion and floodplain sedimentation rates, which in turn would influence sediment load estimations at the catchment outlet. Additionally the temporal variation of changes to overland sediment generation and delivery to the catchment has not been considered within these scenarios, which would also strongly influence sediment yields at the catchment outlet.

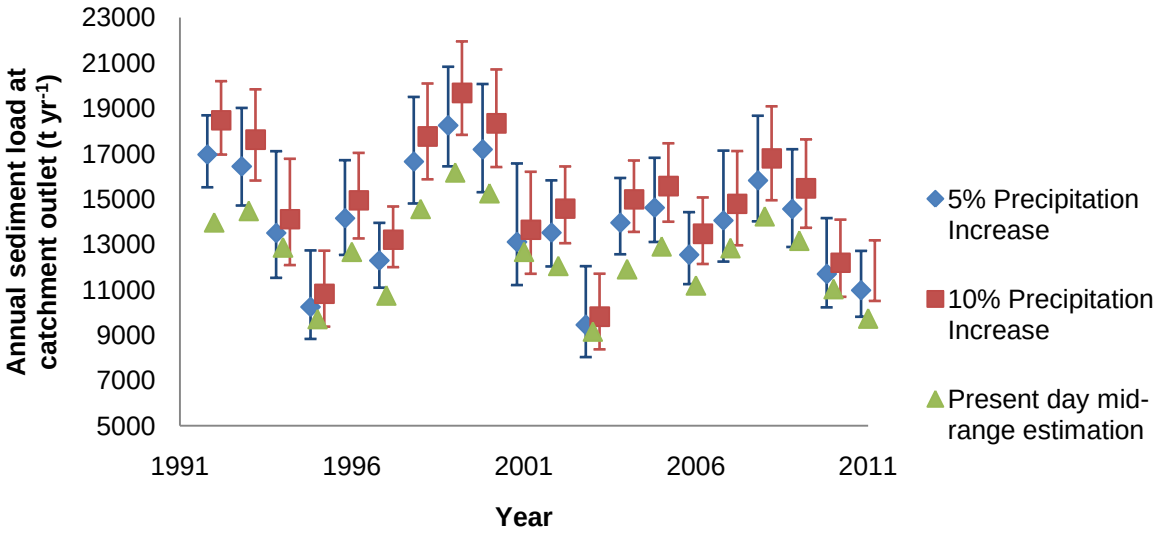

Figure 5.24: Annual sediment load at the catchment outlet predicted under different climate scenarios by the sediment budget model.

Table 5.20: Average annual sediment load at the catchment outlet over 20-year simulation period for climate scenarios with 5% increase of precipitation.

Simulation no.	Climate change scenario	a	μ	θ	Sediment load at catchment outlet (t yr^{-1})
1	1	1.20	0.035	0.930	13175
2	1	1.00	0.035	0.930	12876
3	1	1.20	0.030	0.900	14445
4	1	1.00	0.030	0.900	14115
5	1	1.40	0.030	0.900	14774
6	1	1.40	0.035	0.930	13475
7	1	1.40	0.040	0.930	12978
8	1	1.20	0.040	0.930	12690
9	1	1.00	0.040	0.930	12403
10	2	1.20	0.035	0.930	13717
11	2	1.00	0.035	0.930	13418
12	2	1.20	0.030	0.900	15038
13	2	1.00	0.030	0.900	14709
14	2	1.40	0.030	0.900	15368
15	2	1.40	0.035	0.930	14016
16	2	1.40	0.040	0.930	13500
17	2	1.20	0.040	0.930	13213
18	2	1.00	0.040	0.930	12925
19	3	1.20	0.035	0.930	14259
20	3	1.00	0.035	0.930	13960
21	3	1.20	0.030	0.900	15632
22	3	1.00	0.030	0.900	15303
23	3	1.40	0.030	0.900	15961
24	3	1.40	0.035	0.930	14558
25	3	1.40	0.040	0.930	14022
26	3	1.20	0.040	0.930	13735
27	3	1.00	0.040	0.930	13448

Table 5.21: Average annual sediment load at the catchment outlet over 20-year simulation period for climate scenarios with 10% increase of precipitation.

Simulation no.	Climate change scenario	a	μ	θ	Sediment load at catchment outlet (t yr^{-1})
28	4	1.20	0.035	0.930	13058
29	4	1.00	0.035	0.930	12754
30	4	1.20	0.030	0.900	14353
31	4	1.00	0.030	0.900	14017
32	4	1.40	0.030	0.900	14689
33	4	1.40	0.035	0.930	13363
34	4	1.40	0.040	0.930	12860
35	4	1.20	0.040	0.930	12568
36	4	1.00	0.040	0.930	12276
37	5	1.20	0.035	0.930	14080
38	5	1.00	0.035	0.930	13775
39	5	1.20	0.030	0.900	15475
40	5	1.00	0.030	0.900	15139
41	5	1.40	0.030	0.900	15811
42	5	1.40	0.035	0.930	14384
43	5	1.40	0.040	0.930	13843
44	5	1.20	0.040	0.930	13552
45	5	1.00	0.040	0.930	13260
46	6	1.20	0.035	0.930	15101
47	6	1.00	0.035	0.930	14797
48	6	1.20	0.030	0.900	16597
49	6	1.00	0.030	0.900	16261
50	6	1.40	0.030	0.900	16932
51	6	1.40	0.035	0.930	15405
52	6	1.40	0.040	0.930	14827
53	6	1.20	0.040	0.930	14535
54	6	1.00	0.040	0.930	14243

5.4. Conclusions

Within this chapter a coupled catchment sediment budget model has been developed using insights from previous chapters; a bank erosion model has been developed to incorporate an existing bank erosion index, and factors identified previously in this thesis to influence bank erosion rates. Additionally a floodplain sedimentation methodology based on a power-law relationship has been applied to the Exe catchment. Both these models have been incorporated within a water and sediment routing model to create a catchment sediment budget model.

The bank erosion model has been calibrated against observational bank erosion data from the literature for the Exe catchment. The model incorporates several factors known to influence bank erosion; the composition of channel bank material (silt-clay content), shear stress acting on the channel bank and exceedence of critical bank shear stress, channel confinement, and sinuosity. The inclusion of these factors results in an improvement of the physical realism of bank erosion models compared to existing methodologies. The range of average annual bank eroded sediment production within the catchment was found to be within the range of observed values.

The floodplain sedimentation model has also been calibrated against observational bank erosion data from the literature. A range of parameter values for the Exe catchment have been established. The wide range of possible parameter values and sediment input scenarios resulted in a large uncertainty range of model estimations, however observed values of floodplain sedimentation were within the model's predicted range.

The errors within the input data to the sediment budget model (from the APT model output) pose a limitation on the calibration and validation of the model at present. The uncertainty of the sediment input to the catchment was accounted for by completing several model simulations with a range of possible input data scenarios, and consequently uncertainty of model outputs increases. The sediment input data used for the model was modified in 2 different ways to produce 6 different scenarios which were chosen to represent a range of

plausible sediment delivery time-series to the catchment based on average annual sediment delivery.

Additional sources/sinks of sediment such as channel bed erosion/deposition are not considered within the sediment budget model. As noted in the previous chapters, bank erosion and floodplain sedimentation have been observed as a significant sediment source and sink respectively within catchments. The magnitude of excluded processes is not thought to be as significant, and therefore their exclusion should not significantly alter the accuracy of the model. However a further development of the model could involve inclusion of such processes.

The climate change scenarios analysed here represent an increase of precipitation by either 5 or 10%. For each of these precipitation change scenarios three possible sediment delivery scenarios were simulated. Based on analysis of present day simulations a smaller range of parameter values for bank erosion and floodplain sedimentation were identified, and resulting changes to the magnitudes of these processes were analysed. As expected, both bank erosion and floodplain sedimentation increase as a result, but the different magnitudes of change indicate varying levels of sensitivity of these processes to climatic change. Changes to the variation of precipitation events and seasonal effects of climatic change were not accounted for. Additionally, in reality a complex relationship between precipitation and overland sediment generation exists (as opposed to the simplistic increase in sediment generation in response to increased precipitation as represented here). Future work could include running the APT model for different climate scenarios which could reduce uncertainty of sediment response to climatic changes. The use of these different outputs as inputs to the sediment budget model developed here would enable a more comprehensive analysis of the effect of climate change. A similar analysis could be performed with land-use change.

The model developed has been tested on only the Exe catchment, UK and therefore it is not possible to comment here on the model's ability to represent these processes at additional catchments. However, the data used to generate the bank erosion model (and sinuosity and channel confinement factor within the model) was based on several UK catchments and therefore it is likely that this component of the model would perform well in alternative locations.

The routing methodology should perform with the same degree of accuracy for any alternative location. Therefore with some calibration the model could be applied to additional UK catchments.

The APT model estimates overland sediment generation, and water and sediment delivery to channels throughout catchments. The sediment budget model developed in this chapter provides an extension to this model by routing both the water and sediment through the catchment and accounting for sediment generation through bank erosion and sediment loss through floodplain sedimentation. The combined model therefore provides a holistic estimation of the catchment sediment budget by incorporating several processes and considering the catchment as a whole. This model will be a valuable tool for assessing the impact of potential future changes within the catchment (such as climate and land-use change). Additionally the model enables identification of key sources and sinks of sediment within catchments. This will be useful for implementing effective management and mitigation strategies, enabling catchments to comply with policy targets. Potentially effective mitigation strategies include the use of buffer strips: a strip of land between agricultural areas and channel banks where natural vegetation is allowed to grow. Buffer strips trap sediments and enhance infiltration of pollutants, preventing them from reaching the channel. Additionally, the presence of a riparian zone within the buffer strip enhances bank stability reducing the risk of bank erosion. Alternative strategies may include fencing along channel banks (to prevent a reduction in bank stability caused by trampling), crop rotation strategies (to maximise soil stability and reduce overland sediment generation), and conservation tillage practices.

6. Conclusions

The overall aim of this thesis was to develop a catchment sediment budget model that could be coupled to existing overland sediment generation models. The objectives of the catchment budget model included an improved representation of sediment sources and sinks within catchments, to enable a more comprehensive representation than is available with existing models. This has been achieved through incorporation of a channel bank erosion and floodplain sedimentation model within the budget model. A minimal input data requirement of the model was also considered desirable as this would allow ease of application of the model within several catchments nationally. The sediment budget model was also required to be computationally efficient to allow coupling to existing overland sediment generation models, and to enable numerous simulations to be performed to analyse the influence of a variety of climate and land use scenarios to the sediment budget.

The importance of considering the catchment as a whole for effective management was discussed in chapter one, and noted by Walling and Collins (2008). Sediment modelling provides a means of assessing several sediment processes, and the interaction of these processes at a catchment scale, over longer time periods than is possible compared with observational techniques. The relevance of sediment loads to the chemical and ecological state of river catchments, and uncertainties regarding the scenarios of future environmental change and catchment responses to such changes were also discussed in chapter one. Sediment budget models provide a means of assessing catchment scale response, and estimating changes to sediment generation, transport, and storage processes as a result of various environmental change scenarios. Additionally catchment sediment budget models provide a means of assessing management strategies to enable effective implementation of mitigation measures.

Chapter two investigated the influence of several physical factors on bank erosion rates within UK catchments. Field-based methodologies provide only short-term datasets at small spatial scales. Therefore a GIS methodology modified from previous studies (Hooke and Kain, 1982; Gurnell *et al*, 1994) was

used to allow estimation of bank erosion rates over periods of up to 150 years across 7 UK river catchments. The results of this analysis indicated the importance of the physical factors upstream catchment area, channel confinement (within the floodplain), channel sinuosity and slope. Additionally the analysis highlighted the significance of bank erosion as a sediment source, and the spatial and temporal variation of bank erosion rates both within and between catchments. Additionally, the results highlighted the importance of bank erosion as a sediment source within river catchments, and the variability of sediment production from bank erosion both within and between catchments. The relationship observed between bank erosion and upstream catchment area was thought to be significant as this independent variable is a surrogate of discharge magnitude. As channel confinement ratio increased (which is equivalent to channels becoming less confined within floodplains) bank erosion was found to increase. This is due to the lack of restriction within the floodplain, thereby allowing the channel to migrate.

The relationship between sinuosity and bank erosion from chapter two appeared to be non-linear and therefore chapter three investigated the existence of a threshold value of sinuosity. To enable analysis of the influence of sinuosity over longer timescales (greater than 400 years) a meander migration model was used. The results of this analysis indicated that as sinuosity increases (from a value of 0, a straight line channel) bank erosion rates increase. As sinuosity increases above values of approximately 1.5 bank erosion rates were found to decrease with additional increase to channel sinuosity. This relationship is similar to that between channel radius of curvature and bank erosion rates. The formation of secondary circulation and positioning of maximum velocity within the channel was believed to account for this relationship, and also the point of maximum bank erosion being located downstream of the bend apex. In straight channels the maximum flow velocities are located within the centre of the channel, hence bank erosion rates are low. As sinuosity increases, the positioning of maximum velocity moves towards the channel bank on the outside of the bend, and consequently bank erosion rates increase. Above sinuosities of ~1.5, with any further increase in sinuosity the maximum flow velocities move towards the centre of the channel, reducing bank erosion rates.

The current version of PSYCHIC/ADAS APT model (which is a newer version of PSYCHIC, still in development stages at the time of writing) estimates delivery of sediment and water to the channel network. Currently neither of these models includes a channel routing component. Chapter four of this thesis used ADAS APT model output data of water/runoff delivery to the channel network as input for a computationally efficient catchment water routing model based on the variable parameter Muskingum-Cunge methodology. This model was tested on the Exe catchment, Devon, UK for a 20-year period from 1991-2011. The model performance was assessed using gauging station data at 5 locations across the catchment. After some modification of the input data the model was found to perform with a reasonable degree of accuracy (R^2 values 0.6-0.86 and NSE 0.55-0.80).

As noted in chapters one and two, bank erosion may form a significant sediment source within catchments, and due to the influence of several controlling factors varies both spatially and temporally. In the fifth chapter, an existing national bank erosion index developed by ADAS was used as the basis for the formulation of a bank erosion model. Both the bank erosion index and the bank erosion model developed incorporate the influence of silt-clay content of channel banks (which influences bank cohesion and values of critical shear stress). The ADAS bank erosion index estimates the percentage of the year where flows exceed the critical shear stress, and from this estimate the mass of bank eroded sediment which reaches the catchment outlet. This approach was modified to estimate bank erosion based on exceedence of critical shear stress at each model time step (1.5 hours). Additionally, the developed model estimates the total mass of bank eroded sediment. The findings from chapters two and three were incorporated by inclusion of sinuosity and channel confinement factors.

Sediment routing was incorporated to the catchment routing methodology developed in chapter four. Additionally, a bank erosion model was developed to incorporate the findings of chapters two and three. A floodplain sedimentation model developed by Nicholas *et al*, (2006), whereby a power law relationship between discharge in excess of bankfull and sedimentation rate was applied. Finally, the fully coupled catchment sediment budget model, including both the bank erosion and floodplain sedimentation components was

applied to the Exe catchment, and ADAS APT sediment delivery estimation data were used as input data for the simulations. Whilst validation of the model is difficult due to lack of detailed observational sediment data, calibration of the model indicated the ability of the sediment budget model to reproduce average annual values of bank erosion, floodplain sedimentation, and sediment load at the catchment outlet within the range of observational data values.

Representations of bank erosion within existing sediment models normally include very few of these factors; SedNet accounts for the length of channel bank covered by vegetation, and SHETRAN accounts for the exceedence of shear stress by channel flow and application of an erodibility parameter. Neglecting several of these additional factors known to influence bank erosion will result in poor reproduction of the spatial variability of bank erosion rates (both within and between catchments) and inaccurate prediction of the magnitude of bank erosion rates. The bank erosion model developed within this thesis is an improvement upon existing approaches due to the incorporation of additional factors known to influence bank erosion rates. The improved representation of bank erosion will enable spatial variation of bank erosion rates between catchments (and within catchments) to be captured by the model. The inclusion of sinuosity makes the model more suitable when considering longer term environmental response, particularly climatic changes. However, several existing models (including the catchment model developed in this thesis) do not represent changes to channel planform (including sinuosity) over time. Therefore the ability of the model to estimate bank erosion over longer timescales could be improved by inclusion of channel migration within catchment models. This however would greatly increase the computational demands of the model and therefore was not within the remit of this thesis.

Additional factors which could improve the representation of bank erosion include the incorporation of the influence of vegetation within the model. As discussed in chapter one, vegetation affects bank stability in several ways; hydrological, mechanical, with both positive and negative influences on bank stability. However the overall influence of vegetation is assumed to promote bank stability (Simon and Collison, 2002). Inclusion of a vegetation parameter could also enhance the model's ability to represent changes as a result of various land use scenarios.

The bank erosion model developed in this thesis has been based on an empirical approach, the data for which has been taken from several UK river catchments. Relationships between bank erosion and factors observed will most likely vary between locations, and therefore even though the model may perform well at one location but will need validation at other sites. Further validation of the model, by applying the model to alternative catchments within the UK (and elsewhere) is required. Whilst calibration between catchments may be necessary, it is thought that within the UK at least the model is likely to perform with a similar level of accuracy as the dataset used for the analysis was drawn from a range of UK catchments, so as to enable the development of a catchment scale model that could be applied nationally.

Additional data for calibration and validation of the model would enable greater confidence in the model's ability. Further work could include application of the model within an area with sufficient observational data of bank erosion rates (from field data in addition to GIS based data to enable ground truthing), floodplain sedimentation rate data, and sediment load data (at the catchment outlet and upstream locations). At present, sources of such data are incredibly limited, if available.

Chapter five noted the significance of floodplain sedimentation as a key sediment sink within river catchments. Whilst, complex numerical models which enable representation of the spatial variability of sedimentation and inundation patters exist these approaches are computationally complex and have large data requirements. Therefore, these models are only applied at spatial scales much smaller than catchments, making them unsuitable for incorporation within the catchment sediment budget model to be developed in this thesis. The floodplain sedimentation model applied within this sediment budget model provides an efficient means of representing floodplain sedimentation at a catchment scale. Additionally, this approach requires minimal input data in comparison to more complex alternatives.

Figure 6.1 illustrates the processes included within the sediment budget model developed within this thesis. The ADAS APT model provided input data for the sediment budget model of sediment (and water) delivery to the channel network. The APT model includes representation of overland sediment generation (by processes such as rainsplash detachment and entrainment

within surface runoff), the influence of varying soil erodibilties, land use and vegetation coverage, hydrological routing of sediment and the proportion of sediment re-deposited before reaching the channel (sediment delivery ratio). The routing model developed in chapters four and five provide a means of estimating both water and sediment transport throughout the catchment.

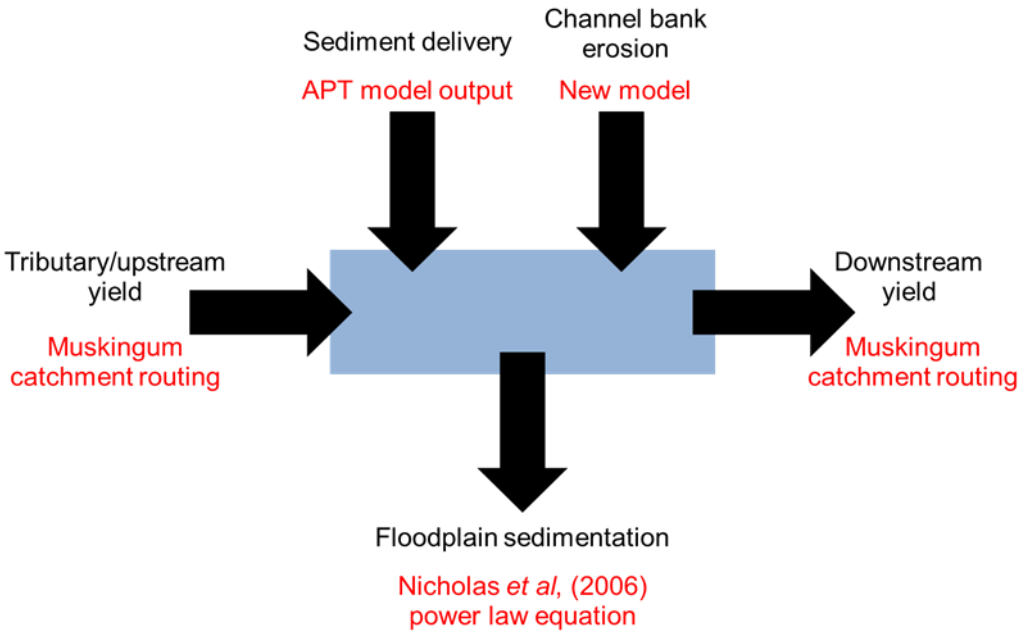

Figure 6.1: Schematic representation of the catchment sediment budget model developed within this thesis, and the processes included within the model.

Several existing sediment generation models do not include a representation of channel bank erosion as a sediment source (eg: PSYCHIC/ADAS APT, RUSLE/USLE, CREAMS etc.). The sediment budget model developed within this thesis is therefore an improvement upon existing approaches due to the inclusion of this process as a source of sediment. Additionally, the inclusion of floodplain sedimentation as a sink of sediment within the catchment provides a more complete representation of sediment processes within river catchments.

Additional sediment processes not represented within the model include scouring of floodplain sediment and channel bed, and channel deposition. The

floodplain sedimentation model is calibrated against observational data of net sedimentation rates, and therefore whilst scour is not explicitly represented within the model, this removal of this sediment from the floodplain store/inclusion within the channel is accounted for within the model. The magnitude of channel bed deposition and scour are considerably lower than sediment sources and sinks within the model and therefore the exclusion of these processes will not greatly influence model results.

As indicated in chapter five, the level of uncertainty within model estimations is high. This is largely due to the range of possible parameter values within the model, (particularly the bank erosion and floodplain sedimentation models). Each of the model components was calibrated against available observational data. The limited spatial coverage of observational data results in a large range of possible values for these processes at a catchment scale. Therefore there is a range of plausible parameter values, and parameter combinations for each of these processes which accounts for a large proportion of this uncertainty.

An assessment of potential climate change was performed within chapter five of this thesis by way of systematic increase of water delivery to the catchment. The results of this analysis indicated the magnitudes of sediment generated through bank erosion, sediment deposition on floodplains, and sediment load at the catchment outlet all increased when considering increased water delivery scenarios. Floodplain sedimentation was observed to be more sensitive to increased water delivery than bank erosion. Similarly to the present day model estimates, uncertainty of the model estimates in response to climate change is high. This is partly due to the range of plausible parameter values, and uncertainty surrounding the simulated climatic changes. The parameter values for these model simulations were based on values from present day scenarios, therefore and assumption is made that these values would still be suitable in future. As the APT model was still in development stages during this project duration, additional APT outputs based on a range of potential future climate and land use scenarios was unavailable. A future development of this project could include further model simulations using various APT model scenarios as input data.

This thesis has contributed to scientific understanding of factors controlling channel bank erosion rates within several UK catchments, and the development of an existing methodology of monitoring bank erosion rates. This has lead to the development of a new bank erosion model that is an improvement on existing modelling approaches due to the inclusion of additional controlling factors. A catchment sediment budget model has been developed incorporating the new bank erosion model and a floodplain sedimentation model, providing a more complete representation of catchment sediment processes than current alternatives.

7. Appendices

7.1.Appendix A

Aggregate class	Aggregate class number[1]	Broad Habitat	LCM2007 class	LCM2007 class number[2]
Broadleaf woodland	1	'Broadleaved, Mixed and Yew Woodland'	Broadleaved woodland	1
Coniferous woodland	2	'Coniferous Woodland'	'Coniferous Woodland'	2
Arable	3	'Arable and Horticulture'	'Arable and Horticulture'	3
Improved grassland	4	'Improved Grassland'	'Improved Grassland'	4
Semi-natural grassland	5	Rough Grassland	Rough grassland	5
		'Neutral Grassland'	'Neutral Grassland'	6
		'Calcareous Grassland'	'Calcareous Grassland'	7
		'Acid Grassland'	Acid grassland	8
		'Fen, Marsh and Swamp'	'Fen, Marsh and Swamp'	9
Mountain, heath, bog	6	'Dwarf Shrub Heath'	Heather	10
			Heather grassland	11
		'Bog'	'Bog'	12
		'Montane Habitats'	'Montane Habitats'	13
		'Inland Rock'	'Inland Rock'	14
Saltwater	7	Saltwater	Saltwater	15
Freshwater	8	Freshwater	Freshwater	16
Coastal	9	'Supra-littoral Rock'	'Supra-littoral Rock'	17
		'Supra-littoral Sediment'	'Supra-littoral Sediment'	18
		'Littoral Rock'	'Littoral Rock'	19
		'Littoral Sediment'	Littoral sediment	20
			Saltmarsh	21
Built-up areas and gardens	10	'Built-up Areas and Gardens'	Urban	22
			Suburban	23

Figure 7.1: Aggregate classes and broad habitat classes for LCM 2007 data. From Land Cover Map data documentation 2007. (CEH, 2007).

LCM2007 class	Brief Review
Broadleaved woodland	Broadleaved woodlands are characterised by stands >5 m high with tree cover >20%; scrub (<5 m) requires cover >30% for inclusion in this BH. Such fine distinctions cannot be made through remote sensing. Open-canopy woodland (stands with trees <50%) is a particular problem, albeit occurring relatively rarely, and may not often be mapped consistently, due to the dominance of the non-woodland plants. Stands with near-closed canopies can be interpreted easily in the field and pure examples can normally be found for training the classifier. Broadleaved evergreen trees (part of this BH) rarely occur in stands >1ha (an area large enough to create suitable training areas appropriate for classification). Mixed woodland (with >20% broadleaved trees) was trained separately. Where individual stands of broad-leaved or evergreen trees exceeded the minimum mappable unit, they were treated as separate blocks within the woodland; in many parts of the UK, truly 'mixed woodlands' as opposed to those with mosaic-blocks of broadleaved and coniferous trees, are unusual.
'Coniferous Woodland'	*'Coniferous Woodland'* includes semi-natural stands and plantations, with cover >20%. The recognition of coniferous woodland is generally straightforward. Rare examples of open canopy semi-natural pinewoods may have been classified according to the dominant understorey class. The BH includes new plantation and recently felled areas (this is a class where the BH definition is based on land use, i.e. forestry, rather than cover). New plantations, predominantly heather and/or grass, for example, are recorded as such by the spectral classification of image data. New plantations are only consistently recorded as conifers when tree cover is sufficient to strongly influence the reflectance. LCM2007 includes newly felled areas. Once they are fully recolonised by rough grass, heath or scrub, they are recorded according to that cover. Deciduous larch is discernible from other deciduous trees and is generally correctly included with other conifers.
'Arable and Horticulture'	This Broad Habitat includes annual crops, perennial crops such as berries and orchards and freshly ploughed land. Orchards with a ground flora are hard to distinguish.
'Improved Grassland'	Improved grassland is distinguished from semi-natural grasslands based on its higher productivity, lack of winter senescence and location and/or context. In some cases heavy grazing can cause mis-classification with semi-natural grassland, or even arable land. Some confusion occurs between *'Improved Grassland'* and *'Calcareous Grassland'* and *'Neutral Grassland'*, as *'Calcareous Grassland'* and *'Neutral Grassland'* are often very productive grassland and so spectrally very similar to *'Improved Grassland'*.

'Neutral Grassland'	In the production of LCM2007 grassland is mapped by classifying images into *'Improved Grassland'* and **Rough grassland**. The knowledge-based enhancement rules determine whether **Rough grassland** should be reclassified as *'Neutral Grassland'*, *'Calcareous Grassland'* or *'Acid Grassland'*, or whether it should remain as **Rough grassland.** In the field *'Neutral Grassland'* is determined based on botanical composition and it also includes semi-improved grasslands managed for silage, hay or pasture (Jackson, 2000), which in LCM2007 will often be classified as *'Improved Grassland'*.
'Calcareous Grassland'	*The same methods apply as for 'Neutral Grassland' (see above).*
'Acid Grassland'	*The same methods apply as for 'Neutral Grassland' (see above).* Bracken can be mapped using LCM2007 methods, but it depends on image timing and suitable training areas (bracken often fails to offer stands sufficiently extensive for classification and training), so for consistency it is assigned to *'Acid Grassland'*. However, some stands of bracken can be identified at the subclass level.
Rough grassland	The knowledge-based enhancement rules determine whether **Rough grassland** should be reclassified as *'Neutral Grassland'*, *'Calcareous Grassland'* or *'Acid Grassland'*, or whether it should remain as **Rough grassland**. The grass that remains as Rough grassland is therefore a mix of areas of managed, low productivity grassland, plus some areas of semi-natural grassland, which could not be assigned Neutral, Calcareous or Acid grassland with confidence by the knowledge-based enhancements.
Note about grassland classes	The comparisons between LCM2007 and other data sets (the ground reference polygons and Countryside Survey in 2007 Broad Habitat maps) (Morton *et al.*, 2011), showed that *'Neutral Grassland'* and *'Calcareous Grassland'* were often mis-classified as *'Improved Grassland'*. Users requiring *'Neutral Grassland'* and *'Calcareous Grassland'* should read Section 3.9 and Chapter 4 of the LCM2007 final report (Morton *et al.*, 2011). Other users may wish to aggregate the grassland classes together, if appropriate to their needs.
'Heather' and 'Heather grassland' (together form the *'Dwarf Shrub Heath'* Broad Habitat)	*'Dwarf Shrub Heath'* is divided into two classes, depending on the density of Heather, producing 'Heather' and 'Heather grassland' classes respectively. This is similar to LCM1990's and LCM2000s Open and Dense Shrub Heath classes. Note: comparing LCM2007 to other data sets (ground reference data set (Section 3.9 of Morton *et al.*, 2011) and Countryside Survey in 2007 (Chapter 4 of Morton *et al.*, 2011)) shows confusion over the separation of *'Bog'* and *'Dwarf Shrub Heath'*, however, this only affects the separation of these two BHs and they are often difficult to separate in the field. Note, the Broad Habitat classification treats ericaceous vegetation on peat > 0.5 m depth as *'Bog'*. A soil map showing peat-soils is used to distinguish heaths from ericaceous bogs.

'Fen, Marsh and Swamp'	*'Fen, Marsh and Swamp'* includes fen, fen meadows, rush pasture, swamp, flushes and springs. From a remote sensing perspective *'Fen, Marsh and Swamp'* is problematic as it is can be comprised of a wide range of land cover types and many patches of Fen are below the LCM2007 MMU. The small size of *'Fen, Marsh and Swamp'* patches, plus their typically mosaic nature make it difficult to find representative areas of sufficient size to conduct a spectral classification. Soil data is of limited use in assisting as it shows the historical land cover, so large swathes of East Anglia have a peaty, fen soil, but subsequent drainage and management have changed them to arable.
'Bog'	*'Bog'* includes ericaceous, herbaceous and mossy swards in areas with a peat depth > 0.5 m. *'Bog'* forms part of an ecological continuum covering *'Acid Grassland'*, *'Dwarf Shrub Heath'* and some types of *'Fen, Marsh and Swamp'* and the separation of these habitats can be difficult, as the surface vegetation (i.e. land cover) maybe very similar and the division rests on the depth of peat. The division in the field can account for species presence, plus peat depth, but for LCM2007 the division is based on soil data sets.
Saltwater	Saltwater is mapped to a limited extent around the coastline of the UK.
Freshwater	This is based on merging two freshwater BHs (*'Standing Open Water and Canals'* and *'Rivers and Streams'*), as they cannot be reliably separated from each other using the methods and data used for LCM2007. In many cases small and/or narrow water bodies fall below the MMU. Water bodies > 0.5 ha are readily mapped, as are very wide rivers (>50 m).
'Montane Habitats'	The montane distribution for LCM2007 is assigned based on altitude (see Section 3.7 of Morton *et al.*, 2011), whereas the Broad Habitat definition is based on vegetation type. The Broad Habitat definitions produced by JNCC note (Jackson, 2000) that if other habitats, such as *'Calcareous Grassland'* and *'Bog'*, occur within the *'Montane Habitats'* zone they should not be recorded as *'Montane Habitats'*. In the production of LCM2007 it was not possible to determine whether a *'Montane Habitats'* reclassification based on altitude has greater validity than the original spectral classification. This should be taken into account by users interested specifically in the *'Montane Habitats'* class. LCM2007 above the montane altitude LCM2007 maps three Broad habitats: *'Montane Habitats'*, **Freshwater** and *'Inland Rock'*.
'Inland Rock'	This Broad Habitat type covers both natural and artificial exposed rock surfaces which are >0.25ha, such as inland cliffs, caves, screes and limestone pavements, as well as various forms of excavations and waste tips such as quarries and quarry waste. To be classified as *'Inland Rock'* the rock has to be the dominant spectral signature.
'Urban' and 'Suburban' (together form the *'Built-up*	Within the *'Built-up Areas and Gardens'* Broad Habitat LCM2007 recognises two categories that can be determined reliably: 'Urban' and 'Suburban'. 'Urban' includes dense urban, such as town and city centres, where there is typically little vegetation. 'Urban' also includes areas such as dock sides, car parks and industrial estates.

Areas and Gardens' Broad Habitat)	'Suburban' includes suburban areas where the spectral signature is a mix of urban and vegetation signatures.
'*Supra-littoral Rock*'	Features that may be present in this coastal class include vertical rock, boulders, gullies, ledges and pools. Very limited areas are mappable using satellite remote sensing.
'*Supra-littoral Sediment*'	This class includes sand-dunes, which are reliably mapped in this class. Areas of coastal sand may be confused between this class and the 'Littoral sediment' class.
'*Littoral Rock*'	These classes are those in the maritime mask zone on a rocky coastline. They are generally more extensive than supra-littoral rock and thus more readily mappable from satellite images.
'Littoral sediment' and 'Saltmarsh' (together form the '*Littoral Sediment*' Broad Habitat)	Littoral sediment is mapped as two classes: 'Saltmarsh' and 'Littoral sediment'. Saltmarsh is a Priority Habitat and of sufficient extent and spectral distinction to be mapped consistently. The remaining 'Littoral Sediment' is mapped spectrally, although there maybe some confusion with the 'Supra-littoral sediment' class.

Figure 7.2: Description of LCM aggregate classes.

Table 7.1: Erosion estimates from GIS overlay data for all WFD sub-catchments. Table continued on next page.

Number	Channel	Erosion (kg ha^{-1} yr^{-1})	Retreat rate (m yr^{-1})	Width averaged retreat rate (m m^{-1} yr^{-1})
1	Avon	450	0.1660	0.0065
2	Avon	58	0.1296	0.0052
3	Avon	555	0.1429	0.0055
4	Avon	409	0.1350	0.0072
5	Bourne	120	0.1234	0.0138
6	Ebble	419	0.1104	0.0128
7	Nadder	775	0.1262	0.0065
8	Nadder	316	0.0774	0.0084
9	Nadder	996	0.1228	0.0101
10	Wylye	686	0.1142	0.0082
11	Wylye	9	0.0805	0.0080
12	Wylye	153	0.0709	0.0061
13	Exe	1327	0.1269	0.0048
14	Exe	1207	0.0765	0.0041
15	Exe	116	0.1191	0.0033
16	Exe	3029	0.1127	0.0042
17	Exe	702	0.1632	0.0132
18	Exe	1364	0.0978	0.0064
19	Creedy	1310	0.1375	0.0088
20	Creedy	671	0.0790	0.0096

Number	Channel	Erosion (kg ha^{-1} yr^{-1})	Retreat rate (m yr^{-1})	Width averaged retreat rate (m m^{-1} yr^{-1})
21	Culm	1434	0.1129	0.0101
22	Culm	692	0.1153	0.0130
23	Eye	1389	0.0863	0.0072
24	Ouse	151	0.0572	0.0069
25	Ouse	867	0.1149	0.0031
26	Ouse	1394	0.0956	0.0061
27	Ouse	1000	0.0670	0.0079
28	Ouse	1113	0.1022	0.0024
29	Ouse	527	0.1103	0.0035
30	Ouse	1673	0.1638	0.0044
31	Swale	3321	0.0993	0.0045
32	Swale	2336	0.2291	0.0081
33	Swale	406	0.0858	0.0035
34	Nidd	400	0.1257	0.0064
35	Nidd	1391	0.0987	0.0053
36	Nidd	431	0.0840	0.0035
37	Wharf	155	0.0474	0.0082
38	Wharf	522	0.0797	0.0021
39	Wharf	1130	0.1137	0.0034
40	Stour	147	0.0764	0.0085
41	Stour	294	0.0679	0.0052
42	East Stour	247	0.0544	0.0089
43	East Stour	17	0.0706	0.0082
44	Little Stour	144	0.0966	0.0108
45	Sarre Penn	186	0.0819	0.0131
46	Test	153	0.0933	0.0053
47	Test	48	0.0707	0.0036
48	Test	53	0.0898	0.0058
49	Test	118	0.0833	0.0049
50	Itchen	83	0.1273	0.0105
51	Itchen	214	0.0901	0.0062
52	Itchen	153	0.0730	0.0049
53	Wye	581	0.0587	0.0040
54	Wye	1708	0.0495	0.0011
55	Wye	198	0.0279	0.0008
56	Wye	1292	0.0594	0.0013
57	Wye	1319	0.0754	0.0015
58	Wye	1354	0.0611	0.0013
59	Wye	2081	0.1081	0.0021
60	Munnow	1054	0.0909	0.0050
61	Munnow	250	0.0417	0.0044
62	Munnow	931	0.1117	0.0096
63	Lugg	718	0.0563	0.0034
64	Lugg	2683	0.0997	0.0078
65	Lugg	71	0.1270	0.0079

Table 7.2: Estimated values of upstream area, sinuosity, slope and confinement for each WFD. Table continued on next page.

Number	Channel	Upstream Catchment area (km^2)	Average Sinuosity	Slope
1	Avon	24	2.1115	0.00230
2	Avon	117	1.5613	0.00000
3	Avon	1717	1.8938	0.00131
4	Avon	397	1.8604	0.00186
5	Bourne	174	1.6260	0.00291
6	Ebble	117	1.4586	0.00320
7	Nadder	684	1.6425	0.00155
8	Nadder	69	1.7095	0.00295
9	Nadder	214	1.6972	0.00229
10	Wylye	454	1.3446	0.00085
11	Wylye	83	1.5239	0.00224
12	Wylye	309	1.4277	0.00250
13	Exe	626	1.5307	0.00326
14	Exe	265	1.2393	0.00682
15	Exe	1235	1.1698	0.00159
16	Exe	912	1.3604	0.00159
17	Exe	48	1.5468	0.00776
18	Exe	90	1.3445	0.00724
19	Creedy	271	1.3972	0.00244
20	Creedy	91	1.4559	0.00399
21	Culm	281	1.4321	0.00314
22	Culm	86	1.3032	0.00590
23	Eye	339	1.5740	0.00138
24	Ouse	60	1.2859	0.00000
25	Ouse	991	1.4938	0.00044
26	Ouse	2319	1.5490	0.00019
27	Ouse	4605	1.8542	0.00203
28	Ouse	3522	1.4056	0.00018
29	Ouse	515	1.4758	0.00347
30	Ouse	711	1.7342	0.00343
31	Swale	876	1.7103	0.00000
32	Swale	644	1.6506	0.00541
33	Swale	3522	1.6177	0.00000
34	Nidd	219	1.4271	0.00335
35	Nidd	530	2.4041	0.00077
36	Nidd	365	1.6389	0.00207
37	Wharf	4605	1.7382	0.00203
38	Wharf	528	1.32038	0.00212
39	Wharf	973	1.5203	0.00204
40	Stour	71	1.7460	0.00282
41	Stour	374	1.4383	0.00143
42	East Stour	71	1.3738	0.00203

Number	Channel	Upstream Catchment area (km^2)	Average Sinuosity	Slope
43	East Stour	374	1.1118	0.01945
44	Little Stour	207	1.2713	0.00248
45	Sarre Penn	52	1.3261	0.00107
46	Test	864	1.2234	0.00107
47	Test	342	1.2238	0.00158
48	Test	178	1.3924	0.00331
49	Test	482	1.4690	0.00143
50	Itchen	75	1.2931	0.00377
51	Itchen	414	1.6380	0.00253
52	Itchen	38	1.6671	0.00000
53	Wye	78	1.5045	0.00000
54	Wye	828	1.5298	0.00760
55	Wye	437	1.4155	0.00658
56	Wye	1975	1.4791	0.00090
57	Wye	3262	2.5434	0.00103
58	Wye	4057	2.2984	0.00135
59	Wye	1789	1.9649	0.00209
60	Munnow	435	2.0059	0.00429
61	Munnow	24	1.2810	0.06401
62	Munnow	80	1.4245	0.00160
63	Lugg	890	1.9440	0.00379
64	Lugg	377	1.7842	0.00371
65	Lugg	3262	1.4147	0.00329

Table 7.3: Estimated values of channel confinement. The numbered version of confinement relates to the numbered confinement methodology outlined in the previous section. Values shown in red are below the threshold value of 3.8 and can therefore be classified as confined. Table continued on next page.

Number	Channel	CC1	CC2	CC3	CC4
1	Avon	3.83	1.82	0.57	0.60
2	Avon	8.08	1.29	1.21	1.28
3	Avon	10.51	5.55	1.58	1.65
4	Avon	8.98	4.83	1.34	1.47
5	Bourne	6.86	4.22	1.02	1.23
6	Ebble	23.40	16.04	3.47	4.20
7	Nadder	20.56	12.52	3.07	3.35
8	Nadder	6.50	3.80	0.97	1.16
9	Nadder	15.10	8.90	2.25	2.60
10	Wylye	13.97	10.39	2.08	2.36
11	Wylye	4.12	2.70	0.61	0.72
12	Wylye	14.19	9.94	2.11	2.47
13	Exe	8.98	5.86	1.35	1.41
14	Exe	9.79	7.90	1.46	1.60
15	Exe	6.13	5.24	0.92	0.93
16	Exe	12.07	8.87	1.81	1.89
17	Exe	5.21	3.36	0.77	0.89
18	Exe	6.63	4.93	0.99	1.11
19	Creedy	13.98	10.01	2.09	2.34
20	Creedy	22.05	15.14	3.27	3.98
21	Culm	17.48	12.20	2.60	3.04
22	Culm	22.81	17.51	3.38	4.08
23	Eye	15.83	10.06	2.36	2.73
24	Ouse	14.39	11.19	2.13	2.60
25	Ouse	6.81	4.56	1.03	1.03
26	Ouse	26.98	17.42	4.03	4.51
27	Ouse	35.65	19.23	5.29	6.41
28	Ouse	6.36	4.52	0.96	0.94
29	Ouse	5.97	4.05	0.90	0.92
30	Ouse	4.27	2.46	0.64	0.64
31	Swale	13.24	7.74	1.98	2.13
32	Swale	6.04	3.66	0.91	0.94
33	Swale	11.32	7.00	1.70	1.80
34	Nidd	4.33	3.03	0.65	0.70
35	Nidd	7.17	2.98	1.07	1.17
36	Nidd	4.50	2.74	0.67	0.71
37	Wharf	52.40	30.15	7.74	9.87
38	Wharf	3.88	2.94	0.58	0.58
39	Wharf	8.24	5.42	1.24	1.26

Number	Channel	CC1	CC2	CC3	CC4
40	Stour	22.65	12.97	3.36	4.05
41	Stour	9.92	6.90	1.48	1.70
42	East Stour	21.89	15.94	3.24	4.10
43	East Stour	14.92	13.42	2.21	2.68
44	Little Stour	16.93	13.32	2.51	3.03
45	Sarre Penn	98.11	73.99	14.50	18.31
46	Test	3.37	2.76	0.50	0.56
47	Test	2.87	2.35	0.43	0.47
48	Test	1.83	1.32	0.27	0.31
49	Test	3.37	2.30	0.50	0.56
50	Itchen	3.34	2.59	0.50	0.58
51	Itchen	10.20	6.23	1.52	1.72
52	Itchen	4.63	2.78	0.69	0.78
53	Wye	5.64	3.75	0.84	0.95
54	Wye	4.54	2.97	0.68	0.67
55	Wye	2.28	1.61	0.34	0.35
56	Wye	4.42	2.99	0.67	0.65
57	Wye	6.51	2.56	0.98	0.95
58	Wye	2.38	1.03	0.36	0.35
59	Wye	4.80	2.44	0.72	0.69
60	Munnow	6.96	3.47	1.04	1.14
61	Munnow	3.16	2.47	0.47	0.56
62	Munnow	6.94	4.87	1.03	1.20
63	Lugg	10.35	5.32	1.54	1.72
64	Lugg	10.31	5.78	1.53	1.77
65	Lugg	20.22	14.29	3.02	3.37

Table 7.4: Distribution of variables.

Erosion kg/ha/yr

N	Valid	65
	Missing	0
Mean		796.57
Median		555.00
Mode		153
Skewness		1.392
Std. Error of Skewness		.297
Kurtosis		2.016
Std. Error of Kurtosis		.586
Minimum		16
Maximum		3321

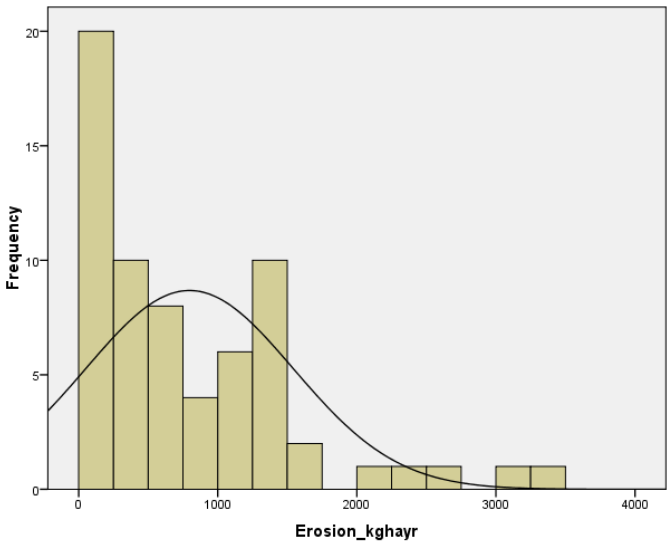

Retreat rate m/yr

N	Valid	65
	Missing	0
Mean		.1010077
Median		.0978000
Mode		.02790[a]
Skewness		.813
Std. Error of Skewness		.297
Kurtosis		1.382
Std. Error of Kurtosis		.586
Minimum		.02790
Maximum		.22910

a. Multiple modes exist. The smallest value is shown

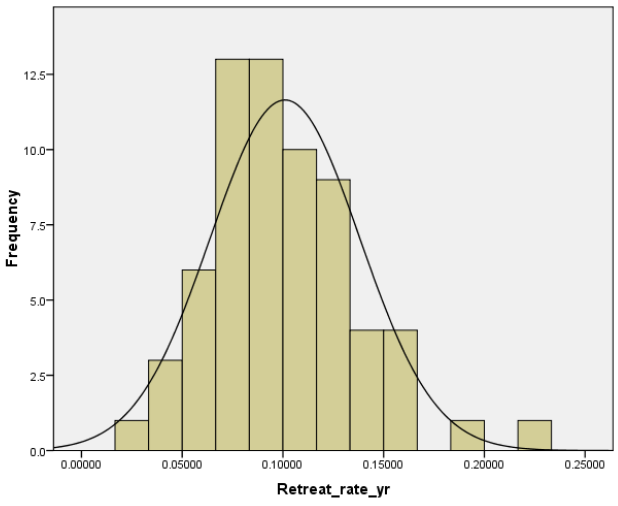

Width average retreat rate m/yr

N	Valid	65
	Missing	0
Mean		.0065723
Median		.0061000
Mode		.00350
Skewness		.530
Std. Error of Skewness		.297
Kurtosis		-.494
Std. Error of Kurtosis		.586
Minimum		.00080
Maximum		.01400

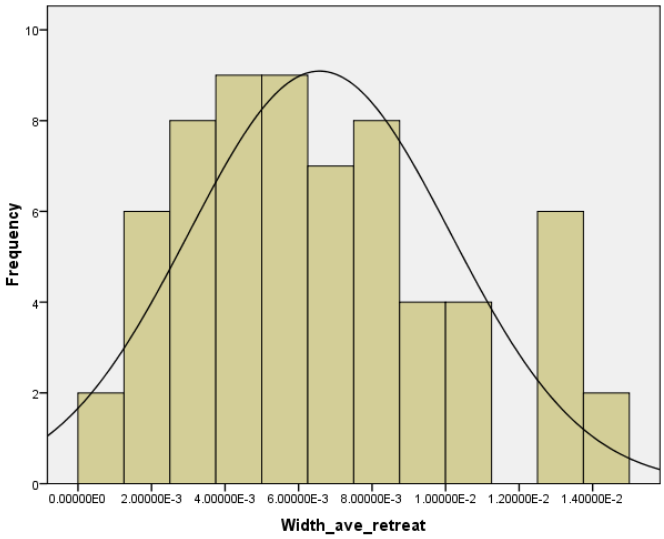

Sinuosity

N	Valid	65
	Missing	0
Mean		1.5661689E0
Median		1.5045000E0
Mode		1.11180E0[a]
Skewness		1.341
Std. Error of Skewness		.297
Kurtosis		2.238
Std. Error of Kurtosis		.586
Minimum		1.11180
Maximum		2.54340

a. Multiple modes exist. The smallest value is shown

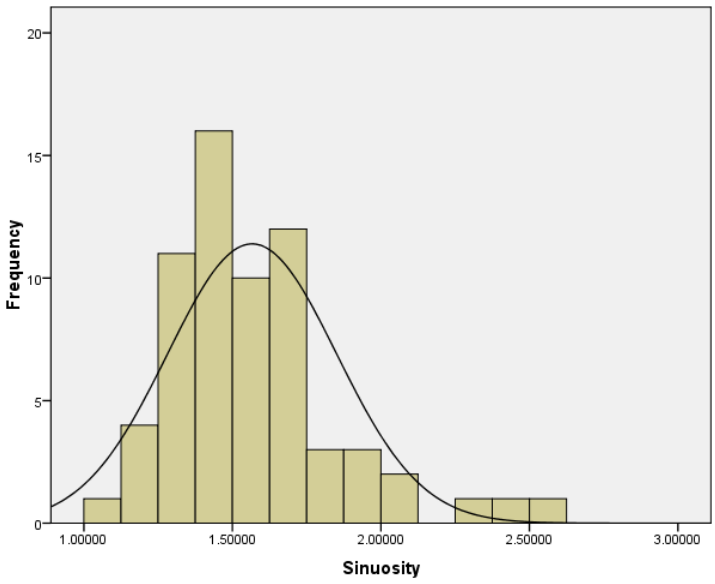

Slope

N	Valid	65
	Missing	0
Mean		.0036894
Median		.0021200
Mode		.00000
Skewness		6.747
Std. Error of Skewness		.297
Kurtosis		49.725
Std. Error of Kurtosis		.586
Minimum		.00000
Maximum		.06401

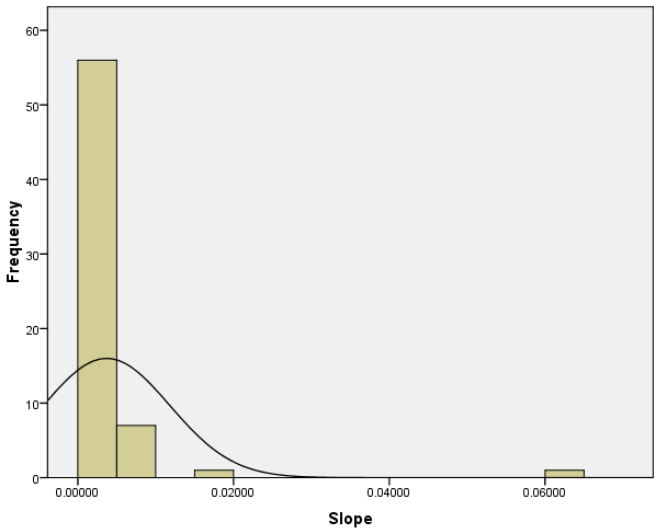

Upstream catchment area km^2

N	Valid	65
	Missing	0
Mean		840.37
Median		377.00
Mode		24[a]
Skewness		2.056
Std. Error of Skewness		.297
Kurtosis		3.339
Std. Error of Kurtosis		.586
Minimum		24
Maximum		4605

a. Multiple modes exist. The smallest value is shown

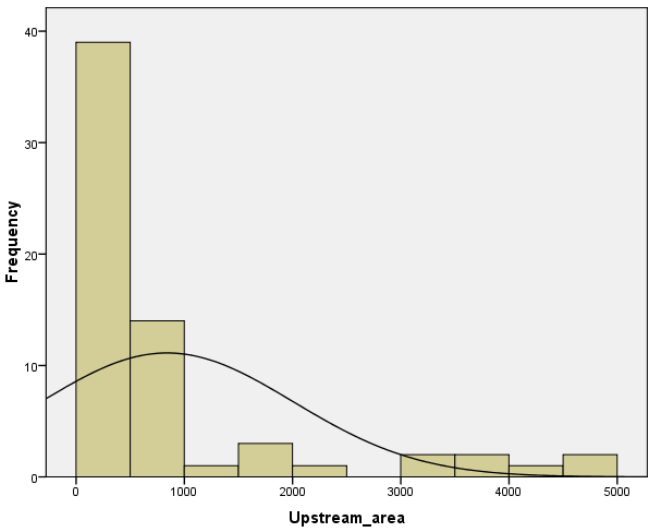

CC1

N	Valid	65
	Missing	0
Mean		12.1715
Median		8.0800
Mode		3.37[a]
Skewness		4.231
Std. Error of Skewness		.297
Kurtosis		23.188
Std. Error of Kurtosis		.586
Minimum		1.83
Maximum		98.11

a. Multiple modes exist. The smallest value is shown

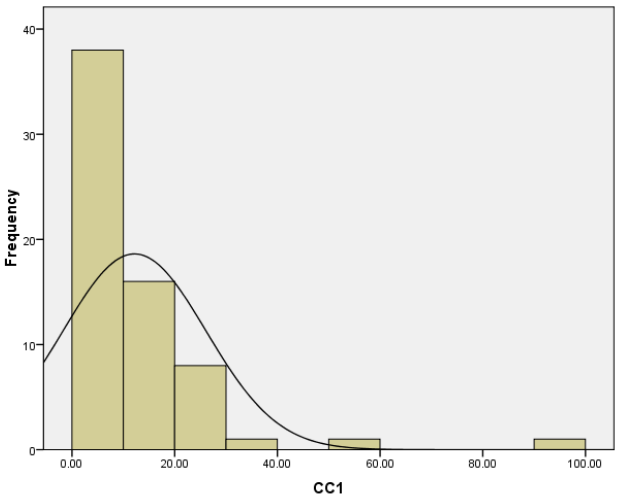

CC2

N	Valid	65
	Missing	0
Mean		8.0398
Median		4.9300
Mode		1.03[a]
Skewness		4.797
Std. Error of Skewness		.297
Kurtosis		29.753
Std. Error of Kurtosis		.586
Minimum		1.03
Maximum		73.99

a. Multiple modes exist. The smallest value is shown

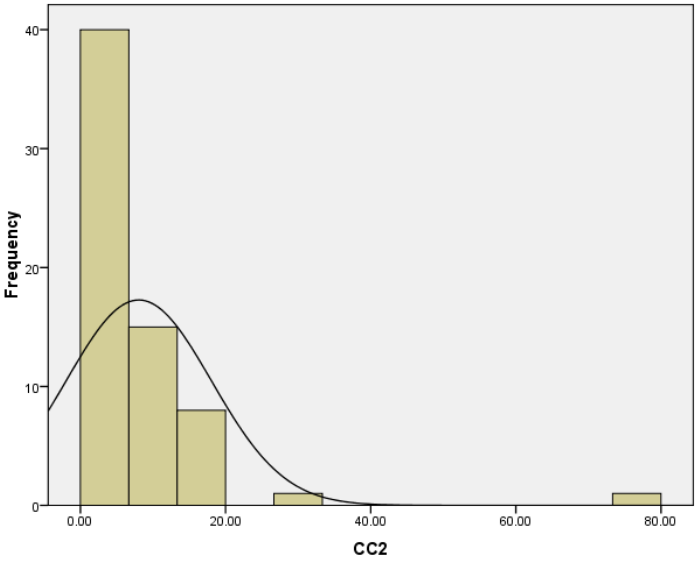

CC3

N	Valid	65
	Missing	0
Mean		1.8112
Median		1.2100
Mode		.50
Skewness		4.216
Std. Error of Skewness		.297
Kurtosis		23.076
Std. Error of Kurtosis		.586
Minimum		.27
Maximum		14.50

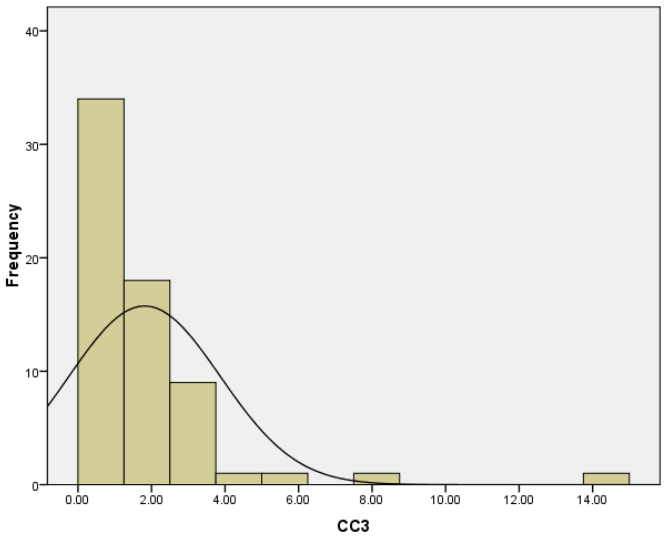

CC4

N	Valid	65
	Missing	0
Mean		2.1003
Median		1.2600
Mode		.56
Skewness		4.357
Std. Error of Skewness		.297
Kurtosis		24.108
Std. Error of Kurtosis		.586
Minimum		.31
Maximum		18.31

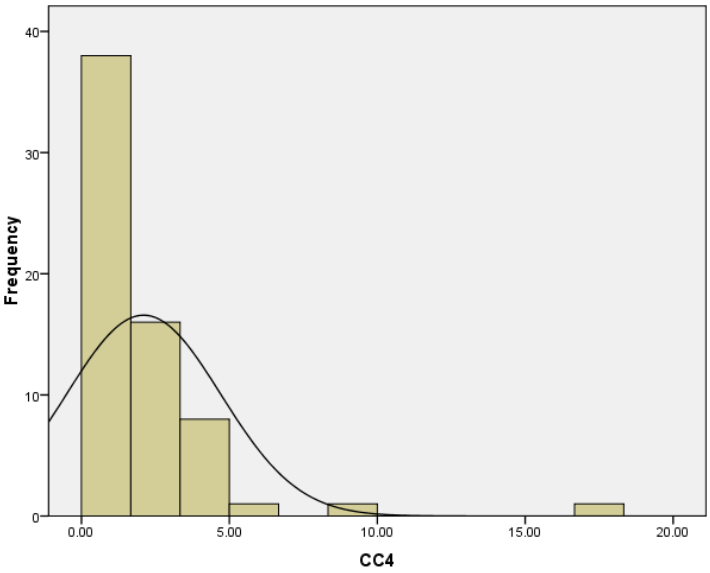

LOG Erosion kg/ha/yr

N	Valid	65
	Missing	0
Mean		2.6593
Median		2.7443
Mode		2.18
Skewness		-.705
Std. Error of Skewness		.297
Kurtosis		.039
Std. Error of Kurtosis		.586
Minimum		1.20
Maximum		3.52

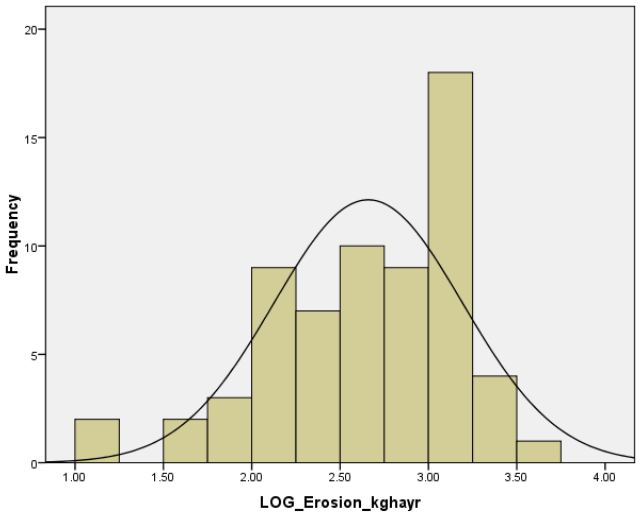

LOG Sinuosity

N	Valid	65
	Missing	0
Mean		.1885
Median		.1774
Mode		.05[a]
Skewness		.799
Std. Error of Skewness		.297
Kurtosis		.789
Std. Error of Kurtosis		.586
Minimum		.05
Maximum		.41

a. Multiple modes exist. The smallest value is shown

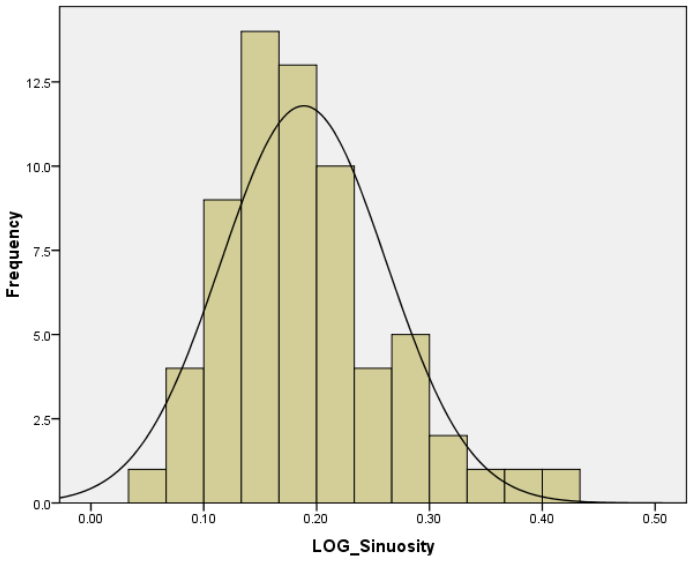

LOG Slope (+0.0001)

N	Valid	65
	Missing	0
Mean		-2.7267
Median		-2.6536
Mode		-4.00
Skewness		-.759
Std. Error of Skewness		.297
Kurtosis		1.684
Std. Error of Kurtosis		.586
Minimum		-4.00
Maximum		-1.19

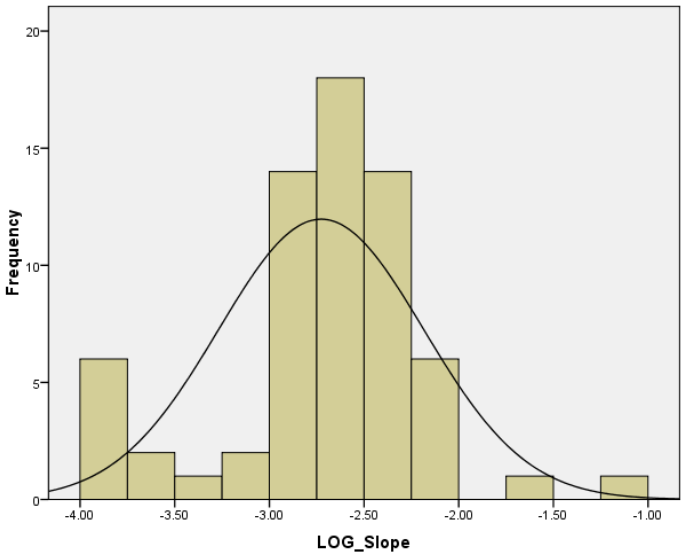

LOG Upstream area

N	Valid	65
	Missing	0
Mean		2.5619
Median		2.5763
Mode		1.38[a]
Skewness		.027
Std. Error of Skewness		.297
Kurtosis		-.677
Std. Error of Kurtosis		.586
Minimum		1.38
Maximum		3.66

a. Multiple modes exist. The smallest value is shown

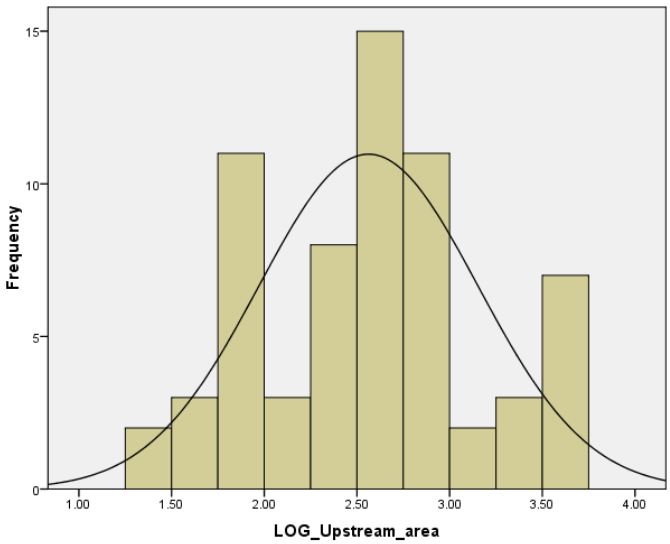

LOG CC1

N	Valid	65
	Missing	0
Mean		.9369
Median		.9074
Mode		.53[a]
Skewness		.506
Std. Error of Skewness		.297
Kurtosis		.407
Std. Error of Kurtosis		.586
Minimum		.26
Maximum		1.99

a. Multiple modes exist. The smallest value is shown

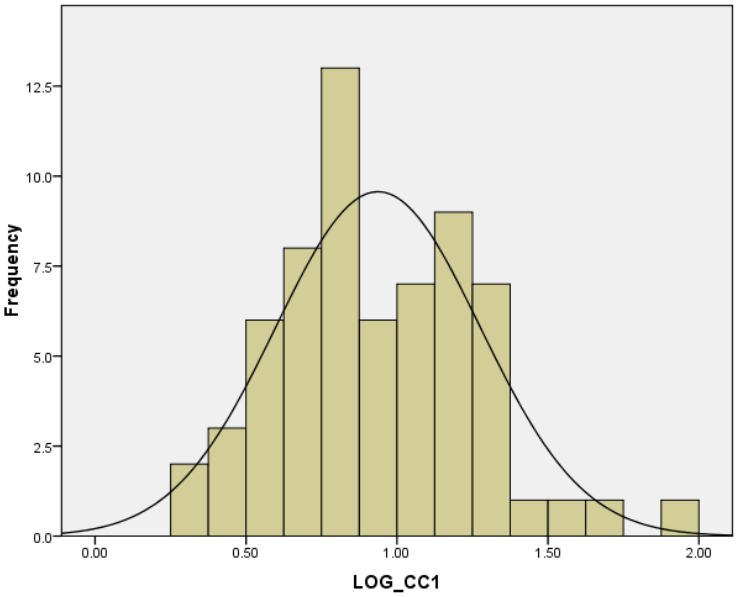

LOG CC2

N	Valid	65
	Missing	0
Mean		.7392
Median		.6928
Mode		.01[a]
Skewness		.466
Std. Error of Skewness		.297
Kurtosis		.274
Std. Error of Kurtosis		.586
Minimum		.01
Maximum		1.87

a. Multiple modes exist. The smallest value is shown

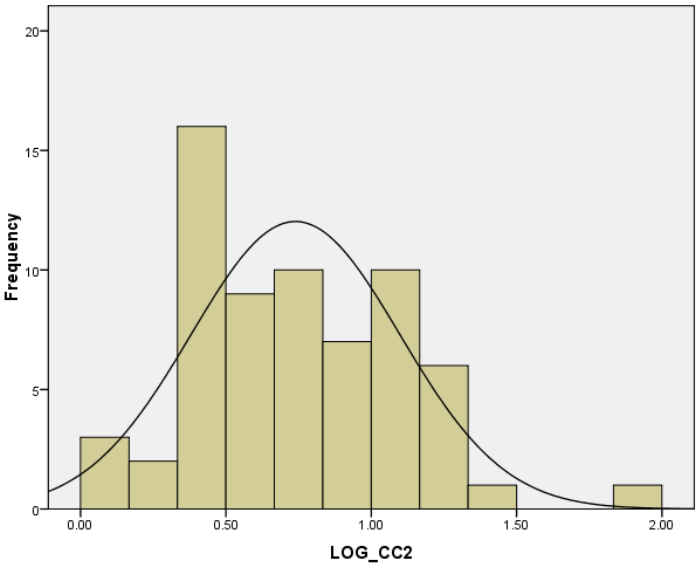

LOG CC3

N	Valid	65
	Missing	0
Mean		.1107
Median		.0828
Mode		-.30
Skewness		.496
Std. Error of Skewness		.297
Kurtosis		.405
Std. Error of Kurtosis		.586
Minimum		-.57
Maximum		1.16

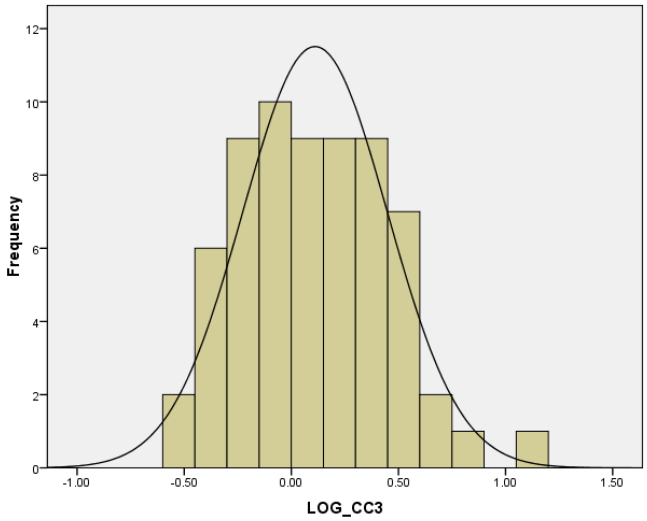

LOG CC4

N	Valid	65
	Missing	0
Mean		.1555
Median		.1004
Mode		-.25
Skewness		.558
Std. Error of Skewness		.297
Kurtosis		.375
Std. Error of Kurtosis		.586
Minimum		-.51
Maximum		1.26

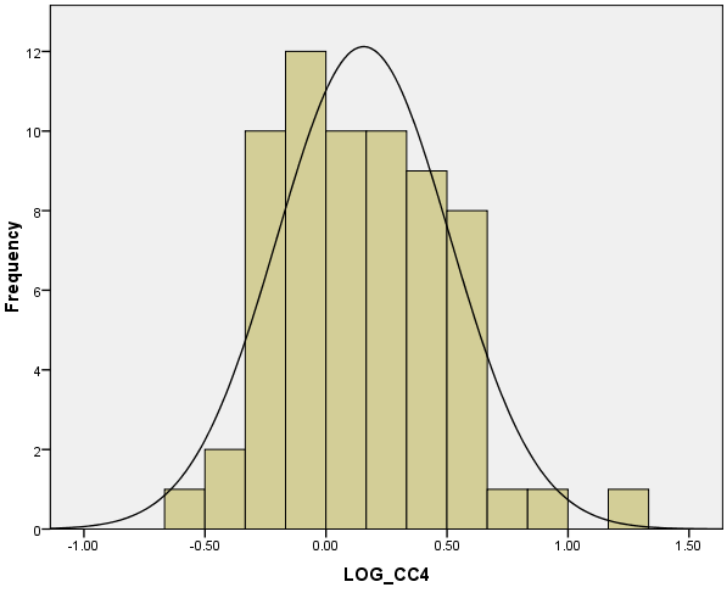

Table 7.5: Residuals from regression of erosion rate (kg/ha/yr). Table continued on next page.

Number	Channel	WFD	Standardized Residual
11	Wylye	33	-3.12
43	East	8	-2.14
65	Lugg	23	-1.80
37	Warf	10	-1.63
2	Avon	9	-1.60
48	Test	18	-1.51
47	Test	17	-1.43
5	Bour	23	-1.13
49	Test	22	-1.10
40	Stou	7	-0.94
50	Itch	6	-0.80
51	Itch	7	-0.79
15	Exe	8	-0.79
12	Wyly	36	-0.73
52	Itch	30	-0.70
33	Swal	17	-0.58
46	Test	14	-0.58
55	Wye	20	-0.55
3	Avon	10	-0.52
57	Wye	23	-0.52
4	Avon	19	-0.49
44	Litt	3	-0.46
58	Wye	24	-0.32
63	Lugg	4	-0.24
24	Ouse	2	-0.22
8	Nadd	17	-0.22
41	Stou	8	-0.21
1	Avon	5	-0.19
36	Nidd	21	-0.16
27	Ouse	10	-0.14
45	Sarr	5	-0.08
35	Nidd	20	-0.03
42	East	6	0.03
60	Munn	1	0.16
34	Nidd	19	0.17
29	Ouse	22	0.19
7	Nadd	13	0.24
6	Ebbl	9	0.28
61	Munn	6	0.39
38	Warf	24	0.42
25	Ouse	7	0.48
59	Wye	25	0.55
53	Wye	3	0.57
9	Nadd	29	0.60

Number	Channel	WFD	Standardized Residual
28	Ouse	17	0.61
10	Wyly	32	0.64
26	Ouse	9	0.67
39	Warf	25	0.68
56	Wye	22	0.73
20	Cree	14	0.74
17	Exe	11	0.76
30	Ouse	23	0.79
13	Exe	1	0.88
23	Eye	58	0.97
22	Culm	3	1.01
54	Wye	15	1.05
62	Munn	27	1.09
32	Swal	15	1.21
19	Cree	13	1.22
21	Culm	2	1.24
64	Lugg	18	1.25
31	Swal	13	1.38
14	Exe	7	1.41
18	Exe	12	1.53
16	Exe	10	1.79

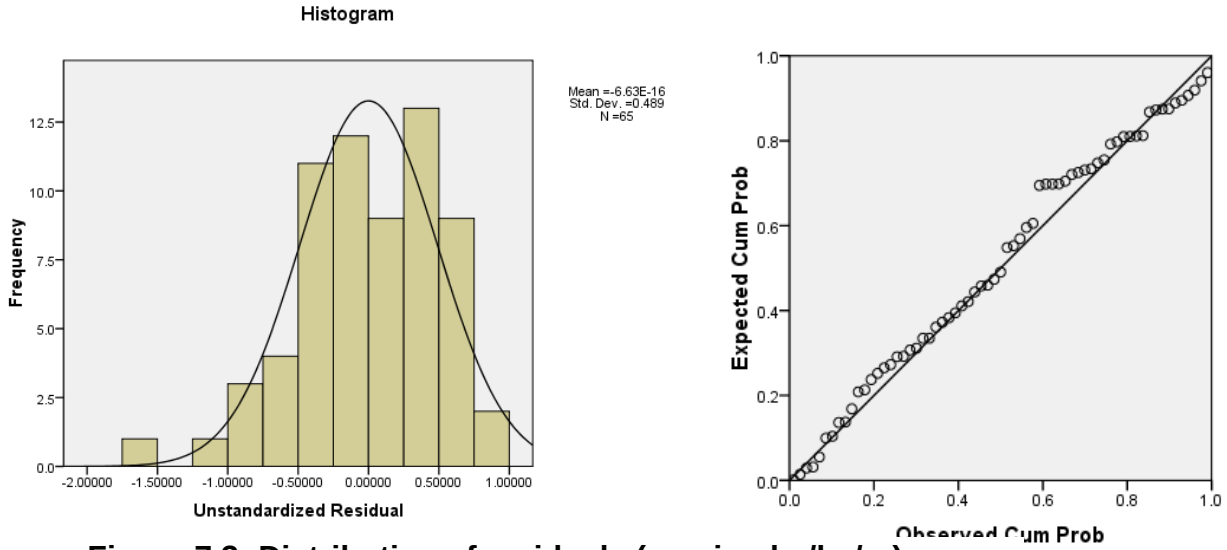

Figure 7.3: Distribution of residuals (erosion kg/ha/yr).

Table 7.6: Residuals Width averaged retreat rate (m m yr^{-1}). Table continued on next page.

Number	Channel	WFD	Standardized Residual
61	Munn	6	-2.19
14	Exe	7	-1.66
54	Wye	15	-1.54
63	Lugg	4	-1.32
55	Wye	20	-1.27
40	Stou	7	-1.14
12	Wyly	36	-0.88
42	East	6	-0.86
53	Wye	3	-0.84
38	Warf	24	-0.84
29	Ouse	22	-0.81
16	Exe	10	-0.79
39	Warf	25	-0.75
18	Exe	12	-0.74
24	Ouse	2	-0.70
41	Stou	8	-0.66
36	Nidd	21	-0.61
52	Itch	30	-0.59
57	Wye	23	-0.58
13	Exe	1	-0.54
45	Sarr	5	-0.54
1	Avon	5	-0.52
20	Cree	14	-0.50
60	Munn	1	-0.50
7	Nadd	13	-0.49
56	Wye	22	-0.44
59	Wye	25	-0.39
2	Avon	9	-0.37
25	Ouse	7	-0.33
23	Eye	58	-0.28
43	East	8	-0.27
51	Itch	7	-0.27
15	Exe	8	-0.23
31	Swal	13	-0.17
47	Test	17	-0.03
26	Ouse	9	0.07
35	Nidd	20	0.09
37	Warf	10	0.12
30	Ouse	23	0.21
8	Nadd	17	0.22
28	Ouse	17	0.30
33	Swal	17	0.32
64	Lugg	18	0.34

Number	Channel	WFD	Standardized Residual
3	Avon	10	0.37
4	Avon	19	0.44
19	Cree	13	0.45
34	Nidd	19	0.46
27	Ouse	10	0.46
58	Wye	24	0.54
49	Test	22	0.60
10	Wyly	32	0.67
11	Wyly	33	0.75
21	Culm	2	0.75
9	Nadd	29	0.83
65	Lugg	23	0.92
48	Test	18	0.98
44	Litt	3	0.99
62	Munn	27	1.01
22	Culm	3	1.04
6	Ebbl	9	1.20
46	Test	14	1.21
32	Swal	15	1.44
50	Itch	6	2.07
17	Exe	11	2.47
5	Bour	23	3.34

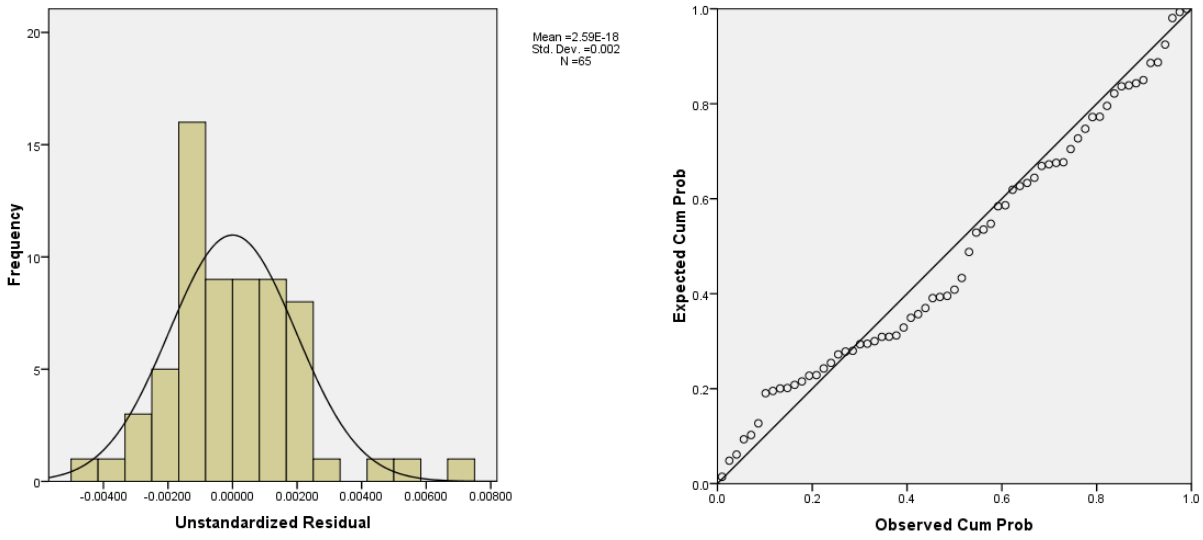

Figure 7.4: Distribution of residuals (width averaged retreat rate m m yr^{-1}).

Table 7.7: Residuals width averaged retreat rate m m yr^{-1} after case 61 removed. Table continued on next page.

Number	Channel	WFD	Standardized Residual
14	Exe	7	-1.94
54	Wye	15	-1.80
55	Wye	20	-1.56
63	Lugg	4	-1.42
40	Stou	7	-1.29
18	Exe	12	-1.04
42	East	6	-1.00
38	Warf	24	-0.99
12	Wyly	36	-0.98
29	Ouse	22	-0.97
16	Exe	10	-0.82
39	Warf	25	-0.81
53	Wye	3	-0.77
1	Avon	5	-0.75
36	Nidd	21	-0.72
41	Stou	8	-0.72
20	Cree	14	-0.66
13	Exe	1	-0.64
60	Munn	1	-0.62
24	Ouse	2	-0.60
45	Sarr	5	-0.55
52	Itch	30	-0.54
43	East	8	-0.54
57	Wye	23	-0.48
7	Nadd	13	-0.47
56	Wye	22	-0.42
59	Wye	25	-0.40
51	Itch	7	-0.33
23	Eye	58	-0.28
15	Exe	8	-0.28
25	Ouse	7	-0.26
2	Avon	9	-0.23
47	Test	17	-0.15
8	Nadd	17	0.07
31	Swal	13	0.11
30	Ouse	23	0.13
35	Nidd	20	0.17
64	Lugg	18	0.28
37	Warf	10	0.30
34	Nidd	19	0.31
26	Ouse	9	0.34
19	Cree	13	0.40
4	Avon	19	0.44
3	Avon	10	0.47

Number	Channel	WFD	Standardized Residual
28	Ouse	17	0.51
49	Test	22	0.57
11	Wyly	33	0.62
58	Wye	24	0.63
27	Ouse	10	0.65
33	Swal	17	0.68
21	Culm	2	0.71
10	Wyly	32	0.74
48	Test	18	0.81
9	Nadd	29	0.82
22	Culm	3	0.91
62	Munn	27	0.94
44	Litt	3	0.96
65	Lugg	23	1.01
6	Ebbl	9	1.17
46	Test	14	1.24
32	Swal	15	1.39
50	Itch	6	1.93
17	Exe	11	2.31
5	Bour	23	3.39

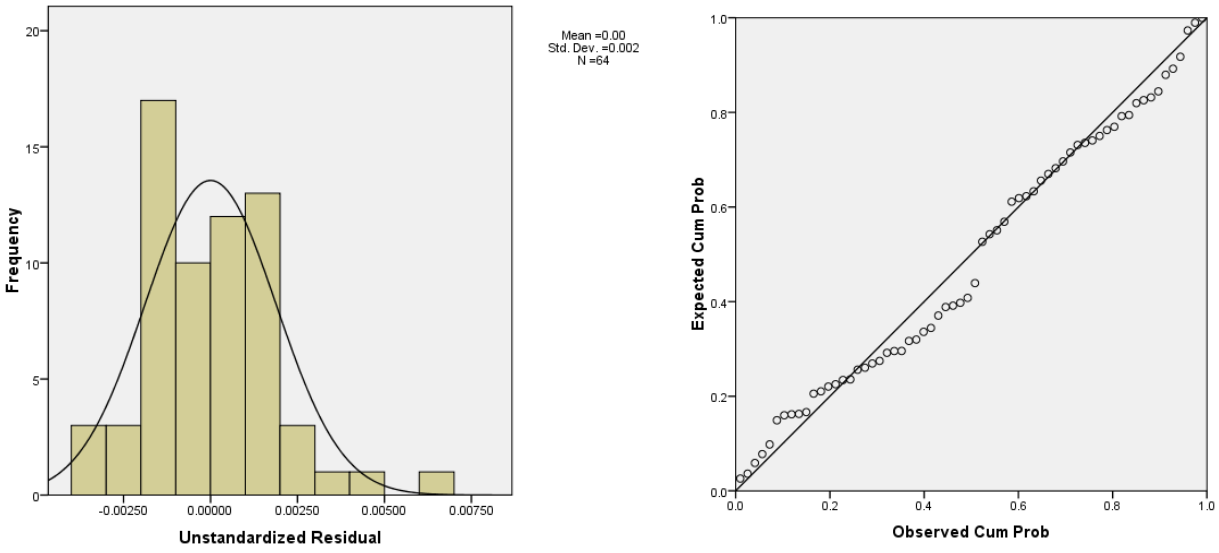

Figure 7.5: Distribution of residuals (width averaged retreat rate m m yr^{-1}) after case 61 removed.

7.2.Appendix B

Table 7.8: Combination of parameter sets used for the model within the calibration range. Average erosion, average sinuosity, and correlation for the period of dynamic equilibrium for each output is also shown. Table continued on next page.

E	Alpha	Gamma	CO	Ave E	Ave s	correl
0.3	0.5	1.5	2	0.016	1.302	0.437
0.3	0.5	2.0	2	0.011	1.282	0.754
0.3	0.6	1.5	2	0.014	1.291	0.309
0.3	0.6	2.0	2	0.010	1.270	0.193
0.4	0.5	1.5	2	0.021	1.292	0.628
0.4	0.5	2.0	2	0.015	1.278	0.252
0.4	0.6	1.5	2	0.019	1.293	0.447
0.4	0.6	2.0	2	0.012	1.266	0.300
0.3	0.5	1.5	3	0.015	1.575	-0.032
0.3	0.5	2.0	3	0.010	1.564	0.023
0.3	0.6	1.5	3	0.014	1.553	-0.335
0.3	0.6	2.0	3	0.009	1.509	-0.385
0.4	0.5	1.5	3	0.021	1.548	-0.124
0.4	0.5	2.0	3	0.015	1.544	-0.021
0.4	0.6	1.5	3	0.018	1.557	0.057
0.4	0.6	2.0	3	0.011	1.544	0.098
0.3	0.5	1.5	4	0.015	1.775	-0.500
0.3	0.5	2.0	4	0.010	1.790	-0.655
0.3	0.6	1.5	4	0.017	1.763	-0.238
0.3	0.6	2.0	4	0.009	1.784	-0.885
0.4	0.5	1.5	4	0.020	1.741	-0.470
0.4	0.5	2.0	4	0.014	1.734	-0.294
0.4	0.6	1.5	4	0.013	1.781	-0.181
0.4	0.6	2.0	4	0.011	1.783	-0.696
0.3	0.5	1.5	5	0.015	1.902	-0.555
0.3	0.5	2.0	5	0.009	1.898	-0.570
0.3	0.6	1.5	5	0.012	1.962	-0.582
0.3	0.6	2.0	5	0.008	1.893	-0.118
0.4	0.5	1.5	5	0.020	1.925	-0.492
0.4	0.5	2.0	5	0.013	1.921	-0.137
0.4	0.6	1.5	5	0.016	1.971	-0.678
0.4	0.6	2.0	5	0.011	1.933	-0.834
0.3	0.5	1.5	6	0.013	2.124	-0.616
0.3	0.5	2.0	6	0.010	2.203	-0.794
0.3	0.6	1.5	6	0.012	2.192	-0.591
0.3	0.6	2.0	6	0.008	1.997	-0.867
0.4	0.5	1.5	6	0.018	2.024	-0.291

E	Alpha	Gamma	CO	Ave E	Ave s	correl
0.4	0.5	2.0	6	0.012	2.045	-0.531
0.4	0.6	1.5	6	0.015	2.122	-0.600
0.4	0.6	2.0	6	0.010	2.105	-0.430
0.3	0.5	1.5	7	0.014	2.212	-0.706
0.3	0.5	2.0	7	0.009	2.244	-0.779
0.3	0.6	1.5	7	0.012	2.192	-0.720
0.3	0.6	2.0	7	0.012	2.269	-0.939
0.4	0.5	1.5	7	0.018	2.185	-0.522
0.4	0.5	2.0	7	0.012	2.130	-0.463
0.4	0.6	1.5	7	0.015	2.172	-0.718
0.4	0.6	2.0	7	0.011	2.197	-0.563
0.3	0.5	1.5	8	0.013	2.267	-0.543
0.3	0.5	2.0	8	0.008	2.296	-0.873
0.3	0.6	1.5	8	0.011	2.402	-0.235
0.3	0.6	2.0	8	0.007	2.138	-0.912
0.4	0.5	1.5	8	0.018	2.274	-0.612
0.4	0.5	2.0	8	0.011	2.247	-0.742
0.4	0.6	1.5	8	0.016	2.338	-0.388
0.4	0.6	2.0	8	0.009	2.335	-0.713
0.3	0.5	1.5	9	0.014	2.399	-0.851
0.3	0.5	2.0	9	0.009	2.521	-0.854
0.3	0.6	1.5	9	0.011	2.492	-0.903
0.3	0.6	2.0	9	0.007	2.483	-0.986
0.4	0.5	1.5	9	0.017	2.342	-0.331
0.4	0.5	2.0	9	0.019	2.364	-0.793
0.4	0.6	1.5	9	0.015	2.382	-0.434
0.4	0.6	2.0	9	0.010	2.346	-0.653

Table 7.9: Combination of parameter sets used for the model when run with a lower chute cut-off parameter. Average erosion, average sinuosity, and correlation for the period of dynamic equilibrium for each output is also shown.

E	Alpha	Gamma	CO	Ave E	Ave s	correl
0.4	0.6	2.0	1.5	0.011	1.152	0.534
0.4	0.6	2.0	1.2	0.008	1.061	0.615
0.4	0.6	2.0	1.3	0.011	1.126	0.273
0.4	0.6	2.0	1.4	0.010	1.095	0.657
0.4	0.6	2.0	1.1	0.006	1.032	0.750
0.3	0.6	2.0	1.5	0.009	1.149	0.627
0.3	0.6	2.0	1.4	0.008	1.126	0.560
0.3	0.6	2.0	1.3	0.008	1.097	0.827
0.3	0.6	2.0	1.2	0.006	1.060	0.928
0.3	0.6	2.0	1.1	0.005	1.031	0.861
0.4	0.6	2.0	1.6	0.012	1.172	0.588
0.4	0.6	2.0	1.7	0.013	1.205	0.732
0.4	0.6	2.0	1.8	0.013	1.239	0.549
0.4	0.6	2.0	1.9	0.012	1.258	0.055
0.3	0.6	2.0	1.6	0.009	1.167	0.690
0.3	0.6	2.0	1.7	0.009	1.205	0.577
0.3	0.6	2.0	1.8	0.010	1.232	0.641
0.3	0.6	2.0	1.9	0.010	1.237	0.629
0.3	0.5	1.5	1.9	0.017	1.270	0.674
0.3	0.5	1.5	1.8	0.016	1.233	0.581
0.3	0.5	1.5	1.7	0.015	1.212	0.558
0.3	0.5	1.5	1.6	0.015	1.182	0.607
0.3	0.5	1.5	1.5	0.014	1.152	0.723
0.3	0.5	1.5	1.4	0.013	1.118	0.752
0.3	0.5	1.5	1.3	0.011	1.089	0.658
0.3	0.5	1.5	1.2	0.010	1.059	0.800
0.3	0.5	1.5	1.1	0.007	1.029	0.679
0.4	0.5	1.5	1.9	0.022	1.266	0.509
0.4	0.5	1.5	1.8	0.021	1.253	0.404
0.4	0.5	1.5	1.7	0.021	1.214	0.719
0.4	0.5	1.5	1.6	0.020	1.178	0.704
0.4	0.5	1.5	1.5	0.018	1.146	0.679
0.4	0.5	1.5	1.4	0.017	1.116	0.703
0.4	0.5	1.5	1.3	0.016	1.087	0.733
0.4	0.5	1.5	1.2	0.013	1.059	0.688
0.4	0.5	1.5	1.1	0.010	1.030	0.679

7.3.Appendix C

Table 7.10: Largest 24 events for calibration period 1 (1/10/1993-30/9/2001) at station 45001.

Event no.	Obs Day	Obs Q	Sim Day	Sim Q	Error %	Day error
1	2587	218	2587	134.3	-38.4	0
2	454	203.5	454	118.3	-41.9	0
3	1857	183.7	1858	81.4	-55.7	-1
4	395	174.1	396	124.9	-28.3	-1
5	1850	172.2	1851	66.7	-61.3	-1
6	81	170.7	81	91.2	-46.6	0
7	2625	160	2626	87	-45.6	-1
8	2278	156	2278	82.1	-47.4	0
9	1556	149.7	1556	75.8	-49.4	0
10	484	143	485	98.3	-31.3	-1
11	2270	143	2271	111.2	-22.2	-1
12	2263	138	2263	79.6	-42.3	0
13	813	126.8	814	72.8	-42.6	-1
14	1231	124	1232	52.6	-57.6	-1
15	1937	122	1934	63.9	-47.6	3
16	1619	118.5	1619	47.6	-59.8	0
17	2593	114	2588	124.9	9.5	5
18	1913	112.9	1914	58.2	-48.4	-1
19	97	111	97	78.2	-29.5	0
20	1366	104.6	1366	31.5	-69.8	0
21	73	103.7	74	56	-46	-1
22	1520	103	1520	63.6	-38.2	0
23	1979	102	1981	49.2	-51.7	-2
24	405	96.4	406	78.2	-18.9	-1

Table 7.11: Largest 24 events for calibration period 2 (1/10/2003-30/9/2011) at station 45001.

Event no.	Obs Day	Obs Q	Sim Day	Sim Q	Error %	Day error
1	1802	174	1803	127.5	-26.7	-1
2	1530	150	1531	98.1	-34.6	-1
3	2662	148.3	2662	94.8	-36.1	0
4	74	140	74	111.6	-20.3	0
5	1744	121	1745	69.2	-42.8	-1
6	768	116	768	47.2	-59.3	0
7	104	115	104	97.9	-14.9	0
8	1568	109	1569	64	-41.3	-1
9	1152	105	1152	88.8	-15.4	0
10	2129	105	2130	82.2	-21.7	-1
11	1524	101	1529	80.1	-20.7	-5
12	2250	97.4	2252	77.4	-20.5	-2
13	2300	92.4	2301	39	-57.8	-1
14	1959	92.3	1960	57.4	-37.8	-1
15	1574	85.2	1569	64	-24.9	5
16	395	82.7	395	65.5	-20.8	0
17	1901	79.3	1901	58.2	-26.6	0
18	1253	79.2	1253	67.1	-15.3	0
19	1941	77.8	1942	65.3	-16.1	-1
20	1198	74.2	1198	67.2	-9.4	0
21	1779	73.1	1778	52	-28.9	1
22	795	71.5	796	51.6	-27.8	-1
23	2599	71	2601	42.7	-39.8	-2
24	446	69.5	446	72.4	4.2	0

Table 7.12: Largest 24 events for calibration period 1 (1/10/1993-30/9/2001) at station 45002.

Event no.	Obs Day	Obs Q	Sim Day	Sim Q	Error %	Day error
1	453	157.9	454	104.8	-33.6	-1
2	1857	137.6	1858	75.4	-45.2	-1
3	395	134.8	396	116.5	-13.6	-1
4	2587	132.6	2587	124.5	-6.1	0
5	1850	125.9	1851	60.8	-51.7	-1
6	81	108.5	81	73.6	-32.2	0
7	1556	103.9	1558	64.6	-37.9	-2
8	484	99.8	485	82.8	-17	-1
9	1618	99.3	1619	43	-56.7	-1
10	1231	98	1231	47.5	-51.5	0
11	2263	97.6	2263	67.1	-31.3	0
12	2278	97.6	2278	64.3	-34.1	0
13	2625	97.4	2626	76.3	-21.7	-1
14	2270	94.8	2271	99.1	4.6	-1
15	813	89.7	813	60.5	-32.5	0
16	1937	85.1	1934	57.1	-32.9	3
17	1913	82.6	1913	51.1	-38.2	0
18	1979	81.7	1980	39.4	-51.8	-1
19	1366	79.3	1366	28.5	-64.1	0
20	73	73.7	74	47.7	-35.2	-1
21	97	72.2	96	62.7	-13.1	1
22	1520	70.2	1520	56.1	-20.1	0
23	2593	69.9	2588	52.3	-25.3	5
24	185	69.3	186	83.4	20.4	-1

Table 7.13: Largest 24 events for calibration period 2 (1/10/2003-30/9/2011) at station 45002.

Event no.	Obs Day	Obs Q	Sim Day	Sim Q	Error %	Day error
1	1802	105	1803	117.6	12	-1
2	74	102.7	74	107	4.2	0
3	2662	101.8	2662	83.6	-17.8	0
4	1530	97.4	1531	87.1	-10.5	-1
5	104	77.5	104	87.5	12.9	0
6	768	77.2	768	42.9	-44.5	0
7	1744	76	1745	65.3	-14.1	-1
8	1151	70.1	1152	82.2	17.2	-1
9	2250	69.1	2251	60.5	-12.4	-1
10	1568	68.2	1568	51	-25.2	0
11	1524	66.6	1529	69	3.6	-5
12	2129	64.6	2130	79.9	23.7	-1
13	1574	61.9	1569	45	-27.4	5
14	1197	58.9	1198	57.3	-2.8	-1
15	2300	53.1	2300	29.7	-44.1	0
16	395	51.5	395	52.7	2.3	0
17	2599	51.3	2601	38.6	-24.7	-2
18	1253	50.8	1252	50.6	-0.3	1
19	1941	50.2	1941	52.2	4	0
20	501	47.8	501	51.3	7.4	0
21	1208	47.3	1206	43.7	-7.6	2
22	1779	47	1778	48.1	2.3	1
23	755	46.1	756	44.9	-2.6	-1
24	124	45.6	129	57.3	25.7	-5

Table 7.14: Largest 24 events for calibration period 1 (1/10/1993-30/9/2001) at station 45003.

Event no.	Obs Day	Obs Q	Sim Day	Sim Q	Error %	Day error
1	2625	66.5	2625	42.2	-36.5	0
2	81	56.9	80	28.1	-50.6	1
3	2587	56.1	2586	35.2	-37.3	1
4	405	48.7	404	22.3	-54.2	1
5	2278	45.3	2277	27.4	-39.4	1
6	2270	43.8	2270	26.1	-40.4	0
7	2593	43.1	2588	8.4	-80.5	5
8	1406	37.5	1405	11.2	-70.2	1
9	813	37.2	812	16.1	-56.8	1
10	1850	37	1850	8.9	-76	0
11	2377	36.8	2376	6.5	-82.4	1
12	1857	34	1857	13.9	-59.2	0
13	484	33.7	484	25.3	-24.8	0
14	1556	31.8	1557	20.1	-36.8	-1
15	97	31.4	96	24.2	-23.1	1
16	1937	29	1937	15.7	-45.7	0
17	1510	28.9	1509	13.9	-52	1
18	126	27.9	125	16.1	-42.3	1
19	2180	27.5	2179	20.7	-24.9	1
20	2031	27.4	2030	14.9	-45.6	1
21	830	26.9	830	21.4	-20.5	0
22	1520	25.6	1519	15.4	-39.8	1
23	1146	25.2	1145	7.4	-70.8	1
24	453	25.1	453	18.2	-27.6	0

Table 7.15: Largest 24 events for calibration period 2 (1/10/2003-30/9/2011) at station 45009.

Event no.	Obs Day	Obs Q	Sim Day	Sim Q	Error %	Day error
	1959	64	1959	26.6	-58.4	0
2	1857	53.4	1856	61.7	15.6	1
3	794	51.4	793	23.6	-54.1	1
4	1901	42.1	1900	25.4	-39.6	1
5	1530	39.3	1530	20.2	-48.6	0
6	1568	36.4	1567	18.6	-48.8	1
7	1802	36.3	1802	9.9	-72.8	0
8	104	35.5	103	18.4	-48.3	1
9	1251	34.4	1252	22.5	-34.7	-1
10	2300	31.8	2305	17.3	-45.7	-5
11	2605	29.9	2605	10.6	-64.7	0
12	768	27.2	767	6.4	-76.4	1
13	446	26	447	9.1	-65.2	-1
14	1703	25.3	1703	7.5	-70.3	0
15	1868	24.3	1868	19	-21.8	0
16	395	23.9	393	20.2	-15.7	2
17	1744	23.4	1744	4.5	-80.7	0
18	2246	22.8	2251	19.6	-13.9	-5
19	1623	21.5	1628	18.5	-14.2	-5
20	124	21.4	128	19.7	-7.8	-4
21	2333	21.2	2332	7.6	-64.2	1
22	2259	20.5	2258	17.8	-13.3	1
23	2306	20.5	2305	17.3	-15.7	1
24	1232	20.1	1232	14.7	-26.7	0

Table 7.16: Largest 24 events for calibration period 1 (1/10/1993-30/9/2001) at station 45009.

Event no.	Obs Day	Obs Q	Sim Day	Sim Q	Error %	Day error
1	454	68.9	454	60.9	-11.6	0
2	2586	59.6	2586	66.5	11.6	0
3	395	50.6	395	61.5	21.5	0
4	1850	49.9	1850	35.6	-28.7	0
5	1857	49.2	1858	43.8	-10.9	-1
6	484	41	485	43.8	6.8	-1
7	80	40.6	80	37	-8.9	0
8	2625	38.2	2626	40.7	6.7	-1
9	1366	37.6	1366	14.8	-60.7	0
10	1558	37.4	1555	34.3	-8.2	3
11	1619	37.4	1619	27.2	-27.3	0
12	1913	34.4	1913	34.8	1.3	0
13	1231	32.4	1236	32.8	1.4	-5
14	1980	30.6	1980	21	-31.3	0
15	2277	30.5	2277	30.1	-1.4	0
16	2263	29.5	2263	40.1	35.9	0
17	1937	29	1934	35.6	22.9	3
18	813	28.1	813	32.8	16.6	0
19	97	26.7	96	30.4	13.9	1
20	2271	26.6	2270	54.4	104.4	1
21	2631	25.4	2626	40.7	60.4	5
22	2593	24.6	2590	18.2	-26	3
23	1922	24.3	1920	27.1	11.6	2
24	2346	23.3	2346	25.2	8.3	0

Table 7.17: Largest 24 events for calibration period 2 (1/10/2003-30/9/2011) at station 45009.

Event no.	Obs Day	Obs Q	Sim Day	Sim Q	Error %	Day error
1	1802	40.6	1802	64.9	59.8	0
2	2662	34.5	2662	48.1	39.5	0
3	1530	34.4	1531	47.8	39	-1
4	1573	31.2	1568	28.2	-9.5	5
5	74	29.7	74	67.6	127.7	0
6	1152	27.6	1152	51.1	85.3	0
7	104	26.9	104	49.6	84.2	0
8	2250	25.9	2246	30.8	18.9	4
9	768	24.5	768	26.7	8.8	0
10	1524	24.2	1529	41	69.4	-5
11	1198	22.9	1198	31.5	37.6	0
12	1253	21.4	1252	26.5	24	1
13	2599	20.6	2604	22.5	9.4	-5
14	395	19.6	390	31.3	59.6	5
15	2129	19.6	2130	51.4	162.3	-1
16	1208	19.5	1206	24.6	26.1	2
17	1942	19.4	1941	29.1	50	1
18	125	18.2	129	31.2	71.7	-4
19	2300	17.5	2300	16.4	-6.4	0
20	1744	17	1744	41.3	142.9	0
21	1629	16.8	1629	42.6	153.5	0
22	1162	16.5	1167	25	51.3	-5
23	1168	15.8	1168	25.4	60.6	0
24	1565	15.7	1568	28.2	79.8	-3

Table 7.18: Largest 24 events for calibration period 1 (1/10/1993-30/9/2001) at station 45012.

Event no.	Obs Day	Obs Q	Sim Day	Sim Q	Error %	Day error
1	505	516	502	16.5	-96.8	3
2	499	504	502	16.5	-96.7	-3
3	2614	108	2609	17.8	-83.5	5
4	2259	89	2262	36.5	-59	-3
5	2576	71.4	2571	8.7	-87.8	5
6	81	70.7	80	30.6	-56.7	1
7	2267	61.8	2270	73.9	19.6	-3
8	2582	53.6	2586	46.7	-12.9	-4
9	1846	51	1850	18.8	-63.1	-4
10	126	47.3	125	16.4	-65.4	1
11	482	42.8	481	32.2	-24.8	1
12	2597	39.4	2595	13.6	-65.4	2
13	1547	38.5	1547	12.4	-67.9	0
14	819	38.4	814	18.5	-51.9	5
15	2717	35.2	2720	6.2	-82.3	-3
16	454	34.6	453	49.3	42.6	1
17	2661	34.1	2656	9.1	-73.4	5
18	97	32.7	96	26.8	-18.2	1
19	1815	31.9	1810	1.4	-95.6	5
20	802	31.8	798	4.2	-86.9	4
21	146	31.7	148	22.9	-27.7	-2
22	434	29.3	433	18	-38.6	1
23	1839	28.7	1842	6.9	-76.1	-3
24	1926	28.4	1921	14.1	-50.4	5

Table 7.19: Largest 24 events for calibration period 2 (1/10/2003-30/9/2011) at station 45012.

Event no.	Obs Day	Obs Q	Sim Day	Sim Q	Error %	Day error
1	1959	81.1	1959	31.6	-61	0
2	2300	46.6	2305	15.1	-67.5	-5
3	1901	41.2	1900	24.6	-40.3	1
4	795	37.3	793	14.6	-60.8	2
5	1228	33.8	1232	18.5	-45.3	-4
6	480	32.3	480	8.7	-73	0
7	445	32	445	14.2	-55.7	0
8	1253	31.1	1252	22.9	-26.4	1
9	1802	29.9	1802	25.6	-14.5	0
10	395	29.6	394	18.4	-37.7	1
11	2252	26.9	2251	25.5	-5.2	1
12	2246	26	2251	25.5	-1.9	-5
13	768	25.9	767	9.8	-62.2	1
14	1154	25.5	1151	21.5	-15.6	3
15	2237	24.9	2236	17.3	-30.5	1
16	1568	24.8	1567	21.7	-12.6	1
17	1530	24.5	1530	25.8	5.2	0
18	2282	24.3	2282	14.9	-38.7	0
19	100	24	103	27.6	14.9	-3
20	2662	23.6	2661	23.7	0.1	1
21	124	23.2	128	22.1	-4.9	-4
22	1628	22.3	1628	18.2	-18.3	0
23	1160	22.1	1155	10.1	-54.3	5
24	1364	21.8	1369	4.3	-80.4	-5

8.Bibliography

Abam, T., 1993. Factors affecting distribution of instability of river banks in the Niger delta. Engineering Geology 35, 123–133.

Abernethy, B., Rutherfurd, I.D., 1998. Where along a river's length will vegetation most effectively stabilise stream banks? Geomorphology 23, 55–75.

Allan, D., Erickson, D., Fay, J., 1997. The influence of catchment land use on stream integrity across multiple spatial scales. Freshwater Biology 37, 149–161.

Allison, M.A., Kuehl, S.A., Martin, T.C., Hassan, A., 1998. Importance of flood-plain sedimentation for river sediment budgets and terrigenous input to the oceans : Insights from the Brahmaputra-Jamuna River. Geology 26, 175–178.

Allison, P., 1999. Multiple regression : A primer.

Anthony, S., 2003. The MCDM model: a monthly calculation of water balance for use in the decision support systems. Unpublished ADAS internal document.

Armour, J.D., Hateley, L.R., Pitt, G.L. 2009. Catchment modelling of sediment, nitrogen and phosphorus nutriend loads within SedNet/ANNEX in the Tully-Murray basin. Marine and Freshwater Research 60, (11) 1091-1096.

Ascough, J., Baffaut, C., Nearing, M., Liu, B., 1997. WEPP Watershed Model: 1 Hydrology and Erosion. Fort Collins, CO, USA.

Ashbridge, D., 1995. Processes of river bank erosion and their contribution to the suspended sediment load of the River Culm, Devon, in: Foster, I., Gurnell, A., Webb, B. (Eds.), Sediment and Water Quality in River Catchments. Wiley, Chichester, UK, pp. 229–245.

Asselman, N., Middelkoop, H., 1995. Floodplain sedimentation: Quantities patterns and processes. Earth Surface Processes and Landforms 20, 481–499.

Aswathy, M.V., Vijith, H., Sathessh, R., 2008. Factors influencing the sinuosity of Pannagon River, Kottayam, Kerala, India: An assessment using remote sensing and GIS. Environmental Monitoring and Assessment 138, 173–180.

Bailey, R., Spackman, E., 1996. A model for estimating soil moisture changes as an aid to irrigation scheduling and crop water-use studies : 1 Operational details and description. Soil Use and Management 122–128.

Baker, V., 1977. Stream-channel response to floods, with examples from central Texas. Geological Society of America Bulletin 88, 1057–1071.

Barry, D. a., Bajracharya, K., 1995. On the Muskingum-Cunge flood routing method. Environment International 21, 485–490.

Bartley, R., Hartcher, M., Henderson, A., Chen, Y., Brodie, J., 2004. Application of SedNet Model to the Bowen Catchment, Queensland: assessment of sediment and nutrient loads at a sub-catchment scale under different grazing scenarios. CSIRO Land and Water Client Report.

Bates, P.., De Roo, a. P.., 2000. A simple raster-based model for flood inundation simulation. Journal of Hydrology 236, 54–77.

Bathurst, J.C., Thorne, C.R., Hey, R.D., 1977. Direct measurements of secondary currents in river bends. Nature 269, 504–506.

Beeson, C., Doyle, P., 1995. Comparison of bank erosion at vegetated and non-vegetated channel bends. JAWRA Journal of the American Water Resources Association 31, 983–990.

Bell, V., Kay, A., 2007. Development of a high resolution grid-based river flow model for use with regional climate model output. Hydrology and Earth System Sciences 11, 532–549.

Beuselinck, L., Govers, G., Hairsine, P., 2002. The influence of rainfall on sediment transport by overland flow over areas of net deposition. Journal of Hydrology 257, 145–163.

Biedenharn, D., Thorne, C., 1994. Magnitude-frequency analysis of sediment transport in the Lower Mississippi river. Regulated Rivers: Research & Management 9, 237–251.

Biedenharn, D.., Combs, P.G., Hill, G.J., Pinkard, C.F., Pinkston, C.B., 1989. Relationship between channel migration and radius of curvature on the Red River, in: Wang, S.Y. (Ed.), Sediment Transport Modeling: Proceedings of the International Symposium. Hydraulics Division, American Society of Civil Engineers, pp. 536–541.

Biftu, G.F., Gan, T.Y., 2004. A semi-distributed, physics-based hydrologic model using remotely sensed and Digital Terrain Elevation Data for semi-arid catchments. International Journal of Remote Sensing 25, 4351–4379.

Bilotta, G.S., Brazier, R.E., 2008. Understanding the influence of suspended solids on water quality and aquatic biota 42, 2849–2861.

Birkinshaw, S.J., Bathurst, J.C., 2006. Model study of the relationship between sediment yield and river basin area. Earth Surface Processes and Landforms 31, 750–761.

Blake, W.H., Walling, D.E., He, Q., 2002. Using cosmogenic beryllium-7 as a tracer in sediment budget investigations. Geografiska Annaler, Series A: Physical Geography 84, 89–102.

Blake, W.H., Ficken, K.J., Taylor, P., Russell, M.A., Walling, D.E., 2012. Tracing crop-specific sediment sources in agricultural catchments. Geomorphology 139-140, 322-329.

Blanckaert, K., 2002. Secondary currents measured in sharp open-channel bends, in: Bousmar, D., Zech, Y. (Eds.), River Flow. Louvain, Belgium, pp. 117–125.

Blanckaert, K., De Vriend, H.J., 2004. Secondary flow in sharp open-channel bends. Journal of Fluid Mechanics 498, 353–380.

Blanckaert, K., Graf, W.H., 2001. Mean flow and turbulence in open-channel bend. Journal of hydraulic engineering 127, 835–847.

Boorman, D.B., Hollist, J.M., Lilly, A., 1995. Hydrology of soil types : a hydrologically based classification of the soils of the United Kingdom Report no. 126. Wallingford, Oxfordshire UK.

Boroughs, C., Zagona, E., 2002. Daily flow routing with the Muskingum-Cunge method in the Pecos river riverware model, in: The Second Federal Interagency Hydrologic Modeling Conference, Las Vegas.

Bras, R., 1990. Hydrology : An Introduction to Hydrologic Sciences. Addison-Wesley Publishing Company, New York.

Brice, J., 1973. Meandering pattern of the White River in Indiana: An analysis, in: Morisawa, M. (Ed.), Fluvial Geomorphology. University of New York, Binghampton.

Brodie, I., Rosewell, C., 2007. Theoretical relationships between rainfall intensity and kinetic energy variants associated with stormwater particle washoff. Journal of Hydrology 340, 40–47.

Brunner, G.W., Garbrecht, J.G., 1991. A Muskingum-Cunge Channel Flow Routing Method for Drainage Networks.

Bryan, R., 2000. Soil erodibility and processes of water erosion on hillslope. Geomorphology 32, 385–415.

Bryan, R., Rockwell, D., 1998. Water table control on rill initiation and implications for erosional response. Geomorphology 23, 151–169.

Bull, L.J., 1997. Magnitude and variation in the contribution of bank erosion to the suspended sediment load of the River Severn, UK. Earth Surface Processes and Landforms 22, 1109–1123.

Cabot, P., 2006. Relating sediment and phosphorus movement at multiple scales using fallout cesium-137, phosphorus soprtion dynamics and precision conservation technology. University of Wisconsin-Madison.

Cammeraat, E., 2004. Scale dependent thresholds in hydrological and erosion response of a semi-arid catchment in southeast Spain. Agriculture, ecosystems & environment 104, 317–332.

Carlston, C., 1965. The relation of free meander geometry to stream discharge and its geomorphic implications. American Journal of Science 263, 864–885.

Carson, M., Lapointe, M., 1983. The Inherent Asymmetry of River Meander Planform Author. The Journal of Geology 91, 41–55.

Carter, J., Owens, P., Walling, D., Leeks, G., 2003. Fingerprinting suspended sediment sources in a large urban river system. The Science of The Total Environment 314-316, 513–534.

Chadwick, A., Morfett, J., Borthwick, M., 2004. Hydraulics in Civil and Environmental Engineering, 4th Editio. ed. CRC Press.

Chaplin, J.J., 2005. Development of Regional Curves Relating Bankfull-Channel Geometry and Discharge to Drainage Area for Streams in Pennsylvania and Selected Areas of Maryland - Scientific Investigations Report, Development. Reston, Va. : U.S. Dept. of the Interior, U.S. Geological Survey.

Choudhury, P., 2002. Flood routing in river networks using equivalent Muskingum inflow. Journal of Hydrologic Engineering 413–419.

Chow, V.T., 1959. Open-channel hydraulics. McGraw Hill, New York.

Christensen, J.H., Christensen, O.B., 2002. Severe summertime flooding in Europe. Nature 421, 805–806.

Cole, S.J., Moore, R.J., 2009. Advances in Water Resources Distributed hydrological modelling using weather radar in gauged and ungauged basins. Advances in Water Resources 32, 1107–1120.

Collins, A., Strőmqvist, J., Davison, P.S., Lord, E.I., 2007. Appraisal of phosphorus and sediment transfer in three pilot areas identified for the catchment sensitive farming initiative in England: application of the prototype PSYCHIC model. Soil Use and Management 23, 117–132.

Collins, A., Walling, D., Leeks, G., 1997a. Fingerprinting the Origin of Fluvial Suspended Sediment in Larger River Basins : Combining ASsessment of Spatial Provenance and Source Type. Geografiska annaler. Series A. Physical geography 79, 239–254.

Collins, A., Walling, D., Leeks, G., 1997b. Source type ascription for fluvial suspended sediment based on a quantitative composite fingerprinting technique. Catena 29, 1–27.

Collins, A.L., Anthony, S.G., Hawley, J., Turner, T., 2009. The potential impact of projected change in farming by 2015 on the importance of the agricultural sector as a sediment source in England and Wales. Catena 79, 243–250.

Connell, R., Painter, D., Beffa, C., 2001. Two-dimensional flood plain flow. 2: Model Validation. Journal of Hydrologic Engineering 406–415.

Costa, M.H., Botta, A., Cardille, J.A., 2003. Effects of large-scale changes in land cover on the discharge of the Tocantins River, Southeastern Amazonia. Journal of Hydrology 283, 206-207.

Couper, P., 2003. Effects of silt–clay content on the susceptibility of river banks to subaerial erosion. Geomorphology 56, 95–108.

Couper, P., Stott, T.I.M., Maddock, I.A.N., 2002. Insights into river bank erosion processes derived from analysis of negative erosion-pin recordings: Observations from three recent UK studies. Earth Surface Processes and Landforms 79, 59–79.

Couper, P.R., Maddock, I.A.N.P., 2001. Subaerial river bank erosion processes and their interaction with other bank erosion mechanisms on the River Arrow, Warwickshire, UK. Earth Surface Processes and Landforms 646, 631–646.

Craft, C.B., Casey, W.P., 2000. Sediment and nutrient accumulation in floodplain and depressional freshwater wetlands of Georgia, USA. Wetlands 20, 323–332.

Crosato, A., 1989. Meander migration prediction. Excerpta 4, 169–198.

Crosato, A., 2009. Physical explanations of variations in river meander migration rates from model comparison. Earth Surface Processes and Landforms 34, 2078–2086.

Cunge, J.A., 1969. On the subject of flood propagation computiational method (Muskingum method). Journal of Hydraulic Research 7, 205–230.

Darby, S., Thorne, C., 1996. Development and testing of riverbank-stability analysis. Journal of hydraulic engineering 443–454.

Davie, T., 2008. Fundamentals of Hydrology. Routledge, Oxford UK.

Davies, T.R.H., Tinker, C.C., 1984. Fundamental characteristics of stream meanders. Geological Society of America Bulletin 95, 505–512.

Davison, P.S., Withers, P.J. a., Lord, E.I., Betson, M.J., Strömqvist, J., 2008. PSYCHIC – A process-based model of phosphorus and sediment mobilisation and delivery within agricultural catchments. Part 1: Model description and parameterisation. Journal of Hydrology 350, 290–302.

De Vriend, H.J., 1981. Steady flow in shallow channel bends. Delft University of Technology.

Desmet, P.J.J., Govers, G., 1996. A GIS procedure for automatically calculating the USLE LS factor on topographically complex landscape units. Journal of Soil and Water conservation 51, 427-433.

Dickinson, W., Rudra, R., Wall, G., 1986. Identification of soil erosion and fluvial sediment problems. Hydrological Processes 1, 111–124.

Douglas, I., 1967. Man, Vegetation and the Sediment Yields of Rivers. Nature 215, 925–928.

Duan, J., Julien, P., 2005. Numerical simulation of the inception of channel meandering. Earth surface processes and landforms 30, 1093–1110.

Duijsings, J., 1987. A sediment budget for a forested catchment in Luxembourg and its implications for channel development. Earth Surface Processes and Landforms 12, 173–184.

Dury, G., 1973. Magnitude-frequency analysis and channel morphology, in: Morisawa, M. (Ed.), Fluvial Geomorphology. Allen and Unwin, London, pp. 91–121.

Ebisemiju, F., 1990. Sediment delivery datio prediction equations for short catchment slopes in a humid tropical environment. Journal of Hydrology 114, 191–208.

Ebisemiju, F.S., 1994. The sinuosity of alluvial river channels in the seasonally wet tropical environment: case study of river Elemi, southwestern Nigeria. Catena 21, 13–25.

Edwards, A., Withers, P., 1998. Soil phosphorus management and water quality : a UK perspective. Soil use and Management 14, 124–130.

Environment Agency, 2008. River Habitat Survey.

Environment Agency, 2012. 2012 Check on progress report.

Environment Protection Agency, U., 2013. EPA [WWW Document]. Channel stability analysis. URL http://water.epa.gov/scitech/datait/tools/warsss/pla_box07.cfm (accessed 9.1.13).

Environment Waikato, 2008. Wharekawa Estuary Sediment Sources - Report 2008.

Erskine, W., Saynor, M., 1996. Effects of catastrophic floods on sediment yields in southeastern Australia, in: Erosion and Sediment Yield: Global and Regional Perspectives. pp. 381–388.

Ewen, J., Parkin, G., O'Connell, P., 2000. Shetran: Distributed River Basin Flow and Transport Modeling System. Journal of Hydrologic Engineering 5, 250–258.

FAO (Food and Agriculture Organisation of the UN), 1996. Control of water pollution from agriculture, FAO irrigation and drainage paper 55.

Ferro, V., Minacapilli, M., 1995. Sediment delivery processes at basin scale. Hydrological Sciences Journal 40, 703–717.

Field, A., 2005. Discovering Statistics Using SPSS. Sage.

Finnegan, N.J., Dietrich, W.E., 2011. Episodic bedrock strath terrace formation due to meander migration and cutoff. Geological Society of America Bulletin 2011068.

Fisher, K., Dawson, H., 2003. DEFRA / Environment Agency Flood and Coastal Defence R & D Programme Roughness Review By Karen Fisher and Hugh Dawson. London.

Flanagan, D., Gilley, J., Franti, T., 2007. Water Erosion Prediction Project (WEPP) : Development history, model capabilities, and future enhancements. Transactions of the ASABE 50, 1603–1612.

Fornis, R.L., Vermeulen, H.R., Nieuwenhuis, J.D., 2005. Kinetic energy–rainfall intensity relationship for Central Cebu, Philippines for soil erosion studies. Journal of Hydrology 300, 20–32.

Fotherby, L., 2009. Valley confinement as a factor of braided river pattern for the Platte River. Geomorphology 103, 562–576.

Fowler, H., Ekström, M., 2009. Multi-model ensemble estimates of climate change impacts on UK seasonal precipitation extremes. International Journal of Climatology 416, 385–416.

Fox, D., Bryan, R., 1999. The relationship of soil loss by interrill erosion to slope gradient. Catena 211–222.

Franchini, M., Bernini, A., Barbetta, S., Moramarco, T., 2011. Forecasting discharges at the downstream end of a river reach through two simple Muskingum based procedures. Journal of Hydrology 399, 335–352.

Fread, D.L., 1992. Flow Routing, in: Maidment, D.L. (Ed.), Handbook of Hydrology. McGraw.

Friedkin, J.F., 1945. A Laboratory Study of the Meandering of Alluvial Rivers - Waterways Experimentation Report.

Fuller, I.C., 2008. Geomorphic impacts of a 100-year flood: Kiwitea Stream, Manawatu catchment, New Zealand. Geomorphology 98, 84–95.

Furbish, D., 1991. Spatial autoregressive structure in meander evolution. Geological Society of America Bulletin 103, 1576–1589.

Garbrecht, J., Brunner, G., 1991. Hydrologic channel-flow routing for compound sections. Journal of Hydraulic Engineering 117, 629–642.

Gardiner, T., 1981. Some Factors Promoting Channel Bank Erosion , River Lagan , County Down. Journal of Earth Sciences 5, 231–239.

Gautier, E., Brunstein, D., Vauchel, P., Roulet, M., Fuertes, O., Guyot, J., Darozzes, J., Bourrel, L., 2007. Temporal relations between meander deformation, water discharge and sediment fluxes in the floodplain of the Rio Beni (Bolivian Amazonia). Earth Surface Processes and Landforms 32, 230–248.

Gerbersdorf, S., Jancke, T., Westrich, B., 2007. Sediment Properties for Assessing the Erosion Risk of Contaminated Riverine Sites. An approach

to evaluate sediment properties and their covariance patterns over. Journal of Soils and Sediments 7, 25–35.

Giardino, J., Lee, A., 2011. Rates of Channel Migration on the Brazos River.

Goldich, S., 1938. A Study in Rock-Weathering. The Journal of Geology 46, 17–58.

Golosov, V., 2002. Soil erosion and small river aggradation in Russia, in: ISCO Conference. Beijing.

Gomez, B., Coleman, S., 2007. Channel change, bankfull and effective discharges on a vertically accreting, meandering, gravel-bed river. Earth Surface Processes and Landforms 785, 770–785.

Goovaerts, P., 1999. Using elevation to aid geostatistical mapping of rainfall erosivity. Catena 34, 227-242.

Govers, G., Poesen, J., 1988. Assessment of the interrill and rill contributions to total soil loss from an upland field plot. Geomorphology 1, 343–354.

Gregory, K.., 1987. Energetics of the Physical Environment : Energetic approaches to Physical Geography. John Wiley and Sons, Ltd.

Gruszowski, K.E., Foster, I.D.L., Lees, J. A., Charlesworth, S.M., 2003. Sediment sources and transport pathways in a rural catchment, Herefordshire, UK. Hydrological Processes 17, 2665–2681.

Guo, J., Julien, P., 2005. Shear Stress in Smooth Rectangular Open-Channel Flows. Journal of hydraulic engineering 30, 30–37.

Gupta, H., Sorooshian, S., Yapo, P., 1999. Status of Automatic calibration for hydrologic models: Comparison with mutilevel expert calibration. Journal of Hydrologic Engineering 4, 135–143.

Gurnell, A., 1994. Channel planform change on the river Dee meanders, 1876-1992. Regulated Rivers: Research & Management 9, 187–204.

Hall, J.E., Holzer, D.M., Beechie, T.J., 2007. Predicting River Floodplain and Lateral Channel Migration for Salmon Habitat Conservation. Journal of the American Water Resources Association 43, 786–797.

Haltas, I., Kavvas, M., 2009. Ensemble-Averaged Flow Routing in Channel Networks : Kinematic Wave Equation. Journal of Hydrologic Engineering 655–662.

Hazelton, P., Murphy, B., 2007. Interpreting soil test results. CSIRO Publishing.

He, Q., Owens, P., 1995. Determination of suspended sediment provenance using caesium-137, unsupported lead-210 and radium-226 : a numerical

mixing model approach, in: Foster, I., Gurnell, A., Webb, B. (Eds.), Sediment and Water Quality in River Catchments. John Wiley and Sons, Ltd., Chichester, UK.

Heathwaite, A., Johnes, P., 1996. Contribution of nitrogen species and phosphorus fractions to stream water quality in agricultural catchments. Hydrological Processes 10, 971–983.

Hey, R.D., Thorne, C.., 1986. Stable channels with moblie gravel beds. Journal of Hydraulic Engineering ASCE 112, 671–689.

Hey, R.D., Thorne, C.R., 1975. Secondary flow in river channels. Area 7, 191–195.

Heywood, M., 2003. Sedimentation of salmonid spawning gravels: an investigation of associated sediment dynamics in the Hampshire Avon catchment. PhD thesis,University of Exeter, UK.

Hickin, E., 1978. Mean flow structure in meanders of the Squamish River, British Columbia. Canadian Journal of Earth Sciences 15, 1833–1849.

Hickin, E., Nanson, G., 1975. The Character of Channel Migration on the Beatton River , Northeast British. Geological Society of America Bulletin 86, 487–494.

Hicks, F., Peacock, T., 2005. Suitability of HEC-RAS for flood forecasting. Canadian Water Resources Journal 30, 159–174.

Hoogmoed, W., Stroosnijder, L., 1984. Crust formation on Sandy Soils in the Sahel 1. Rainfall and Infiltration. Soil and Tillage Research 4, 5–23.

Hooke, J., 1979. An analysis of the processes of river bank erosion. Journal of Hydrology 42, 39–62.

Hooke, J., 1980. Magnitude and distribution of rate of river bank erosion. Earth surface processes 5, 143–157.

Hooke, J., 1987. No Changes in meander morphology, in: Gardiner, V. (Ed.), International Geomorphology. John Wiley and Sons, Ltd., Chichester, UK, pp. 591–609.

Hooke, J., 1997. Styles of channel change, in: Thorne, C., Hey, R., Newson, M. (Eds.), Applied Fluvial Geomorphology for River Engineering and Management. John Wiley and Sons, Ltd., Chichester, UK, pp. 237–268.

Hooke, J., 2003. Coarse sediment connectivity in river channel systems: a conceptual framework and methodology. Geomorphology 56, 79–94.

Hooke, J., Kain, R., 1982. Historical change in the Physical Environment. Butterworth, London.

Hooke, J., Yorke, L., 2010. Rates, distributions and mechanisms of change in meander morphology over decadal timescales, River Dane, UK. Earth Surface Processes and Landforms 35, 1601–1614.

Hooke, J.M., 2007a. Complexity, self-organisation and variation in behaviour in meandering rivers. Geomorphology 91, 236–258.

Hooke, J.M., 2007b. Spatial variability, mechanisms and propagation of change in an active meandering river. Geomorphology 84, 277–296.

Hooke, J.M., 2008. Temporal variations in fluvial processes on an active meandering river over a 20-year period. Geomorphology 100, 3–13.

Hough, M., Jones, R., 1997. The United Kingdom Meteorological Office rainfall and evaporation calculation system : MORECS version 2.0-an overview. Hydrology and Earth System Sciences 1, 227–239.

Howard, A., Knutson, T., 1984. Sufficient conditions for River Meandering: A Simulation Approach. Water Resources Research 20, 1659–1667.

Howard, A.., 1992. Modeling channel migration and floodplain sedimentation in meandering streams, in: Carling, P.A., Petts, G.E. (Eds.), Lowland Floodplain Rivers: Geomorphological Perspectives. pp. 1–40.

Howard, A.D., Hemberger, A.T., 1991. Multivariate characterization of meandering. Geomorphology 4, 161–186.

Huang, M., Gallichand, J., Dong, C., Wang, Z., Shao, M., 2007. Use of soil moisture data and curve number method for estimating runogg in the loess Plateau of China. Hydrological Processes 21, 1471–1481.

Hudson, P.F., Kesel, R.H., 2000. Channel migration and meander-bend curvature in the lower Mississippi River prior to major human modification. Geology 28, 531–534.

Hurkmans, R.T.W.L., de Moel, H., Aerts, J.C.J.H., Troch, P. a., 2008. Water balance versus land surface model in the simulation of Rhine river discharges. Water Resources Research 44, n/a–n/a.

Ikeda, S., Parker, G., Sawai, K., 1981. Bend theory of river meanders. Part 1. Linear development. Journal of Fluid Mechanics 112, 363 377.

Institute of Water Research, 2002. Institute of Water Research: RUSLE - On-line soil erosion assessment tool [WWW Document]. URL http://35.8.121.139/rusle/index.html (accessed 11.2.10).

IPCC, 2007. Climate Change 2007 : An Assessment of the Intergovernmental Panel on Climate Change, Change. IPCC.

Jansen, J., Codilean, A., Bishop, P., Hoey, T., Persano C, 2006. Channel sinuosity: another angle on steady state and transient response in bedrock rivers draining active mountain belts. Geophysical Research Abstracts 8.

Jarritt, N., Lawrence, D., 2007. Fine sediment delivery and transfer in lowland catchments: modelling suspended sediment concentrations in response to hydrological forcing. Hydrological Processes 2744, 2729–2744.

Jepsen, R., Roberts, J., Lick, W., 1997. Effects of bulk density on sediment erosion rates. Water, Air and Soil Pollution 99, 21–31.

Jiongxin, X., 1996. Channel pattern change downstream from a reservoir: An example of wandering braided rivers. Geomorphology 15, 147–158.

Julian, J., Torres, R., 2006. Hydraulic erosion of cohesive riverbanks. Geomorphology 76, 193–206.

Kay, A.L., Jones, R.G., Reynard, N.S., 2006. RCM rainfall for UK flood frequency estimation. II. Climate change results. Journal of Hydrology 318, 163–172.

Keesstra, S.D., Bruijnzeel, L.A., Huissteden, J. Van, 2009. Meso-scale catchment sediment budgets : combining field surveys and modeling in the Dragonja catchment , southwest Slovenia 1561, 1547–1561.

Kemp, J., 2004. Flood channel morphology of a quiet river, the Lachlan downstream from Cowra, southeastern Australia. Geomorphology 60, 171–190.

Kosmos, C., Danalatos, N., Cammeraat, L.H., Chabart, M., Diamantopoulos, J., Farand, R., Gutierrez, L., Jacob, A., Marques, H., Martinez-Fernandez, J., Mizara, A., Moustakas, N., Nicolau, J.M., Oliveros, C., Pinna, G., Puddu, R., Puigdefabregas, J., Roxo, M., Simao, A., Stamou, G., Tomasi, N., Usai, D., Vacca, A., 1997. The effect of land use on runoff and soil erosion rates under Mediterranean conditions. Catena 29, 45-59.

Kimaro, D.N., Poesen, J., Msanya, B.M., Deckers, J.A., 2008. Catena Magnitude of soil erosion on the northern slope of the Uluguru Mountains , Tanzania : Interrill and rill erosion 75, 38–44.

King, K., Arnold, J., Bingner, R., 1999. Comparison of Green-Ampt and Curve number methods on Goodwin Creek watershed using SWAT. Transactions of the ASAE 42, 919–925.

Kinnell, P.I. a., 2005. Raindrop-impact-induced erosion processes and prediction: a review. Hydrological Processes 19, 2815–2844.

Knighton, D., 1998. Fluvial Forms and Processes. Arnold.

Knisel, W., 1980. CREAMS A field scale model for Chemicals Runoff and Erosion from Agricultural Management Systems, USDA Conservation Research Report.

Knisel, W.., Williams, J.., 1995. Hydrology Component of CREAMS and GLEAMS Models, in: Singh, V.. (Ed.), Computer Models of Watershed Hydrology. Water Resources Publication, pp. 1069–1114.

Kondolf, G., Piégay, H., Landon, N., 2002. Channel response to increased and decreased bedload supply from land use change : contrasts between two catchments. Geomorphology 45, 35–51.

Koussis, A.D., Mazi, K., Lykoudis, S., Argiriou, A.A., 2012. Reverse flood routing with the inverted Muskingum storage routing scheme. Natural Hazards and Earth System Science 12, 217–227.

Kumar, D., Baliarsingh, F., Raju, K., 2011. Extended Muskingum method for flood routing. Journal of Hydro-environment Research 5, 127–135.

Laflen, J., Elliot, W., Simanton, J., Holzey, C., Kohl, K., 1991. WEPP Soil erodibility experiments for rangeland and cropland soils. Journal of Soil and Water Conservation 46, 39–44.

Lambert, A.C.P., Walling, D.E., 1987. Floodplain sedimentation: A preliminary investigation of contemporary deposition within the lower reaches of the River Culm, Devon, UK. Geografiska Annaler, Series A: Physical Geography 69, 393–404.

Lancaster, S.T., Bras, R.L., 2002. A simple model of river meandering and its comparison to natural channels. Hydrological Processes 26, 1–26.

Lane, L.., Renard, K., Foster, G., Laflen, J., 1992. Development and application of modern soil erosion prediction technology - the USDA experience. Australian Journal of Soil Research 30, 893–912.

Langbein, W., Schumm, S., 1958. Yield of Sediment in Relation to Mean Annual Precipitation. American Geophysical Union Transactions 39, 1076–1084.

Langendoen, E., Motta, D., García, M., Abad, J., 2010. An improved meander migration formulation based on streambank erosion processes, in: River Flow Conference. Braunsweig, Germany.

Lauer, J.W., Parker, G., 2008. Net local removal of floodplain sediment by river meander migration. Geomorphology 96, 123–149.

Lawler, D., 1986. River bank erosion and the influence of frost: a statistical examination. Transactions of the Institute of British Geographers 11, 227–242.

Lawler, D.M., 1993. Needle ice processes and sediment mobilization on river banks: the River Ilston, West Glamorgan, UK. Journal of Hydrology 150, 81–114.

Lawler, D.M., Grove, J.R., Couperthwaite, J.S., Leeks, G.J.L., 1999. Downstream change in river bank erosion rates in the Swale ± Ouse system , northern England 992.

Leece, S.A., 1997. Spatial patterns of historical overbank sedimentation and floodplain evolution, Blue River, Wisonsin. Geomorphology 18, 224–244.

Legates, D.R., McCabe, G.J., 1999. Evaluating the use of “goodness-of-fit” measures in hydrologic and hydroclimatic model validation. Water Resources Research 35, 233–241.

Lewin, G., Brindle, B., 1977. Confined Meanders, in: Gregory, K. (Ed.), River Channel Changes. Wiley, pp. 221–233.

Leys, K.F., Werritty, A., 1999. River channel planform change : software for historical analysis. Geomorphology 29, 107–120.

Longfield, S., Macklin, M., 1999. The influence of recent environmental change on flooding and sediment fluxes in the Yorkshire Ouse basin. Hydrological Processes 1066, 1051–1066.

Lu, H., Moran, C., Prosser, I., 2006. Modelling sediment delivery ratio over the Murray Darling Basin. Environmental Modelling & Software 21, 1297–1308.

Lu, H., Moran, C., Prosser, I., DeRose, R., 2004. Investment prioritization based on broadscale spatial budgeting to meet downstream targets for suspended sediment loads. Water Resources Research 40.

Lukey, B., Sheffield, J., Bathurst, J., 1995. Simulating the Effect of Vegetation Cover on the Sediment Yield of Mediterranean Catchments Using SHETRAN. Physics and Chemistry of the Earth 20, 427–432.

Luppi, L., Rinaldi, M., Teruggi, L., Darby, S., Nardi, L., 2008. Monitoring and numerical modelling of riverbank erosion processes : a case study along the Cecina River (central Italy). Earth Surface Processes and Landforms 34, 530–546.

Lyons, J., Weigel, B., Paine, L., Undersander, D., 2000. Influence of intensive rotational grazing on bank erosion, fish habitat quality, and fish communities in southwestern Wisconsin trout streams. Journal of Soil and Water Conservation 55, 271–276.

Mackey, S.D., Bridge, J.S., 1992. A revised FORTRAN program to simulate alluvial stratigraphy. Computers & Geosciences 18, 119–181.

Magilligan, F.J., 1992. Thresholds and the spatial variability of flood power during extreme floods. Geomorphology 5, 373–390.

Malmon, D. V., Reneau, S.L., Dunne, T., Katzman, D., Drakos, P.G., 2005. Influence of sediment storage on downstream delivery of contaminated sediment. Water Resources Research 41, W05008.

Mattia, C., Bischetti, G., Gentile, F., 2005. Biotechnical characteristics of root systems of typical Mediterranean species. Plant and Soil 278, 23–32.

McCarthy, G.T., 1938. The unit hydrograph and flood routing. US Engineering Office, Providence RI.

McCool, D., Foster, G., Renard, K., Yoder, D., Weesies, G., 1995. The Revised Universal Soil Loss Equation, in: Department of Defense/Interagency Workshop on Technologies to Address Soil Erosion on Dpeartment of Defense Lands.

McMichael, C.E., Hope, A.S., Loaiciga, H. a., 2006. Distributed hydrological modelling in California semi-arid shrublands: MIKE SHE model calibration and uncertainty estimation. Journal of Hydrology 317, 307–324.

Meakin, P., Sun, T., Jøssang, T., Schwarz, K., 1996. A simulation model for meandering rivers and their associated sedimentary environments. Physica A 233, 606–618.

Mekawi, A., 2010. Flood Propagation of the Blue Nile in the Sudan Using Muskingum Routing. Nile Basin Water Science & Engineering Journal 3, 39–50.

Merkel, W., 2002. Muskingum-Cunge Flood Routing Procedure in NRCS Hydrologic Models. USDA NRCS National Water and Climate Center 20, 1–12.

Merritt, W.S., Letcher, R. A., Jakeman, A. J., 2003. A review of erosion and sediment transport models. Environmental Modelling & Software 18, 761–799.

Michalková, M., Piégay, H., Kondolf, G.M., Greco, S.E., 2011. Lateral erosion of the Sacramento River, California (1942-1999), and responses of channel and floodplain lake to human influences. Earth Surface Processes and Landforms 36, 257–272.

Micheli, E., Kirchner, J., 2002. Effects of wet meadow riparian vegetation on streambank erosion. 1. Remote sensing measurements of streambank migration and erodibility. Earth Surface Processes and Landforms 27, 627–639.

Micheli, E., Larsen, E., 2011. River channel cutoff dynamics, Sacramento river, California, USA. River Research and Applications 344, 328–344.

Middelkoop, H., Asselman, N.E.M., 1998. Spatial variability of floodplain sedimentation at the event scale in the Rhine–Meuse delta, The Netherlands. Earth Surface Processes and Landforms 23, 561–573.

Middelkoop, H., Van Der Perk, M., 1998. Modelling spatial patterns of overbank sedimentation on embanked floodplains. Geografiska Annaler, Series A: Physical Geography 80, 95–109.

Miller, A., 1990. Flood hydrology and geomorphic effectiveness in the central Appalachians. Earth Surface Processes and Landforms 15, 119–134.

Millward, A.A., Mersey, J.E., 1999. Adapting the RUSLE to model soil erosion potential in a mountainous tropical watershed. Catena 38, 109-129.

Milne, J., 1983. Patterns of confinement in some stream channels of upland Britain. Geografiska annaler. Series A. Physical geography 65, 67–83.

Montgomery, D.R., Buffington, J.M., 1997. Channel-reach morphology in mountain drainage basins. Geological Society of America Bulletin 109, 596–611.

Moramarco, T., Barbetta, S., 2006. A real-time stage Muskingum forecasting model for a site without rating curve. Hydrological sciences … 51, 37–41.

Moramarco, T., Singh, V., 2000. A practical method for analysis of river waves and for kinematic wave routing in natural channel networks. Hydrological processes 62, 51–62.

Morgan, R., 2005. Soil erosion and conservation, 2nd ed. Longman.

Morgan, R., Quinton, J., Smith, R.E., Govers, G., Poesen, W.A., Auerswald, K., Chisci, G., Torri, D., Styczen, M.E. 1998. The European Soil Erosion Model (EUROSEM) : A dynamic approach for predicting sediment transport from

fields and small catchments. Earth Surface Processes and Landforms 544, 527–544.

Morgan, R.P.., 2001. A simple approach to soil loss prediction: a revised Morgan–Morgan–Finney model. Catena 44, 305–322.

Moriasi, D.N., Arnold, J.G., 2007. Model Evaluations Guidelines for Systematic Quantification of Accuracy in Watershed Simulations. Transactions of the ASABE 50, 885–900.

Mosselman, E., 1998. Morphological modelling of rivers with erodible banks. Hydrological Processes 1370, 1357–1370.

Myers, T., Swanson, S., 1992. Variation of stream stability with stream type and livestock bank damage in Northern Nevada. JAWRA Journal of the American Water Resources Association 28, 743–754.

Nanson, G., Hickin, E., 1986. A statistical analysis of bank erosion and channel migration in western Canada. Geological Society of America Bulletin 97, 497–504.

Nash, D., 1994. Effective Sediment-Transporting Discharge from Magnitude-Frequency Analysis. The Journal of Geology 102, 79–95.

Nash, D., 2001. Arid geomorphology. Progress in Physical Geography 25, 409–427.

Nearing, M., Foster, G., Lane, L., Finkner, S., 1989. A process-based soil erosion model for USDA-Water Erosion Prediction Project technology. Trans. ASAE 32, 1587–1593.

Neller, R., 1988. A comparison of channel erosion in small urban and rural catchments, Armidale, New South Wales. Earth Surface Processes and Landforms 13, 1–7.

Nicholas, A., Walling, D., 1998. Numerical modelling of foodplain hydraulics and suspended sediment transport and deposition. Hydrological Processes 1355, 1339–1355.

Nicholas, A., Walling, D., Sweet, R.J., Fang, X., 2006. Development and evaluation of a new catchment-scale model of floodplain sedimentation. Water resources Research 42, 1–13.

Nicholas, A.P., Mitchell, C. a., 2003. Numerical simulation of overbank processes in topographically complex floodplain environments. Hydrological Processes 17, 727–746.

Nicholls, D., 2001. The source and behaviour of fine sediment in the River Torridge Devon and their implications for salmon spawning. PhD thesis, University of Exeter, UK.

Nicoll, T.J., Hickin, E.J., 2010. Planform geometry and channel migration of confined meandering rivers on the Canadian prairies. Geomorphology 116, 37–47.

Norusis, M., n.d. SPSS guide to data analysis. Prentice Hall.

Orlandini, S., Rosso, R., 1998. Parameterization of stream channel geometry in the distributed modeling of catchment dynamics. Water Resources Research 34, 1971–1985.

Owens, P., Batalla, R., 2005. Fine-grained sediment in river systems : Environmental significance and management issues. River Research and … 717, 693–717.

Owens, P.N., Walling, D.E., Leeks, G.J.L., 2000. Tracing fluvial suspended sediment sources in the catchment of the River Tweed, Scotland using composite fingerprints and a numerical mixing model, in: Foster, I.D.. (Ed.), Tracers in Geomorphology. Wiley, Chichester, UK, pp. 291–308.

Palmer, T.N., Ralsanen, J., 2002. Quantifying the risk of extreme seasonal precipitation events in a changing climate. Nature 415, 512–514.

Peltier, L., 1950. The Geographic Cycle in Periglacial Regions as It is Related to Climatic Geomorphology. Annals of the Association of American Geographers 40, 214–236.

Perşoiu, I., Rădoane, M., 2011. Spatial and temporal controls on historical channel responses - study of an atypical case: Someşu Mic River, Romania. Earth Surface Processes and Landforms 36, 1391–1409.

Perumal, M., 1992. Multilinear Muskingum flood routing method. Journal of Hydrology 133, 259–272.

Perumal, M., Sahoo, B., 2008. Volume conservation controversy of the variable parameter Muskingum–Cunge method. Journal of Hydraulic Engineering C, 475–485.

Phillips, J., 2002. Geomorphic impacts of flash flooding in a forested headwater basin. Journal of Hydrology 269, 236–250.

Pickup, G., 1991. Event frequency and landscape stability on the floodplain systems of arid Central Australia. Quaternary Science Reviews 10, 463–473.

Pieri, L., Bittelli, M., Wu, J., Dun, S., Flanagan, D., Pisa, P., Ventura, F., Salvatorelli, F., 2007. Using the Water Erosion Prediction Project (WEPP) model to simulate field-observed runoff and erosion in the Apennines mountain range. Journal of Hydrology 336, 84–97.

Pizzuto, J.E., 1987. Sediment diffusion during overbank flows. Sedimentology 34, 301–317.

Ponce, V., Changanti, P., 1994. Variable-parameter Muskingum-Cunge method revisited. Journal of Hydrology 162, 433–439.

Ponce, V., Lohani, A., Scheyhing, C., 1996. Analytical verification of Muskingum-Cunge routing. Journal of hydrology 174, 235–241.

Ponce, V.M., 1994. Engineering Hydrology: Principles and Practices. Prentice Hall.

Ponce, V.M., Theurer, F.D., 1982. Accuracy criteria in diffusion routing. Journal of Hydraulic Division ASCE 108, 747–757.

Ponce, V.M., Yevjevich, V., 1978. Muskingum-Cunge method with variable parameters. Journal of Hydraulic Division ASCE 104, 1663–1667.

Potter, K.W., 1991. Hydrological impacts of changing land management practices in a moderate-sized agricultural catchment. Water Resources Research, 27. 845-855.

Prosser, I., Rustomji, P., Young, B., Moran, C., Hughes, A., 2001. CSIRO Report : Constructing River Basin Sediment Budgets for the National Land and Water Resources Audit.

Prosser, I., Young, I., Rustomji, P., Hughes, A., Moran, C., 2001. A Model of River Sediment Budgets as an Element of River Health Assessment, in: International Congress on Modelling and Simulation. pp. 1–6.

Prudhomme, C., Jakob, D., Svensson, C., 2003. Uncertainty and climate change impact on the flood regime of small UK catchments. Journal of Hydrology 277, 1–23.

Rankinen, K., Thouvenot-Korppoo, M., Lazar, a., Lawrence, D.S.L., Butterfield, D., Veijalainen, N., Huttunen, I., Lepistö, a., 2010. Application of catchment scale sediment delivery model INCA-Sed to four small study catchments in Finland. Catena 83, 64–75.

Rapp, C., Abbe, T., 2003. A framework for delineating channel migration zones.

Rejman, J., Brodowski, R., 2005. Rill characteristics and sediment transport as a function of slope length during a storm event on loess soil. Earth Surface Processes and Landforms 239, 231–239.

Renard, K., Ferreira, V., 1993. RUSLE Model Description and Database Sensitivity. Journal of Environmental Quality 22, 389–638.

Renard, K., Foster, G., 1997. Predicting soil erosion by water : A guide to conservation planning with the Revised Universal Soil Loss Equation (RUSLE), Agriculture Handbook.

Riezebos, H.T.H., Epema, G.F., 1985. DROP SHAPE AND EROSIVITY PART 11 : SPLASH DETACHMENT , TRANSPORT AND EROSIVITY INDICES 10, 69–74.

Rinaldi, M., 2003. Recent channel adjustments in alluvial rivers of Tuscany, central Italy. Earth Surface Processes and Landforms 28, 587–608.

Roberts, R., Church, M., 1986. The sediment budget in severely disturbed watersheds, Queen Charlotte Ranges, British Columbia. Canadian Journal for Research 16, 1092–1106.

Rosgen, D.L., 1994. A classification of natural rivers. Catena 22, 169–199.

Russell, M. A, Walling, D.E., Hodgkinson, R. A, 2001. Suspended sediment sources in two small lowland agricultural catchments in the UK. Journal of Hydrology 252, 1–18.

Sadeghi, S.H., Singh, J.K., 2010. Derivation of Flood Hydrographs for Ungauged Upstream Subwatersheds Using a Main Outlet Hydrograph. Journal of Hydrologic Engineering 1059–1069.

Santhi, C., Arnold, J.G., Williams, J.., Dugas, W.A., Srinivasan, R., Hauck, L.., 2001. Validation of the SWAT model on a large river basin with point and nonpoint sources. Journal of the American Water Resources Association 37, 1169–1188.

Sarma, J., 1986. Sediment transport in the Burhi Dihing River, India. IAHS PUBLICATION 159, 199–215.

Schilling, K., Wolter, C., 1999. Detailed GPS survey of Walnut Creek, Iowa: channel characteristics and spatial relationships [WWW Document]. Iowa Geological and Water Survey. URL http://www.igsb.uiowa.edu/Mapping/WaterQualityAg/walnut/wntpost/wntpost.htm (accessed 11.26.13).

Schumm, S., Khan, H., 1972. Experimental study of channel patterns. Geological Society of America Bulletin 83, 1755–1770.

Schumm, S., Rutherford, L., Brooks, J., 1994. Pre-cutoff morphology of the lower Mississippi River, in: Schumm, S., Winkley, B. (Eds.), The Variability of Large Alluvial Rivers. American Society of Civil Engineers Press, New York, pp. 13–44.

Schumm, S.A., 1968. River Adjustment to Altered Hydrologic Regimen, Murrumbidgee River and Paleochannels, Australia.

Selby, M., 1982. Hillslope materials and processes. Oxford University Press, Oxford, UK.

Seminara, G., Zolezzi, G., Tubino, M., Zardi, D., 2001. Downstream and upstream influence in river meandering. Part 2. Planimetric development. Journal of Fluid Mechanics 438, 213–230.

Shrestha, S., Bastola, S., Babel, M., 2007. The assessment of spatial and temporal transferability of a physically based distributed hydrological model parameters in different physiographic regions of Nepal. Journal of Hydrology 347, 153–172.

Silgram, M., Hatley, D., Gooday, R., 2007. IRRIGUIDE: a decision support tool for drainage estimation and irrigation scheduling, in: Proceedings of the 6th Biennial Conference of the European Federation of IT in Agriculture (EFITA). Glasgow.

Simm, D., Walling, D., 1998. Lateral variability of overbank sedimentation on a Devon flood plain. Hydrological sciences journal 43, 715–732.

Simm, D.J., 1995. The rates and patterns of overbank deposition on a lowland floodplain, in: Foster, I.D.L., Gurnell, A., Webb, B.W. (Eds.), Sediment and Water Quality in River Catchments. pp. 247–262.

Simon, A., Collison, A., 2002. Quantifying the mechanical and hydrologic effects of riparian vegetation on streambank stability. Earth Surface Processes and Landforms 27, 527–546.

Singh, J., Knapp, H., Demissie, M., 2004. Hydrologic Modeling of the Iroquois River Watershed Using HSPF and SWAT., Illinois State Water Survey: Champaign, Ill.

Singh, P., Quiroga, A., 1987. A Dam-Breach Erosion Model : I . Formulation 1, 177–197.

Singh, R., Panda, R., Satapathy, K., Ngachan, S., 2012. Runoff and Sediment Yield Modelling for a Treated Hilly Watershed in Eastern Himalaya Using the Water Erosion Prediction Project Model. Water Resources Management 26, 643.

Singh, V., McCann, R., 1980. Some notes on Muskingum method of flood routing. Journal of Hydrology 48, 343–361.

Sivapalan, M., Jothityangkoon, C., Menabde, M., 2002. Linearity and non-linearity of basin response as a function of scale: discussion of alternative definitions. Water Resources Research 38, 41–45.

Smithson, P., Addison, K., Atkinson, K., 2008. Fundamentals of the Physical Environment, 4th ed. Routledge.

Soulsby, C., Youngson, A., Moir, H., Malcolm, I.A., 2001. Fine sediment influence on salmonid spawning habitat in a lowland agricultural stream: a preliminary assessment. Science of the Total Environment 265, 295–307.

Stolum, H.H., 1996. River Meandering as a Self-Organization Process. Science 271, 1710–1713.

Stolum, H.H., 1998. Planform geometry and dynamics of meandering rivers. Geological Society Of America Bulletin 110, 1485–1498.

Strömqvist, J., Collins, A. L., Davison, P.S., Lord, E.I., 2008. PSYCHIC – A process-based model of phosphorus and sediment transfers within agricultural catchments. Part 2. A preliminary evaluation. Journal of Hydrology 350, 303–316.

Summerfield, M., 1991. Global Geomorphology : an introduction to the study of landforms. Longman.

Surian, N., 1999. Channel changes due to river regulation: the case of the Piave River, Italy. Earth Surface Processes and Landforms 24, 1135–1151.

Surian, N., Cisotta, A., 2007. Channel adjustments, bedload transport and sediment sources in a gravel-bed river, Brenta River, Italy. Earth Surface Processes and Landforms 32, 1641–1656.

Surian, N., Mao, L., 2009. Morphological effects of different channel-forming discharges in a gravel-bed river. Earth Surface Processes and Landforms 1107, 1093–1107.

Swanson, K.M., Watson, E., Aalto, R., Lauer, J.W., Bera, M.T., Marshall, A., Taylor, M.P., Apte, S.C., Dietrich, W.E., 2008. Sediment load and floodplain

deposition rates: Comparison of the Fly and Strickland rivers, Papua New Guinea. Journal of Geophysical Research 113, F01S03.

Sweet, R.J., Nicholas, A. P., Walling, D.E., Fang, X., 2003. Morphological controls on medium-term sedimentation rates on British lowland river floodplains. Hydrobiologia 494, 177–183.

Takeuchi, K., Ao, T., Ishidaira, H., 1999. Introduction of block-wise use of TOPMODEL and Muskingum-Cunge method for the hydroenvironmental simulation of a large ungauged basin. Hydrological Sciences Journal 44, 633–646.

Tang, X., Knight, D., Samuels, P., 1999. Volume conservation in variable parameter muskingum-cunge method. Journal of Hydraulic Engineering 125, 610–620.

Taylor, K., Owens, P., 2008. Sediment and contaminant sources and transfers in river basins, in: Owens, P. (Ed.), Sustainable Management of Sediment Resources: Sediment Management at the River Basin Scale. Elsevier B.V, pp. 83–135.

Tewolde, M., Smithers, J., 2006. Flood routing in ungauged catchments using Muskingum methods. Water SA 32, 379–388.

Theurer, F., 1998. Environment Agency Report: Impact of sediment pollution on Salmon and Trout fisheries.

Thomas, H., Nisbet, T., 2007. An assessment of the impact of floodplain woodland on flood flows. Water and Environment Journal 21, 114–126.

Thorne, C., 1990. Effects of vegetation on riverbank erosion and stability, in: Thornes, J. (Ed.), Vegetation and Erosion. Wiley, Chichester, UK, pp. 125–144.

Thorne, C., 1991. Bank erosion and meander migration of the Red and Mississippi rivers, USA. IAHS PUBL, IAHS, WALLINGFORD,(ENGL), 1991, 301–313.

Thorne, C.R., Hey, R.D., 1979. Direct measurements of secondary currents at a river inflection point. Nature 280, 226–228.

Thornes, J., 2003. Extremeness of extreme events. Geographica Polonica 76, 157–174.

Tiwari, A., Risse, L., Nearing, M., n.d. Evaluation of WEPP and its comparison with USLE and RUSLE 43, 1129–1135.

Tooth, S., 2000. Downstream changes in dryland river channels: the Northern Plains of arid central Australia. Geomorphology 34, 33–54.

Tooth, S., McCarthy, T.S., Brandt, D., Hancox, P.J., Morris, R., 2002. Geological controls on the formation of alluvial meanders and floodplain wetlands: the example of the Klip River, eastern Free State, South Africa. Earth Surface Processes and Landforms 27, 797–815.

Torizzo, M., Pitlick, J., 2004. Magnitude-frequency of bed load transport in mountain streams in Colorado. Journal of Hydrology 290, 137–151.

Torri, D., Poesen, J., 1992. The Effect of Soil Surface Slope on Raindrop Detachment 1 Introduction 19, 561–578.

Trimble, S., 1977. The fallacy of stream equilibrium in contemporary denudation studies. American Journal of Science 277, 876–887.

Tucker, G.E., Slingerland, R., 1997. Drainage basin responses to climate change. Water Resources Research 33, 2031–2047.

U.S. Army Corps of Engineers, 1994. Chapter 9 - Streamflow and Reservoir Routing, in: Flood Run-off Analysis.

USGS (United states Geological Survey) 2007. Nutrient and Suspended-Sediment Transport and Trends in the Columbia River and Puget Sound Basins, 1993–2003. Scientific Investigations report 5186.

United States Department of Agriculture, 1986. Urban Hydrology for Small Watersheds, Techincal Release 55.

Vaikasas, S., Rimkus, A., 2003. Hydraulic modelling of suspended sediment deposition in an inundated floodplain of the Nemunas Delta. Nordic hydrology 34, 519–530.

Van Asselen, S., Stouthamer, E., Smith, N.D., 2010. Factors Controlling Peat Compaction in Alluvial Floodplains: A Case Study in the Cold-Temperate Cumberland Marshes, Canada. Journal of Sedimentary Research 80, 155–166.

Van Dijk, P., Bruijnzeel, L.A., Rosewell, C.J., 2002. Rainfall intensity and kinetic energy relationships : a critical literature appraisal 261, 1–23.

Van Dijk, P., Kwaad, F., 1998. Modelling suspended sediment supply to the river Rhine drainage network; a methodological study. IAHS PUBLICATION 165–176.

Van Liew, M., Arnold, J.G., Garbrecht, J.G., 2003. Hydrologic sumulation on agricultural watersheds: Choosin between two models. Transactions of the ASAE 46, 1539–1551.

Wade, A.J., Whitehead, P.G., Butterfield, D., 2002. The Integrated Catchments model of Phosphorus dynamics (INCA-P), a new approach for multiple source assessment in heterogeneous river systems: model structure and equations. Hydrology and Earth System Sciences 6, 583–606.

Walling, D.E., 1983. The Sediment Delivery Problem. Journal of Hydrology 65, 209–237.

Walling, D.E., 2005. Tracing suspended sediment sources in catchments and river systems. Science of the total environment 344, 159–84.

Walling, D.E., Amos, C., 1999. Source , storage and mobilisation of fine sediment in a chalk stream system. Hydrological processes 340, 323–340.

Walling, D.E., Bradley, S., 1989. Rates and Patterns of Contemporary Floodplain Sedimentation : A Case Study of the River Culm, Devon, UK. GeoJournal 19, 53–62.

Walling, D.E., Collins, A.L., 2008. The catchment sediment budget as a management tool. Environmental Science & Policy 11, 136–143.

Walling, D.E., Collins, A.L., Jones, P. A., Leeks, G.J.L., Old, G., 2006. Establishing fine-grained sediment budgets for the Pang and Lambourn LOCAR catchments, UK. Journal of Hydrology 330, 126–141.

Walling, D.E., Collins, A.L., Stroud, R.W., 2008. Tracing suspended sediment and particulate phosphorus sources in catchments. Journal of Hydrology 350, 274–289.

Walling, D.E., Fang, D., Nicholas, A.P., Sweet, R.J., 2004. The grain size characteristics of overbank deposits on the flood plains of British lowland rivers 226–234.

Walling, D.E., He, Q., 1997. Investigating spatial patterns of overbank sedimenation on river floodplains. Water, Air and Soil Pollution 99, 9–20.

Walling, D.E., He, Q., 1998. The spatial variability of overbank sedimentation on river floodplains. Geomorphology 24, 209–223.

Walling, D.E., He, Q., Blake, W.H., 2000. River floodplains as phosphorus sinks. The role of erosion and sediment transport in nutrient and contaminent transfer. IAHS Pub. 263, 211-128.

Walling, D.E., He, Q., Nicholas, A.., 1996. Floodplains as suspended sediment sinks, in: Anderson, M.G., Walling, D., Bates, P.D. (Eds.), Floodplain Processes. pp. 399–439.

Walling, D.E., Owens, P.N., Leeks, G.J.L., 1999a. Rates of contemporary overbank sedimentation and sediment storage on the floodplains of the main channel systems of the Yorkshire Ouse and River Tweed , UK. Hydrological Processes 13, 993–1009.

Walling, D.E., Owens, P.N., 2003. The role of overbank floodplain sedimentation in catchment contaminant budgets. Hydrobiologia 494, 83–91.

Walling, D.E., Owens, P.N., Foster, I.D.L., Lees, J. A., 2003. Changes in the fine sediment dynamics of the Ouse and Tweed basins in the UK over the last 100-150 years. Hydrological Processes 17, 3245–3269.

Walling, D.E., Owens, P.N., Leeks, G.J.L., 1998. The role of channel and floodplain storage in the suspended sediment budget of the River Ouse, Yorkshire, UK. Geomorphology 22, 225–242.

Walling, D.E., Owens, P.P.N., Leeks, G.J.L.G., 1999b. Fingerprinting suspended sediment sources in the catchment of the River Ouse , Yorkshire , UK. Hydrological Processes 975, 955–975.

Walling, D.E., Quine, T.A., 1993. Using Chernobyl-derived fallout radionuclides to investigate the role of downstream conveyance losses in the suspended sediment budget of the River Severn, United Kingdom. Physical Geography 14, 239–253.

Walling, D.E., Russell, M., Hodgkinson, R., Zhang, Y., 2002. Establishing sediment budgets for two small lowland agricultural catchments in the UK. Catena 47, 323–353.

Walling, D.E., Woodward, J., 1995. Tracing sources of suspended sediment in river basins: a case study of the River Culm, Devon, UK. Marine Freshwater Research 46, 327–336.

Webb, B.W., Walling, D.E., 1982. The magnitude and frequency characteristics of fluvial transport in a Devon drainage basin and some geomorpohological implications. Catena 9, 9–23.

Whitehead, P.G., Wilson, E., Butterfield, D., 1998. A semi-distributed integrated nitrogen model for multiple source assessment in catchments (INCA) : Part

1-model structure and process equations. Science of the Total Environment 210, 547–558.

Williams, G., 1986. River meanders and channel size. Journal of Hydrology 88, 147–164.

Wilson, L., 1973. Variations in mean annual sediment yield as a function of mean annual precipitation. American Journal of Science 273, 335–349.

Winterbottom, S.J., Gilvear, D.J., 2000. A GIS-based approach to mapping probabilities of river bank erosion : regulated river Tummel, Scotland. Regulated Rivers: Research & Management 16, 127–140.

Wischmeier, W., Smith, D., 1962. Soil-loss estimation as a toll in soil and water management planning. Bulletin of the International Associationo of Scientific Hydrology 59, 148–159.

Wischmeier, W., Smith, D., 1978. Predicting rainfall losses - a guide to conservation planning. Washington, DC.

Wischmeier, W., Mannering, J.V., 1969 Relation of Soil Properties to its Erodibility. Soil Science Society of America Journal 33, 131-137.

Wolman, M., Miller, J., 1960. Magnitude and Frequency of Forces in Geomorphic Processes. The Journal of Geology 68, 54–74.

Wood, P., Armitage, P., 1997. Biological Effects of Fine Sediment in the Lotic Environment. Environmental Management 21, 203–217.

Wu, Y., Zheng, Q., Zhang, Y., Liu, B., Cheng, H., Wang, Y., 2008. Development of gullies and sediment production in the black soil region of northeastern China. Geomorphology 101, 683–691.

Yalin, M., 1963. An expression for bed-load transportation. Journal of Hydraulic Division 89, 221–250.

Zaimes, G., 2006. Riparian land uses and precipitation influences on stream bank erosion in Central Iowa. JAWRA Journal of the American Water Resources Association 42, 83–97.

Zawejska, J., Wyzga, B., 2010. Twentieth-century channel change on the Dunajec River, southern Poland: Patterns, causes and controls. Geomorphology 117, 234–246.

Zolezzi, G., Seminara, G., 2001. Downstream and upstream influence in river meandering. Part 1. Planimetric development. Journal of Fluid Mechanics 438, 183–211.